CERTIFIED MAIL
RETURN RECEIPT REQUESTED

RDM-07-012
October 24, 2007

U.S. Nuclear Regulatory Commission,
ATTN: Jessica Glenny, Project Scientist
Division of Spent Fuel Storage and Transportation,
Office of Nuclear Material Safety and Safeguards,
Washington, DC 20555-0001

Subject: **NRC Request for Additional Information, Docket No. 71-9319, TAC No. 24069**

Reference: **1) NRC Request for Additional Information for Review of the Model No. MAP-12 and MAP-13 Packages, dated September 6, 2007.**

2) AREVA NP Inc Letter dated 03/13/07, "Application for a Certificate of Compliance for the MAP-12/MAP-13 Packages, Revision 0, Docket No. 71-9319".

Ms. Glenny:

AREVA NP Inc. hereby submits the attached response to the Request for Additional Information (RAI) dated September 6, 2007. AREVA appreciates the thorough review given to the Safety Analysis Report, and is confident that all issues are resolved with this submittal. Included within this submittal are the following documents:

- Three (3) paper copies of updated information for the Safety Analysis Report (SAR) for the MAP-12/MAP-13 Packages (Attachment A), including response to RAI questions (Attachment B), provided in three separate folders.
- Three (3) electronic copies are provided in PDF format of the updated SAR, including response to RAI questions (Attachment C).

The electronic copies are contained on CDs in three separate envelopes labeled, "MAP-12/MAP-13 Docket 71-9319, Revision 1".

One copy of each (paper copy and CD) is also being sent to the NRC Document Control Desk.

Revised sections and/or page changes that make up revision 1 to the MAP SAR, in response to the NRC RAI, are provided with revision bars in the right page margin. In addition, a summary description of the nature of page changes is provided with a further description of the sections and/or page changes to update revision 0 of the MAP SAR to revision 1 status.

The majority of SAR changes were made to delete references to the shipment of loose rods and/or rod containers. AREVA is not seeking approval for the transportation of loose fuel rods. Another global change involved revising the description of the borated-aluminum neutron absorber plates as either Boral or borated metal matrix composite.

An additional change to the SAR was initiated by AREVA in response to a nonconformance of the polyurethane foam. The foam manufacturer, General Plastics, notified AREVA on 10/19/2007 that the foam supplied for the fleet of MAP packages had a slightly higher thermal conductivity than specified for use with the MAP. The thermal conductivity was originally specified to be within the range of 0.17 to 0.25 BTU-in/hr-ft^2-°F, per General Plastics recommendation. However, General Plastics notified AREVA that the batch measurements of the foam could have a maximum thermal conductivity of 0.28 BTU-in/hr-ft^2-°F. AREVA evaluated the nonconformance and found that the slightly higher thermal conductivity would not impact the performance of the package. Therefore, the SAR has been updated to allow this slightly higher thermal conductivity range up to 0.30 BTU-in/hr-ft^2-°F. This change affects Section 8.1.5.1.4.

If you or your staff have any questions, require additional information, or wish to discuss the matter further, please contact me at 434-832-5172. Please reference the unique document identification number in any correspondence concerning this letter.

Sincerely,

Richard D. Montgomery, Advisory Engineer
Nuclear Criticality Safety & Shipping Containers

Cc:
Document Control Desk
Spent Fuel Project Office
Office of Nuclear Material Safety and Safeguards,
U.S. Nuclear Regulatory Commission,
Washington, DC 20555-0001

Attachment A

Paper Copy
MAP-12/MAP-13 Package
Safety Analysis Report (SAR)

AREVA NP INC.
An AREVA and Siemens company

3315 Old Forest Road, P.O. Box 10935, Lynchburg, VA 24506-0935
Tel.: (434) 832-3000 - Fax: (434) 832-3840

AREVA

AREVA NP Inc.,

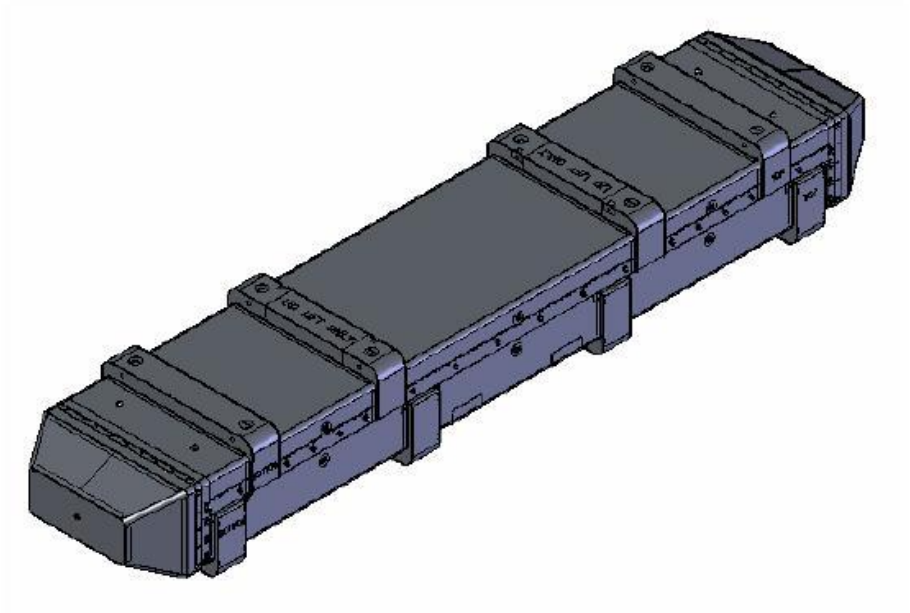

Document Identification No.
51-9026593-001

Application for Certificate of Compliance for the MAP Series of PWR Fuel Shipping Packages

NRC Certificate of Compliance USA/9319/B(U)F-96 Docket 71-9319

Revision 1
October 2007

AREVA NP Inc.,

Document Identification No.
51-9026593-001

Application for Certificate of Compliance for the MAP Series of PWR Fuel Shipping Packages

NRC Certificate of Compliance USA/9319/B(U)F-96 Docket 71-9319

Revision 1
October 2007

Safety Analysis Report

AREVA NP Inc.,

MAP PWR Fuel Shipping Package

Certificate of Compliance No: USA/9319/B(U)F-96

Docket No: 71-9319

Record of Revisions

Revision 0 – March 2007
Revision 1 – October 2007

Nature of Changes
Revision 1

Item	Paragraph or Page(s)	Description and Justification
1	Section 1.1	Add discussion and footnote for modeled package array and justification for calculated CSI value of 2.8 (RAI 1-3)
2	All	Changed description of neutron absorber plates as borated aluminum to either Boral or borated metal matrix composite (RAI 6-2)
3	All	Deleted reference to shipment of loose rods and use of loose rod container (RAI 1-2). Deleted Sections 1.2.1.4,
4	Sections 1.2.2 and 1.2.2.2	Change reference from ^{234}U to ^{236}U with regard to Type B material designation (RAI 1-1)
5	Table 1-1	Changed use of Gadolinia to Absorbers
6	Table 1-3	Add entry for typical rod pressures of 145 to 450 psig (RAI 4-5)
7	Section 2.11	Corrected cited references to Sections 2.12.1 and 4.0 (RAI 4-2)
8	Section 2.12.1	Minor format changes for consistency
9	Table 2.12.1-3	Add further details regarding testing of CTU3 in regards to thermal test duration, condition of assembly and moderator after tests (RAI 2-1)
10	Sections 2.12.1.4.1, 2.12.1.4.2, 2.12.1.4.4	Add further details including figures and discussion regarding fuel assembly geometry, fuel cavity geometry and condition of rod cladding after HAC testing (RAI 4-2)
11	Section 2.12.1.4.4	Provide further clarification of thermal test and results with added discussion and figures. Provided summary table and figures for all moderator segments post HAC testing. Changed reporting basis for moderator from volume to mass for consistency between pre test calculated and post test measured results. Clarified 85% credit assumed for Lid moderator (RAI 2-1, 3-4, and 3-7)
12	Section 2.12.1.5	Add further clarification regarding fuel assembly geometry, fuel cavity geometry, condition of rod cladding, and condition of moderator after HAC testing (RAI 2-1, 3-4, 3-7, and 4-2)
13	Section 2.12.1.6.2	Add further clarification regarding fuel rod pressure for simulate payload (RAI 4-5)
14	Section 3	Revised identified pages to incorporate omitted references (RAI 3-1)
15	Sections 3.3, 3.3.1.1, and 3.5.2	Modified sections and added new Figure 3-2 to present enlarged view of transient shown in Figure 3-1 (RAI 3-2)
16	Sections 3.2.1 and 3.5.2	Modified sections to describe how the solar absorptivity values listed in Table 3-6 of the SAR were applied to the thermal model (RAI 3-3)
17	Section 3.4.2	Modified section to clarify the sequence of events related to the fire test of the MAP (RAI 3-4)
18	Section 3.4.2	Modified section to include justification for the heat input ratio between the regulatory and fire test results (RAI 3-5)
19	Section 3.2.2 and 3.4.3	Modified Sections 3.2.2 and 3.4.3 to provide clarification of the basis for the estimated temperatures reached during the fire (RAI 3-6)
20	Section 3.4.3.1	Add more detailed discussion as further provided in Section 2.12.1 (RAI 3-7)
21	Section 3.5.3	Modified Section 3.5.3 (RAI 3-8, 3-10, and 3-11)
22	Section 4.2.3	Leakage rate change to be consistent with Section 8.1.4 (RAI 4-1)

Item	Paragraph or Page(s)	Description and Justification
23	Section 4	Revised section discussion to indicate that test results are documented in Section 2.12.1 (RAI 4-2)
24	Section 4.2.1.2	Add discussion of weight of fuel equivalent to an A quantity (RAI 4-4)
25	Section 4 and 2.12.1	Add discussion of initial pressure for fuel rods (RAI 4-5)
26	Section 6.2.1.3.2.1	Revised description and allowed form of borated-aluminum neutron absorber to Boral or borated metal matrix composite (RAI 6-1 and 6-2)
27	Sections 6.2.1.4.2, 6.4.5.1.3	Add details and reference for Nylon 6,6 moderator including credit for 90% for the moderator block and 100% for theoretical density (RAI 6-3)
28	Sections 6.3.1, 6.4.2.1, and 6.4.5	Revised Table 6-3 and applicable sections to include summary parameters and calculation results for flooded-gap calculations (RAI 6-4 and 6-5)
29	Section 6.7.7	Revised section and Figure 6-29 to explain the keff curves (RAI 6-6)
30	Section 8	Revised page 8-3, upper limit of thermal conductivity acceptance criteria for foam from 0.25 to 0.30 for consistency with General Plastics reported range. The thermal protection offered by the foam is primarily a function of its density, which determines how much energy is required to char the foam. A relatively small change (0.05 BTU-in/hr-ft^2-^{o}F) to the thermal conductivity of un-charred foam would have little to no perceptible change on the package temperatures for NCT or HAC.

Description of Section/Page Changes
Revision 1

Section or Page Removed	Section or Page Inserted	Basis for Change
Cover Page, Record of Revisions, revision 0	Replace with Cover Page, Record of Revisions, revision 1	Response to RAI
Section 1, revision 0	Replace with Section 1, revision 1	Response to RAI
Section 2, pages 2-1, 2-3, 2-25, and 2-54, revision 0	Replace with Section 2, pages 2-1, 2-3, 2-25, and 2-54, revision 1	Response to RAI
Section 2.12.1, revision 0	Replace with Section 2.12.1, revision 1	Response to RAI
Section 3, revision 0	Replace with Section 3, revision 1	Response to RAI
Section 4, revision 0	Replace with Section 4, revision 1	Response to RAI
Section 6, revision 0	Replace with Section 6, revision 1	Response to RAI
Section 8, page 8-3, revision 0	Replace with Section 8, page 8-3, revision 1	Consistency with General Plastics reported range

Table of Contents

Page

1.0 GENERAL INFORMATION

1.1 INTRODUCTION

The MAP package is designed to transport both Type A and Type B fissile material in the form of unirradiated nuclear fuel assemblies containing sintered uranium dioxide fuel pellets enriched up to 5.0 weight percent ^{235}U. The Criticality Safety Index (CSI) for the MAP is 2.8 when transporting fuel assemblies. The criticality assessment documented in Section 6 modeled a 36 package array for optimum conditions that remained below the derived Upper Safety Limit (USL) as further defined in Section 6[1].

1.2 PACKAGE DESCRIPTION

The major components of the MAP package are presented in Figure 1-1 through Figure 1-7. Detailed drawings are included in Appendix 1.3.1. There are two versions of the MAP packaging: the MAP-12 and the MAP-13. The primary difference between the two versions is the active fuel length of the payload assembly: the MAP-12 is used to ship 144" nominal active fuel and the MAP-13 is used to ship 150" nominal active fuel lengths. The packaging for the two versions is essential identical with the exception of the longer package length.

1.2.1 Packaging

The MAP package is designed to carry two (2) PWR fuel assemblies. The package consists of two basic components: a Base and a Lid. A typical cross-section showing the components of the package is depicted in Figure 1-2 and Figure 1-3. Figure 1-2 is a cross sectional view of the package at the inner stiffeners of the Base and Lid. Figure 1-3 is a cross-sectional view of the package at the location of the moderator and absorber interface within the Base and Lid. The Lid includes independent impact limiters at opposite ends of the package. A close-up view of the package closure is shown in Figure 1-4.

[1] For the 36 package array, 2N=36, N=18 and the CSI is derived by 50/18 which is rounded conservatively to 2.8.

1.2.1.1 MAP Base

The Base consists of a fixed stainless steel strong-back which supports the fuel assembly or Rod Container. The "W" shaped strong-back is secured in the Base using a riveted construction through a fiberglass thermal barrier. A series of inner stiffeners are secured to the underside of the strong-back to provide additional support to the fuel assembly during transport. A neutron moderator and absorber are positioned directly beneath the strong-back between each inner stiffener. The Base inner stiffeners are further retained by a stainless steel cover. The Base stiffener region is not filled with polyurethane foam; however, this volume of the package is sealed from the elements. Each stiffener is perforated to reduce weight and prevent partial flooding of the region during HAC.

Exterior to the cover is a layer of rigid polyurethane foam and an outer shell of 11 gauge stainless steel. An additional 12 gauge stainless steel sheet is provided between the two middle stiffeners to provide local protection against HAC puncture. Four stainless steel outer stiffeners support the package Base and further allow stacking.

The payload rests on the "W" shaped strong-back (referred to as a W-plate) and is held in place with hinged and latched aluminum doors. Inserts are used, as necessary, to provide support for shorter fuel assembly designs at the upper and lower end fittings of the Fuel Assembly. A hold-down bar provides positive axial pressure on the upper end fitting to prevent shifting of the payload during shipment.

1.2.1.2 MAP Lid

The construction of the MAP Lid is very similar to that of the Base – a "W" shaped stainless steel inner shell is fitted with a series of inner stiffeners, neutron moderator and absorbers, and a stainless steel cover is fitted over the stiffeners. A layer of rigid polyurethane foam provides impact and thermal protection and the outer shell of the packaging is fabricated using 11-gauge stainless steel. An additional 12 gauge stainless steel sheet is provided between the two middle stiffeners to provide local protection against HAC puncture. Unlike the inner stiffeners in the Base of the package, the Lid inner stiffeners are not fully imbedded in the polyurethane foam. The

outer stiffeners on the Lid are offset from the Base outer stiffeners to allow for stacking, and are reinforced at the package lift points.

The MAP Lid is fitted with trapezoidal impact limiters at each end. The impact limiters are constructed from rigid polyurethane foam encased by the package outer stainless steel skin. Both the Base and the Lid include end plates with interfacing angles. These angles interlock when the package is assembled, providing strength to the closure and limiting fire ingress during HAC. Figure 1-5 shows a lengthwise cross sectional view. Figure 1-6 provides an enlarged view of the end impact limiters. Figure 1-7 shows an enlargement of the interlocking angle of the Base with the end impact limiters of the Lid.

The polyurethane foam in the Lid and Base is insulated from the outer shell with two layers of ceramic fiber paper. The Lid and Base for a stepped joint with a fibrous high temperature seal and closure using ball lock fasteners.

1.2.1.3 MAP Materials of Construction

The MAP is primarily constructed from: stainless steel, aluminum, and rigid polyurethane foam. Other materials used are fiberglass reinforced polyester resin, refractory insulation, Nylon 6,6 and borated metal matrix composite. Each end impact limiter contains 10 lb/ft^3 polyurethane foam. The balance of the polyurethane foam used is 6 lb/ft^3. The foam is rigid, closed cell polyurethane that is an excellent impact absorber and thermal insulator and has well defined characteristics that make it ideal for this application. Fiberglass strips and a fibrous high temperature seal provide a thermal barrier between the exterior shell and the strong-back. The neutron absorber consists of a borated metal matrix composite in the form of a thin plate. Blocks of Nylon 6,6 are used as a neutron moderator. This thermoplastic is self-extinguishing and has a relatively high melting point. The neutron moderator and absorber are significant components used for criticality safety. Further discussion is presented in Section 6, Criticality Evaluation, and Section 8, Acceptance Tests and Maintenance Program.

1.2.1.4 Containment System

The Containment System for the MAP is the fuel rod cladding. Requirements for containment are described in Section 4.

1.2.1.5 Package Weights and Dimensions

MAP-12 (144-in Nominal Fuel Length)

• Maximum Gross Weight	8,630 pounds (3,923 kg)
• Maximum Payload Weight	3,400 pounds (1,545 kg)
• Overall Outer Dimensions	208" x 45" x 31" high (5,283 mm x 1,143 mm x 787 mm)

MAP-13 (150-in Nominal Fuel Length)

• Maximum Gross Weight	8,630 pounds (3,923 kg)
• Maximum Payload Weight	3,400 pounds (1,545 kg)
• Overall Outer Dimensions	221" x 45" x 31" high (5,613 mm x 1,143 mm x 787 mm)

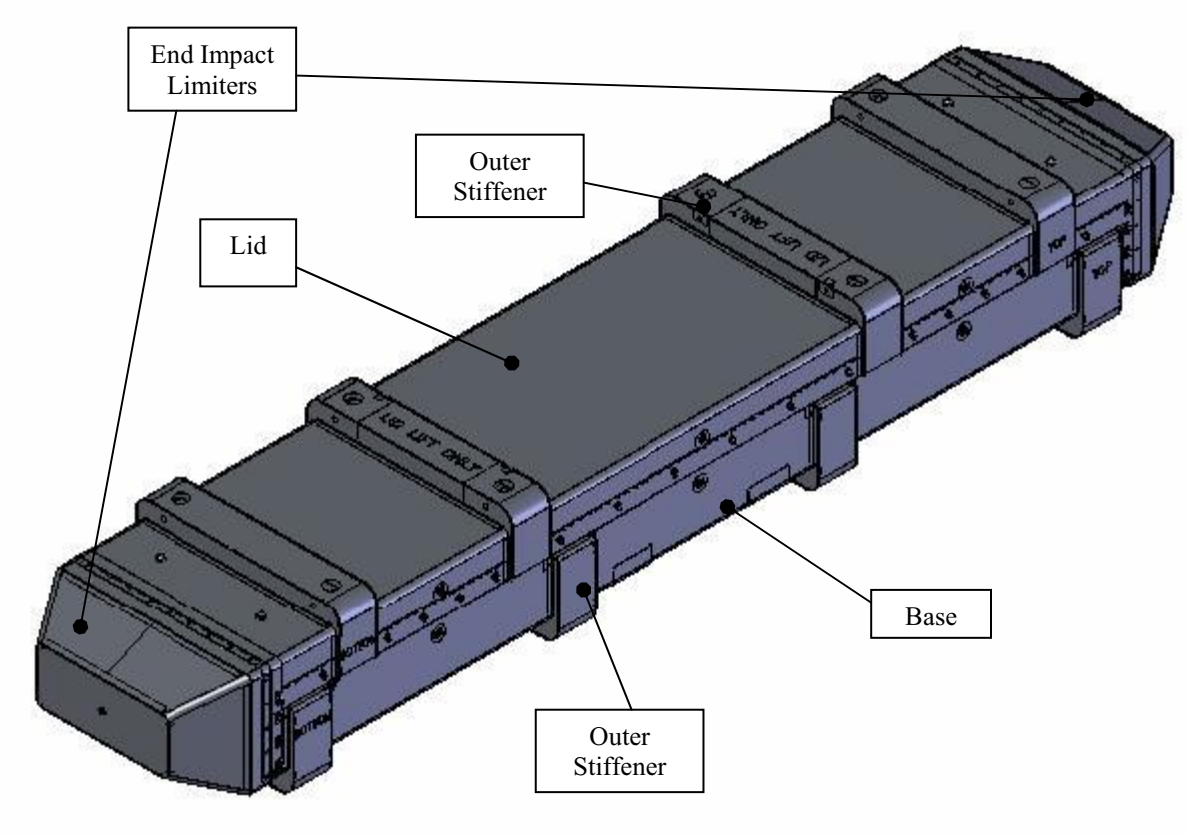

Figure 1-1 MAP Package – Isometric View

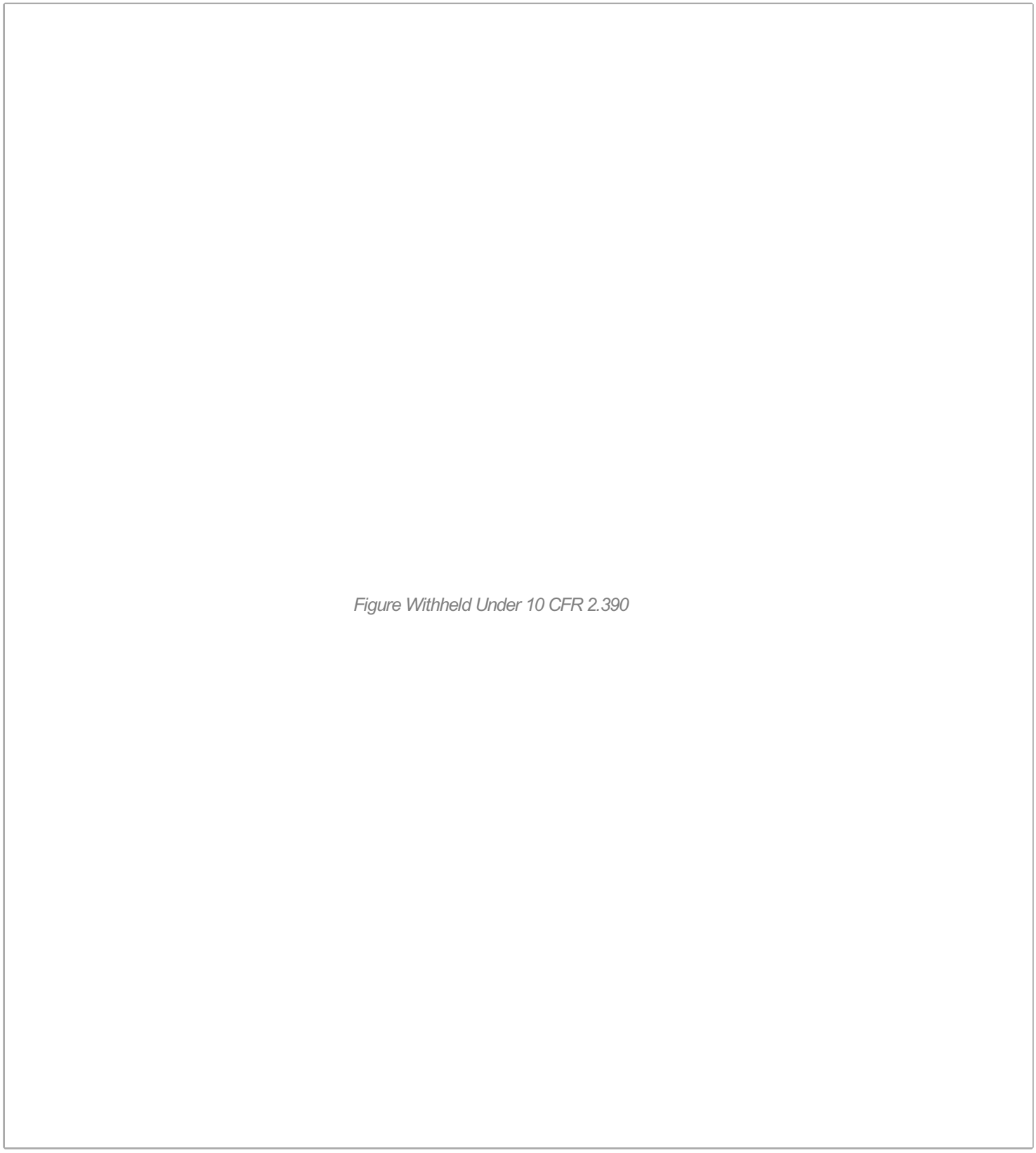

Figure 1-3 MAP Package – Cross Section at Moderator and Absorber

Figure Withheld Under 10 CFR 2.390

Figure 1-4 MAP Package – Close-up of Closure Cross Section

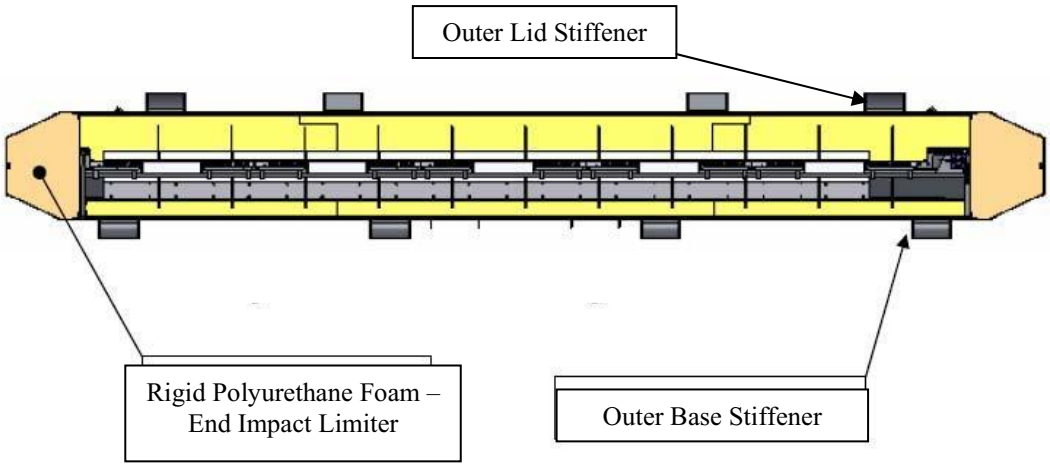

Figure 1-5 MAP Package – Cross Section Lengthwise through Center

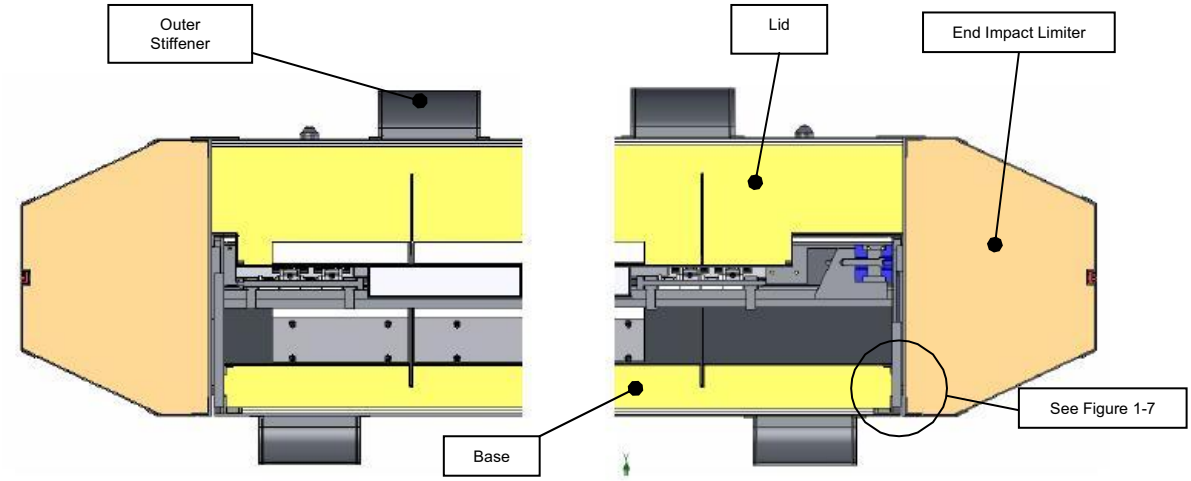

Figure 1-6 MAP Package – Cross Section through Center at Bottom and Top (Left to Right)

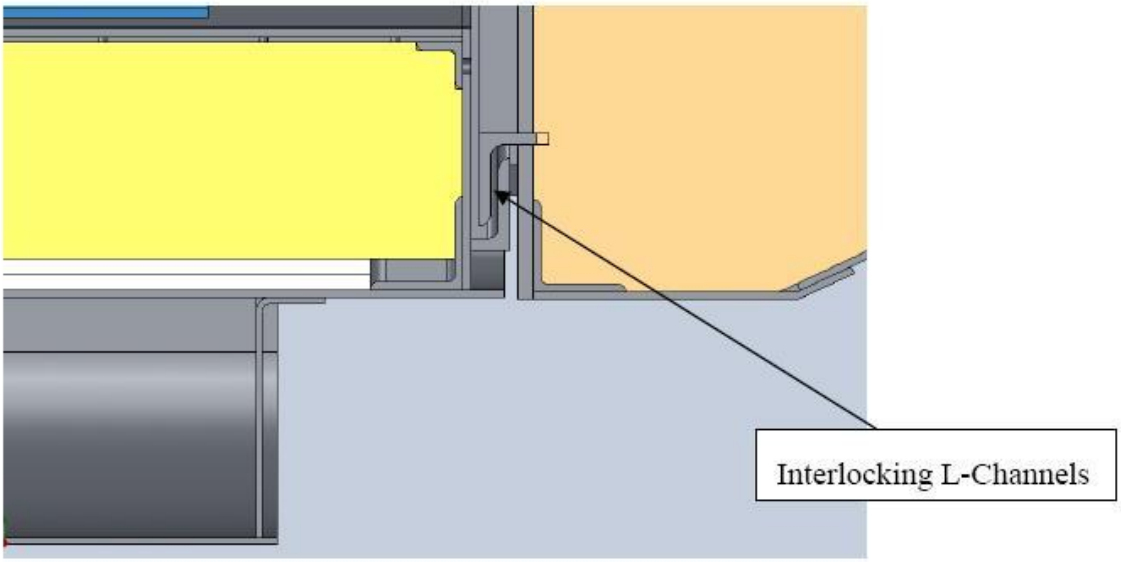

Figure 1-7 MAP Package – Cross Section at Interlocking L-Channels at End Impact Limiters

1.2.2 Contents

Table 1-1 provides a listing of the type, form and mass of material that may be shipped in the MAP. Both Type A and Type B materials are allowed for shipment for materials meeting the isotopic requirements listed in Table 1-2. The fuel assemblies may be of various model and type

as long as they meet the specified requirements delineated in Section 6.0. Typical dimensions of the main components in the fuel assemblies are listed in Table 1-3.

The chemical and physical form of the Type A and Type B contents are the same and are described in Section 1.2.2.1 and 1.2.2.2. The primary difference between the Type A and a Type B content is the uranium fuel for the Type B content has elevated concentrations of ^{236}U. An example of structural materials of the fuel assembly is provided in Table 1-4. Zirconium alloy, stainless steel and Ni-Cr-Fe alloy are chemically stable materials, and are stable to temperatures above 1,475˚F.

In additional to the fuel assembly configuration described previously, each fuel assembly may be shipped with an absorber or control rod cluster inserted into the assembly. The absorber and control rods consist of a very strong thermal neutron absorber clad in metal tubes and further clustered for insertion within a fuel assembly for either reactor flux conditioning or reactor control. The clusters are very effective in reducing the multiplication factor for the package and array of packages such that criticality is not possible in any configuration. However, for purposes of this application, such strong neutron absorbers are not credited for criticality control.

The decay heat of the contents is essentially zero. Neutron and gamma shielding is not required or provided.

1.2.2.1 Type A Contents

The Type A content of the packaging is fresh unirradiated low enriched uranium Pressurized Water Reactor (PWR) nuclear fuel assemblies. A maximum of two fuel assemblies are placed in each packaging. The packaging is designed and analyzed to ship fuel configured either in a 14x14, 15x15, 16x16 or 17x17 array and positioned in one or both sides on the strong-back.

The nuclear fuel pellets loaded in rods and contained in the packaging are uranium oxides primarily as ceramic UO_2 and U_3O_8. The fuel assembly maximum enrichment is less than or equal to 5.0 wt% ^{235}U.

1.2.2.2 Type B Contents

The Type B content of the packaging is unirradiated low enriched uranium Pressurized Water Reactor (PWR) nuclear fuel assemblies derived from off-specification high enriched uranium or reprocessed uranium. The increase in ^{236}U causes the contents to fall under the Type B requirements. A maximum of two fuel assemblies are placed in each packaging. The mixture A_2 value is 0.17 as calculated in Section 4.0. The packaging is designed and analyzed to ship fuel configured either in a 14x14, 15x15, 16x16 or 17x17 array and positioned on one or both sides of the strong-back.

The nuclear fuel pellets loaded in rods and contained in the packaging are uranium oxides primarily as UO_2 and U_3O_8. The fuel assembly maximum enrichment is less than or equal to 5.0 wt% ^{235}U.

1.2.2.3 Quantity of Radioactive Materials of Main Nuclides

The fuel assemblies in this packaging are loaded with low enrichment uranium dioxide less than or equal to 5 wt% ^{235}U. When used as a Type A package the contents conform to the A_1 and A_2 values for a Type A package. Table 1-1 shows the quantity of uranium and enrichment common to both the Type A and Type B contents. These values are carried forward to Table 1-2 to calculate total activity for the mixtures. Activity fractions and A_2 for the mixtures are determined in Section 4.0, Containment.

Fuel rods assembled into the fuel assemblies are those loaded with sintered pellets of uranium dioxide and/or with sintered pellets of uranium dioxide mixed with various additives (e.g., Chromium, Boron, Gadolinium, and Europium). These neutron absorbers are not credited in the safety basis.

1.2.2.4 Packing Materials

A number of packing materials may be used to protect the fuel assembly from superficial damage during shipment (e.g., Neoprene, polyethylene bags).

1.2.3 Special Requirements for Plutonium

Plutonium will not be shipped in the MAP; therefore, this section is not applicable.

Table 1-1 Quantity of Radioactive Materials for Shipment in MAP (Type A and B)

Allowable Assembly Arrays	14x14, 15x15, 16x16 and 17x17
Main Nuclides	Low enriched uranium ≤ 5 wt% ^{235}U
State of Uranium	Uranium oxide ceramic pellet, Solid Normal Form
Fuel Assembly Maximum Enrichment	5.0 wt% Maximum
Number of Fuel Rods Containing Absorbers	Unlimited
Maximum mass of Uranium Dioxide Pellets	574 kg per Fuel Assembly 1,148 kg per Package
Maximum ^{235}U mass	25.5 kg per Fuel Assembly 51.0 kg per Package

Table 1-2 Maximum Allowable Quantity of Radioactive Material

Isotope	Maximum content, g/gU	Maximum mass, g	Total Activity, TBq	Total Activity, Ci
^{232}U	2.00E-09	2.02E-03	1.68E-03	4.54E-02
^{234}U	2.00E-03	2.02E+03	4.65E-01	1.26E+01
^{235}U	5.00E-02	5.06E+04	4.05E-03	1.09E-01
^{236}U	2.50E-02	2.53E+04	6.07E-02	1.64E+00
^{238}U	9.23E-01	9.34E+05	1.12E-02	3.03E-01
^{237}Np	1.66E-06	1.68E+00	4.37E-05	1.18E-03
^{238}Pu	6.20E-11	6.27E-05	3.95E-05	1.07E-03
^{239}Pu	3.04E-09	3.08E-03	7.07E-06	1.91E-04
^{240}Pu	3.04E-09	3.08E-03	2.58E-05	6.98E-04
Gamma Emitters	6.46E+05 MeV-Bq/kgU			

Table 1-3 Typical Dimensions of the Main Components of Fuel Assembly and Fuel Rod

Attribute	Dimensions			
Package Type	MAP-12		MAP-13	
Fuel Type	Pressurized Water Reactor			
Maximum Fuel Assembly Length (including cluster assembly), inches	172		184	
Active Fuel Length (Maximum Nominal Length of enriched material zone), inches	144		150	
Maximum Nominal Fuel Grid Envelope, inches	8.546		8.546	
Fuel Assembly Type	14x14	15x15	16x16	17x17
Maximum Nominal Active Fuel Length, inches	144	144	150	144
Nominal Fuel Pellet Diameter, inches	0.367 – 0.381	0.360 – 0.375	0.327	0.319 – 0.322
Nominal Cladding Wall Thickness, inches	0.025 – 0.028	0.024 – 0.030	0.024	0.022 – 0.024
Nominal Cladding Inner Diameter, inches	0.374 – 0.387	0.364 – 0.380	0.334	0.326 – 0.329
Nominal Fuel Rod Outer Diameter, inches	0.424 – 0.440	0.416 – 0.430	0.382	0.374 – 0.376
Number of Fuel Rods	176 – 179	204 – 216	236	264
Fuel Rod Helium Cover Gas Pressure, psig	145 – 450			

Table 1-4 Typical Fuel Structure Materials

Component parts	Structural Materials	Typical Density
Pellets	Sintered Uranium Dioxide (in some cases uranium dioxide blended with other non-fissile additives)	10.96 g/cm^3 (0.396 lb/in^3)
Cladding tube	Zirconium alloy, metallic zirconium	6.5 g/cm^3 (0.24 lb/in^3)
Internal spring	Stainless steel	7.8 g/cm^3 (0.28 lb/in^3)
Upper and Lower end plug	Zirconium alloy	6.5 g/cm^3 (0.24 lb/in^3)
Guide/Instrument Tube	Zirconium alloy or stainless steel	6.5 to 7.8 g/cm^3 (0.24 to 0.28 lb/in^3)
Upper and Lower tie plate	Stainless steel	7.8 g/cm^3 (0.28 lb/in^3)
Spacer	Zirconium alloy and Ni-Cr-Fe alloy	6.5 to 8.5 g/cm^3 (0.24 to 0.31 lb/in^3)
Finger spring	Zirconium alloy and Ni-Cr-Fe alloy	6.5 to 8.5 g/cm^3 (0.24 to 0.31 lb/in^3)
Expansion spring	Zirconium alloy and Ni-Cr-Fe alloy	6.5 to 8.5 g/cm^3 (0.24 to 0.31 lb/in^3)

1.2.4 Operational Features

The primary operational feature of the package is the ball-lock closure pins used to secure the Lid to the Base. Fork lift pockets are provided on the Base of the package. Stacking brackets, which double as lift points, are attached on the Lid and Base at four (4) locations. The package must be up-righted onto one end for loading and unloading. No valves or rate-monitored seals are used.

1.3 APPENDICES

1.3.1 Package Drawings

2.0 STRUCTURAL EVALUATION

This chapter identifies and describes the principal structural design aspects of the MAP package, and demonstrates the structural safety of the packaging and compliance with the structural requirements of 10 CFR 71[1].

For normal conditions of transport (NCT), demonstration of compliance is by performance testing for free drop and penetration, by calculation for stacking, and by reasoned argument for the water spray requirements. For hypothetical accident conditions (HAC), including the free drop, puncture drop, and fire tests, demonstration of compliance is accomplished by performance testing utilizing multiple, prototypic, full-scale MAP packages.

The compliance of the MAP package with all applicable general structural requirements is discussed in the following sections. The results of the NCT and HAC performance tests are summarized in Section 2.6, *Normal Conditions of Transport*, and Section 2.7, *Hypothetical Accident Conditions*, respectively. Detailed results from all testing is found in Appendix 2.12.1, *MAP Shipping Package Certification Tests*.

2.1 DESCRIPTION OF STRUCTURAL DESIGN

2.1.1 Discussion

The MAP package is designed to carry two (2) PWR fuel assemblies. The fuel assemblies are arranged side-by-side and orientated in a diamond configuration with respect to the package transportation surface.

A detailed description of the package components is provided in Section 1.2, *Packaging Description*, and on the drawings in Appendix 1.3.1, *Package Drawings*.

[1] Title 10, Code of Federal Regulations, Part 71 (10 CFR 71), *Packaging and Transportation of Radioactive Material*, 01-01-06 Edition.

The structural components relied on for NCT and HAC protection are the Lid and Base outer shell and stiffeners, polyurethane foam, fiberglass thermal breaks, ball lock pins and the "W" plate.

2.1.3 Weights and Centers of Gravity

Weights of the MAP packaging components and the maximum gross weight of the loaded package are presented in Section 1.2.1.6. The weights shown in the table are for both the long and short version of the package. The difference in actual tare weights between the two packages is allotted to the fuel weight in the shorter package, which actually carries the heavier fuel. The calculated center of gravity (CG) of the empty package assembly is located at the geometric center for the width and height, and 1 3/4 inches towards the bottom for the length. The calculated CG of the loaded package assembly is also located at the geometric center for the width and height, but 2 2/3 inches towards the bottom for the length, as shown in Figure 2-1. The loaded package CG assumes an even distribution throughout the package cavity of the payload weight.

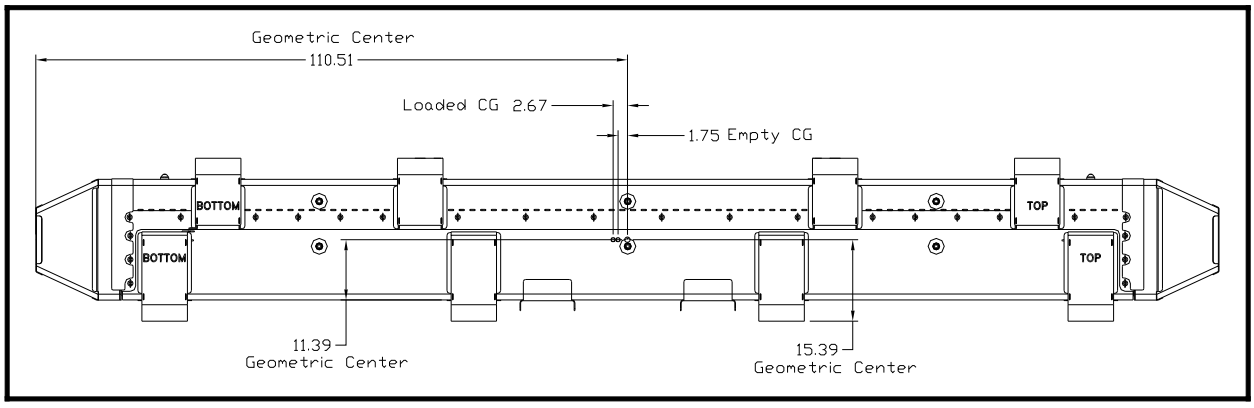

Figure 2-1 – MAP Package CG

2.1.4 Identification of Codes and Standards for Package Design

In lieu of extensive reliance on the use of codes or standards in design, compliance with requirements is demonstrated via full scale testing of the MAP package under both NCT and HAC, resulting in a high level of confidence in the integrity of the design.

Prior to performing the HAC, 30 ft free drop tests, the CTUs were thermally conditioned to a temperature of 120 ºF. The foam temperatures recorded just prior to the tests ranged between 100 ºF and 120 ºF. CTU1 and CTU3 were tested at warm temperature in order to obtain maximum deformations. Warm temperature is also bounding for CTU2, which is focused on maximum impact. This is because the polyurethane foam in the end impact limiter approaches compression to a "solid" before all of the drop energy is absorbed, which allows the last stage of the impact to be uncushioned. This is a more severe case than cold foam which, due to greater strength, does not become "solid".

A summary and discussion of the certification tests is provided in Sections 2.7.1 through 2.7.8. The tests performed, and their sequence, are summarized in Table 2-3 and depicted in Figure 2-30 through Figure 2-32.

2.7.1 Free Drop

10 CFR §71.73(c)(1) requires the drop of the package onto an essentially unyielding surface from a height of 9 m (30 ft) in the orientation for which maximum damage is expected. As discussed in Section 2.6.7, *Free Drop*, certain HAC free drops from a height of 30 ft were preceded by a NCT free drop from a height of 4 ft in the same orientation.

2.7.1.1 End Drop – Justification of Drop Angle

The MAP Package is slightly different, internally, from the top end to the bottom end. The top has an aluminum restraint bar for applying a slight axial preload to the fuel assemblies. The preload helps minimize movement of the fuel assemblies inside the package during transport. The end impact limiters are the same. Both have the same shape, volume, and density of polyurethane foam. The stainless steel shells are also of similar construction. Therefore, the impact force between the top and bottom end drops should be virtually the same with regard to the package. The fuel assemblies, however, are bounded by a bottom drop. Each fuel rod has an internal spring assembly in the top to permit thermal growth of the pellets. During an impact, these spring assemblies act as an energy absorber for the fuel pellets, which make up most of the weight of the fuel. Also, the top fuel assembly hold down spring further cushions the top. A

2.8 ACCIDENT CONDITIONS FOR AIR TRANSPORT OF PLUTONIUM

The MAP package is not transported by air; hence, this section does not apply.

2.9 ACCIDENT CONDITIONS FOR AIR TRANSPORT OF FISSILE MATERIAL PACKAGES

The MAP package is not transported by air; hence, this section does not apply.

2.10 SPECIAL FORM

Since special form is not claimed for the MAP package or fuel, this section does not apply.

2.11 FUEL RODS

In each event evaluated either by analysis or by test, the fuel rods were protected by the MAP package so that they sustained no significant damage. Fuel rod cladding is considered to provide containment of radioactive material under both normal and accident test conditions. Discussion of this cladding and its ability to maintain sufficient mechanical integrity to provide such containment is described in Section 2.12.1 "*MAP Shipping Package Certification Tests*" and Section 4.0 "*Containment*".

Table of Contents **Page**

2.12.1 MAP Shipping Package Certification Tests

2.12.1.1 Introduction

A total of eight (8) tests as discussed in this Section were conducted at the National Transportation Research Center in Oak Ridge, Tennessee, on February 12, 2007. A single thermal test as discussed in this section was further conducted at the Carolina Fire Academy in Columbia, South Carolina, on February 15, 2007. Additional testing and inspections were conducted at the AREVA NP Inc., Mount Athos Road Facility in Lynchburg, Virginia, on February 19 and 20, 2007.

- Three (3) MAP shipping packages were subjected to the following on February 12, 2007.
  - Five (5) free drop tests, two (2) NCT and three (3) HAC.
  - Three (3) puncture tests.
- One (1) MAP shipping package was subject to the following on February 15, 2007.
  - One (1) HAC thermal test.
- One (1) MAP shipping package was subject to the following on February 19, 2007.
  - One (1) penetration rod test.

2.12.1.2 Pre-Test Measurements and Inspections

Detailed fabrication travelers documented the configuration of three (3) prototype MAP-13 units. These packages were verified and further identified as Certification Test Units (CTU) 1, 2, and 3.

2.12.1.2.1 Test Distribution

Table 2.12.1-1 shows the various tests completed for each CTU.

Table 2.12.1-1 – MAP-13 CTU Certification Tests

CTU #	Penetration	Puncture	4' NCT	30' HAC
1	n/a	1) 20° Oblique puncture through CG on lid 2) CG over base side closure joint puncture	10° slap-down on base	30° slap-down on base
2	Lid impact	n/a	n/a	Vertical bottom end
3	n/a	20° Oblique puncture through CG on lid	Horizontal lid down	Horizontal lid down

2.12.1.2.2 Weight Distribution

Each package weight was measured and recorded as shown in Table 2.12.1-2.

Table 2.12.1-2 – CTU Weight Characterization

CTU #	Empty CTU Weight, lb	Fuel Assembly/ Ballast Weight, lb	Adjusted Package Weight, Internal/External, lb	Gross Package Weight, lb
1	5,078	3,400	132/20	8,630
2	5,079	3,400	131/20	8,630
3	5,077(1)	3,400	133/20	8,630

(1) The doubler plates installed on both the lid and base increased the empty weight by 150 lb. This is discussed further in Sections 2.12.1.4.2 and 2.12.1.4.3 for the 20° oblique puncture bar tests of CTU 1 and CTU 3, respectively.

2.12.1.2.3 Puncture Bar Measurements

Puncture bar size and weight: Steel cylindrical bar measured at 6" diameter x 36" tall with a radius of curvature of the bar of less than ¼". The bar had a square mounting base which was bolted to the drop pad.

2.12.1.2.4 Penetration Rod Measurements

Penetration rod size and weight: Steel cylindrical rod measured at 1.25" diameter x 39" long with one end being hemispherical. The rod weight was measured at 13.55 lb.

2.12.1.2.5 Test Pad Characterization

The larger (exterior) drop pad (target) at the National Transportation Research Center (NTRC), Packaging Research Facility (PRF), has been demonstrated to meet the regulatory definition of a flat, essentially unyielding, horizontal surface for packages weighting up to 28,184 lb (12,811 kg) as certified in Oak Ridge National Laboratory Report ORNL/NTRC-001. Several packages exceeding the tested weight of the MAP-13 package have been previously tested at the NTRC.

2.12.1.3 Summary of Tests and Results

2.12.1.3.1 Initial Conditions

Each CTU was dimensionally inspected to the fabrication drawings. The fabrication records were also reviewed prior to accepting each package for testing.

The CTUs were heated in the large bay at the NTRC. CTUs 1 and 3 were wrapped with two (2) 1,500 watt heat strips and insulated with 6" of insulation. CTU 2 was also wrapped with two (2) 1,500 watt heat strips, only the bottom half, since this package was used in the end drop.

CTU 3 was reinsulated for transport to the Carolina Fire Academy and further heated prior to the burn test.

CTUs were heated for at least 48 hours prior to testing to maintain a package temperature of near 100 ^{o}F. The foam temperature in the area of the impending impact region was measured and recorded immediately prior to the corresponding test. Figure 2-12.1-1 shows the packages being heated at the NTRC.

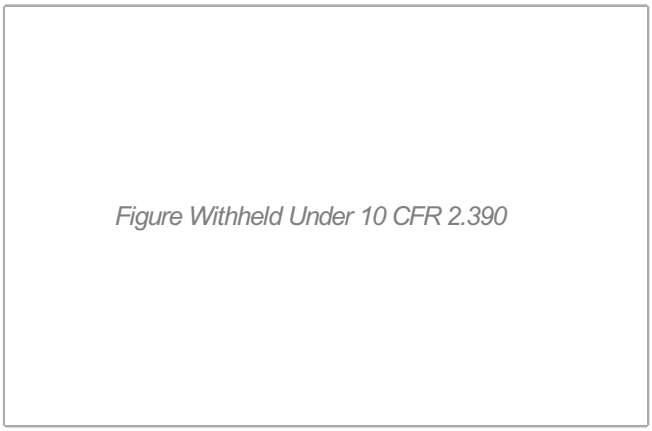

Figure 2.12.1-1 – View showing CTU 3 (left) and CTU 2 (right) during heating.

2.12.1.3.2 Test Description and Results

Table 2.12.1-3 includes a summary description and results of the tests conducted for each CTU. The tests are listed in the sequence performed. Based on the worst damage received and the potential to challenge the moderator in the thermal test, CTU 3 was designated, packaged, and shipped for further testing to the Carolina Fire Academy.

Table 2.12.1-3 – Summary of Drop Tests and Results

CTU No.	Drop Height	Test Designation/Description	Test Results
2	40 in	Penetration test on lid	Slight indentation
2	30 ft	HAC vertical free drop on end	Package end impact limiter crush from 14.25" to ~8.37". Total crush of 5.88". No physical damage to other portions of the package. No loose or damaged closure pins
1	4 ft	10° slap-down on base	Minor compression to top/bottom stiffeners in impact region of base. Single closure pin (ballast side, second from top) fell out after impact
1	30 ft	30° slap-down on base	Top two stiffeners crushed flat. Shoulders sheared off on five bottom closure pins on ballast side with four being sheared off on fuel assembly side. Two pins on opposite sides restrict further removal of lid. Bottom impact limiter movement upward ~1" with the edge of the braided fibrous sleeving visible. Closure along inner rail maintained with no direct path for flame entry. Bottom impact limiter gap between bottom plate of base increased from ~5/8" to ~1.38" on bottom edge but remained at ~5/8" at top. Closure angles remained intact with no direct path for flame entry. Top impact limiter gap remained at 5/8".
3	4 ft	Horizontal lid down	Minor compression to top/bottom stiffeners in impact region of lid.
3	30 ft	Horizontal lid down	Outer (inboard) stiffeners were torn from package side. Outer (outboard) stiffeners were crushed. Lid deformed ½" along stiffeners. Lid deformed further in lifting area ~ 1.5". Six closure pins sheared but their bases remained in place.
1	40 in	20° Oblique puncture through CG on lid	Maximum puncture depth of 7" with moderator hold down strap visible. Longitudinal tearing of shell.

CTU No.	Drop Height	Test Designation/Description	Test Results
1	40 in	CG over base side closure joint puncture	Maximum puncture depth of 3 ½". Minor longitudinal tearing of shell.
3	A double plate was added to the lid and base of CTU 3 and the oblique puncture repeated. This added 150 lb to the existing package weight of 8,630 lb.		
3	40 in	20° Oblique puncture through CG on lid	Maximum puncture depth of 3.5". No longitudinal tearing of shell.
2	Closure pins were easily removed to facilitate internal inspections. The fuel assembly remained in very good condition with no rod movement or lattice expansion. The fuel assembly bottom end fitting bowed at its edge mid-span on all four sides by less than 1/16". There was no impact between the end fitting and pedestal gage used to monitor movement of the bottom end fitting. There were no bent rods, no visible rod cladding cracks and therefore no loose pellets. There was also no fuel assembly lattice expansion. The neoprene on the doors and strong-back was not damaged. The bottom span of the ballast collapsed which caused the support rods to expand beyond its fabricated envelope and impact and break two sections along the hinge of the bottom door.		
1	A single closure pin fell out during the normal testing. Nine closure pins had sheared shoulders as a result of the 30 ft drop. A tenth pin which was likely to have also sheared fell off during the puncture testing. Three closure pins were drilled out to permit lid removal. The lid was easily removed once two additional pins in the bottom section were further sheared during lid removal. The shoulders on these two pins were sheared off during the 30 ft test. The fuel assembly experienced lattice compression of ~0.4" at the mid-span with no compression or expansion at the assembly ends. Two grid sections at the assembly mid-span broke allowing one rod to move freely. Rod ends were randomly gapped from the bottom end fitting due to the slap down effect. A similar effect was observed at the top end fitting. There was no fuel assembly bottom end fitting bowing. There was no impact between the end fitting and pedestal gage used to monitor movement of the bottom end fitting. There were no bent rods, no visible rod cladding cracks and therefore no loose pellets. The neoprene on the doors and strong-back was not damaged. There were broken rivets on both the ballast and fuel assembly side along the fiberglass thermal barrier of the base. The ballast side was more severe than the fuel assembly side since the ballast was more rigid. There was a gap at the top portion of the fiberglass thermal barrier on the ballast side but multiple remaining rivets kept the bottom portion of the fiberglass and unit intact. The puncture depth on the package lid was excessive while the puncture depth on the package closure was limited. Due to more severe foam compression experienced with CTU 3 in the 30 ft drop test, the oblique puncture was repeated with CTU 3 however doubler plates were installed in the lid and base to limit the migration of the pin into the package. The penetration of the bar within CTU 1 would have been similar to CTU 3 as discussed below had the double plates been installed prior to testing of CTU 1.		

CTU No.	Drop Height	Test Designation/Description	Test Results
3	The outer (inboard) stiffeners were torn in local regions from the package side. The outer (outboard) stiffeners were crushed contiguous to the lid shell. The lid deformed ½" along the stiffeners. The lid further deformed in the lifting areas of the inboard stiffeners by ~ 1.5". Due to more severe foam compression with CTU 3 experienced in the 30 ft drop test, the oblique puncture was repeated with CTU 3 however doubler plates were installed in the lid and base to limit the migration of the pin into the package. The penetration of the bar within CTU 3 was still more severe than the impact along the package closure of CTU 1. CTU 3 was selected for the thermal test due to the more severe package crush and greater potential to challenge the moderator. The level of penetration of the bar within the lid of CTU 1 would have been reduced similar to that observed with CTU 3 had the doubler plates also been installed on CTU 1 prior to the test. As noted, six closure pins were removed prior to the burn test. The package was subjected to at least an 800 ^{o}C fire for at least 38 minutes. The package was further subjected to fire for 6-7 minutes as the remaining fuel burned. Off gas from the package continued to burn for approximately 1 hour. On cooling, foam char was observed in the blowout plugs and also surrounding the puncture. Ten closure pins were drilled out to permit lid removal that were most likely stuck due to thermal expansion of the package. The lid was easily removed. The fuel assembly experienced lattice compression of ~0.2" along the entire length. There was no lattice expansion. There was no impact between the end fitting and pedestal used to monitor movement of the bottom end fitting. There were no bent rods, no visible rod cladding cracks and therefore no loose pellets. The neoprene on the doors and strong-back was not damaged. Further disassembly of the lid and base was permitted using grinding wheels however some cutting torches were also used. The ceramic fiber paper was charred but remained in-place within the lid and base. The foam regions consisted primarily of foam char with some portions being unburnt. There was no melting of the moderator in the base of the package however some moderator melted in the local vicinity of the puncture. Moderator melting was observed in the peaks of two moderator blocks closest to the exterior of the package. The moderator in the lid was inspected with the worst case melted portion, based on visual examination, removed for further examination. Based on a mass comparison two moderator blocks that had melted the most, actually melting together, experienced a 6.6% weight loss based on the moderator minimum design requirements. No other weight losses were measured.		

Notes:

All NCT free drops are from 4 ft, HAC drops are from 30 ft, and all puncture drops are from 40 in. Distance is measured by the closest package point to the impact surface or object.

Packages subject to all NCT, HAC and Thermal testing were heated to approximately 100 ^{o}F prior to test, however due to unpredictable/uncontrolled ambient thermal gradient (convection and radiation effect) the package surface temperature varied somewhat. The high temperature was held for a minimum of 30 minutes with package being reinsulated between testing and prior to conduct of the thermal test.

2.12.1.4 Certification Tests

2.12.1.4.1 CTU 2

30 ft HAC Vertical Bottom End Drop

Pre Test

- Ambient temperature: 48 – 51 ^{o}F
- CTU foam temperature: 105 ^{o}F
- Time: 1115 hours, 02/12/2007
- Drop Height: 30 ft

The package was rigged, stabilized and lifted 30 ft by crane over the pad, Figure 2.12.1.-2.

The vertical package with bottom end down was dropped accurately on the steel pad.

Post Test

There was minor damage to the bottom end impact limiter as shown in Figure 2.12.1-3. Note that the package came to rest firmly on the test pad.

Figure 2.12.1-2 – CTU2 prior to drop

Figure 2.12.1-3 – CTU2 immediately after drop

CTU 2 Post Test Inspection

There was no lattice expansion within the fuel assembly or yielding of the bottom end fitting as shown in Figures 2.12.1-4 through 2.12.1-7. Based on observation and physical measurements,

there was no lattice expansion or compression of the fuel assembly. There were no bent or cracked rods (cladding) and no loose pellets (rods loaded with Tungsten Carbine pellets were used in the Fuel Assembly fabrication). There was also no significant deformation to either the bottom or top fuel assembly end fittings. The fuel cavity geometry was maintained. The fuel assembly did not shift outside of the original envelope placement on the strong-back nor did it axially shift outside of the flux trap region. No change in the geometric placement of the surrounding flux trap components of the package was observed. Based on these observations and physical measurements the HAC drop tests performed on CTU 2 had no impact on criticality or containment.

Figure 2.12.1-4 – Bottom end fitting

Figure 2.12.1-5 – Bottom view of end fitting

Figure 2.12.1-6 – Assembly mid-span

Figure 2.12.1-7 – Top end fitting

There was also no significant package internal damage as shown in Figures 2.12.1-8 and 2.12.1-9.

Figure 2.12.1-8 – Base interior after impact

Figure 2.12.1-9 – Side view of Base after impact

2.12.1.4.2 CTU 1

NCT 4 ft 10^{o} slap-down on base

Pre Test

- Ambient temperature: 48 ^{o}F
- Time: 1140 hours, 02/12/2007
- Drop Height: 4 ft

The package was rigged, stabilized and lifted 4 ft by crane over the pad, Figure 2.12.1-10.

The package oriented at a 10^{o} for the slap-down was dropped accurately on the steel pad.

Post Test

There was minor damage to the bottom end stiffener as shown in Figure 2.12.1-11.

Figure 2.12.1-10 – CTU1 prior to NCT test

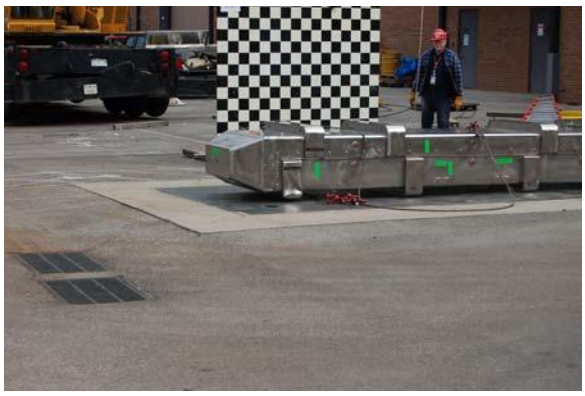

Figure 2.12.1-11 – CTU1 after impact

HAC 30 ft 30^{o} slap-down on base

Pre Test

- Ambient temperature: 48 ^{o}F
- Time: 1150 hours, 02/12/2007
- Drop Height: 30 ft

The package was rigged, stabilized and lifted 30 ft by crane over the pad, Figure 2.12.1-12.

The package oriented at a 30^{o} for the slap-down was dropped accurately on the steel pad.

Post Test

There was minor damage to the bottom end stiffener as shown in Figures 2.12.1-13 through 2.12.1-15. The close-up view in Figure 2.12.1-14 shows that five closure pins had sheared off on the ballast side of the package. On the opposite (fuel assembly) side, four bottom pins were further sheared off. Portions of the pins remained in place indicating that only the pin shoulders had sheared off. These views show that the closure is maintained. Remaining closure pins were removed to facilitate lid removal. However during lid removal, single pins on each side within the bottom end impact limiter prevented lid removal since they were still engaged. These two pins were further sheared during lid removal. Once sheared the lid was easily removed. Figure

2.12.1-15 shows an inverted package after the side puncture test. This view shows that the closure and interlocking angles remained intact. There was no significant compression of the body (e.g., foam) of the package.

Figure 2.12.1-12 – CTU1 prior to impact

Figure 2.12.1-13 – CTU1 after impact

Figure 2.12.1-14 – CTU1 close-up of impact end

Figure 2.12.1-15 – CTU1 inverted for puncture test

20° Oblique puncture through CG on lid

Pre Test

- Ambient temperature: 50 °F
- Time: 1450 hours, 02/12/2007
- Drop Height: 40 in

The package was rigged, stabilized and lifted 40 in by crane over the test bar, Figure 2.12.1-16.

The package with lid oriented down at a 20° oblique angle was dropped accurately on the puncture bar. The angle of the orientation is shown in Figure 2.12.1-17.

Post Test

The package came to rest on the puncture bar as shown in Figure 2.12.1-18. The puncture bar protruded into the package (as measured by the depth of the sheet metal shell) approximately 5.5" as shown in Figure 2.12.1-19. On closer inspection a hold-down strap for the moderator was visible which corresponded to a depth of approximately 7". Based on these observations, it appeared that the puncture bar entered the lid to a depth of approximately 7" and that the sheet metal shell retracted with foam expansion to a depth of 5.5". This same drop orientation was duplicated with CTU 3 using a doubler plate since the protrusion into CTU 1 was greater than desired for the subsequent thermal testing. The puncture did not compromise the fuel cavity and

had no effect on the fuel assembly envelope. The only concern being the survivability of the moderator in the thermal test.

Figure 2.12.1-16 – CTU1 prior to puncture

Figure 2.12.1-17 – Angle of CTU1

Figure 2.12.1-18 – CTU1 on impact

Figure 2.12.1-19 – CTU1 impact area

CG over base side closure joint puncture

Pre Test

- Ambient temperature: 50 ^{o}F
- Time: 1530 hours, 02/12/2007
- Drop Height: 40 in

The package was rigged, stabilized and lifted 40 in by crane over the test bar, Figure 2.12.1-20.

The package with side closure oriented down was dropped accurately on the puncture bar.

Post Test

The puncture bar protruded into the package 3 ½" as shown in Figure 2.12.1-21. The package impacted the puncture bar, bounced and impacted the puncture bar a second time prior to falling off the bar and landing lid down on the test pad. This impact did not compromise the package closure.

Figure 2.12.1-20 – CTU1 side puncture test

Figure 2.12.1-21 – CTU1 side puncture area

CTU 1 Post Test Inspection

The bottom barrel nut housing on the ballast side fractured however the second latch remained intact as shown in Figure 2.12.1-22. Figure 2.12.1-23 shows a portion of the rivets that failed along the fiberglass thermal barrier. This also shows that the barrier is maintained. Figure 2.12.1-24 shows the thermal barrier along the inner length on the fuel assembly as being intact. Figures 2.12.1-25 and 2.12.1-26 show the locking angles in the top closure that experienced minor bending but remained intact. These figures also show the weld failure on the top and the inner closure flange that connect to the fiberglass thermal barrier. Figures 2.12.1-27 and 2.12.1-28 show the locking angles in the bottom closure that experienced minor bending but remained intact. These figures also show the weld failure on the bottom end and the inner closure flange that connects to the thermal barrier. Figure 2.12.1-29 shows essentially no damage to the underlining of the lid and the closure angles of the lid bottom.

Figure 2.12.1-30 shows the rod movement at the bottom end fitting and further shows no lattice expansion or rod migration beyond the end fitting. Figure 2.12.1-31 indicates that the bottom end

fitting is intact and undamaged. Figure 2.12.1-32 shows the single rod that protruded from a damaged grid at the mid-span of the fuel assembly. Figure 2.12.1-33 further shows that the lattice was compressed at the mid-span by about 0.4". Figure 2.12.1-34 shows the corresponding rod movement at the upper end fitting and further shows no lattice expansion or rod migration beyond the end fitting.

There was no lattice expansion and only minor compression of the fuel assembly at the mid-span. There were no bent or cracked rods (cladding) and no loose pellets (rods loaded with Tungsten Carbine pellets were used in the Fuel Assembly fabrication). There was also no significant deformation or yielding to either the bottom or top fuel assembly end fittings. A single grid broke mid-span on the fuel assembly however this did not lead to bending or cracking of the fuel rod. The fuel cavity geometry was maintained. The fuel assembly did not shift outside of the original envelope placement on the strong-back nor did it axially shift outside of the flux trap region. No change in the geometric placement of the surrounding flux trap components of the package was observed. Based on these observations and physical measurements the HAC drop tests performed on CTU 1 had no impact on criticality or containment.

Figure 2.12.1-22 – Cracked barrel housing

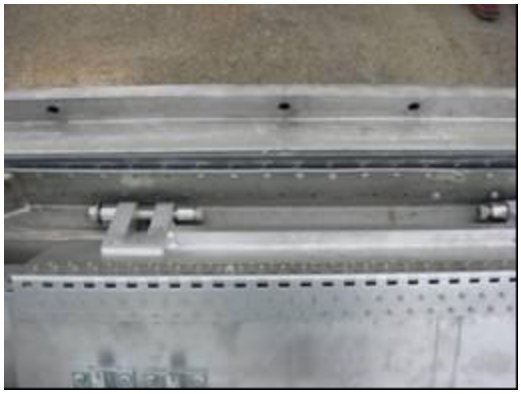

Figure 2.12.1-23 – Location of broken rivets

Figure 2.12.1-24 – No door damage

Figure 2.12.1-25 – Cracked top weld

Figure 2.12.1-26 – Cracked top weld

Figure 2.12.1-27 – Cracked bottom weld

Figure 2.12.1-28 – No damage to bottom closure

Figure 2.12.1-29 – No damage to lid interior

Figure 2.12.1-30 – Slight rod movement (bottom)

Figure 2.12.1-31 – Bottom end fitting

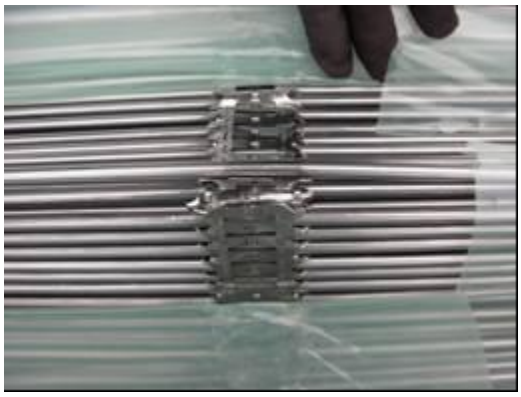

Figure 2.12.1-32 – Mid-span edge grid failure

Figure 2.12.1-33 – Mid-span lattice compression

Figure 2.12.1-34 - Slight rod movement (top)

2.12.1.4.3 CTU 3

NCT 4 ft Horizontal lid down

Pre Test

- Ambient temperature: 48 °F
- CTU foam temperature: 94 °F
- Time: 1330 hours, 02/12/2007
- Drop Height: 4 ft

The package was rigged, stabilized and lifted 4 ft by crane over the pad, Figure 2.12.1-35.

The horizontal package with lid down was dropped accurately on the steel pad.

Post Test

There was minor damage to the bottom end stiffener as shown in Figure 2.12.1-36.

Figure 2.12.1-35 – CTU3 prior to NCT test

Figure 2.12.1-36 – CTU3 after NCT test

HAC 30 ft Horizontal lid down

Pre Test

- Ambient temperature: 48 °F
- CTU foam temperature: 94 °F

- Time: 1400 hours, 02/12/2007
- Drop Height: 30 ft

The package was rigged, stabilized and lifted 30 ft by crane over the pad, Figure 2.12.1-37.

The horizontal package with lid down was dropped accurately on the steel pad, Figure 2.12.1-38.

Post Test

There was damage to the top end stiffeners as shown in Figures 2.12.1-39 through 2.12.1-40.

Figure 2.12.1-37 – CTU3 prior to HAC test

Figure 2.12.1-38 – CTU3 after impact

Figure 2.12.1-39 – CTU3 lid impact area

Figure 2.12.1-40 – CTU3 lid impact area

Figure 2.12.1-41 and Figure 2.12.1-42 show that the outboard stiffeners have buckled and that the inboard stiffeners have torn away from the side of the package. Figure 2.12.1-42 shows that the lid compression ranges from ½" to 1 ½" in the vicinity of the lid lifting brackets.

Figure 2.12.1-41 – CTU3 inverted

Figure 2.12.1-42 – CTU3 lid deformation measurement

20^{o} Oblique puncture through CG on lid

Pre Test

- Ambient temperature: 50 ^{o}F
- Time: 1625 hours, 02/12/2007
- Drop Height: 40 in

The package was rigged, stabilized and lifted 40 in by crane over the test bar, Figure 2.12.1-43.

This test is essentially identical to the test documented in Section 2.12.1.4.2 for CTU 1 however two (2) 12 GA doubler plates were added to the lid and base increasing the package weight by 150 lb. The plates were skip welded in place to prevent movement during the puncture test. The package with lid oriented down at a 20^{o} oblique angle was dropped accurately on the puncture bar as show in Figure 2.12.1-44.

Figure 2.12.1-43 – CTU3 prior to puncture test

Figure 2.12.1-44 – CTU3 on impact

Post Test

The puncture bar protruded into the package 3.5" as shown in Figures 2.12.1-45 and 2.12.1-46. The puncture depth for this test was the same as reported for the CG over side closure in Section 2.12.1.4.2 for CTU 1. Since the moderator in the lid is more susceptible to potential melting as opposed to the moderator in the base, CTU 3 was selected as the target for thermal testing.

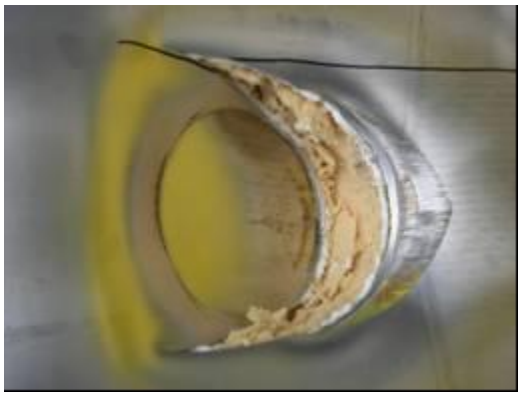

Figure 2.12.1-45 – CTU3 puncture area

Figure 2.12.1-46 – CTU3 puncture depth measurement

HAC 30 Minute Thermal Test

Pre Test

- Ambient temperature: 55 ^{o}F
- CTU foam temperature: 73 ^{o}F

- Time: 1829 hours, 02/15/2007
- Height above pad: 40 in

The package was rigged, stabilized and positioned 40 in above the pool, Figure 2.12.1-47, on an insulated test stand.

When the test article was mounted on the test stand, the distance between the sides of the test article and the inside walls of the weir varied between 39.5 inches (100 cm) and 45.25 inches (115 cm). The sides of the test article were between 71.5 inches (182 cm) and 77.25 inches (196 cm). The lowest corner of the package (stiffener) was approximately 39.9 inches (101 cm) above the normal waterline when the pool is filled to maximum capacity. The test article was mounted onto this stand with the top lid and bottom surfaces 14 degrees from vertical. This provided maximum exposure of the package penetration due to the puncture bar. The desired pre-heat foam and moderator temperature of 100 ^{o}F was not achieved prior to the thermal test due to a short in the heat tape. However, this was compensated for in an extended burn time. Figure 2.12.1-48 and Figure 2.12.1-49 show the location of the six (6) closure pins (three on each side) that were removed from the package prior to the test. This further simulated damage experienced with CTU 1 and allowed further fire ingress into the package. The shoulders of pins in these locations on CTU 1 had sheared, but the base of the pins remained in the package.

Figure 2.12.1-47 – CTU3 thermal test position

Figure 2.12.1-48 – CTU3 lock pin removal

Figure 2.12.1-49 – CTU3 lock pin removal opposite side

2.12.1.4.4 Thermal Test

The fuel in the pool was ignited at 1829 hours and full engulfment was achieved at approximately 1831 hours, however full engulfment of the central portion of the package was achieved after 1 minute. After ignition, fuel flow was maintained at an average rate of approximately 32 gallons per minute until 1858 hours. At this time, all fuel flow was stopped, and fuel valves and pumps were secured. The package remained engulfed until approximately 1909 hours. Between 1900 and 1915 hours, fire suppressant foam was added below the surface of the pool to extinguish the fire. The fire suppressant was introduced to the test setup approximately 31 minutes after the pool was ignited. The fire suppressant was introduced to the test setup via piping below the surface of the fuel pool. At no time did the fire suppressant make contact with any portion of the package or serve to cool the package, nor did the suppressant stop any combustion occurring in or on the package.

Full engulfment of the test article was achieved for approximately 38 minutes as shown in Figure 2.12.1-50. The thermal test involved: 2 minutes to achieve full engulfment, 38 minutes of full engulfment, and approximately 15 minutes until the pool burn was terminated.

Figure 2.12.1-50 – CTU3 fully engulfing fire

Post Test

Fire temperatures averaged above 800°C (1,472°F) with peak temperatures reaching 1,200°C (2,192°F). Within 30 seconds after the start of test, average shell temperatures measured at eight different locations exceeded 800°C (1,472°F). Peak shell temperatures also reached 1,200°C (2,192°F). Fire temperatures below the test article also averaged above 800°C (1,472°F).

CTU 3 Post Test Inspection (Exterior and Interior of Package)

The package was allowed to cool overnight prior to removal from the test pad for inspection. Figure 2.12.1-51 shows a foam char in the vicinity of the puncture. Figure 2.12.1-52 shows the up-righted package being prepared for opening. Ten (10) closure pins had to be drilled to facilitate lid removal. Figures 2.12.1-53 and 2.12.1-54 show typical foam char from the vent ports located in the stiffeners and package side, respectively. Figure 2.12.1-55 further shows foam char from one of the closure pin locations removed prior to the test. Figure 2.12.1-56 shows the lid removal for inspection of the doors, door hardware, package interior, fuel assembly, and ballast.

Figure 2.12.1-51 – Puncture area after thermal test

Figure 2.12.1-52 – Side view after removal from pad

Figure 2.12.1-53 – Vent at stiffener

Figure 2.12.1-54 – Vent on package side

Figure 2.12.1-55 – Foam char in lock pin area

Figure 2.12.1-56 – CTU3 lid removal

Figure 2.12.1-57 and Figure 2.12.1-58 shown that the doors and door hardware remain intact however rivets are visible on the inner closure flange. The fiberglass thermal barrier is coated with residue but is essentially intact with minor gaps along the top. Figure 2.12.1-59 and Figure

2.12.1-60 show that the fuel assembly and ballast are not significantly damaged. The fuel assembly compressed approximately 0.2" along the mid-span but remained intact at the end fittings. The neoprene on the strong-back and doors remained intact and in their fixed locations however the neoprene on the inner mid-span doors on the ballast side became detached during door opening indicating that the adhesive had deteriorated. Figure 2.12.1-61 shows that the fuel assembly polypropylene cover and paper fabrication route card remained intact. Figure 2.12.1-62 shows the pristine condition of the fuel assembly once the polypropylene cover is removed and further indicates no bent or broken rods and no rod movement.

There was no lattice expansion and only minor compression of the fuel assembly at the mid-span. There were no bent or cracked rods (cladding) and no loose pellets (rods loaded with Tungsten Carbine pellets were used in the Fuel Assembly fabrication). There was also no significant deformation or yielding to either the bottom or top fuel assembly end fittings. The fuel cavity geometry was maintained. The fuel assembly did not shift outside of the original envelope placement on the strong-back nor did it axially shift outside of the flux trap region. No change in the geometric placement of the surrounding flux trap components of the package was observed. Based on these observations and physical measurements the HAC drop and thermal tests performed on CTU 3 had no impact on criticality or containment.

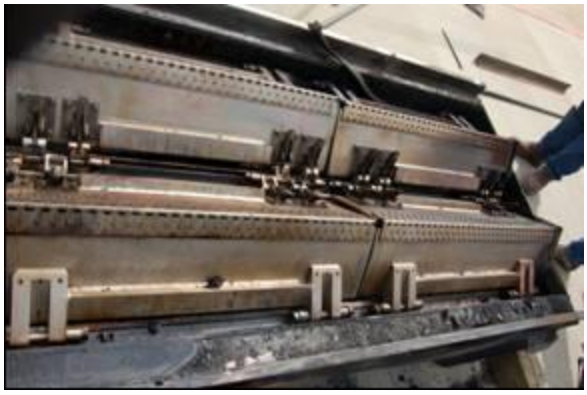

Figure 2.12.1-57 – CTU3 interior

Figure 2.12.1-58 – CTU3 interior

Figure 2.12.1-59 – CTU3 view of fuel assembly and ballast

Figure 2.12.1-60 – Neoprene adhesive degradation during thermal test

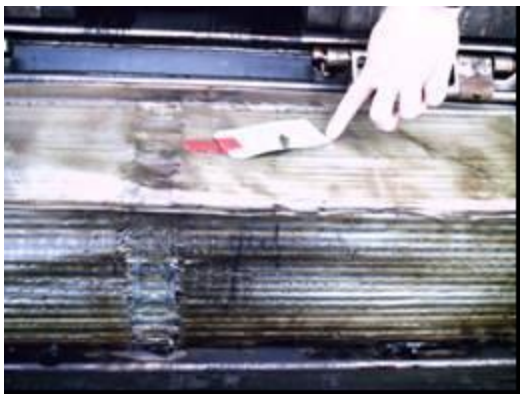

Figure 2.12.1-61 – Polypropylene liner and paper release tag intact

Figure 2.12.1-62 – Polypropylene sheet removal showing bright intact rods

With the internals of the package being characterized, the fuel assembly and ballast were removed and the package shells transported to the AREVA NP Inc, Lynchburg Mount Athos Road Fuel Fabrication Facility for further examination.

CTU 3 Post Test Inspection (Cut Away of Lid and Base)

The sheet metal shell of the lid was cut and removed between the stiffeners and also adjacent to the end impact limiters. Figure 2.12.1-63 shows the package mid-span while Figure 2.12.1-64 shows the section between the bottom stiffeners. These figures show that the ceramic fiber paper was not charred but saturated with condensed products from foam out-gassing. The paper remained in its relative position. Figure 2.12.1-65 and Figure 2.12.1-66 show the removal of the ceramic fiber paper and foam char. Figure 2.12.1-67 shows the emerging moderator to be in good condition. The moderator was covered by remaining un-burnt foam, foam char, and further saturated with condensed products from foam out-gassing. Figure 2.12.1-68 shows the worst case span (segment #5) of moderator in the lid that exhibited melting at the higher peak edges of the blocks. This section of moderator was removed for characterization. The Nylon 6,6 melting with subsequent material loss appeared to be very localized at the peaks of the blocks closest to the puncture location in the lid.

Figure 2.12.1-63 – Ceramic fiber paper middle

Figure 2.12.1-64 – Ceramic fiber paper end

Figure 2.12.1-65 – Foam Char

Figure 2.12.1-66 – Foam Char

Figure 2.12.1-67 – Appearance of Nylon 6,6

Figure 2.12.1-68 – Identification of Segment #5

Figure 2.12.1-69 shows the segment number assignments used in support of characterization of the Nylon 6,6 moderator blocks. Segment #1 is located at the forward of the package (fuel assembly

bottom) while segment #11 is located at the package aft (fuel assembly top). Figure 2.12.1-70 further shows the assignment of the moderator block locations in each segment. The moderator block numbering assignment is consistent with drawing 9045399. Table 2.12.1-4 provides the post burn test characterization of each moderator block specific to segment location and further by position within each segment. The post burn test condition is characterized based on a visual examination of each block while retained within the package. The blocks are characterized by no melt, slight melt, and melt. The moderator blocks are further shown in Figures 2.12.1-71 through 2.12.1-74.

The moderator blocks for segment #1 are not shown in the following figures however their condition is similar to the conditions for segment #11 as indicated in Figure 2.12.1-74. There were no visible signs of melting of the moderator blocks in segment #1 or segment #11. Figure 2.12.1-71 shows the moderator blocks for segments #2, #3, and #4. The Nylon 6,6 shows no visible signs of melting in either segment. Figure 2.12.1-72 shows the moderator blocks for segments #6, #7, and #8. The moderator blocks in segment #5 were removed for characterization and are discussed later in this section. The moderator blocks at locations B3/(7) and B4/(6) showed signs of slight melting at their respective peak edges in segments #6, #7, and #8. Figure 2.12.1-73 shows the moderator blocks for segments #9, #10, and #11. The moderator blocks at locations B3/(7) and B4/(6) also showed signs of slight melting at their respective peak edges in segments #9 and #10. The moderator blocks in segments #6 through #10 had slight melting at peak areas closest to the exterior lid however, in no case did there appear to be any loss of material.

Figure 2.12.1-74 identifies the condition of the moderator blocks within segment #5 prior to removal. The moderator block at location B4/(6) showed signs of melting at its respective peak edge, melting into and attaching to block B6/(5). The moderator block at location B3/(7) showed signs of slight melting at its respective peak edge. The moderator block at location B2/(8) showed signs of slight melting at its outer corners adjacent to the stiffeners along the outer closure. Only moderator block B4/(6) in segment #5 experienced melting with loss of material. The melting with loss of material appeared to be localized.

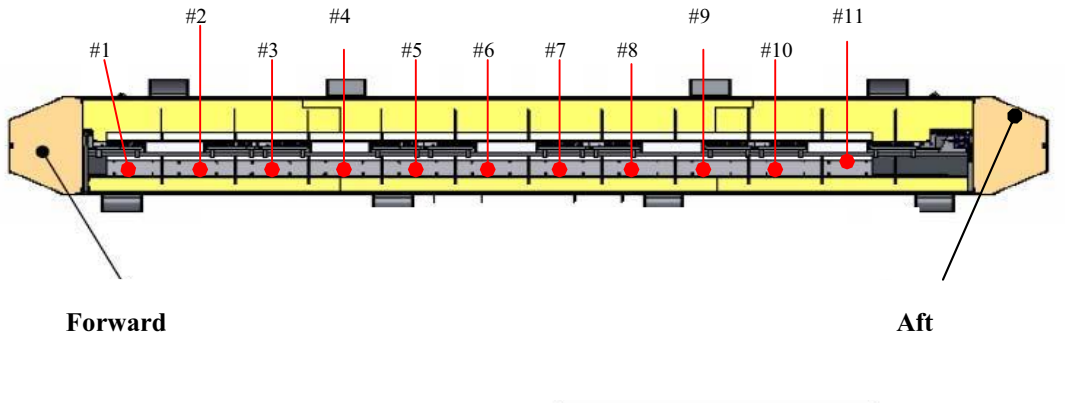

Figure 2.12.1-69 – Nylon 6,6 Segment Locations Designated from Forward to Aft of Package

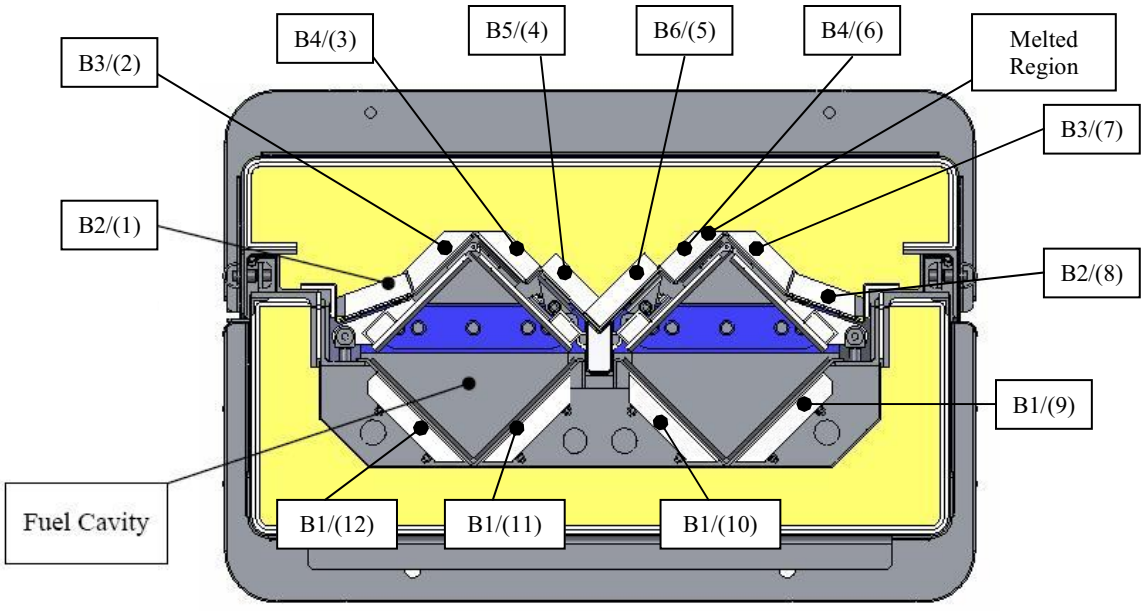

Figure 2.12.1-70 – Nylon 6,6 Moderator Block Nomenclature within each Segment Location (Block Type/Location as indicated in Drawing 9045399)

Table 2.12.1-4 – Post Burn Test Characterization of Moderator in Test Package CTU 3

Moderator Block No./ Label	Visual Observations of Nylon 6,6 from Forward (Segment #1) to Aft (Segment #11) of Test Package					
	Segment #1	**Segment #2**	**Segment #3**	**Segment #4**	**Segment #5**	**Segment #6**
B2/(1)	No Melt	No Melt	No Melt	No Melt	No Melt	No Melt
B3/(2)	No Melt	No Melt	No Melt	No Melt	No Melt	No Melt
B4/(3)	No Melt	No Melt	No Melt	No Melt	No Melt	No Melt
B5/(4)	No Melt	No Melt	No Melt	No Melt	No Melt	No Melt
B6/(5)	No Melt	No Melt	No Melt	No Melt	Slight Melt	No Melt
B4/(6)	No Melt	No Melt	No Melt	No Melt	Melted to B6(5)[1]	Slight Melt
B3/(7)	No Melt	No Melt	No Melt	No Melt	Slight Melt	Slight Melt
B2/(8)	No Melt	No Melt	No Melt	No Melt	No Melt	No Melt
B1/(9)	No Melt	No Melt	No Melt	No Melt	No Melt	No Melt
B1/(10)	No Melt	No Melt	No Melt	No Melt	No Melt	No Melt
B1/(11)	No Melt	No Melt	No Melt	No Melt	No Melt	No Melt
B1/(12)	No Melt	No Melt	No Melt	No Melt	No Melt	No Melt
	Segment #7	**Segment #8**	**Segment #9**	**Segment #10**	**Segment #11**	
B2/(1)	No Melt	No Melt	No Melt	No Melt	No Melt	
B3/(2)	No Melt	No Melt	No Melt	No Melt	No Melt	
B4/(3)	No Melt	No Melt	No Melt	No Melt	No Melt	
B5/(4)	No Melt	No Melt	No Melt	No Melt	No Melt	
B6/(5)	No Melt	No Melt	No Melt	No Melt	No Melt	
B4/(6)	Slight Melt	Slight Melt	Slight Melt	Slight Melt	No Melt	
B3/(7)	Slight Melt	Slight Melt	Slight Melt	Slight Melt	No Melt	
B2/(8)	No Melt	No Melt	No Melt	No Melt	No Melt	
B1/(9)	No Melt	No Melt	No Melt	No Melt	No Melt	
B1/(10)	No Melt	No Melt	No Melt	No Melt	No Melt	
B1/(11)	No Melt	No Melt	No Melt	No Melt	No Melt	
B1/(12)	No Melt	No Melt	No Melt	No Melt	No Melt	

[1] Nylon 6,6 block B4/(6) in Segment #5 was the only block experiencing melting that appeared to have lost material.

Figure 2.12.1-71 – Nylon 6,6 Segments #2, #3, and #4. Foam char is still visible on segment #3.

Figure 2.12.1-72 – Nylon 6,6 Segments #6, #7, and #8. Foam char visible on all segments.

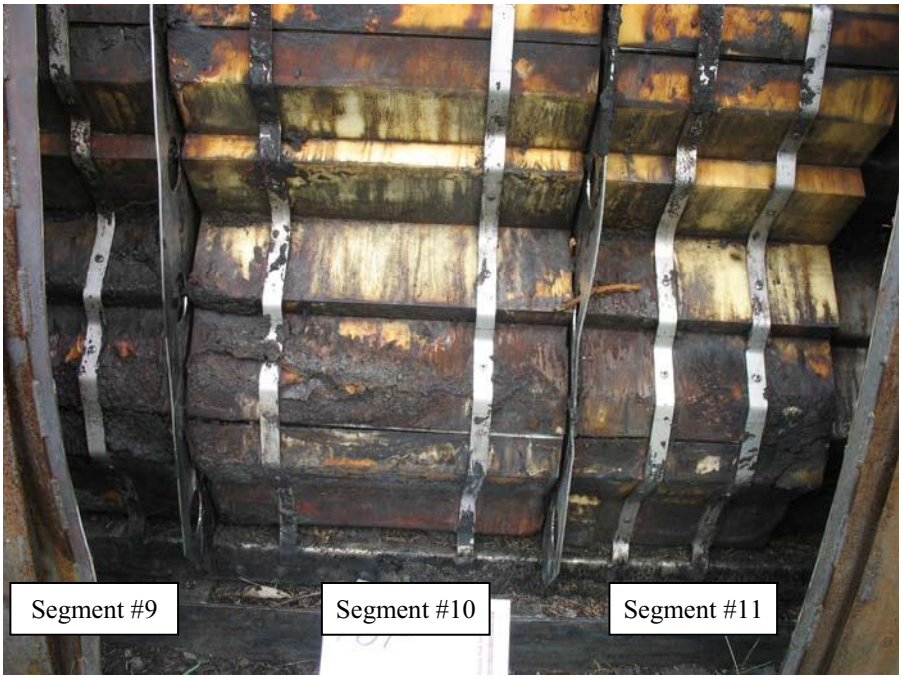

Figure 2.12.1-73 – Nylon 6,6 Segments #9, #10, and #11. Foam char visible on bottom sections of each segment.

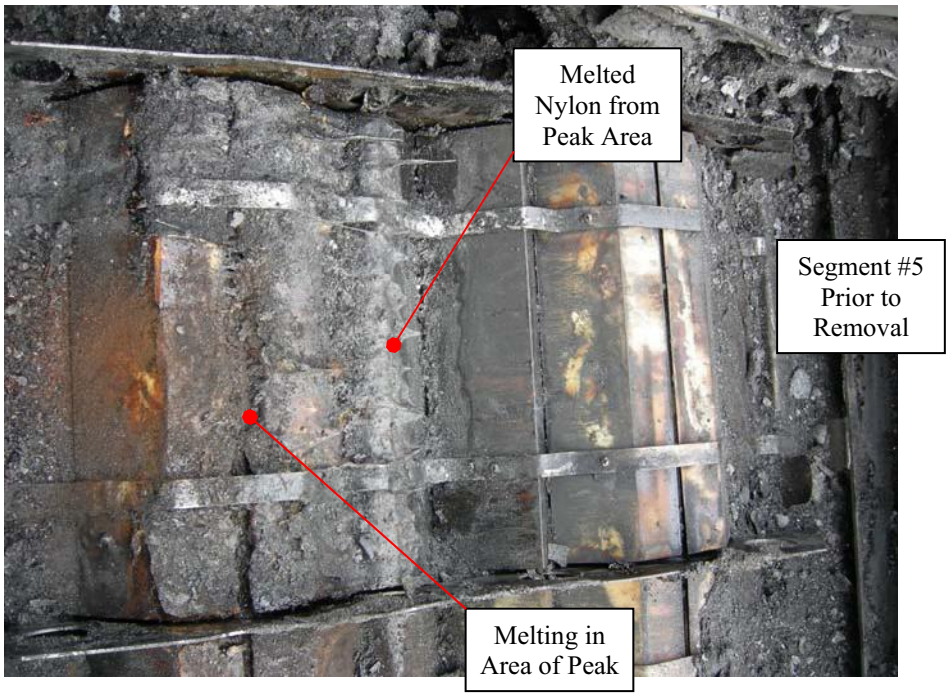

Figure 2.12.1-74 – Nylon 6,6 Segment #5. Melted blocks shown at left with similar non-melted section at right.

Figure 2.12.1-75 shows the section of moderator removed that by visual examination exhibited the most melting. The moderator blocks above the ballast in the peak of the lid exhibited the most

melting with one melting into a second block as shown in Figure 2.12.1-76. The blocks in Figure 2.12.1-75 from left to right (see Figure 2.12.1-70) are B2/(1), B3/(2), B4/(3), B5/(4), B6/(5), B4/(6), B3/(7), B2/(8), respectively. Blocks B6/(5) and B4/(6) are further shown in Figure 2.12.1-76. Block B4/(6) appears to have melted into B6/(5) in segment #5. The melted peak edge on B4(6) is also shown, with jagged edge, in Figure 2.12.1-75.

Figure 2.12.1-75 – Segment #5 after cleaning

Figure 2.12.1-76 – Segment #5 melted piece

The top surface of the moderator was coated with condensed products from the out-gassing of the polyurethane foam. Minor scrapping on the surface of the moderator removed the tar to reveal the white nylon as installed in the package, Figure 2.12.1-76, center of the picture. The moderator was pressure washed to remove foam char and residue which further removed a minor amount on Nylon. The pretest measured mass[2] (block thicknesses ranging from 1.27 to 1.28-inches) and the design required minimum mass (based on a moderator minimum thickness of 1.25-inches) of the two items that bonded together as a result of the test was 6.95 lb and 6.80 lb, respectively. The post test mass was 6.35 lb. By weight characterization the two items lost 8.6% of their pretest mass or 6.6% based on the design minimum required mass. The credited 85% moderator mass (Table 6-7) as specified in the criticality assessment was 5.68 lb. The post test mass of blocks B6/(5) and B4/(6) in segment #5 remained above the 85% modeled mass in the criticality assessment. The average loss of Nylon 6,6 in the lid is much less than 6.6% since only two blocks

[2] The installed Nylon 6,6 mass exceeded the minimum design mass by about 2.2%.

appeared to have a reduce mass due to melting as a result of the thermal test. Averaging the weight loss in segment #5 with the other ten lid segments results is a weight loss of less than 2.1%.

Moderator loss was anticipated but expected to be minimal with the use of a high temperature thermoplastic material. Nylon 6,6 was specifically selected for this application due to its high temperature resistance and self-extinguishing characteristics. Table 2.12.1-5 summarizes the results of these measurements. Figure 2.12.1-70 identifies the location of the moderator blocks with respect to the package. The neutron absorber plates (positioned beneath the moderator blocks) did not experience any deformation or melting

Table 2.12.1-5 – Post Burn Test Characterization of Moderator in Segment #5 (See Figure 2.12.1-70)

Block No./ Label	Pre Test Mass, lb		Minimum Design Mass, lb		Post Test Mass, lb	Moderator Loss, Percent[3]	85%[4] Design Mass, lb		Visual Observations
B2/(1)	3.25		3.18		3.25	0.0	2.70		No Melt
B3/(2)	3.35		3.28		3.35	0.0	2.79		No Melt
B4/(3)	2.90		2.84		2.90	0.0	2.41		No Melt
B5/(4)	3.00		2.93		3.00	0.0	2.49		No Melt
B6/(5)	4.05	6.95	3.96	6.80	6.35	6.6	3.37	5.68	Slight Melt
B4/(6)	2.90		2.84				2.41		Melted to B6/(5)
B3/(7)	3.35		3.28		3.35	0.0	2.79		Slight Melt
B2/(8)	3.25		3.18		3.25	0.0	2.70		No Melt
B1/(9)	5.05		4.94		5.05	0.0	4.45		No Melt
B1/(10)	5.05		4.94		5.05	0.0	4.45		No Melt
B1/(11)	5.05		4.94		5.05	0.0	4.45		No Melt
B1/(12)	5.05		4.94		5.05	0.0	4.45		No Melt
Total	46.25		45.23		45.70	6.6	39.44		
Average Moderator Weight Loss in Segment #5 (Lid)						**2.1 % (Based on Pre Test Mass)**			
Average Moderator Weight Loss in Segment #5 (Lid/Base)						**1.2 % (Based on Pre Test Mass)**			
Average Moderator Weight Loss in Package						**< 0.1 % (Based on Pre Test Mass)**			

[3] Loss based on the minimum design mass.

[4] The criticality assessment in Section 6 credited 85% of the lid and 90% of the base Nylon 6,6. Mass values reported for the base are 90% of the minimum design mass.

The sheet metal shell of the base was also cut and removed between the stiffeners and also adjacent to the end impact limiters. Figure 2.12.1-77 shows the package mid-span while Figure 2.12.1-78 shows the ceramic fiber paper and foam char being removed to expose the inner cover beneath the strong-back. Figure 2.12.1-79 shows the emerging moderator along the outside of the package to be in good condition while Figure 2.12.1-80 shows the emerging moderator along the outside opposite end of the package to also be in good condition. This was typical of the moderator along the full length of the base of the package which exhibited no melting. Figure 2.12.1-81 shows the base moderator in the package aft, Figure 2.12.1-82 shows the base moderator in the center of the package, and Figure 2.12.1-83 shows the moderator in the package forward. Also shown in Figure 2.12.1-81 is a section of moderator that was cleaned to remove condensed off-gases from foam combustion to reveal the white Nylon 6,6. The neutron absorber plates (positioned beneath the moderator blocks) also did not experience any deformation or melting.

Table 2.12.1-4 summarizes the moderator block inspections in the base of the package. Table 2.12.1-5 summarizes the base package moderator block inspections for segment #5. The average loss of Nylon 6,6 due to the thermal test was less than 1.2% based on the pretest mass of the moderator in the lid and base for segment #5. The post test mass of 45.70 lb for segment #5 remained above the minimum design mass of 45.23 lb (minimum 1.25-inch moderator thickness) and significantly above the 39.44 lb mass (85% lid and 90% base) credited in the criticality assessment. The average moderator loss within the package is about ~ 0.1% when considering all eleven Nylon 6,6 segments in the lid and base.

Figure 2.12.1-77 – Ceramic fiber paper in Base

Figure 2.12.1-78 – Base liner with foam char removed

Figure 2.12.1-79 – Base edge Nylon 6,6

Figure 2.12.1-80 – Base edge Nylon 6,6, opposite end

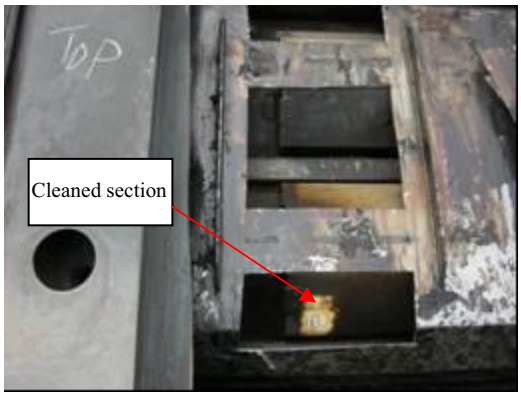

Figure 2.12.1-81 – Nylon 6,6 at top (aft)

Figure 2.12.1-82 –Nylon 6,6 at center

Figure 2.12.1-83 – Base Nylon 6,6 at bottom (forward)

2.12.1.5 Tests Final Results

Upon completion of the Certification Tests, based on the severity of the damage it was determined that CTU 3 was the most damaged package (with doubler plate) in terms of the following thermal

event. Therefore, CTU 3 was sent for thermal testing since its configuration appeared to be most challenging for potential melting and ignition of the credited neutron moderator (Nylon 6,6). The condition of CTU 3 was worsened by the removal of six (6) closure pins in the bottom of the package allowing flame ingress to the interior of the package during the thermal test.

CTU 1 and 2 were opened with CTU 1 requiring drilling to remove three closure pins. The lids were easily removed to view the internals of the package. Based on observation and physical measurements, there was no lattice expansion of the fuel assemblies in either package. Also, there were no loose pellets (Rods loaded with Tungsten Carbine pellets were used in the Fuel Assembly fabrication) and no bent or cracked rods. There was also no significant deformation to either the bottom or top fuel assembly end fittings. There was also no significant damage to the interior of either package including the neoprene supports for the assembly.

CTU 3 was thermally tested exceeding the 30 minute – 1,475 ^{o}F (800 ^{o}C) fully engulfing fire in both duration and temperature. The amount of un-burnt foam remaining within the package shell was minimal however this still did not lead to significant melting of the neutron (nylon) moderator or absorber. The worst case melting (weight loss) was determined to be less than 6.6% for two moderator blocks, with an average weight loss per segment of less than 1.2%. The average weight loss within the package is anticipated to be about 0.1% when considering that only two blocks in a single segment had a reduced mass on inspection after completion of the thermal test. The package criticality analysis modeled the moderator at greater than 10% reduction in both the Lid and Base. The analyzed configuration exceeds the observed damage and is therefore conservatively modeled.

Ten closure pins required drilling to allow removal of the Lid on CTU 3. These were most likely stuck due to thermal expansion and warping of the package. The lid was easily removed to view the internals of the package. Based on observation and physical measurements, there was no lattice expansion of the fuel assembly. The exterior of the rods, being covered by a thin polypropylene sheet, remained in their as fabricated bright condition. The HAC fire test had no further effect on the cladding. Also, there were no loose pellets (rods loaded with Tungsten Carbine pellets were used in the Fuel Assembly fabrication) and no bent or cracked rods. There was also no significant deformation to either the bottom or top fuel assembly end fittings. There

was also no significant damage to the interior of the package including the neoprene supports for the assembly.

A visual inspection of the fuel rods in the CTUs did not identify any bent or damage rods. The test assemblies were removed from the CTUs and further inspected, and no cracked or breached rods were visually identified. A random sample of rods were removed from the most damaged assembly (CTU 1) and checked for pressurization. All were found to be pressurized. Therefore, no leakage or breach of the rods occurred as a result of the performance tests.

Visual inspection of the fuel rod cladding after the drop and thermal test performed for the MAP package demonstrated that the containment boundary (fuel rod cladding) remained intact and leak-free during all normal and hypothetical accident conditions. The immersion tests further specified in 10 CFR 71 (c)(5) for fissile and (6) for all packages, require immersion equivalent to an external water pressure of 21.7 lb/in^2, however intact and leak-free rods can tolerate much higher pressures and remain internally dry. As a result, the immersion tests were not performed. From these results it is also feasible to model the fuel rod fuel-cladding gap as moderator free. However, for conservatism the gap can be modeled under flooded conditions in the criticality assessment.

2.12.1.6 Certification Test Unit Description

This section describes the certification test units and simulated payload used for the normal conditions of transport (NCT) and hypothetical accident condition (HAC) tests performed in accordance with 10 CFR §71.

2.12.1.6.1 Certification Test Units

Certification tests of the MAP packaging utilized full-scale CTUs that were fabricated, inspected, and received in accordance with quality procedures.

Through the design and fabrication process, a single design was proposed and three (3) certification test units were fabricated in accordance with an NRC approved quality assurance program. The drawings presented in Appendix 1.3.1, *Packaging Drawings*, fully represent the design of these CTUs.

Additional weight was added to each CTU both internally and externally to increase the weight and provide margins for fabrication. The gross package test weight of each CTU was 8,630 lb.

Stainless steel double plates were added to the lid and base of CTU 3 prior to the lid oblique puncture test. This added 150 lb to the unit. It was clear from the three (3) 30 foot drop tests that the package integrity was not challenged, and the small additional weight (1.7%) from the doubler plates would not alter these results. The production packages will require doubler plate installation. This increases the gross package weight to 8,780 lb. Sufficient weight margin exists in the gross package tested weight of 8,630 lb such that the increased weight of the double plates does not need to be included during the initial package approval. However, this margin may need to be licensed at a later date to facilitate shipment of all fuel assembly designs in the MAP-13 package.

2.12.1.6.2 Simulated Payload

Each CTU was loaded with a dummy fuel assembly and a ballast weight. The fuel assembly design selected for testing was chosen due to its weaker structure, thinnest rod and cladding wall thickness of all current AREVA NP Inc. designs. Certification testing of the package with a fuel assembly with the above traits is likely to lead to more fuel assembly damage in all drop test orientations considered. The weaker structure is likely to lead to more assembly lattice expansion and more rod movement during the drop tests increasing the potential for rod bending and subsequent failure. The thinner rod and cladding wall thickness is also likely to increase the potential for rod bending and subsequent failure.

Each rod was loaded with Tungsten Carbide (WC) pellets with dimensions and density similar to current uranium oxide fabricated pellets. Two different rods were loaded for testing; 1) Rods with a 24” WC section in the bottom of the rod followed by 10-12” sections of lead rod followed by a WC pellet cap producing a 144” nominal length material zone, and 2) Rods loaded entirely with WC pellets producing a 144” nominal length material zone. In prior drop tests, rod bending was observed in the bottom section of the assembly generally between the end fitting and the first grid. The 24” WC section will provide ample coverage for rod bending within this region. However, rods loaded entirely with WC pellets will identify any performance differences. Based on the tests

documented in Section 2.12.1.4, there appeared to be no observable performance differences between either rods design.

All rods were pressurized with Helium gas to the maximum design pressure for the tested assembly type, 225 +0/-15 psig. Following the 10 CFR 71 HAC performance tests, no leakage was observed. Thus, the post-test leakage rate is the same as the pre-test leakage rate (on the order of 1E-7 ref-cc/s) and the expected leakage rate is much less that the allowable post-HAC leakage rate (2.25E+3 ref-cc/s assuming aerosol leakage) as calculated in Section 4. Thus, there is significant margin to the allowable leakage rate.

The use of WC pellets as a non-fuel replacement for uranium oxide pellets in axially oriented drop tests will conservatively envelope the dynamic response of uranium pellets. WC is harder, stronger in compressive strength and has a higher elastic modulus as compared to uranium oxide pellets. In a pure axial rod drop test these properties would make the use of WC produce at least equivalent and probably greater impact loads than uranium oxide pellets. The WC pellets used in rod fabrication do not have dished or chamfered ends as compared to uranium pellets such that movement of the WC pellet within the rod is more likely to engage the cladding and lead to more damage due to its sharper edges. In an axial drop test, the major parameter to reproduce is the mass in the clad. Mass per unit length is probably a second-order effect. In this case, WC is an appropriate replacement for uranium pellets. Should there be any lateral forces induced into the drop test, then pellet diameter, length, and mass per unit length need to be duplicated so that the cladding support, and hence the fuel rod lateral dynamics, will be reproduced. The higher density, higher modulus and higher compressive strength will cause more clad damage than uranium pellets. This will increase the conservatism of the test.

The weight of each dummy fuel assembly was increased by loading of lead in the guide and instrument tubes. This additional weight increases the likelihood of damage to the fuel assembly in either lateral or axial drop orientations. The lead did not increase the stiffness of the fuel assembly. A ballast weight consisting of stacked 1.5” steel plates and 5/8” steel threaded rod was used to simulate a second assembly and also add additional weight to the package. The fuel assembly and ballast weights were shimmed within the package fuel cavity. The total weight of fuel assembly and ballast was 3,400 lb as loaded into each CTU for package certification testing.

Table of Contents **Page**

List of Figures **Page**

List of Tables **Page**

3.0 THERMAL EVALUATION

This chapter identifies and describes the principal thermal design aspects of the MAP Series of PWR Fuel Shipping Packages (MAP Package). Further, this chapter presents the evaluations that demonstrate the thermal safety of the MAP Package and compliance with the thermal requirements of 10 CFR 71.

Specifically, all package components are shown to remain within their respective temperature limits under the normal conditions of transport (NCT). Further, per 10 CFR §71.43(g), the maximum accessible package surface temperature is demonstrated to be less than 122 °F (50 °C) for the maximum decay heat loading, an ambient temperature of 100 °F (38 °C), and no insolation. Finally, the MAP Package is shown to retain sufficient thermal protection following the HAC drop scenarios to maintain all package component temperatures within their respective short term limits during the regulatory fire event and subsequent package cool-down.

3.1 Description of Thermal Design

The MAP Packaging, illustrated in Figures 1-1 through 1-7 from Section 1.0, *General Information*, consists of two basic components: a Base and a Lid. There are two configurations of the MAP: the MAP-12 and the MAP-13. The MAP-12 is capable of handling assemblies with 144-in nominal active fuel lengths and has a gross weight of 8,630 pounds (3,909 kg), a tare weight of approximately 5,200 pounds (2,364 kg), and approximate outer dimensions of 208" long x 45" wide x 31" high. The MAP-13 configuration is capable of handling assemblies with 150-in nominal active fuel lengths and has the same gross weight as the MAP-12 configuration, and is approximately 221" long x 45" wide x 31" high. The gross weight for MAP-13 package remains the same as the shorter MAP-12 package since the fuel to be transported is lighter. Both package configurations have the same thermal design features.

A detailed description of the package components is provided in Section 1.2, *Packaging Description*, and on the drawings in Appendix 1.3.1, *Package Drawings*.

3.1.1 Design Features

The primary heat transfer mechanisms within the MAP packaging are conduction and radiation, while the principal heat transfer from the exterior of the packaging is via convection and radiation to the ambient environment.

The Base and Lid serve as the primary impact and thermal protection. The design of the Base and Lid are similar in that each consist of a stainless steel outer shell, a layer of rigid polyurethane foam, and an inner stainless steel shell. The stainless steel provides structural strength and a protective covering for the foam. A typical cross-section showing key elements of the package is depicted in Figure 1-2 and Figure 1-3. Figure 1-2 is a cross sectional view of the package at the inner stiffeners of the Base and Lid. Figure 1-3 presents a similar cross sectional view of the package, but at the location of the moderator and absorber interface within the Base and Lid.

The polyurethane foam in the Base is sandwiched between the stainless steel cover and the exterior shell of the Base and provides the principal thermal protection for the Fuel Cavity during the HAC fire event. Section, 3.5.3, *'Last-A-Foam' Response under HAC Condition*, describes the prototypic performance of the polyurethane foam under elevated temperatures and the mechanisms through which it achieves its thermal protection. Unlike the Base, the polyurethane foam in the Lid assembly extends down to the backside surface of the neutron moderator with no sheet metal separation or void space. A double layer of ceramic fiber paper insulation is used between the exterior shell of the Base and Lid and the polyurethane foam. Thermal tests (see Section 3.5.3) and experience with other package designs have shown that the use of ceramic fiber paper significantly improves the performance of the polyurethane foam under HAC conditions.

The strong-back is secured to the outer shell of the Base via angle irons that form a stepped, inter-locking joint with the Lid. This design feature creates a labyrinth-like pathway to the package interior and in combination with the braided fibrous high temperature sleeving at the Lid-Base package closure ensures that the hot gases generated during the HAC fire event cannot easily enter the interior cavity of the package. Additional thermal protection is provided by the use of a fiberglass thermal barrier (see Figure 1-4) that eliminates the continuous metallic pathway that would otherwise exist between the exterior shell of the Base and the strong-back assembly.

Impact limiters at each end of the Lid assembly consist of 10 pcf polyurethane foam encased in 11 gauge Type 304 stainless steel. The inner plate of the impact limiters are fitted with L-channels that engage similar L-channels in the Base assembly and lock the impact limiters to the Base of the package. The inter-locking nature of the L-channels restricts the inflow of hot gases generated by the HAC fire. Figure 1-7 illustrates the interlocking engagement of the Base with the end impact limiters of the Lid.

The neutron moderator and the absorber materials are mounted along the length of the Base and Lid W-plates. The neutron moderator material is the most thermally limiting component and is protected from HAC fire conditions by the polyurethane foam, ceramic fiber paper and other design features limiting fire ingress.

3.1.2 Content's Decay Heat

The decay heat loading associated with the fresh, unirradiated low enriched PWR fuel assemblies to be carried within the MAP Package is negligible.

3.1.3 Summary of Temperatures

Table 3-1 provides a summary of the package component temperatures under NCT and HAC. The temperatures for normal conditions are based on an analytical model of the MAP Package for extended operation with an ambient temperature of 100°F and a diurnal cycle for the insolation loading. The temperatures for accident conditions are based on a fire test conducted using a full-scale certification test unit (CTU).

The results for NCT conditions demonstrate that significant thermal margin exists for all package components. This is to be expected since the only thermal loads on the package arise from insolation and ambient temperature changes. Further, the evaluations for NCT demonstrate that the package skin temperature will be within the maximum temperature of 122°F permitted by 10 CFR §71.43(g) for accessible surface temperature in an nonexclusive use shipment when transported in a 100°F environment with no insolation.

The results for HAC also demonstrate that the design of the MAP Package provides sufficient thermal protection to yield component temperatures that are significantly below the acceptable

limits defined for each component. Although a small section of the moderator surface in the Lid was noted to have experienced incidental melting during the fire test, this involved only 2.1% of the moderator material in the worst affected Lid segment. This level of moderator loss is significantly below the acceptable limit established in Chapter 6. There was no moderator melting for the majority of the blocks neither in the Lid nor anywhere in the Base; thus reducing the affected moderator material within the entire package to less than 0.1%. These results are seen as conservative given the fact the CTU test article was subjected to an extended exposure to the HAC environment that exceeded the regulatory requirement in both temperature level and duration (see Section 3.4.3.1, *Maximum HAC Temperatures*, for further discussion).

3.1.4 Summary of Maximum Pressures

Both the maximum normal operating pressure (MNOP) and the maximum pressure developed under the HAC condition are 0 psig. The maximum pressure developed in the fuel rods is 506 psig and 654 psig for NCT and HAC, respectively, assuming a worst case initial rod pressurization of 450 psig. As demonstrated in Chapter 4, *Containment*, these pressure levels do not present a safety issue for this application.

Table 3-1 - Maximum Package Temperatures under NCT and HAC Conditions

Location / Component	NCT	HAC[1]	Maximum Allowable[2]	
			Normal	Accident
Fuel Assembly	131°F	< 300°F	752°F	1,058°F
Polypropylene Wrap (on Fuel Assembly)	131°F	< 300°F [3]	225°F	300°F
Neoprene Rubber (Fuel Cavity)	130°F	< 300°F [3]	225°F	500°F
Fuel Cavity Doors	130°F	< 300°F [3]	400°F	1,100°F
Borated Metal Matrix Composite (MMC) Neutron Absorber	133°F	< 300°F	850°F	1,000°F
Thermoplastic Neutron Moderator	135°F	< 500°F [4]	500°F	500°F
Polyurethane Foam, Body - Maximum - Average	 201°F 148°F [6]	 n/a [5] n/a [5]	 500°F 150°F	 n/a n/a
Polyurethane Foam, Impact Limiter - Maximum - Average	 206°F 141°F [6]	 n/a [5] n/a [5]	 500°F 150°F	 n/a n/a
Fiberglass Thermal Breaks	138°F	< 500°F [7]	250°F	2,900°F
Exterior Shell	210°F	2,192°F	800°F	2,700°F

Table Notes:

1) Except for the exterior sheet, all other listed accident temperatures are estimates based on visual observations of the material condition following the fire test (see Section 3.4.3.1, *Maximum HAC Temperatures*, for further discussion).

2) Maximum allowable temperatures are defined in Section 3.2.2, *Technical Specifications of Components*.

3) Estimated component temperature for accident conditions are listed for information only. Component not required for the package safety.

4) The peak moderator temperature of approximately 500°F (indicated by incidental melting) was noted for approximately 2.1% of the moderator material at the worst affected segment and only about 0.1% of the total moderator material. This level of melting is well within acceptable limits (see Section 3.4.3.1, *Maximum HAC Temperatures*, for further discussion).

5) The polyurethane foam is designed to be consumed during the accident fire event to provide thermal protection to the underlying components. Therefore, temperatures achieved during the fire event are not applicable to the safety evaluation of the package.

6) The average temperature of the polyurethane foam used only to set the structural properties for the drop analyses.

7) Estimate based on observed condition of the fiberglass showing structural members intact with slight surface charring.

3.2 Material Properties and Component Specifications

3.2.1 Material Properties

The thermal material properties for the MAP components are provided in Tables 3-2 through 3-6. The MAP packaging is fabricated primarily of Type 304 stainless steel, 6061-T6 aluminum, polyurethane foam, ceramic fiber paper, and thermoplastic moderator. Lesser amounts of Type A564, Gr 630 and XM-19 stainless steel, structural fiberglass, borated metal matrix composite (MMC), neoprene synthetic rubber, and braided fibrous sleeving are also used in the fabrication of the package.

The payload materials include Type 304 stainless steel, zirconium alloy, Ni-Cr-Fe alloy, uranium dioxide pellets, and polypropylene plastic used as a protective sleeving over the fuel assemblies.

Table 3-2 presents the thermal properties for the Type 304 stainless steel, 6061-T6 aluminum, and borated MMC. Properties between the tabulated values are calculated via linear interpolation within the heat transfer code. Thermal properties for the Type A564, Gr 630 and XM-19 stainless steels are assumed to be the same as Type 304 stainless for NCT. The thermal performance under accident conditions is determined via test and not analytical methods.

The borated MMC neutron absorber material is fabricated as a hot-rolled composite sheet consisting of a core of uniformly distributed boron carbide and aluminum particles enclosed between layers of pure aluminum. Because the material is a composite of two different materials, borated MMC will exhibit a different thermal conductivity for heat being conducted through the material vs. heat being conducted along the material. However, since the presence of the borated MMC material is not critical to the thermal performance of the MAP Package, its thermal properties are simplified to a single, non-temperature dependant value for conductivity and specific heat. The thermal data listed in Table 3-2 is based on the specification for the material.

The thermal properties for the structural fiberglass reinforced plastic (FRP), polyurethane foam, moderator, and neoprene synthetic rubber are assumed to be constant with temperature. The values assumed for the NCT evaluation are presented in Table 3-3.

The polyurethane foam used in the package is based on a proprietary formulation and its thermal properties under NCT conditions are obtained from the manufacturer's on-line website.

The ceramic fiber paper insulation used in the MAP Package is a lightweight refractory material processed from high purity alumina silica fibers that are washed and spun into a highly flexible sheet. The material is easy to cut, wrap or form, offers low thermal conductivity, low heat storage and high heat reflectance, and the material is resilient with excellent compression recovery. The thermal properties are presented in Table 3-3.

The heat transfer within the Fuel Assemblies is a combination of conduction and radiation heat transfer within and between the individual fuel rods. A detailed model of the fuel geometry is not required for the purposes of this evaluation. Instead, the fuel assemblies and the surrounding air space between the edges of the assembly and the internal surfaces of the Fuel Cavity are represented as homogenous solid region with anisotropic thermal properties. The thermal properties are based on a detailed model of typical fuel assembly geometry (see Appendix 3.5.2.1, *Description of Thermal Model for NCT Conditions*). The model accounts for conduction and radiation heat transfer between the individual fuel rods and across the space between the assembly edges and the Fuel Cavity surfaces. The results of the detailed modeling are used to compute an 'effective thermal conductivity' for the radial and the axial directions. Table 3-4 presents the effective, anisotropic thermal properties for the homogenized fuel region.

The thermal properties for air are presented in Table 3-5. Because the thermal conductivity of air varies significantly with temperature, the computer model calculates the thermal conductivity across air spaces as a function of the mean film temperature. All void spaces within the MAP Package are conservatively assumed filled with air at atmospheric pressure.

Table 3-6 presents the emissivity (ε) for each radiating surface and the solar absorptivity (α) value for the exterior surface. The solar absorptivity value is applied by multiplying the incident insolation on the package surfaces by the Table 3-6 value to yield the amount of solar energy actually absorbed by the package[1]. The polyurethane foam, ceramic fiber paper, and the moderating material have an assumed emissivity of approximately 0.90 based on a combination of the material type and

[1] NUREG-1609, "Standard Review Plan for Transportation Packages for Radioactive Material", Spent Fuel Project Office, US NRC, Washington, DC 20555, March 2000. ¶3.5.2.1 states that the thermal absorptivities and emissivities are to be appropriate for the package surface conditions.

surface roughness.

3.2.2 Technical Specifications of Components

Table 3-1 lists the maximum allowable operating temperatures for the MAP package. The materials used in the MAP Package that are considered temperature sensitive are the neutron moderator, the borated metal matrix composite (MMC) absorber plates, the neoprene synthetic rubber, and the polypropylene wrap used as a protective sleeving around the fuel assemblies. Of these materials, only the neutron moderator and absorber materials are considered critical to the safety of the package. The other materials either have temperature limits above the maximum expected temperatures or are not considered essential to the function of the package.

Type 304 stainless steel exhibits only small thermal property variations within the expected normal operating temperature range to be experienced by the MAP Package. Its melting point is above 2,700°F. In compliance with the ASME B&PV Code[2], the maximum allowable temperature of stainless steel used for structural purposes is limited to 800°F. However, the ASME allowable temperature limit applies only to thermal loading conditions where the material's structural properties are relied on for loads postulated to occur in the respective operating mode or load combination (such as the NCT and HAC free drops). Since the containment boundary for the package is the cladding on the fuel assemblies and the package is vented to atmosphere, the appropriate upper temperature limit is 800°F for normal conditions and 2,700°F for accident conditions. The same temperature limits apply for the Type 564 and XM-19 stainless steel components.

Aluminum 6061-T6 has a melting point of approximately 1,100°F; however for strength purposes the normal operational temperature should be limited to 400°F[2]. The temperature limit for the structural fiberglass reinforced plastic (FRP) used for thermal breaks in the package is a combination of the maximum temperature for the glass fibers (2,900°F) and the maximum

[2] American Society of Mechanical Engineers (ASME) Boiler & Pressure Vessel Code, Section III, *Rules for Construction of Nuclear Facility Components*, Division 1, Subsection NB, *Class 1 Components*, & Subsection NG, *Core Support Structures*, 2001 Edition, 2002 Addendum.

temperature for the resin used to bind the fibers (250 to 300°F)[3]. To maintain structural strength under normal conditions, a maximum temperature of 250°F is assumed for the resin temperature within the fiberglass thermal breaks. Under HAC conditions, the resin can be allowed to burn out and the thermal break will still serve its purpose, thus the maximum temperature for HAC is 2,900°F.

The thermoplastic moderator material (i.e., Nylon 6,6) is self-extinguishing, and has a melting point of 490 to 510ºF. Material testing conducted for this application showed that the material has a flash ignition temperature of approximately 752ºF[4]. Although the presence of moderator is required for the safety of the design, a portion of it may be lost due to melting or burning without creating a safety concern. Chapter 6 defines the acceptable limits. The borated MMC neutron absorber material has a recommended temperature limit of 850ºF for continuous operation and 1,000ºF for non-continuous operation[5].

The ceramic fiber paper insulation[6] has a melting point of 3,200°F and recommended continuous use temperature limit of 2,300°F.

Section 3.5.3, *'Last-A-Foam' Response under HAC Condition*, describes the behavior of the rigid polyurethane foam as a function of temperature. Based on this information, a peak NCT temperature limit of approximately 500°F is used to avoid non-reversible changes in the thermal properties. No temperature limit exists under HAC conditions since the thermal decomposition of the foam material plays a significant role in the level of thermal protection the material provides to underlying foam material and components. A design limit of 150°F is imposed for the NCT bulk average foam temperature to establish a lower bound on the foam's structural properties which decrease with increased temperature level.

---

[3] *Fiberglass Reinforced Plastic (FRP) Piping Systems Designing Process/Facilities Piping Systems With FRP: A Comparison To Traditional Metallic Materials*, Specialty Plastics, Inc., Baton Rouge, LA, May 29, 1998

[4] MSDS Sheet for Nylon 101, Quadrant EPP, 2120 Fairmont Avenue, P.O. Box 14235, Reading, PA.

[5] Based on similar specifications contained in AAR Product Sheet, *Standard Specification for Boral Composite Sheet*, AAR Advanced Structures.

[6] Based on Grade 1530-L and 1535-L LyTherm® insulation, Lydall Industrial Thermal Solutions, Inc.

The polypropylene plastic wrap used as a protective sleeve around the fuel assemblies has a melting temperature of approximately 273 to 329°F[7]. For the purposes of this analysis, a limit of 300°F is assumed for accident conditions, while a service temperature limit of 225°F is used for NCT conditions. Loss of the plastic wrap is of no consequence to the safety of the MAP Package since its effect on conductive and radiative heat transfer is negligible. Similarly, the neoprene used to provide cushioning between the Fuel Assemblies and the strong-back is not required for the safety of the package. The neoprene material will undergo thermal decomposition when raised above its recommended service temperature of approximately 250°F[8]. This decomposition begins with the neoprene becoming hard and brittle before charring and outgassing. The allowable temperature for the neoprene under accident conditions is in excess of 500°F for exposures of 30 minutes or less[9]. Given that the neoprene is attached to the strong-back structure using an adhesive with a recommended service temperature of 225°F [10], the allowable NCT temperature for neoprene is set at 225°F.

The materials used in the fabrication of the Fuel Assemblies are chemically stable materials with excellent heat resistance. These materials have a minimum temperature rating of 752°F under NCT conditions and 1,058°F under HAC conditions[11].

The minimum allowable service temperature for all MAP components is below -40 °F.

---

[7] Generic polypropylene, film grade, obtained from online material database, http://www.matweb.com.

[8] DuPont Performance Elastomers LLC, Wilmington, DE 19809.

[9] Parker O Ring Handbook, ORD 5700/USA, 2001, www.parker.com.

[10] Scotch-Grip™ 1300L adhesive, 3M Industrial Adhesives and Tapes Division, St. Paul, MN.

[11] Interim Staff Guidance #11, Rev. 3, "Cladding Considerations for the Transportation and Storage of Spent Fuel", Spent Fuel Project Office, US NRC, Washington D.C., 2003.

Table 3-2 – Thermal Properties of Metallic Materials

Material	Temperature (°F)	Thermal Conductivity (Btu/hr-ft-°F)	Specific Heat (Btu/lb_m-°F)	Density (lb_m/in^3)
Stainless Steel[1] Type 304	-40[4]	8.23	0.112	0.289[5]
	70	8.60	0.114	
	100	8.70	0.115	
	150	9.00	0.117	
	200	9.30	0.119	
	250	9.60	0.122	
	300	9.80	0.123	
Aluminum[2] Type 6061, T6	-40[4]	93.2	0.208	0.0975[5]
	70	96.1	0.214	
	100	96.9	0.216	
	150	98.0	0.220	
	200	99.0	0.222	
	250	99.8	0.224	
	300	100.6	0.227	
Borated MMC[3]	---	65.0	0.220	0.0938

Notes:

1) American Society of Mechanical Engineers (ASME) Boiler and Pressure Vessel Code, Section II, *Materials*, *Part D – Properties*, Table TCD, Material Group K, 2001 Edition, 2002 and 2003 Addenda, New York.

2) American Society of Mechanical Engineers (ASME) Boiler and Pressure Vessel Code, Section II, *Materials*, *Part D – Properties*, Table TCD, 2001 Edition, 2002 and 2003 Addenda, New York.

3) Conservative values for the borated metal matrix composite (MMC) are based on *Standard Specification for Boral Composite Sheet*, AAR Advanced Structures.

4) ASME table values were extrapolated to provide data for this temperature condition.

5) http://www.matweb.com

Table 3-3 – Thermal Properties of Non-Metallic Materials

Material	Temperature (°F)	Thermal Conductivity (Btu/hr-ft-°F)	Specific Heat (Btu/lb_m-°F)	Density (lb_m/in^3)	Comments
Structural Fiberglass[1]	---	0.33	0.28	0.065	
Thermoplastic Neutron Moderator[2]	---	0.14	0.41	0.041	
Neoprene[3]	---	0.23	0.52	0.0443	
Polyurethane foam[4,6]	---	0.025 0.025	0.353 0.353	0.00347 0.00579	6 lb/ft^3 10 lb/ft^3
Ceramic Fiber Paper[5]	-40	0.036	0.194	0.00434	Density may range from 6 to 9 lb/ft^3
	500	0.036			
	800	0.048			
	1,300	0.072			
	1,600	0.084			
	2,000	0.132			

Notes:

1) "Typical Properties – FRP Structural Shapes", Enduro Systems, Inc., www.endurocomposites.com.

2) Quadrant Engineering Plastic Products, Material Data Sheets, www.matweb.com..

3) *Polymer Data Handbook*, Oxford University Press, Inc., 1999.

4) Last-A-Foam™ FR3710 On-line Data Sheet, www.generalplastics.com.

5) Based on Grade 1530-L and 1535-L LyTherm® paper insulation, Lydall Industrial Thermal Solutions, Inc.

6) Table values have been modified to reflect the revised foam specification consistent with Section 8. However, the thermal evaluation uses thermal conductivity values of 0.0170 and 0.0183 for 6 and 10 lb/ft^3, respectively. The impact on the results is considered to be negligible.

Table 3-4 - Effective Thermal Properties for Homogenized Fuel Region

Material	Temperature (°F)	Thermal Conductivity (Btu/hr-ft-°F)[1]		Specific Heat (Btu/lb_m-°F)	Density (lb_m/in^3)
		Axial	Radial		
Homogenized FA Region	46	0.255	--	0.0638	0.124
	80	0.254	--		
	260	0.225	--		
	-20	--	0.0278		
	50	--	0.0323		
	150	--	0.0385		
	275	--	0.0468		

Notes: 1) See Appendix 3.5.2.1, *Description of Thermal Model*, for NCT condition basis of table values

Table 3-5 – Thermal Properties of Air

Temperature (°F)	Density (lb_m/in^3)	Specific Heat (Btu/lb_m-°F)	Dynamic Viscosity (lb_m /ft-hr)	Thermal Conductivity (Btu/hr-ft-°F)	Prandtl No.	Coef. Of Thermal Exp. ($°R^{-1}$)
-40	Use Ideal Gas Law w/ Molecular wt = 28.966 g/mole	0.240	0.0367	0.0121	Compute as $Pr = c_p\mu / k$	Compute as $\beta = 1/(°F+459.67)$
0		0.240	0.0395	0.0131		
50		0.240	0.0429	0.0143		
100		0.241	0.0461	0.0155		
200		0.242	0.0521	0.0178		
300		0.243	0.0576	0.0199		
400		0.245	0.0629	0.0220		

Notes: Based on Rohsenow, Hartnett, and Cho, *Handbook of Heat Transfer*, 3rd edition, McGraw-Hill Publishers, 1998, curve fit equations on pp 2.4

Table 3-6 – Thermal Radiative Properties

Material	Assumed Conditions	Assumed Emissivity (ε)	Absorptivity (α)
Outer Sheet, Exterior Surface (Type 304 Stainless Steel)	Weathered	0.45[2]	0.52[3]
Outer Sheet, Interior Surface and Interior Sheets (Type 304 Stainless Steel)	'As- Received'	0.25[1]	---
Polyurethane Foam, Moderator, & Neoprene	---	0.90[3]	---
Strongback Doors (Type 6061-T6 Aluminum)	Un-oxidized	0.15[4]	---
Polypropylene Plastic Wrap	Not included in Model	Transmittance = 0.75	---
Ambient Environment	---	1.00	N/A

Notes:

1) Frank, R. C., and W. L. Plagemann, *Emissivity Testing of Metal Specimens.* Boeing Analytical Engineering coordination sheet No. 2-3623-2-RF-C86-349, August 21, 1986. Testing accomplished in support of the TRUPACT-II design program.
2) *"Emissivity Measurements of 304 Stainless Steel*", Azzazy, M., prepared for Southern California Edison, September 6, 2000, Transnuclear File No. SCE-01.0100.
3) G. G. Gubareff, J. E. Janssen, and R. H. Torborg, *Thermal Radiation Properties Survey*, 2nd Edition, Honeywell Research Center, 1960.
4) Assumed based on standard aluminum properties.

3.3 Thermal Evaluation for Normal Conditions of Transport

This section presents the thermal evaluation of the MAP Package for normal conditions of transport (NCT). Under NCT, the package is assumed to be mounted horizontally on its transport trailer. This establishes the orientation of the exterior surfaces of the package for determining the free convection heat transfer coefficients and insolation loading. While the package would normally be transported in tiered stacks consisting of 3 packages each, the evaluation for NCT assumes a single package since this will bound the maximum and minimum temperatures achieved within any of the packages. Further, the surface of the transport trailer is conservatively assumed to prevent heat exchange between the package and the ambient. Thus, the bottom of the MAP Package is conservatively treated as an adiabatic surface.

The thermal loading on the MAP Package during NCT arises only from insolation on the outer skin of the package since the decay heat of the payload is essentially zero. The thermal conditions that are considered for NCT are those specified in 10 CFR §71.71(c)(1). Accordingly, an ambient temperature of 100°F with the regulatory insolation (i.e., the NCT Hot condition) is used for heat input to the exterior package surfaces. The combination of the foam and the relatively thin exterior skin of the package results in the peak surface temperatures of the package responding rapidly to changes in the external environment, while the interior of the package response change is significantly slower. Since the regulatory insolation represents the total insolation over a 12-hour period, the modeling for NCT converted the insolation values to a diurnal cycle to permit a transient modeling of the insolation loading. Insolation loading based on a diurnal cycle captures the peak component temperatures near the exterior of the package in a more accurate manner[1] as opposed to that obtained using an average insolation loading.

The details of the thermal modeling used to simulate the MAP Package under NCT conditions, together with the insolation loading based on a diurnal cycle, are provided in Appendix 3.5.2, *Analytical Thermal Model*.

[1] Per IAEA Safety Guide TS-G-1.1, ¶654.4, a time dependant sinusoidal heat flux is the more precise way to model insolation.

3.3.1 Heat and Cold

3.3.1.1 Maximum Temperatures

The maximum temperature distribution for the NCT Hot condition specified by 10 CFR §71.71(c)(1) of 100°F with the regulatory insolation is determined using a transient evaluation and a diurnal cycle for the insolation loading[2]. Figure 3-1 illustrates the expected heat-up transient for the MAP Package calculated using the model described in Appendix 3.5.2, *Analytical Thermal Model*, while Figure 3-2 presents an enlarged view at the end of the evaluated heat up period. As seen from the figures, more than 10 days of insolation are required to reach the maximum temperatures under the NCT Hot conditions. The noted change in the component temperatures over the last 24 hours of the evaluated heat up period (see Figure 3-2) is 0.5°F, or less, thus indicating that steady-state conditions are essentially attained. Table 3-1 presents the maximum temperatures reached for various components of the package. All are within in their respective temperature limits. Figure 3-3 illustrates the predicted temperature distribution within the body of the package at selected time points.

The maximum temperature distribution for the MAP Package without insolation loads occurs with an ambient air temperature of 100°F. Since the package payload dissipates essentially zero watts of decay heat, the thermal analysis of this condition represents a trivial case and no thermal calculations are performed. Instead, it is assumed that all package components achieve the 100°F temperature under steady-state conditions. The resulting 100°F package skin temperature is within the maximum temperature of 122°F permitted by 10 CFR §71.43(g) for accessible surface temperature in a non-exclusive use shipment.

3.3.1.2 Minimum Temperatures

The minimum temperature distribution for the MAP Package occurs with a zero decay heat load and an ambient air temperature of -40°F per 10 CFR §71.71(c)(2). Since the thermal analysis of this condition represents a trivial case, no thermal calculations are performed. Instead, it is assumed that all package components achieve the -40°F temperature under steady-state conditions. As discussed

[2] See Section 3.5.2, *Analytical Thermal Model*, for details of the thermal modeling and a comparison of the results obtained by steady-state and transient modeling of the insolation loading for this application.

in Section 3.2.2, *Technical Specifications of Components*, the -40°F temperature is within the allowable operating temperature range for all MAP Package components.

3.3.2 Maximum Normal Operating Pressure

The maximum normal operating pressure (MNOP) for the package is 0 psig. The containment boundary for the package is defined as the fuel rod cladding. The peak fuel rod cladding temperature of 131°F is reached under extended operations in the NCT Hot environment (i.e., an ambient air temperature of 100°F and a diurnal cycle on insolation).

Given that each fuel rod is internally pressurized with helium to a pressure ranging from 145 to 450 psig, depending on assembly design (see Table 1-3), and assuming a 68°F rod temperature at the time of filling, the maximum internal rod pressure that will occur under NCT conditions is determined using the ideal gas law as follows:

$$\text{Max. rod pressure} = \text{initial fill pressure, psia} \times \left[\frac{\text{absolute rod temp. at NCT}}{\text{absolute rod temp. at fill}} \right]$$

$$\text{Max. rod pressure} = (450 \text{ psig} + 14.7) \times \left[\frac{131^{\circ}\text{F} + 459.67^{\circ}\text{R}}{68^{\circ}\text{F} + 459.67^{\circ}\text{R}} \right]$$

$$\text{Max. rod pressure} = 520.2 \text{ psia} = 506 \text{ psig}$$

The acceptability of this pressure rise of 56 psig from the initial fill condition is provided in Chapter 4, *Containment*.

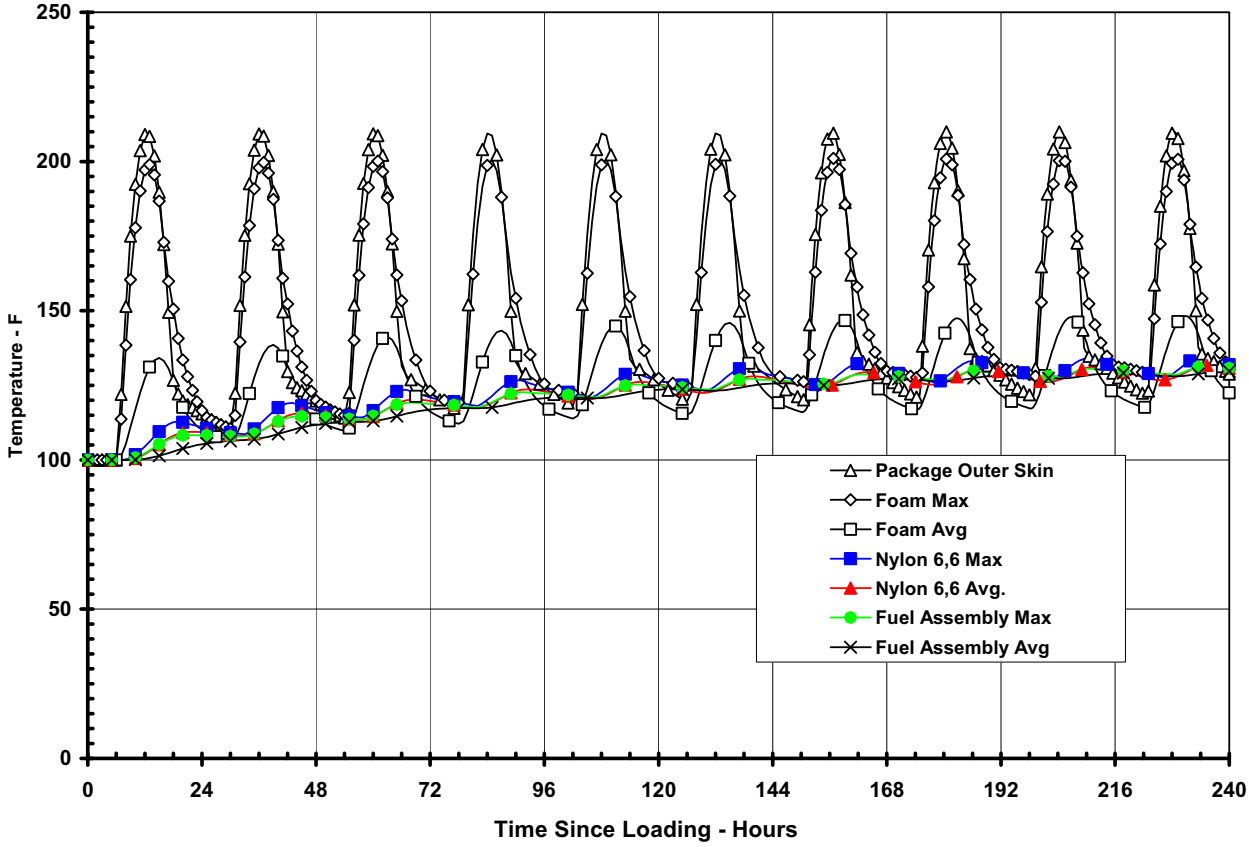

Figure 3-1 - Heat-up of MAP Package under NCT Hot Conditions with Insolation

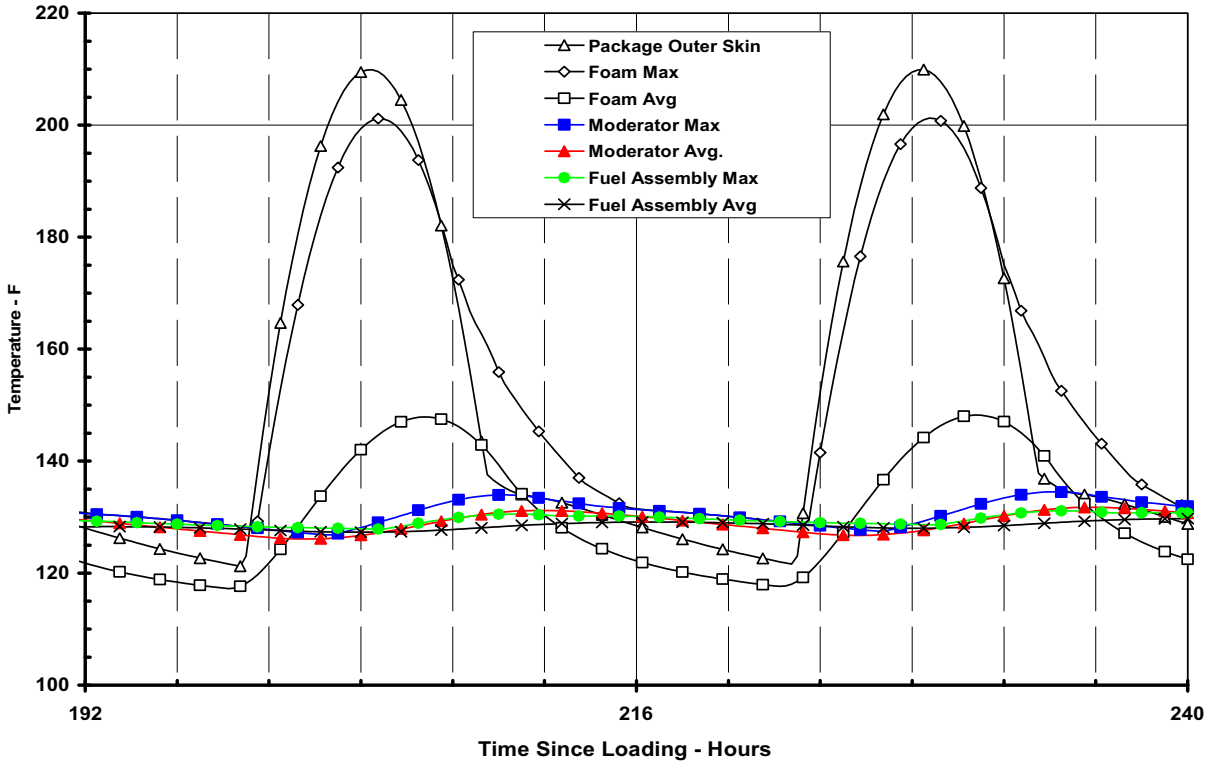

Figure 3-2 - Heat-up of MAP Package under NCT Hot Conditions with Insolation (Enlarged View)

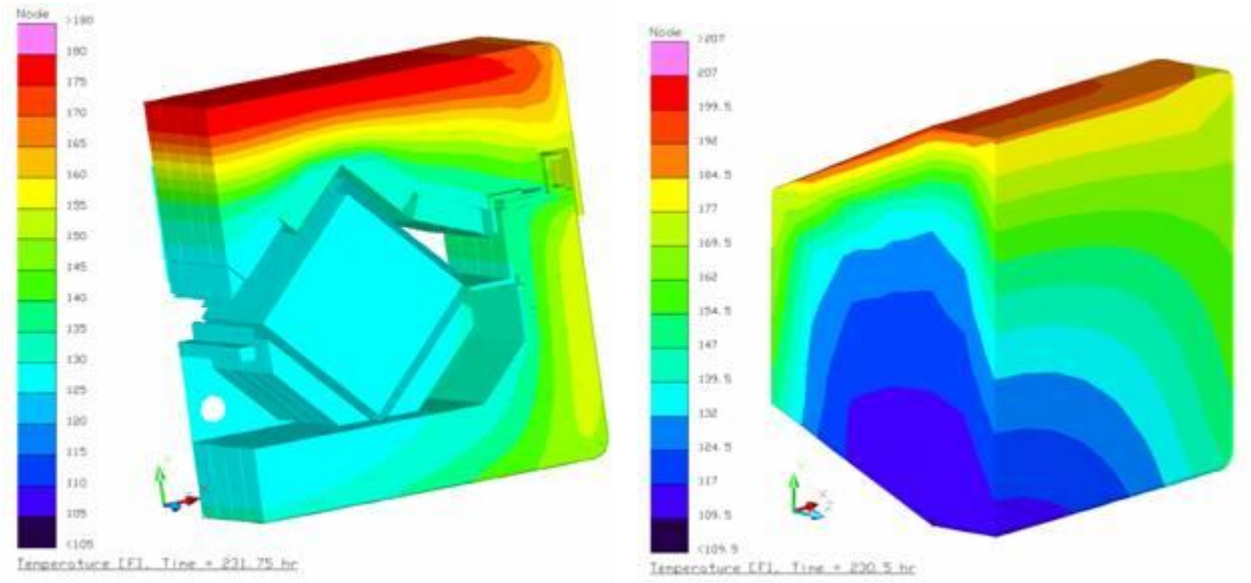

Package @ Time of Peak Fuel Assembly Temperature **Impact Limiter @ Time of Peak Avg. Foam Temperature**

Figure 3-3 - Package Temperature Distributions

3.4 Thermal Evaluation for Hypothetical Accident Conditions

This section presents the thermal evaluation of the MAP Package under the hypothetical accident condition (HAC) specified in 10 CFR §71.73(c)(4). The evaluation is based on a burn test using a full-scale, certification test unit (CTU). The CTU was fabricated to the same specifications as a production MAP Package with the exception of a few thermally insignificant components. For example, 1100 aluminum was substituted for the borated MMC neutron absorber plates. The CTU was loaded with one dummy fuel assembly fabricated to the same specifications as an actual fuel assembly with the exception that the fuel pellets were simulated with Tungsten Carbide Pellets and lead rod. The other position in the Fuel Cavity was occupied by a ballast unit that weighed the same as an actual fuel assembly.

No analytical modeling for the hypothetical accident condition was conducted for this evaluation.

3.4.1 Initial Conditions

Three CTUs were subjected to the free and puncture drop tests specified in 10 CFR §71.71 and 10 CFR §71.73. Different package orientations were used for each CTU. The specific drop orientations tested were selected from a suite of credible drop orientations based on the potential to develop the greatest package damage. Section 2.12.1, *MAP Shipping Package Certification Tests*, presents a summary of the tested orientations and the observed damage noted on each CTU. Evaluations of the damaged CTUs showed that the 'horizontal lid down' orientation with subsequent 20º oblique puncture through the package CG on the lid (i.e., CTU 3) produced the most severe damage to the thermal protection features of the package. Specifically, the observed damage on CTU 3 encompassed the entire length of the package's Lid assembly, whereas the damage noted for CTUs 1 and 2 produced more localized damage, with the area of greatest damage occurring away from the thermally sensitive neutron moderator material. However, to address the loss of closure pins observed during the drop testing on CTU 1, six closure pins (three on each side) were removed from the bottom end of CTU 3 to simulate a similar damage condition (see Section 2.12.1).

Prior to the fire test, CTU 3 was insulated and heated to achieve a mean package temperature of 100ºF, which represents the pre-test package temperature in the most unfavorable ambient condition, as specified in 10 CFR §71.73(c)(4). The 100ºF target package temperature was not achieved due to a combination of ambient temperatures that averaged 55ºF, the need to remove the insulation for extended periods of time to rig the CTU above the test pool, and a short in the heating system. Instead, the average package skin temperature prior to the fire was measured at 73ºF. Although the package began the fire test at less than the desired 100ºF, the impact on the maximum temperatures achieved during the fire was offset by the extended burn time (see below) that more than compensated for the lower starting temperature.

The initial internal package heat load and pressure were identical between test article and the actual MAP Package. Since the MAP payload will consist of fresh fuel assemblies, the zero internal heat load of the CTU essentially matches the internal heat load for a production MAP Package. Likewise, since the MAP Package is not sealed, the internal pressure of the CTU prior to testing was atmospheric.

The fuel rod pressure used for the prototype fuel assembly is the highest batch fuel pressure specified for the AREVA fuel assembly design tested.

3.4.2 Fire Test Conditions

The fire test was performed using one of the test pools at the South Carolina Fire Academy (SCFA) in Columbia, SC. The selected test pool (see Figure 3-4) has inside dimension of 24 by 50 feet and walls that are approximately 24 inches high and 8 inches thick. The facility was modified to perform the regulatory burn test on the MAP CTU by adding a water cooled weir (see Figure 3-5) that limited the burn pool area to approximately 10 by 25 feet. A kerosene-like hydrocarbon fuel was distributed to the burn pool area by two separate fuel lines located below the water level. The fuel distribution system was designed to provide uniform fuel distribution across the surface of the pool. Steel baffles were mounted onto the weir immediately above the water surface and below the bottom of the test article to help control flame direction and minimize the impact of winds on the flame distribution around the test article. The structure also incorporated a steel diffuser around the perimeter. The diffuser increased the effective surface dimensions of the

fire to 14 by 30 feet. The top of the diffuser was approximately 6 feet above the top of the pool surface. The diffuser was also designed to reduce the impact of wind on flame engulfment of the test article.

Water and fuel lines from central pumping stations provided water to fill the pool and to cool support equipment used in the fire test while fuel lines provided liquid fuel for the burn. The pool incorporates a drain provided to empty the pool when desired. A stand-pipe system in the drain is available to maintain a constant water level during testing even with continuous water addition to the pool supplied through the cooling lines.

In accordance with 10 CFR §71.73(c)(4), the MAP CTU was supported by a simple, water-cooled, insulated, steel support stand. This structure, shown in Figure 3-6, consisted of four, 4 inch square tube vertical legs welded to a base of steel channel. The vertical legs were connected, by two square tubes of the same size, one meter above the surface of the pool to form two "H" structures. Cooling water was provided to the support stand to ensure adequate strength during the burn test. The test stand was wrapped with a minimum of one inch of refractory fiber insulation to minimize cooling water requirements and to minimize the local cooling effects at the test article. The MAP CTU test article was mounted on the stand with the top lid surface oriented approximately 14 degrees downward from the vertical position. This orientation was chosen to maximize the heat flux onto the puncture bar damaged area of the package (see Figure 3-7) and allow active flame access to the package closure.

The distance between the MAP CTU test article and the weir's inside walls varied from 39.5 to 45.25 inches at the sides of the test article and from 71.5 to 77.25 inches at the ends. The lowest corner of the package was approximately 39.9 inches above the normal waterline when the pool is filled to maximum capacity. These dimensions comply with the requirements of 10 CFR §71.73(c)(4).

Temperature monitoring during the fire test was accomplished using Inconel sheathed, type K thermocouples. Eight thermocouples were suspended around the test article, approximately 40 inches away from the surface of the package to provided direct measurement of the flame temperature at corners of the pool. Four of these thermocouples were mounted approximately 6

feet above the surface of the pool, while the remaining four were mounted approximately 4 feet above the surface of the pool. In addition, two thermocouples were placed at the mid-point of the steel baffles. The locations of these thermocouples are illustrated in Figure 3-8.

The package shell temperature of the MAP CTU test article was monitored using eight thermocouples that were mounted directly to the test article using sheet metal screws. Three thermocouples were mounted to the Lid's outer shell, three were mounted on the Base's outer shell, and one thermocouple mounted on each of the end impact limiters. The thermocouples on the Lid and Base were roughly centered on the flat surface between stiffeners. The thermocouples mounted on the impact limiters were mounted on the sloped side of the impact limiter shell. Figure 3-9 illustrates the placement of the package shell thermocouples.

The fuel in the burn pool was ignited at 1829 hours on February 15, 2007 and the package was fully engulfed at approximately 1831 hours, formally starting the timed burn test. The package remained essentially engulfed until approximately 1909 hours resulting in a burn test length of approximately 38 minutes during which time the test article was exposed to a fire environment that met or exceeded the temperature requirements of 10 CFR §71.73(c)(4). The flame conditions during this time period are illustrated by Figure 3-10 to Figure 3-12.

At 1900 hours fire suppressant foam was introduced below the surface of the pool to stop the combustion of the fuel remaining in the pool and end the 'fire' portion of the test[1]. Despite this action, combustion of the fuel continued and full engulfment of the package remained until 1909 hours. Thermal input to the package continued until approximately 1924 hours from remnants of fuel that continued to burn in the pool. This added heat input is illustrated by the flame conditions depicted in Figure 3-13 and Figure 3-14. The flames seen at the base of the weir are from the combustion of the remaining fuel, as seen through the vent holes in the weir.

The flames seen higher up at various spots on the package are the result of the flammable gases generated from the thermal decomposition of the polyurethane foam burning after exiting the package at the vent ports and being exposed to a pilot source and air. The combustion of the

foam's outgas began early in the fire duration as the foam began to decompose and continued after the end of the fire until the temperature in the foam components dropped below the decomposition point (i.e., approximately 670ºF) and the gas retained within the foam matrix was expelled. The foam out-gassing and vent port combustion was noted to continue at a relatively vigorous level until approximately 1945 hours, and then subside and extinguish by 2030 hours. This condition is consistent with that noted for other packages using polyurethane foam.

The measured fire flame temperatures averaged above 800°C, with peak temperatures reaching 1,200ºC. The average skin temperature of the test article, as measured at eight different locations, exceeded 800°C within 30 seconds after full engulfment of the test article was achieved. The peak skin temperatures reached 2,192°F. Fire temperatures below the test article, as measured by the thermocouples mounted on the steel baffles, averaged above 800°C. Figure 3-15 presents the transient temperature measurements for the six package skin temperatures located above the temperature sensitive moderator components within the package. As seen from the figure, the average package skin temperatures significantly exceeded the regulatory flame temperature of 1,475°F (800°C) for 38 minutes, with the computed average temperature being 1,746°F. This result confirms that the flame temperature and emissivity generated during the fire test exceeded the requirements of 10 CFR §71.73(c)(4).

Given that the heat transfer via radiation into the package varies with absolute temperature to the fourth power, the heat input into the package is estimated to be approximately 70%[2] higher than that to be expected at the regulatory minimum temperature of 800°C. When combined with the more than 8 additional minutes of flame exposure, the total heat input into the test article is seen to significantly exceed the level from a 30-minute exposure to an 800°C flame.

---

[1] At no time did the fire suppressant make contact with any portion of the package or serve to cool the package, nor did the suppressant stop any combustion occurring in or on the package.

[2] Based on a package skin temperature of 1475°F for a regulatory fire vs. 1746°F for the fire test, a foam char temperature of approximately 650°F, an effective emissivity exchange factor of 0.9, and a convection coef. of 3.5 Btuh/sq. ft-F. The heat input for a regulatory fire would be on the order of ((1475+460)^4 – (650+460)^4)*0.9*1.714e-9 + (1475-650)*3.5 = 22,172 Btuh/sq-ft. The heat input for the observed fire test was on the order of ((1746+460)^4 – (650+460)^4)*0.9*1.714e-9 + (1746-650)*3.5 = 38,026 Btuh/sq-ft. The ratio of heat input is then 38,026/22,172 = 1.72 or 72% higher than a minimum regulatory fire.

3.4.3 Maximum Temperatures and Pressure

3.4.3.1 Maximum HAC Temperatures

The temperatures achieved by the various components within MAP CTU test article were not directly measured. Instead, the maximum temperatures achieved within the test article during the fire test are estimated based on visual observations of the component conditions following the test. Estimating peak temperatures attained in a fire based on the condition of the various components involved is a standard fire investigation technique. Further, given the large thermal margin established below for the fuel assemblies, the accuracy of the predicted temperatures based on this approach is sufficient to assess the safety of the package design.

Figure 3-16 illustrates the Lid cover sheet and puncture bar damage area following the fire test. As seen from the photographs, the intumescent char developed by the polyurethane foam effectively plugged the breach in the outer skin of the package caused by the puncture bar. This protective mechanism of the foam prevents the hot flame gases from entering the interior of the package. A similar result would occur for any other breach in the package.

Figure 3-17 illustrates the condition of the Fuel Cavity following the fire test. The photograph on the left side of the figure demonstrates the Fuel Cavity is undamaged, except for the condensation of the outgas products from the decomposed polyurethane foam and the resin in the fiberglass thermal breaks. Additional photographs of the Fuel Cavity interior are provided in Section 2.12.1, *MAP Shipping Package Certification Tests* (see Figures 2.12.1-57 to 2.12.1-62). The relatively low temperature level reached within the Fuel Cavity was confirmed by examination of the interior of the Fuel Cavity. Not only were the dummy fuel assembly and ballast unit physically undamaged, their surfaces were found to be in pristine condition (see Figure 2.12.1-62). The polypropylene protective wrap on the fuel assembly was undamaged except for a slight ‘curling’ at the base of the fuel assembly. The neoprene showed no signs of curling or hardening, but the adhesive used to attach the neoprene sheets opposite the ballast unit had soften and allowed the neoprene to become detached (see Figure 2.12.1-60).

Given the overall condition of the components within the Fuel cavity as described above, the fact that the polypropylene plastic (with its melting point of approximately 300ºF) was essentially

undamaged, but the neoprene adhesive (with its recommended service temperature limit of 225ºF) had failed in several locations, the peak temperature reached within the Fuel Cavity is estimated to have been below 275ºF. For the purposes of this safety evaluation, a temperature level of 300ºF is used to conservatively bound the peak temperature achieved by the fuel assemblies during the HAC event. This temperature level is well below the allowable HAC temperature limits of 1,058ºF established for the fuel assemblies and the 1,100ºF limit for the borated MMC plates and the fuel cavity doors. Further, the magnitude of these demonstrated thermal margins bounds any reasonable uncertainty in the methodology used to estimate the peak temperature. It should also be noted that the thermal conductivity of the polyurethane foam used in the CTU was 0.24 for the batch, while the current specification allows a maximum of 0.30. This differential in thermal conductivity is consider negligible since the thermal protection offered by the foam is primarily related to the energy required to char the foam which is a function of its density.

Figure 3-18 illustrates the condition of the ceramic fiber paper insulation placed between the polyurethane foam and the outer skin, while Figure 3-19 illustrates the condition of the 6 lb/ft^3 foam. The ceramic fiber paper survived intact although it was saturated with condensed products from the foam out-gassing. In contrast, the 6 lb/ft^3 foam was essentially fully decomposed. As expected, the decomposed foam created a char layer that thermally shields the underlying components. This performance is consistent with the bucket tests described in Appendix 3.5.3, *'Last-A-Foam' Response under HAC Condition*. The fact that very little undamaged foam remained within the package is attributed to the added exposure to the fire conditions that exceeded the regulatory requirements (see Section 3.4.2, *Fire Test Conditions*). Given that the thermal decomposition of the foam proceeds at fairly uniform rate, a reduction in the exposure to the fully engulfing fire condition from the tested 38 minutes to the regulatory required 30 minutes would have resulted in a correspondingly increase in the amount of undamaged foam.

Examination of the neutron moderator components within the package Lid (see Section 2.12.1, *MAP Shipping Package Certification Tests*) showed that the majority of the moderator was undamaged. The principal change from the fabrication condition was due the condensation of tars, etc. generated from the decomposition of the foam and, to a lesser degree, the resin in the fiberglass thermal breaks. Only 13 out of the 88 individual blocks of moderator used in the

package Lid showed any sign of surface melting, with the incidental melting limited to small areas at the edges of the blocks in most cases. No melting or damage of any kind was observed for the 44 moderator blocks used in the package Base. Segment #5 (see Figure 2.12.1-69 for the location of this segment) contains 3 of the affected 13 moderator blocks and these blocks exhibited the worst case melting observed during the post-fire dissection of the package (see Figure 2.12.1-68 and Figures 2.12.1.74 to 2.12.1.76). Although relatively minor, the melting on block B4(6) in this segment does indicate that a local temperature in excess of 500ºF was achieved for a sufficient time to overcome the heat of fusion for the material. The remaining 10 of the 13 moderator blocks showing any sign of melting are dispersed over the adjacent 5 segments (see Table 1.12.1-4). These blocks exhibited only very minor melting at the corners of the blocks where the thermal mass to surface area ratio is the smallest. The location and extent of melting for these blocks demonstrates that the local peak temperature must not have been above 500ºF for long or by much.

A measurement of the moderator blocks in Segment #5 (see Table 2.12.1-5) showed that the weight loss due to melting was approximately 6.6 % by weight for the worst two blocks and 2.1% when averaged over all blocks in Segment #5 of the Lid. The combined weight loss for all moderator blocks in the package is less than 0.1%. As discussed in Chapter 6, *Criticality Evaluation*, this level of moderator loss is well within acceptable limits.

Examination of the Base assembly for the package showed that similar post-fire conditions existed for the ceramic fiber paper and polyurethane foam as was noted in the Lid assembly. As seen from Figure 2.12.1-79 to Figure 2.12.1-83, the moderator blocks in the Base were undamaged with only a slight discoloraton due to condensation of decomposition products from the polyurethane foam.

In conclusion, the fire test demonstrated that the MAP Package design incorporates sufficient thermal protection features to protect the moderator and absorber materials under the HAC conditions. The level of damage noted for the moderator material is well within the safety limits established in Chapter 6, *Criticality Evaluation*. Further, the thermal margin provided by the design of the MAP Package is demonstrated by the fact that the test article was subjected to an

extended exposure to the fully engulfing fire conditions in terms of both time and temperature level during the thermal test, as described in Section 3.4.2, *Fire Test Conditions*, and yet all of the thermal requirements for the components were successfully met.

3.4.3.2 Maximum HAC Pressures

The MAP Package does not contain any sealed enclosures other than the fuel rods contained in the payload. As such, the maximum package pressure developed during the HAC fire event remained near atmospheric conditions at all times. The outgassing which accompanies the thermal decomposition of the polyurethane foam can be expected produced slightly elevated pressures within the various package enclosures containing the foam material, but each of these enclosures contain a plastic 'blow-out' plug designed to fail under either the heat or pressures generated during the fire event.

The maximum rod pressure under HAC conditions is determined in the same manner as that for NCT conditions. Based on a bounding initial rod pressure of 450 psig, a 68°F rod temperature at the time of filling, and a maximum 300°F rod temperature during the HAC fire event, the maximum internal rod pressure under HAC is:

$$\text{Max. rod pressure} = (450\ \text{psig} + 14.7) \times \left[\frac{300^{o}\text{F} + 459.67^{o}\text{R}}{68^{o}\text{F} + 459.67^{o}\text{R}} \right]$$

$$\text{Max. rod pressure} = 669\ \text{psia} = 654\ \text{psig}$$

The acceptability of a pressure rise of 204 psig from the initial fill condition is provided in Chapter 4, *Containment*.

3.4.4 Maximum Thermal Stresses

The MAP Package is fabricated principally of sheet metal and relatively thin structural steel shapes. Further, no pressure containing enclosures exist within the packaging. As such, the thermal stresses developed during the HAC fire event will be low and not significant to the safety of the package.

Viewed from Southwest – Other Structures Are Props Used for Firefighter Training

Figure 3-4 - Fire Test Pool at South Carolina Fire Academy

Viewed from Southwest – Other Structures Are Props Used for Firefighter Training

Figure 3-5 - Weir Structure Setup for Fire Test

Figure 3-6 - MAP CTU 3 Mounted on Insulated Test Stand within Weir

Figure 3-7 - Close-up of MAP CTU 3 on Test Stand Showing Puncture Bar Damage

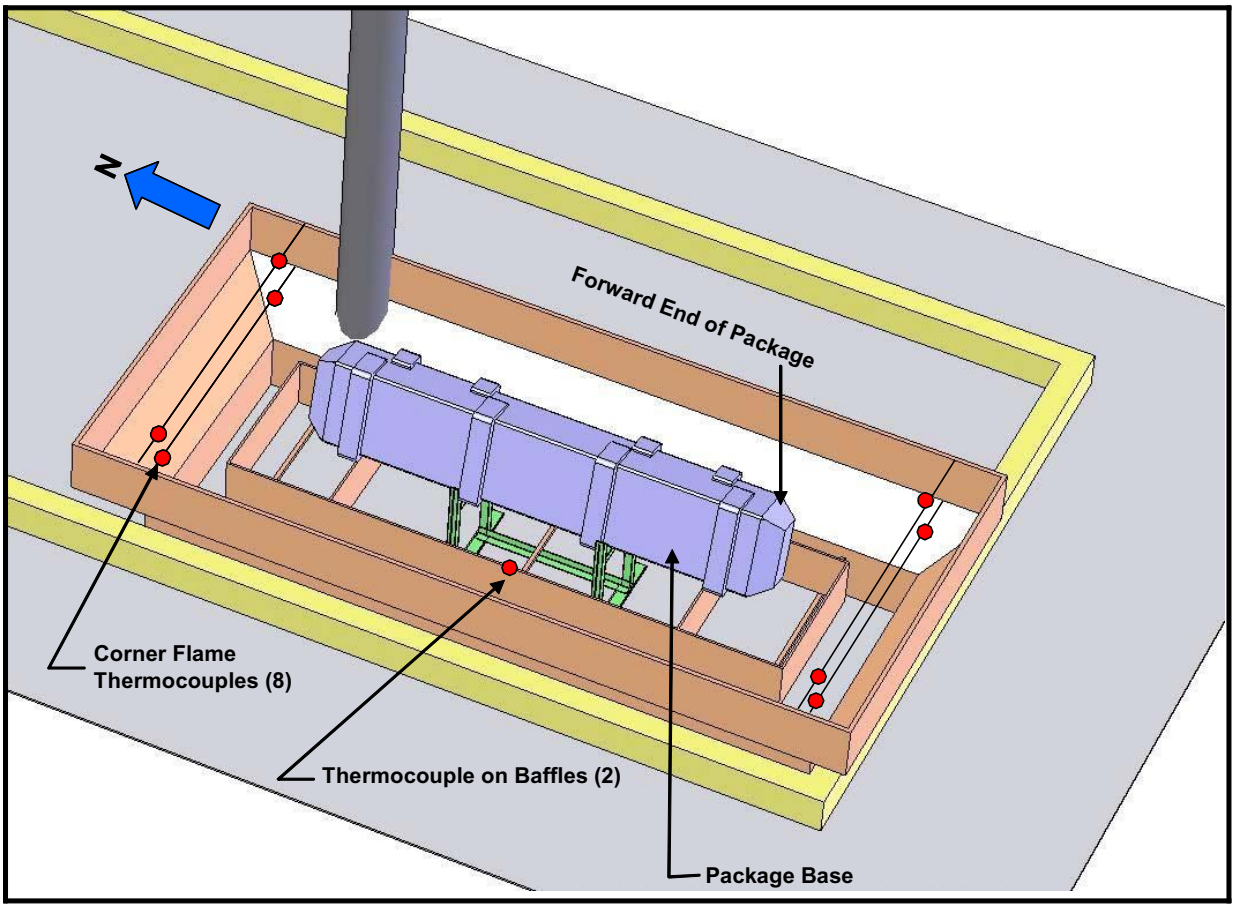

Figure 3-8 - Location of Flame and Baffle Thermocouples

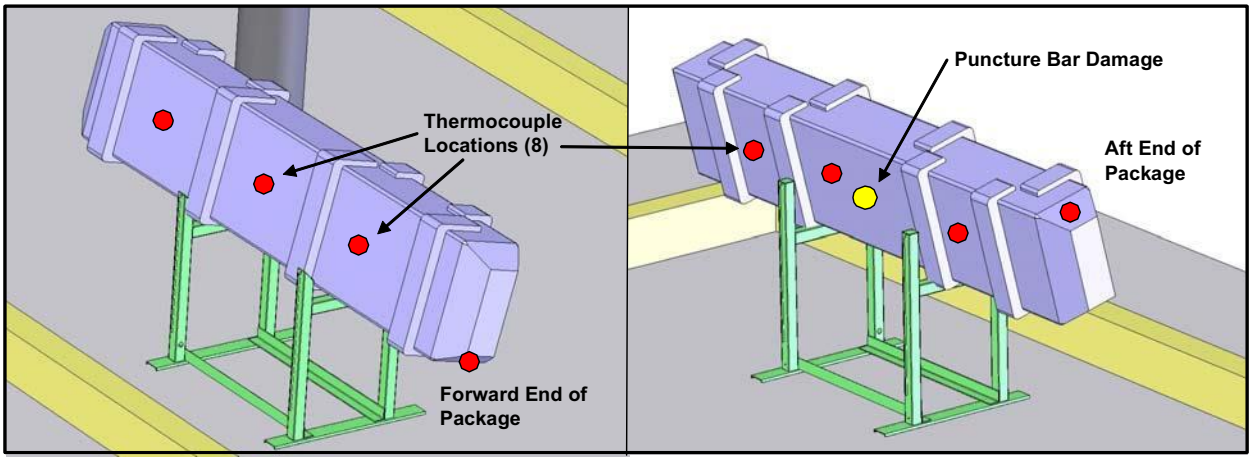

Figure 3-9 - Location of Package Skin Thermocouples

Photo P2150064.JPG

Figure 3-10 - Fire Conditions at Approximately 1833 Hours

Photo P2150121.JPG

Figure 3-11 - Fire Conditions at Approximately 1900 Hours

Photo P2150140.JPG

Figure 3-12 - Fire Conditions at Approximately 1908 Hours

Photo P2150157.JPG

Figure 3-13 - Fire Conditions at Approximately 1916 Hours

Photo P2150167.JPG

Figure 3-14 - Fire Conditions at Approximately 1924 Hours

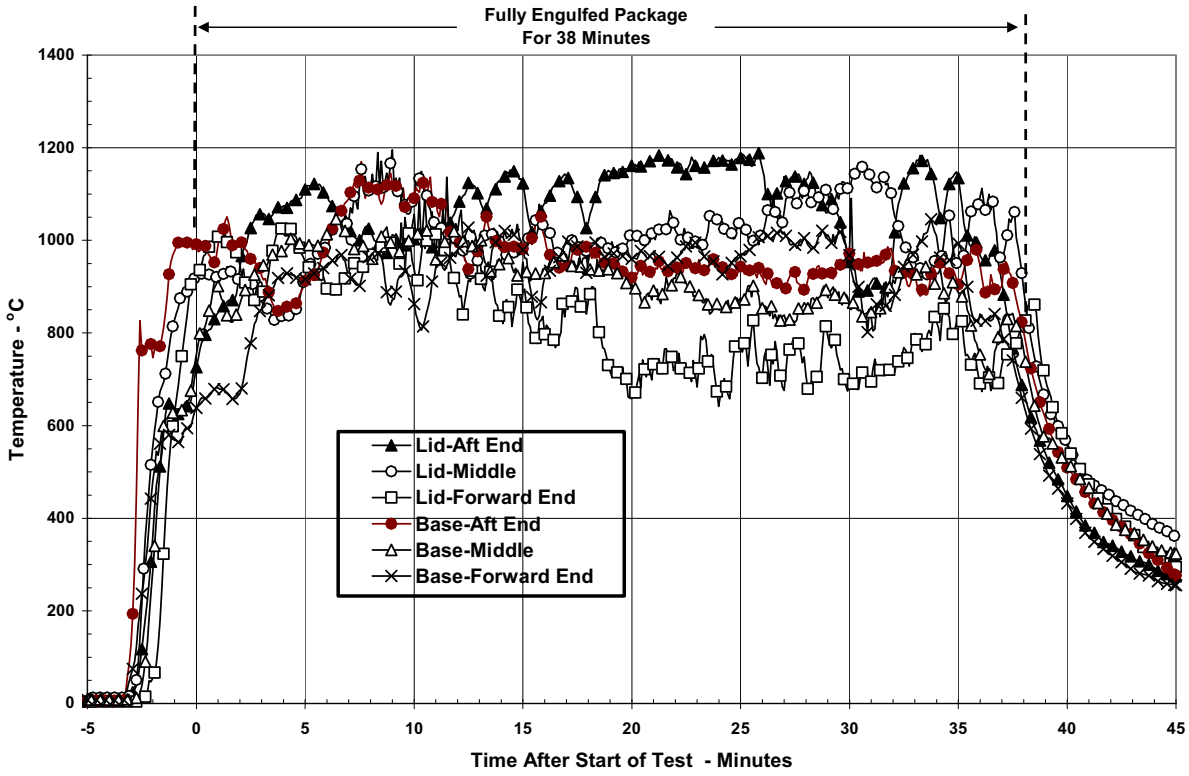

Figure 3-15 – Package Shell (Skin) Temperatures

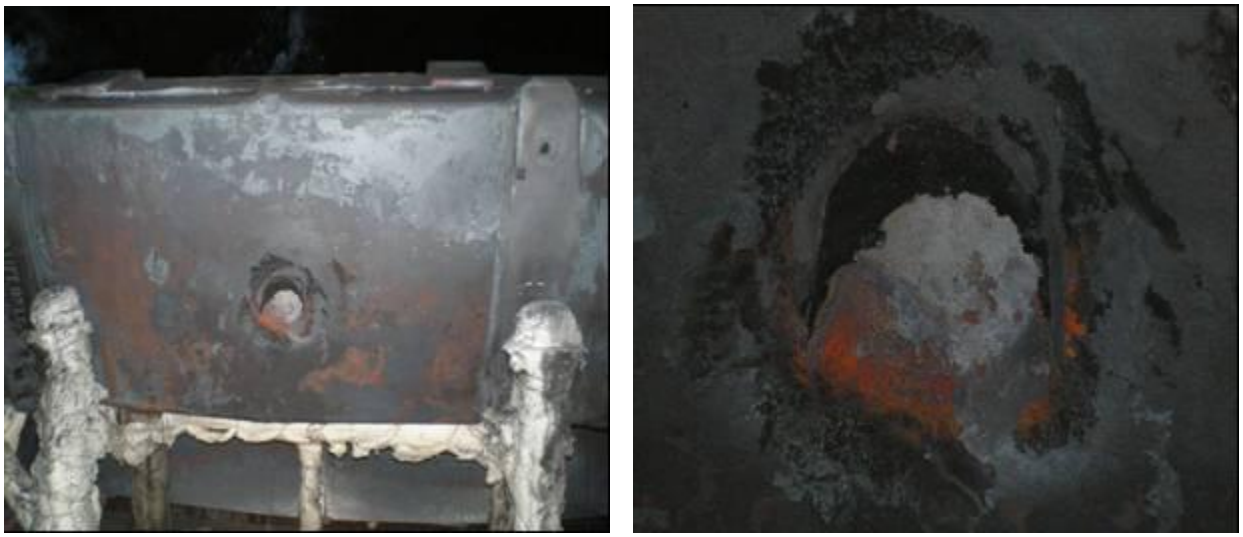

View of Puncture Bar Damage Area

Close-up View of Puncture Bar Damage Area

Figure 3-16 - MAP CTU 3 on Test Stand after Fire Test

View of Fuel Cavity Doors

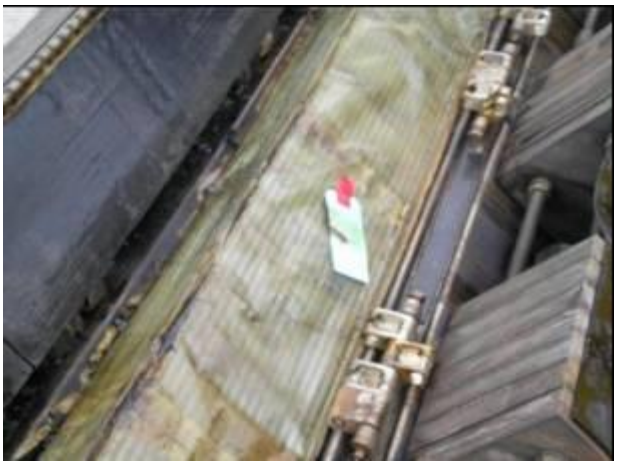

View of Fuel Cavity with Doors Open

Figure 3-17 - MAP CTU 3 after Fire Test: Lid Assembly Removed

View of Lid After Outer Shell Removal

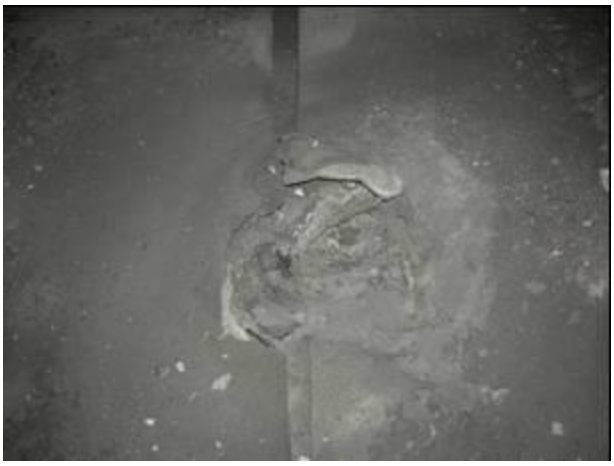

Close-up View of Puncture Bar Damage Area

Figure 3-18 - Dissection of CTU 3 after Fire Test: Lid Outer Shell Removal

Foam Under Ceramic Fiber Paper Intumesced Filling Voids

Sections of Undamaged Foam Remaining

Figure 3-19 - Dissection of CTU 3 after Fire Test: Lid 6 lb/ft^3 Foam Char Removal

3.5 Appendices

3.5.1 Computer Analysis Results

3.5.2 Analytical Thermal Model

3.5.3 'Last-A-Foam' Response under HAC Condition

3.5.1 Computer Analysis Results

Due to the size and number of the output files associated with each analyzed condition, results from the computer analysis are provided on a CD-ROM.

3.5.2 Analytical Thermal Model

The analytical thermal model of the MAP Package was developed for use with the Thermal Desktop®[1] and SINDA/FLUINT[2] computer programs. These programs are designed to function together to build, exercise, and post-process a thermal model. The Thermal Desktop® computer program is used to provide graphical input and output display function, as well as computing the radiation exchange conductors for the defined geometry and optical properties. Thermal Desktop® is designed to run as an AutoCAD® application. As such, all of the CAD tools available for generating geometry within AutoCAD® can be used for generating a thermal model. In addition, the use of the AutoCAD® layers tool provides a convenient means of segregating the thermal model into its various elements.

The SINDA/FLUINT computer program is a general purpose code that handles problems defined in finite difference (i.e., lumped parameter) and/or finite element terms and can be used to compute the steady-state and transient behavior of the modeled system. Although the code can be used to solve any physical problem governed by diffusion-type equations, specialized functions used to address the physics of heat transfer and fluid flow make the code primarily a thermal code.

The SINDA/FLUINT and Thermal Desktop® computer programs have been validated for safety basis calculations for nuclear related projects[3].

Together, the Thermal Desktop® and SINDA/FLUINT codes provide the capability to simulate steady-state and transient temperatures using temperature dependent material properties and heat transfer via conduction, convection, and radiation. Complex algorithms may be programmed into the solution process for the purposes of computing heat transfer coefficients as a function of the local geometry, gas thermal properties as a function of species content, temperature, and pressure, or, for example, to estimate the effects of buoyancy driven heat transfer as a function of density differences and flow geometry.

---

[1] Thermal Desktop®, Version 4.8, Cullimore & Ring Technologies, Inc., Littleton, CO, 2005.

[2] SINDA/FLUINT, Systems Improved Numerical Differencing Analyzer and Fluid Integrator, Version 4.8, Cullimore & Ring Technologies, Inc., Littleton, CO, 2005.

3.5.2.1 Description of Thermal Model for NCT Conditions

Two 3-dimensional thermal models of the MAP Package were developed for the NCT condition. One model is representative of the package along its length and the second simulates one of the end impact limiters. Given the essentially zero decay heat loading of the payload and the level of insulation provided by the polyurethane foam, the thermal performance of the package can be defined through the use of relatively small segments of the package since little axial heat transfer will occur within the package.

Figure 3-20 illustrates the plan and perspective views of the thermal model used to represent the package along its length. The model simulates one-half of the package (i.e., symmetry is assumed about the package's vertical plane) and extends approximately 7.8 inches in the axial direction (e.g., from one stiffener to the mid-point between stiffeners). This modeling choice captures the full height of the package components, one of the two Fuel Cavities, and allows the incorporation of the varying insolation loads that will occur at the top and sides of the package. Program features within the Thermal Desktop® computer program automatically compute the various areas, lengths, thermal conductors, and view factors involved in determining the individual elements that make up the thermal model of the complete assembly.

As seen from the figure, the modeling captures the various components of the packaging, including the use of dual layers of ceramic fiber paper, the stepped joint between the Lid and Base assemblies, the individual angle and channel irons used to connect the strong-back and inner lid assemblies to the outer shells, the moderator, the fiberglass thermal breaks (green solids), the stiffeners, and the fuel assembly (simulated as a homogenous solid region). Also captured, but not easily seen in the figure due to the modeling approach used are the borated MMC neutron absorber plates, the neoprene pads, and the sheet metal used for the strong-back and inner lid assemblies.

The model is composed of solid and plate type elements to represent the various package components. Thermal communication between the various components is via conduction,

---

[3] Software Validation Test Report for Thermal Desktop® and SINDA/FLUINT, Version 4.8, Packaging Technology, Inc., File No. TR-VV-05-001, Rev. 1.

radiation, and surface-to-surface contact. A total of approximately 4,900 nodes, 2,300 planar elements, and 2,000 solid elements are used to simulate the modeled components. In addition, one boundary node is used to represent the ambient environment for convection purposes and a second boundary node is used to represent the ambient temperature for the purpose of radiation heat transfer.

The fuel assemblies are simulated as homogenous solid regions based on a detailed representation of a prototypic fuel assembly. The detailed thermal model, illustrated in Figure 3-21, includes a separate representation of each fuel, poison, and instrumentation rod making up the fuel assembly. Heat transfer between the individual rods is simulated via conduction and radiation across the air space separating the rods. Since the fuel assemblies dissipate essentially zero decay heat, a detail of each fuel assembly type to be transported is not required. Instead, the thermal modeling defining a prototypic 17x17 fuel assembly[4] is acceptable for the purposes of this evaluation. The effective thermal conductivity for the fuel assembly region is determined by exercising the detailed thermal model for a range of temperatures and then converting the resulting temperature rise across the fuel assembly to an effective thermal conductivity based on the methodology for a square solid with distributed heat sources[5]. The results used in this evaluation are provided in Table 3-4.

Figure 3-22 illustrates the plan and perspective 'solid' views of the thermal model used to represent the impact limiters at each end of the Lid assembly. The model simulates one-half of the impact limiter, including the inside skin. A total of approximately 770 nodes, 300 planar elements, and 380 solid elements are used to simulate the modeled components. In addition, one boundary node is used to represent the ambient environment for convection purposes and a second boundary node is used to represent the ambient temperature for the purpose of radiation heat transfer.

---

[4] Packaging Technology Calculation No. 99008-25, *MFFP Thermal Analysis For Transport Conditions*, Rev. 0, Tacoma, Washington, 2004.

[5] "*Spent Nuclear Fuel Effective Thermal Conductivity Report*", prepared TRW Environmental Safety Systems, Inc. for DOE Civilian Radioactive Waste Management System (CRWMS), Report BBA000000-01717-5705-00010, Rev. 0, July 1996.

The heat transfer from the exterior surfaces of the MAP Package is modeled as a combination of convection and radiation exchange. Appendix 3.5.2.2, *Convection Coefficient Calculation*, presents the methodology used to compute the convection coefficients from the various surfaces. In addition, heating of the exterior surfaces due to solar insolation is assumed using a diurnal cycle. A sine wave model is used to simulate the variation in the applied insolation on the surfaces of the package over a 24-hour period, except that when the sine function is negative, the insolation level is set to zero. The timing of the sine wave is set to achieve its peak at 12 pm and peak value of the curve is adjusted to ensure that the total energy delivered matched the regulatory values. As such, the total energy delivered in one day by the sine wave solar model is given by:

$$\int_{6\cdot hr}^{18\cdot hr} Q_{peak}\cdot\sin\left(\frac{\pi\cdot t}{12\cdot hr}-\frac{\pi}{2}\right)dt=\left(\frac{24\cdot hr}{\pi}\right)\cdot Q_{peak}$$

Using the expression above for the peak rate of insolation, the peak rates for top and side insolation may be calculated as follows:

$$Q_{top}=\left(800\frac{cal}{cm^2}\right)\cdot\left(\frac{\pi}{24\,hr}\right)\qquad Q_{top}=2.68\frac{Btu}{hr\text{-}in^2}$$

$$Q_{side}=\left(200\frac{cal}{cm^2}\right)\cdot\left(\frac{\pi}{24\,hr}\right)\qquad Q_{top}=0.67\frac{Btu}{hr\text{-}in^2}$$

Conversion factors of 1 cal/cm^2-hr = 0.0256 Btu/hr-in^2 are used in the above calculations. These peak insolation rates are multiplied by the sine function and the solar absortivity for Type 304 stainless steel (i.e., 0.52) to determine the solar heating on the top and sides of the package as a function of time of day. The use of surface absorptivity to compute the actual insolation absorbed by the package is consistent with ¶3.5.2.1 of NUREG-1609[6] and ¶3.2.1 of RegGuide 7.9[7].

[6] NUREG-1609, "Standard Review Plan for Transportation Packages for Radioactive Material", Spent Fuel Project Office, US NRC, Washington, DC 20555, March 2000.

[7] Regulatory Guide 7.9, "Standard Format and Content of Part 71 Applications for Approval of Packages for Radioactive Material", Office of Nuclear Regulatory Research, US NRC, Washington, DC 20555, March 2005.

Table 3-7 presents a tabulation of the incident insolation on the horizontal surfaces of the package as a function of the time of day as determined using the diurnal cycle described above. The values in the second column of the table represent the instantaneous value of insolation, while the values in the third column represent the time-averaged value of insolation. Summing the values in the third column yields the total insolation value over a 24-hour period. The computed 2,945 Btu/ft^2 value is within 0.2% of the ¶10 CFR 71.71 (c)(1) specified insolation value of 2,950 Btu/ft^2 (800 g-cal/cm^2) for a flat surface. Further, the diurnal cycle applies this insolation over a 12 hour period as specified in ¶10 CFR 71.71 (c)(1).

Confirmation that the use of a diurnal cycle for insolation provides bounding peak temperatures when compared with using an averaged insolation value is presented in Figure 3-23. The left side of the figure presents the predicted package temperature distribution obtained using a diurnal cycle on insolation and a transient analysis, while the right side of the figure presents the predicted package temperature distribution obtained using the 24-hour average insolation value and a steady-state analysis. As seen from the figure, the peak temperatures predicted for the packaging are approximately 34°F higher with the diurnal cycle vs. that obtained using a steady-state insolation loading. The peak and average foam temperatures achieved with the diurnal cycle are 201 and 144°F, respectively, versus 174 and 142°F, respectively, for a steady-state analysis using 24-hour average solar. As such, the two methodologies provide essentially the same average foam temperature, but the diurnal cycle yields a higher peak foam temperature and a larger thermal gradient.

3.5.2.2 Convection Coefficient Calculation

The convective heat transfer coefficient, h_c, has a form of:

$$h_c = Nu \frac{k}{L}$$

where k is the thermal conductivity of the gas at the mean film temperature and L is the characteristic length of the vertical or horizontal surface.

Natural convection from each surface is computed based on semi-emphirical relationships using the local Rayleigh number and the characteristic length for the surface. The Rayleigh number is defined as:

where $$Ra_L = \frac{\rho^2 g_c \beta L^3 \Delta T}{\mu^2} \times Pr$$

g_c = gravitational acceleration, 32.174 ft/s^2 β = coefficient of thermal expansion, °R^{-1}

ΔT = temperature difference, °F ρ = density of air at the film temperature, lb$_m$/ft^3

μ = dynamic viscosity, lb$_m$/ft-s Pr = Prandtl number = (c_p μ) / k

L = characteristic length, ft k = thermal conductivity at film temperature

c_p = specific heat, Btu/lb$_m$-hr-°F Ra_L = Rayleigh #, based on length 'L'

Note that k, c_p, and μ are each a function of air temperature as taken from Table 3-5. Values for ρ are computed using the ideal gas law, β for an ideal gas is simply the inverse of the absolute temperature of the gas, and Pr is computed using the values for k, c_p, and μ from Table 3-5. Unit conversion factors are used as required to reconcile the units for the various properties used.

The natural convection from a discrete vertical surface is computed using Equation 4-33 of Rohsenow, et. al. [8], which is applicable over the range 1 < Rayleigh number (Ra) < 10^{12}:

$$Nu^T = \overline{C}_L Ra^{1/4}$$

$$\overline{C}_L = \frac{0.671}{\left(1 + \left(0.492/Pr\right)^{9/16}\right)^{4/9}}$$

$$Nu_L = \frac{2.0}{\ln\left(1 + 2.0/Nu^T\right)}$$

[8] Rohsenow, Hartnett, and Choi, *Handbook of Heat Transfer*, 3rd edition, McGraw-Hill Publishers, 1998.

$$Nu_t = \frac{C_t^V Ra^{1/3}}{\left(1 + 1.4x10^9\ Pr/\ Ra\right)}$$

$$C_t^V = \frac{0.13\ Pr^{0.22}}{\left(1 + 0.61\ Pr^{0.81}\right)^{0.42}}\left[1 + 0.78\left(\frac{T_{wall}}{T_\infty} - 1\right)\right]$$

where T_{wall} and T_∞ are in terms of absolute temperature.

$$Nu = \frac{h_c L}{k} = \left[(Nu_L)^6 + (Nu_t)^6\right]^{1/6}$$

Natural convection from horizontal surfaces is computed from Equations 4.39 and 4.40 of Rohsenow, et. al.[8], and Equations 3.34 to 3.36 of Guyer [9], where the characteristic dimension (L) is equal to the plate surface area divided by the plate perimeter. For a heated surface facing upwards or a cooled surface facing downwards and Ra > 1:

$$Nu = \frac{h_c L}{k} = \left[(Nu_L)^{10} + (Nu_t)^{10}\right]^{1/10}$$

$$Nu_L = \frac{1.4}{\ln\left(1 + 1.677/\left(\overline{C}_L Ra^{1/4}\right)\right)}$$

$$\overline{C_L} = \frac{0.671}{\left[1 + \left(0.492/Pr\right)^{9/16}\right]^{4/9}}$$

$$Nu_t = 0.14Ra^{1/3}$$

For a heated surface facing downwards or a cooled surface facing upwards and $10^3 < Ra < 10^{10}$, the correlation is as follows:

$$Nu = Nu_L = \frac{2.5}{\ln\left(1 + 2.5/Nu^T\right)}$$

[9] Guyer, E.C., *Handbook of Applied Thermal Design*, McGraw-Hill, Inc., 1989.

$$Nu^{T} = \frac{0.527}{\left(1+\left(1.9/Pr\right)^{9/10}\right)^{2/9}} Ra^{1/5}$$

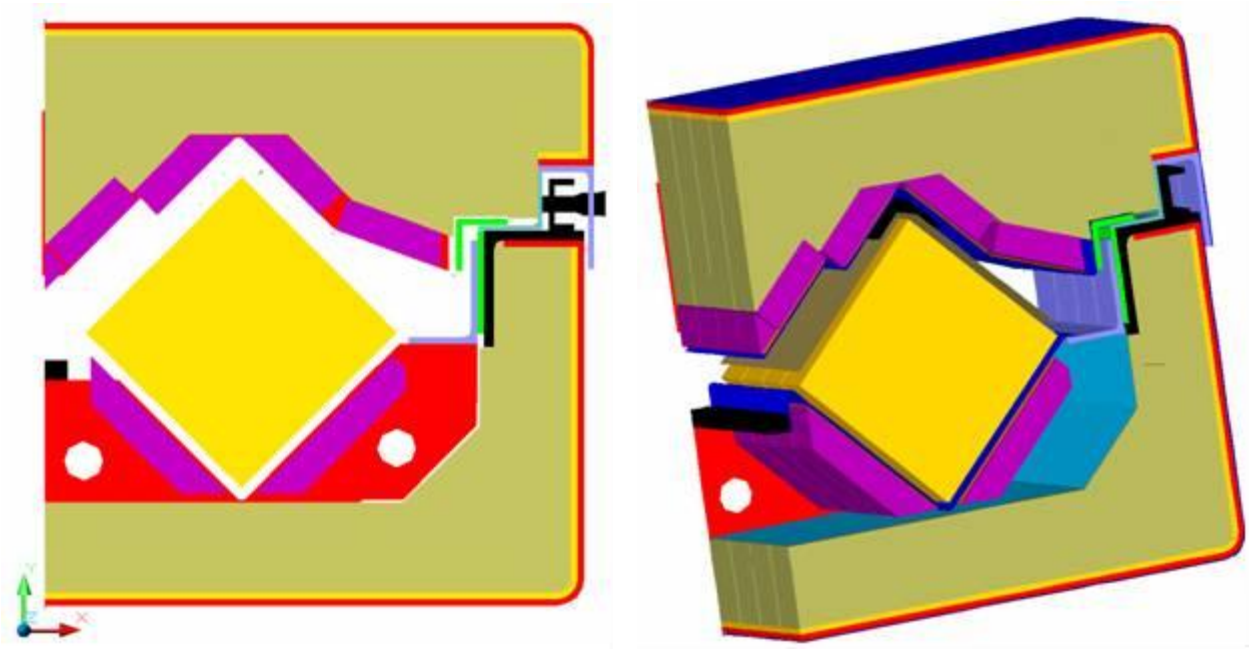

Plan View of Model Between Stiffeners **Perspective View of Model Between Stiffeners**

Figure 3-20 - Plan & Perspective Views of Package Symmetry Thermal Model

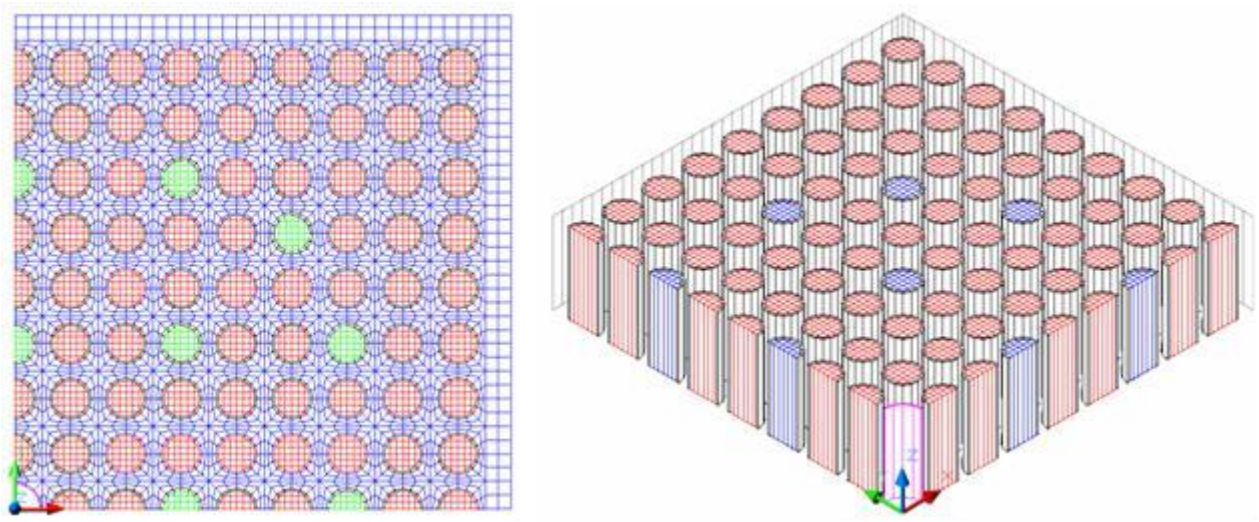

Plan View of Model **Perspective View of Model**

Figure 3-21 - Plan & Perspective Views of Detailed Fuel Assembly Thermal Model

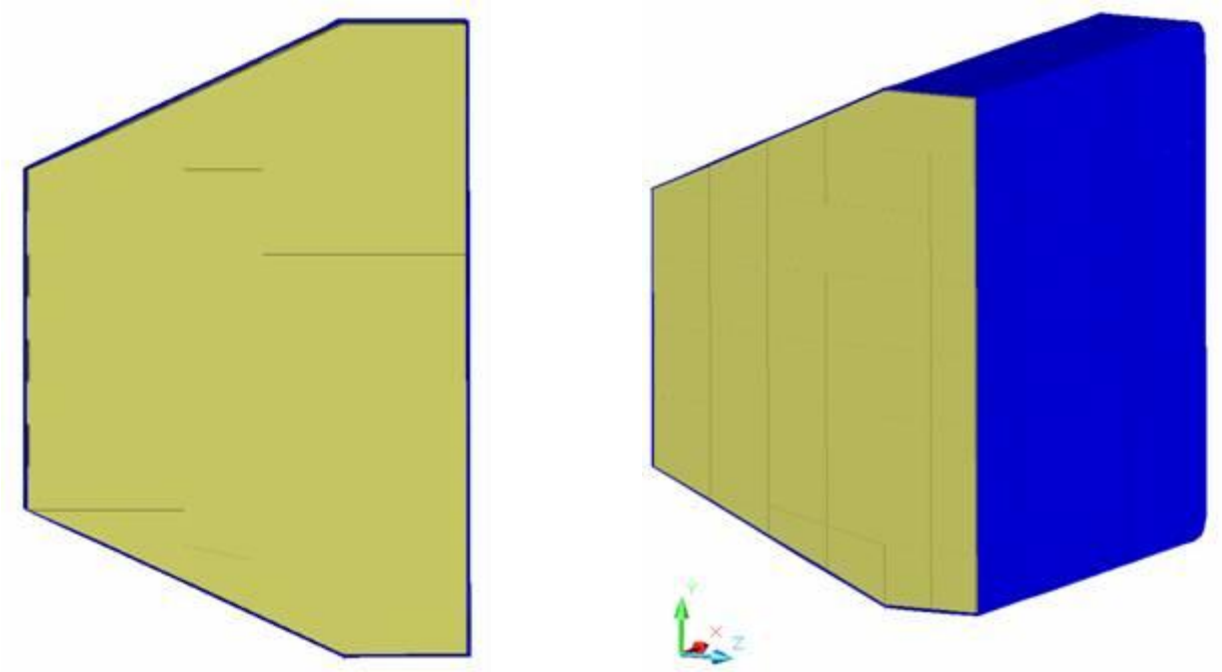

Plan View of Model **Perspective View of Model**

Figure 3-22 - Plan & Perspective Views of Lid End Impact Limiter Thermal Model

Table 3-7 - Diurnal Insolation Values for Horizontal Surfaces

Time (minute)	Transient Insolation Loading (BTU/min-in^2)	Time Avg. Insolation (BTU/in^2)
0 to 330	0	0
360	0	0.08748
390	5.83E-03	0.26103
420	1.16E-02	0.43005
450	1.71E-02	0.5916
480	2.23E-02	0.7431
510	2.72E-02	0.882
540	3.16E-02	1.00575
570	3.55E-02	1.11225
600	3.87E-02	1.1997
630	4.13E-02	1.2666
660	4.32E-02	1.3119
690	4.43E-02	1.3347
720	4.47E-02	1.3347
750	4.43E-02	1.3119
780	4.32E-02	1.2666
810	4.13E-02	1.1997
840	3.87E-02	1.11225
870	3.55E-02	1.00575
900	3.16E-02	0.882
930	2.72E-02	0.7431
960	2.23E-02	0.5916
990	1.71E-02	0.43005
1020	1.16E-02	0.26103
1050	5.83E-03	0.08748
1080 to 1440	0	0
	Daily Sum =	**20.45 Btu/in^2** **2945 Btu/ft^2**

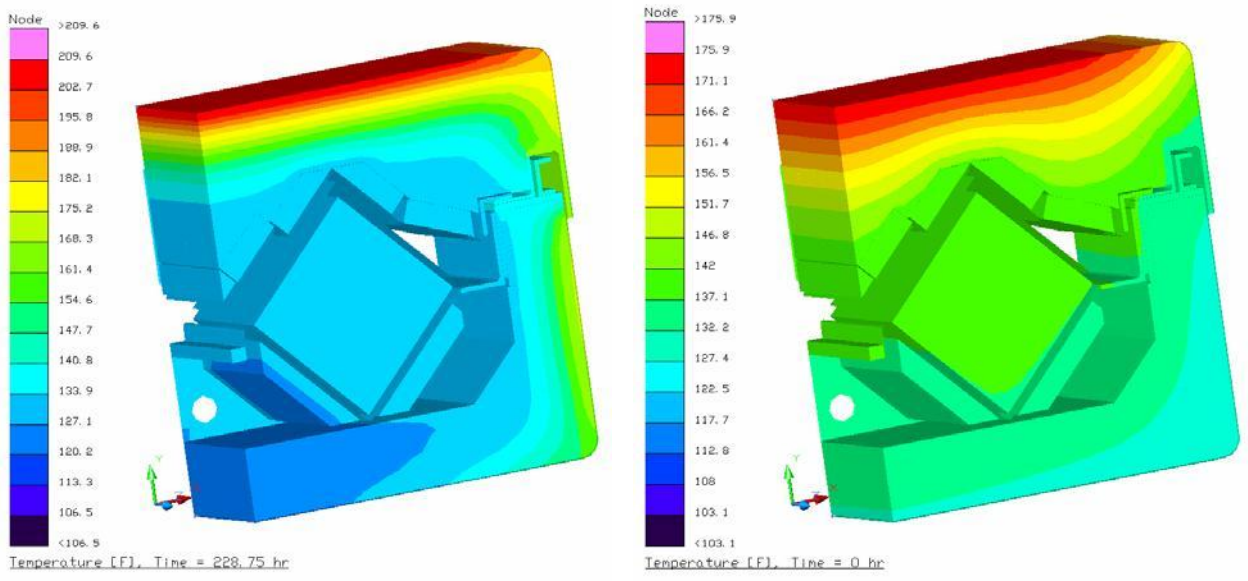

Temperatures with Diurnal Insolation **Temperatures with 24 Hour Avg. Insolation**

Figure 3-23 – Comparison of Package Temperatures with Diurnal vs. Steady-state Insolation Loading

3.5.3 'Last-A-Foam' Response under HAC Condition

The General Plastics LAST-A-FOAM® FR-3700 rigid polyurethane foam[10] has been used in numerous radioactive materials packages[11]. The FR-3700 formulation is specially designed to allow predictable impact-absorption performance under dynamic loading, while also providing an intumescent char layer that insulates and protects the underlying materials, even when exposed to pool-fire conditions. Upon exposure to fire temperatures, this proprietary foam decomposes into an intumescent char that swells and tends to fill voids or gaps created by free drop or puncture bar damage. Because the char has no appreciable structural capacity and will not develop unless there is space available, the char will not generate stresses within the adjacent package components. Without available space the pyrolysis gases developed as a result of the charring process will move the char mass out through the vent ports and prevent its buildup. Only as the charring process continues and space becomes available will char be retained, filling the available space and plugging holes at the surface of the package. Further, the thermal decomposition process for the foam does not alter or cause a chemical reaction within the adjacent materials as attested by the post-fire test physical inspection conducted on this package and others[11].

The thermal decomposition absorbs a significant amount of the heat transferred into the foam, which is then expelled from the package as a high temperature gas. At the same time, the resultant char layer shields the underlying undamaged foam from further direct exposure to the external high temperatures. This behavior has been observed in numerous fire tests of other packages.

Since the decomposition of the foam under elevated temperatures is an endothermic process, the foam is self-extinguishing and will not support a flame once the external fire is removed. However, the gases generated by the decomposition process are combustible and will burn under piloted conditions. Further, a portion of these generated gases could remain trapped within the charred layer of the foam for a period of time after the cessation of the HAC fire event and could support further combustion, although at a much reduced level, until a sufficient time has passed for their depletion from the cell structure.

---

[10] Last-A-Foam™ FR3700 On-line Data Sheet, www.generalplastics.com

[11] Other packages using Last-A-Foam™ FR3700 include TRUPACT-II (CoC #9218), HalfPACT (CoC #9279), MOX Fresh Fuel Package (CoC #9295), and the TN-55 (CoC #9328).

The mechanisms behind the observed variations in the thermal properties and behavior of the FR-3700 foam at elevated temperatures are varied and complex. A series of fire tests[12,13] conducted on 5-gallon cans filled with FR-3700 foam at densities from 6.7 to 25.8 lb/ft^3 helped define the expected performance of the foam under fire accident conditions. Under the referenced fire tests, one end of the test article was subjected to an open diesel fueled burner flame at temperatures of 980 to 1,200ºC (1,800 to 2,200ºF) for more than 30 minutes. A thermal shield prevented direct exposure to the burner flame on any surface of the test article other than the hot face. Each test article was instrumented with thermocouples located at various depths in the foam. In addition, samples of the foam were subjected to thermogravimetric analysis (TGA) to determine the thermal decomposition vs. temperature. The exposure temperatures for the TGA tests varied from 70 to 1,500 ºF, and were conducted in both air and nitrogen atmospheres. The result for the nitrogen environment (see Figure 3-24) is more representative of the low oxygen environment existing within the enclosures encasing the foam components of the MAP Package. These test results indicate that the following steps occur in the thermal breakdown of the foam under the level of elevated temperatures reached during the HAC fire event:

- Below 250 ºF, the variation in foam thermal properties with temperature are slight and reversible. As such, fixed values for specific heat and thermal conductivity are appropriate.
- Between 250 and 500 ºF, small variations in foam thermal properties occur as water vapor and non-condensable gases are driven out of the foam. As such, fixed values for specific heat and thermal conductivity are also appropriate for this temperature range. Further, the observed changes are so slight that the same thermal properties used for temperatures below 250 ºF may also be used to characterize the thermal performance of the foam between 250 and 500 ºF.

---

[12] "*Thermal Assault And Polyurethane Foam Evaluating Protective Mechanisms For Transport Containers*", C.L. Williamson, Z.L. Iams, General Plastics Manufacturing Company, Tacoma, WA, presented at Waste Management '05 Symposium, Tucson, AZ, 2005.

[13] "*Thermal Assault And Polyurethane Foam - Evaluating Protective Mechanisms*", C.L. Williamson, Z.L. Iams, General Plastics Manufacturing Company, Tacoma, WA, presented at PATRAM International Symposium, Berlin, Germany, 2004.

- Irreversible thermal decomposition of the foam begins as the temperature rises above 500ºF and increases non-linearly with temperature. Based on the TGA testing (see Figure 3-24, approximately 2/3's of this decomposition occurs over a narrow temperature range centered about 670°F.
- The decomposition is accompanied by vigorous out-gassing from the foam and an indeterminate amount of internal heat generation. The internal heat generation arises from the gases generated by the decomposition process that are combustible under piloted conditions. However, since the decomposition process is endothermic, the foam will not support combustion indefinitely. Further, the out gassing process removes a significant amount of heat from the package via mass transport.
- The weight loss due to out-gassing not only has direct affect on the heat flux into the remaining virgin foam, but changes the composition of the resulting foam char since the foam constituents are lost at different rates. This change in composition affects both the specific heat and the thermal conductivity of the foam char layer.
- As temperature continues to rise, the developing char layer begins to take on the characteristics of a gas-filled cellular structure where radiative interchange from one cell surface to another becomes the dominant portion of the overall heat transfer mechanism. This change in heat transfer mechanisms causes the apparent heat conductivity to take on a highly non-linear relationship with temperature.
- Finally, at temperatures above 1,250 ºF, the thermal breakdown of the foam is essentially completed and only about 5 to 10% of the original mass is left. In the absence of direct exposure to a flame or erosion by the channeling of the outgas products through the foam, the char layer will be the same or slightly thicker than the original foam depth. This char layer will continue to provide radiative shielding to the underlying foam material.

The sharp transition in the state of the foam noted in Figure 3-24 at or about 670°F can be used to correlate the observed depth of the foam char following a burn test with the occurrence of this temperature level within the foam. Figure 3-25 illustrates the relationship between foam recession (i.e., char depth) and foam density following exposure to a 30-minute fire as complied from a series

of tests. The correlation between the foam recession depth and the foam density is expressed by the relation:

$$y = -0.94681 - 11.64 \times \log_{10}(x)$$

where, y = the recession depth, cm
x = foam density (g/cm^3)

Based on this correlation, the recession depth expected for the nominal 6 pcf density foam used in the Lid and Base Assemblies of the package is estimated to be 4.3 inches. This recession depth does not include the effect of the ceramic fiber paper.

Project Specific Polyurethane Foam Investigations

The beneficial effect of adding 2 layers of ceramic fiber paper adjacent to the exterior skin of the package was investigated using a series of 5-gallon bucket tests conducted specifically for this project[14]. The bucket tests were setup to simulate a prototypic section through the MAP Package Lid Assembly and were conducted as a design verification process prior to proceeding to full scale test unit fabrication to evaluate the combination of the ceramic paper with the thickness of polyurethane foam to be used in the MAP Package Lid. The test setup consisted of the following components (in the order from the outside to the inside):

1) a 11 gauge stainless steel (Type304) lid,
2) one or two layers of ceramic fiber paper insulation,
3) a 3.75 to 4 inch layer of FR-3700 foam (depending on the number of layers of ceramic fiber paper insulation used),
4) a 1.25-inch layer of thermoplastic moderator material,
5) a 0.25-inch thick aluminum plate used to simulate the combined package neutron absorber (borated metal matrix composite) and inner lid sheet,
6) a 1.5-inch thick air gap used to approximate the void region above the Fuel Cavity, and
7) finally, a steel plate that approximated the equivalent fuel weight on a per surface area basis.

[14] AREVA Test Report TR-019, *MAP Foam Bucket Burn Test Report*, Rev. 0, October 2006, prepared by Packaging Technology, Inc., Tacoma, WA.

Figure 3-26 illustrates the setup for the testing of the 6 lb/ft^3 foam with two layers of ceramic fiber paper. The other test setups are similar, with the exception of the foam density and/or the number of layers of ceramic fiber paper used. Care was taken in assembly to isolate all the components from heat input through the side of the bucket.

Figure 3-27 through Figure 3-32 depicts the condition of the test configuration following the simulated HAC fire event. Figure 3-27 demonstrates that the double layer ceramic fiber paper remained intact throughout the test and provided thermal shielding of the underlying polyurethane foam and moderator material. Figure 3-30 depicts the char layer that developed as the polyurethane foam thermally decomposed. The results of the testing demonstrated that the use of two layers of ceramic fiber paper would reduce the degree of foam recession by approximately 24%, or from 4.3 inches to 3.25 inches. The testing showed that the underlying moderator material was undamaged for all configurations tested.

The results seen from the full scale fire test are consistent with the bucket test results, especially when the additional burn time is factored in. This consistency of results demonstrates that the observed thermal performance of the package under the full scale HAC testing is reliable and repeatable (see NUREG-1609, ¶3.5.3.3).

The foam in the end impact limiters of the package has a nominal density of 10 lb/ft^3 and no ceramic fiber paper is used. The combination of the higher foam density and lack of ceramic fiber insulation is expected to yield a recession depth during the fire event of 3.3 inches.

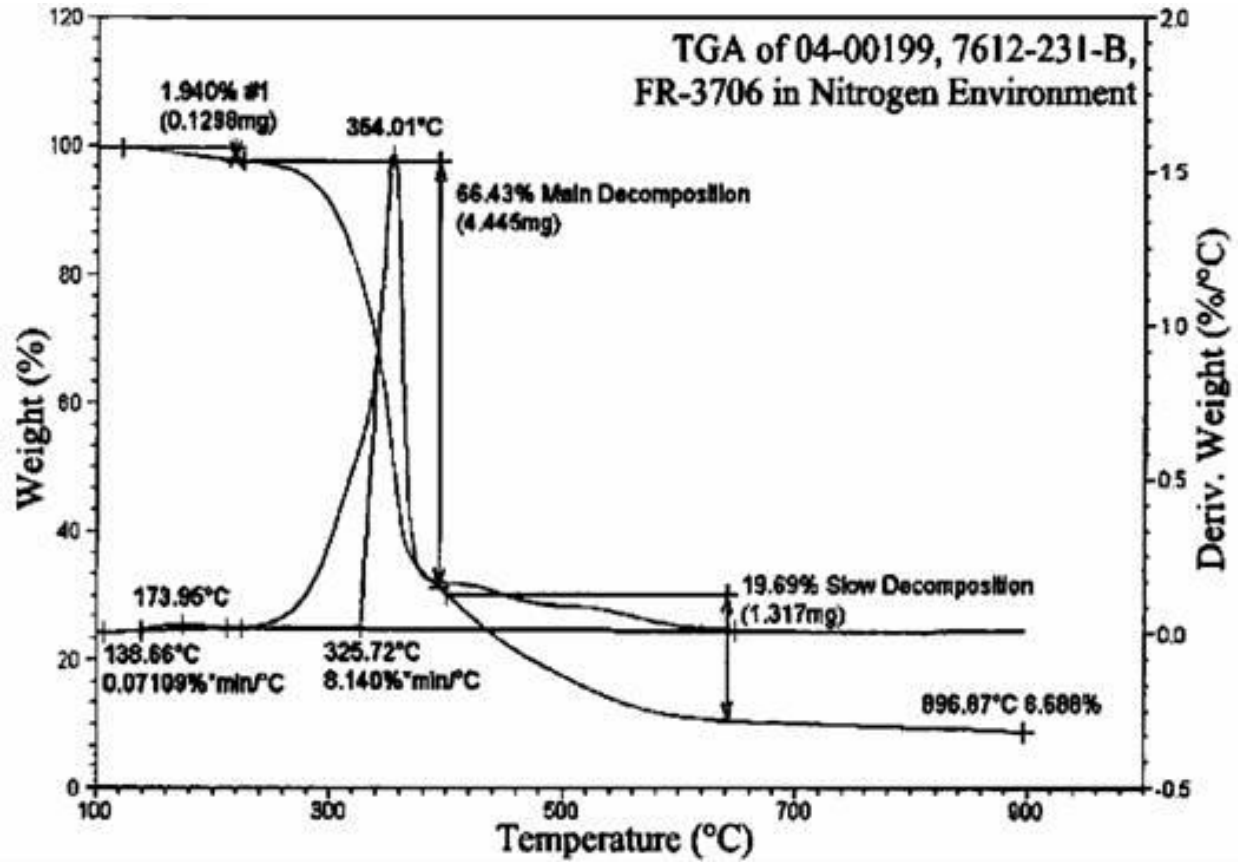

Figure 3-24 - TGA Analysis of Foam Decomposition in Nitrogen

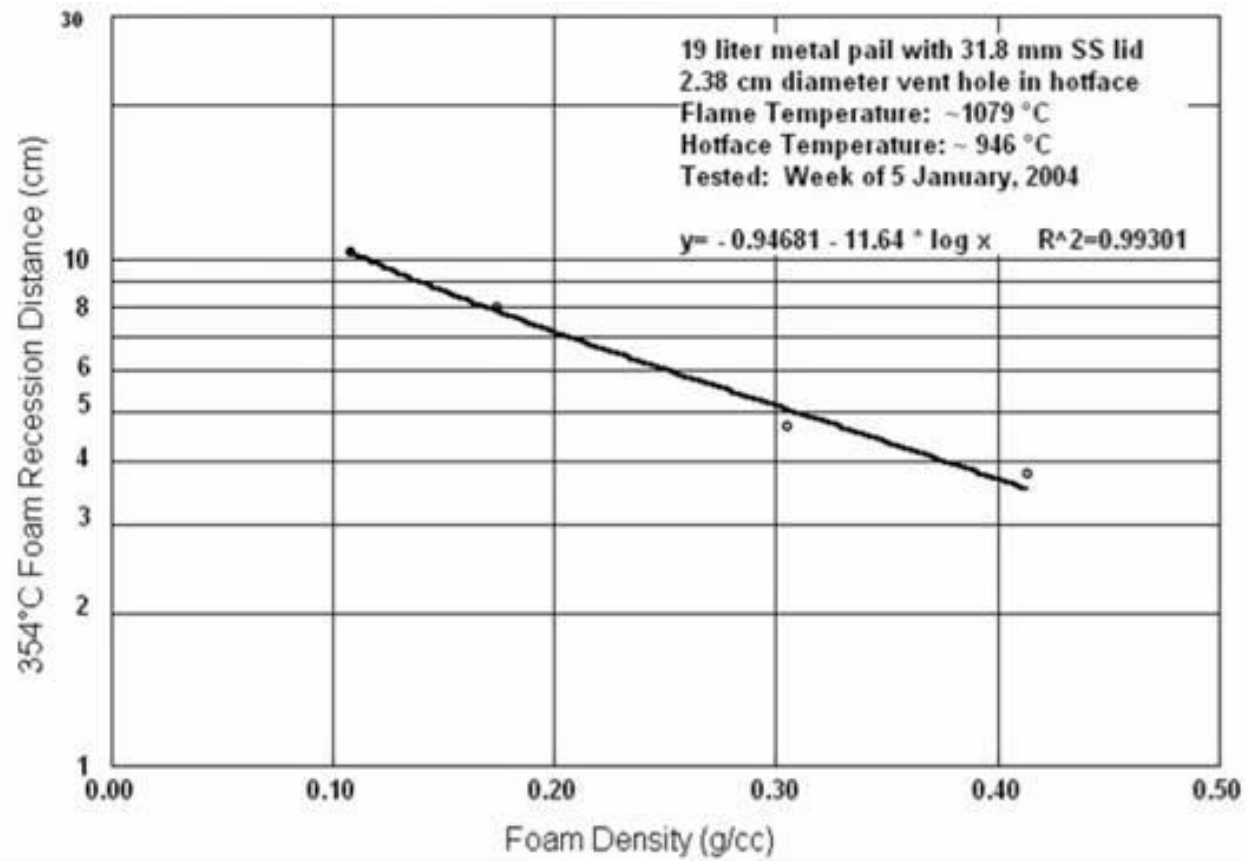

Figure 3-25 - Foam Recession vs. Density for 30-minute Fire

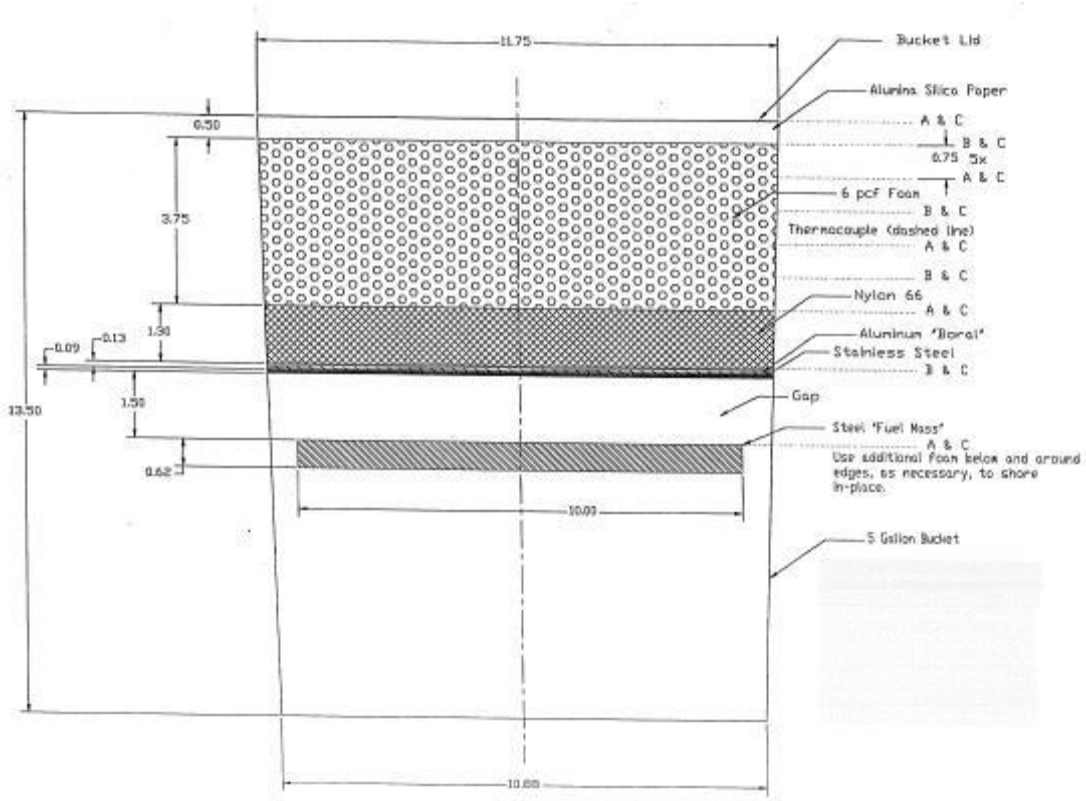

Figure 3-26 - MAP Foam Bucket Burn Test Setup for 6 lb/ft^3 Foam

Figure 3-27 – Intact ceramic fiber following test

Figure 3-28 – Elevation view of dissected bucket

Figure 3-29 – Remaining 6 lb/ft3 foam, backside

Figure 3-30 – Foam char under ceramic fiber paper

Figure 3-31 – Remaining 6 lb/ft^3 foam

Figure 3-32 – Moderator surface, flame side

Table of Contents Page

4.0 CONTAINMENT

The MAP is designed for shipment of fresh pressurized water reactor (PWR) fuel assemblies (Type A or Type B fissile radioactive material in solid form) meeting the specifications given in Section 1. The package is designed in a geometrically controlled configuration and criticality evaluations in this report assume that water does leak into the package interior. Therefore, water-tightness of the package is not assumed for the purpose of maintaining subcriticality.

A detailed description of the MAP and its fabrication is provided in Section 1. The fuel assemblies are loaded and unloaded from the container in a vertical orientation and are shipped in a horizontal orientation (with respect to the fuel assembly longitudinal axis. A maximum of 264 fuel rods (corresponds to a 17x17 array with 24 guide tubes and 1 instrument tube) may be shipped in the MAP. The internal pressure of the fuel rods shipped ranges from 145 to 450 psig.

4.1 Containment Boundary

The containment boundary is defined as the fuel rod cladding.

4.1.1 Containment Penetrations

The MAP containment boundary has no penetrations.

4.1.2 Seals and Welds

The applicable containment boundary welds are the fuel rod end plug welds (the cladding is seamless). All welds are examined for flaws prior to shipment in the MAP. Additionally, all rods are tested for leakage following the fabrication process. The fuel rods are pressurized with Helium as a final step in the fabrication process. The fuel rods are leak tested in a vacuum chamber such that the cover is essentially a vacuum and the trace gas or tracer is Helium. The test has a sensitivity of 3E-08 ref-cc/sec and all rods are demonstrated to have a leakage rate less than 1E-07 ref-cc/sec at that sensitivity prior to shipment in the MAP.

4.1.3 Closure

The MAP utilizes a minimum of 44 stainless steel locking pins to secure the package lid to the package base. These closures do not include or affect the containment boundary of the package.

4.2 Requirements for Normal Conditions of Transport

4.2.1 Containment of Radioactive Material

The package contents, as defined in Section 1.2.2 are assumed to be completely releasable in solid form. The total radioactivity contained in the package is variable, depending upon the payload.

4.2.1.1 Type A Shipments

For Type A payloads, the containment criterion requires no loss or dispersal of the radioactive contents under the normal transport conditions delineated by 10CFR71.71. The performance testing discussed in Section 2.12.1 demonstrates that the MAP effectively protects the payload against dispersal during normal conditions of transport without further leakage evaluations.

4.2.1.2 Type B Shipments

The performance testing discussed in Section 2.12.1 demonstrates that the MAP effectively protects the payload against dispersal during normal conditions of transport and is capable of maintaining the fuel pellets within the containment boundary under normal conditions of transport. For Type B packages, 10CFR71.51 further requires that any leakage be limited to less than 10^{-6} A_2 per hour.

The maximum payload weight is 1,148 kg UO_2. The maximum total radioactivity contained in the package is 16.4 Ci (calculated in Table 4-1). The radioactivity concentration (releasable activity per unit mass) of the package for both Normal and Hypothetical Accident conditions is therefore:

$$16.4 \text{ Ci} / 1{,}148 \text{ kg} = 0.0143 \text{ Ci/kg}.$$

The A_2 value for the mixture in the package is 0.17 Ci (calculated in Table 4-2).

The maximum allowable release rate for normal conditions, per ANSI N14.5-1997, is:

$$10^{-6} A_2 \text{ per hour} = 10^{-6} (0.17 \text{ Ci}) \text{ per hour} = 4.87\text{E-}11 \text{ Ci/sec}.$$

The maximum allowable leakage rate for normal conditions is:

$$4.87\text{E-}11 \text{ Ci/sec} / 0.0143 \text{ Ci/kg} = 3.40\text{E-}9 \text{ kg/sec Type B payload}.$$

For the normal condition, the Type B payload is a solid. The release mechanism for the solid payload through a small leak is assumed to be entrainment of suspended payload into leaking air (aerosol leakage). Per ANSI N14.5-1997, a reasonable bounding assessment of the mass density of a powder aerosol is 9E-6 g/cm^3. Therefore, the maximum allowable leakage rate for the Type B payload for the normal condition is:

$$3.40\text{E-}9 \text{ kg/sec} / 9\text{E-}6 \text{ g/cm}^3 = 0.38 \text{ ref-cm}^3\text{/sec}.$$

For assemblies containing low-enriched commercial grade uranium dioxide, the A_2 value is unlimited; therefore, there is no corresponding limiting weight. For assemblies containing blended low-enriched (BLEU) uranium dioxide, the mixture A_2 value is 0.175 Ci and the specific activity of the material is 0.0143 Ci/kg. Thus, the limiting mass for Type A shipment of BLEU material is 0.175/0.0143=12.2 kg (about 2000 pellets).

The packaging used for low-enriched commercial grade uranium dioxide is the same as the packaging used for the BLEU material. Additionally, the leak tests used to confirm the integrity of the BLEU fuel rods to a rate less than 1E-07 ref-cc/sec is the same as the leak tests used for the low-enriched commercial grade rods. Thus, the leakage rate of the low enriched commercial grade material following the 10CFR71.73 HAC sequence of tests is expected to be the same as that demonstrated for the BLEU material. Since the leakage requirement for low enriched uranium dioxide is no dispersal, the limit established for the package based on BLEU material bounds the limit for the low-enriched commercial grade material.

4.2.2 Pressurization of Containment Vessel

The containment boundary of the package is defined as the fuel rod cladding, and each fuel rod is internally pressurized with helium to a pressure ranging from 145 to 450 psig. Assuming the rod is filled at 68°F and attains a temperature of 131°F during Normal Conditions of Transport, the maximum internal pressure attained is 506 psig (a maximum increase of 56 psig) as calculated in Section 3.3.2 for the normal hot condition as described. The payload is a stable solid-form material to temperatures well above the Normal Hot condition; therefore, pressurization due to form changes, chemical reactions, or destabilization of the payload is not credible.

4.2.3 Containment Criterion

For the Type B payload specified by Tables 1-1 and 1-2, the maximum allowable leakage rate is 0.377 ref-cm^3/sec as bounded by the Normal condition. However, ANSI N14.5-1997 specifies 0.100 ref-cm^3/sec as an upper limit on the maximum allowable leakage rate; therefore, the maximum allowable leakage rate for the Type B payload is 0.100 ref-cm^3/sec. Leakage tests are performed on each rod fabricated to confirm the containment boundary leakage rate is less than 3E-08 ref-cc/sec prior to shipment.

4.3 Containment Requirements for Hypothetical Accident Conditions (HAC)

4.3.1 Fission Gas Products

Fission gas products are not present in the contents to be transported in the MAP.

4.3.2 Containment of Radioactive Material

The package contents, as defined in Section 1.2.2 are assumed to be completely releasable in solid form. The total radioactivity contained in the package is variable, depending upon the payload.

4.3.2.1 Type A Shipments

The containment criteria under HAC (delineated by 10CFR71.73) for the Type A payload requires no loss or dispersal of the radioactive contents. The performance testing discussed in

Section 2.12.1 demonstrates that the MAP effectively protects the payload against dispersal during HAC without further leakage evaluations.

4.3.2.2 Type B Shipments

The performance testing discussed in Section 2.12.1 demonstrates that the MAP effectively protects the payload against dispersal during normal conditions of transport and is capable of maintaining the fuel pellets within the containment boundary under HAC. For Type B packages, 10CFR71.51 further requires that any leakage be limited to less than 1 A_2 per week.

The maximum internal pressure attained for the fuel rods is calculated based on the observed temperature of the payload during the performance tests described in Section 2.12.1. Assuming the rod is filled to the maximum rod design pressure of 450 psig at a temperature of 68°F and attains a temperature of 300°F during the fire event, the maximum internal pressure attained is 654 psig (a maximum increase of 204 psig) as calculated in Section 3.4.3.2.

The maximum total radioactivity contained in the package, calculated in Section 4.2.1.2 is 16.4 Ci (calculated in Table 4-1). The radioactivity concentration (releasable activity per unit mass) of the package, also calculated in Section 4.2.1.2 is 0.0143 Ci/kg. The A_2 value for the mixture in the package is 0.17 Ci (calculated in Table 4-2).

The maximum allowable release rate for HAC, per ANSI N14.5-1997, is:

A_2 per week = (0.175 Ci) per week = 2.89E-7 Ci/sec.

The maximum allowable leakage rate for HAC is:

2.89E-7 Ci/sec / 0.0143 Ci/kg = 2.02E-5 kg/sec Type B payload.

For HAC, the Type B payload is a solid. The release mechanism for the solid payload is assumed to be entrainment of suspended payload into leaking air (aerosol leakage). Per ANSI N14.5-1997, a reasonable bounding assessment of the mass density of a powder aerosol is 9E-6 g/cm^3 (value is not pressure dependent). Note that the assumption that aerosol leakage occurs is conservative, since there was essentially no damage to the fuel rods resulting from the HAC tests and past experience with handling pellets indicates that sintered pellets do not readily release particulates (if at all).

Additionally, the mass density used to calculate the allowable leakage rate for the BLEU material (9E-6 g/cc) is a reasonable bounding assessment per ANSI N14.5-1997 for powder materials. Since only sintered pellets will be used in the assemblies, the use of this value is extremely conservative and adds additional margin to the evaluation.

Thus, the margin to the allowable is significant (more than 1,000 times less than the allowable) and differential leakage due to the initial differential rod pressure is considered negligible.

Therefore, the maximum allowable leakage rate for the Type B payload for HAC is:

$$2.02E\text{-}5 \text{ kg/sec} / 9E\text{-}6 \text{ g/cm}^3 = 2.25E+3 \text{ cm}^3/\text{sec}$$

Although this leakage rate is calculated assuming an aerosol leakage mechanism, sintered UO_2 pellets are too hard and brittle to produce a large volume of small particulates for aerosol leakage. It is more likely that the pellets would be fragmented upon impact, and these fragments would need to migrate through cracks developed in the cladding. In fact, the pellets are much harder than the cladding; thus, damage to the cladding and release of pellets or pellet fragments is much more likely than aerosol leakage. The allowable leakage rate can also be correlated to pellet leakage:

$$2.02E\text{-}5 \text{ kg/sec} / 0.006 \text{ kg/pellet} = 12.6 \text{ pellets/hr.}$$

The performance tests documented in Section 2.12.1 demonstrate that no pellets are released from the cladding as a result of the 10CFR71.73 postulated hypothetical accident conditions.

4.3.3 Containment Criterion

The containment criteria for HAC is bounded by the Normal Condition Criteria (Section 4.2.3).

Table 4-1 Package Total Maximum Radioactivity for Type B Payload[1]

Isotope	Maximum content	Maximum mass, g	Specific Activity[2], TBq/g	Total Activity, TBq	Total Activity, Ci
^{232}U	2.00E-09 g/gU	2.02E-03	0.83	1.68E-03	4.54E-02
^{234}U	2.00E-03 g/gU	2.02E+03	2.3E-04	4.65E-01	1.26E+01
^{235}U	5.00E-02 g/gU	5.06E+04	8.0E-08	4.05E-03	1.09E-01
^{236}U	2.50E-02 g/gU	2.53E+04	2.4E-06	6.07E-02	1.64E+00
^{238}U	9.23E-01 g/gU	9.34E+05	1.2E-08	1.12E-02	3.03E-01
^{237}Np	1.66E-06 g/gU	1.68E+00	2.6E-05	4.37E-05	1.18E-03
^{238}Pu	6.20E-11 g/gU	6.27E-05	6.3E-01	3.95E-05	1.07E-03
^{239}Pu	3.04E-09 g/gU	3.08E-03	2.3E-03	7.07E-06	1.91E-04
^{240}Pu	3.04E-09 g/gU	3.08E-03	8.4E-03	2.58E-05	6.98E-04
Gamma Emitters	6.38E+05 MeV-Bq/kgU	n/a		6.46E-02 [3]	1.74E+00
Total				**0.607**	**16.4**

[1] Based on a maximum payload of 1,148 kg UO_2 per package

[2] 10CFR71, Appendix A

[3] Assumed gamma energy of 0.01 MeV to maximize total content

Table 4-2 Mixture A_2 Calculation for Type B Payload

Isotope	Maximum Radioactive content (Ci)	10CFR71 A_2 per isotope (Ci)	Activity Fraction	A_2 Fraction
^{232}U	4.54E-02	0.027	2.76E-03	1.02E-01
^{234}U	1.26E+01	0.16	7.66E-01	4.79E+00
^{235}U	1.09E-01	Unlimited	N/A	N/A
^{236}U	1.64E+00	0.16	9.99E-02	6.24E-01
^{238}U	3.03E-01	Unlimited	N/A	N/A
^{237}Np	1.18E-03	0.054	7.19E-05	1.33E-03
^{238}Pu	1.07E-03	0.027	6.50E-05	2.41E-03
^{239}Pu	1.91E-04	0.027	1.16E-05	4.31E-04
^{240}Pu	6.98E-04	0.027	4.25E-05	1.57E-03
Gamma Emitters	1.74E+00	0.54	1.06E-01	1.97E-01
Total	**16.4**			5.72
Mixture A_2				**0.17 Ci**

Table of Contents Page

List of Figures Page

List of Tables Page

6.0 CRITICALITY

6.1 INTRODUCTION

The following analyses demonstrate that the MAP packages (MAP-12 and MAP-13, otherwise referred to as MAP in this evaluation) comply fully with the requirements of 10CFR71[1]. The nuclear criticality safety requirements for Type B fissile packages are satisfied for a single package and package array configurations under normal conditions of transport and hypothetical accident conditions. A comprehensive description of the MAP packaging is provided in Section 1. This section provides a description of the package (i.e., packaging and contents) that is sufficient for understanding the features of the MAP that maintain criticality safety.

Specifically, this criticality evaluation presents the following information[2]:

- Description of the contents and packaging, including maximum and minimum mass of materials, maximum ^{235}U enrichment, physical parameters, type, form, and composition.
- Description of the calculational models, including sketches with dimensions and materials, pointing out the differences between the models and actual package design, with explanation of how the differences affect the calculations.
- Justification for the credit assumed for the fixed neutron absorber content, including reference to the acceptance tests that verify the presence and uniformity of the absorber.
- Justification for assuming 90% credit for fixed moderating material.
- Description of the most reactive content loading and the most reactive configuration of the contents, the packaging, and the package array in the criticality evaluation.
- Description of the codes and cross-section data used.

---

[1] Title 10, Code of Federal Regulations, Part 71 (10CFR71), Packaging and Transportation of Radioactive Material, edition effective Oct 2004.

[2] NUREG/CR-5661, Recommendations for Preparing the Criticality Safety Evaluation of Transport Packages.

- Discussion of software capabilities and limitations of importance to the criticality safety evaluations.
- Description of validation procedures to justify the bias and uncertainties associated with the calculational method, including use of the administrative subcritical margin of 0.05 delta k to set an upper safety limit (USL) of 0.94.
- Demonstration that the effective neutron multiplication factor (k_{eff}) calculated in the safety analysis is less than the USL after consideration of appropriate bias and uncertainties for the following.
    - A single package with optimum moderation within the package, close water reflection, and the most reactive configuration consistent with the effects of either normal conditions of transport or hypothetical accident conditions, whichever is more reactive.
    - An array of 5N undamaged packages (packages subject to normal conditions of transport) with nothing between the packages and close water reflection of the array.
    - An array of 2N damaged packages (packages subject to hypothetical accident conditions) if each package were subjected to the tests specified in §71.73, with optimum interspersed moderation and close water reflection of the array.
- Calculation of the Criticality Safety Index (CSI) based on the value of N determined in the array analyses. The evaluation supports a CSI of 2.8.

6.2 DESCRIPTION OF CRITICALITY DESIGN

6.2.1 Design Features

This section describes the design features of the MAP that are important for criticality. The MAP shipping package carries up to two PWR fuel assemblies. Figures 6-1 and 6-2 provide isometric and cross-sectional views of the MAP package.

The MAP is divided into two major systems for the criticality evaluation: Outer Cavity and Fuel Cavity. The Outer Cavity consists of a top and bottom portion. The top portion is the removable lid. Borated neutron absorbing plates coupled with neutron-moderating nylon blocks are affixed to the lower angled inner surfaces of the stainless steel shell that defines the top portion, such that the top absorber-moderator layers are in close proximity to the envelope for a fuel assembly residing in the Fuel Cavity. Additionally, there are spacers welded to the central angle, spaced incrementally over the length of the package, that consist of beveled nylon blocks clad in stainless steel. The remainder of the steel shell is filled with polyurethane foam material.

The bottom portion of the Outer Cavity defines the foundation for the Fuel Cavity which contains the fuel. As in the top portion, angled nylon blocks coupled with borated plates are positioned in close proximity to the envelope for a fuel assembly residing in the Fuel Cavity. The bottom portion consists of a stainless steel shell which is filled with polyurethane foam.

The top surfaces of the Fuel Cavity are defined by the bottom surface of the top portion of the Outer Cavity (angled stainless steel plates). The bottom surfaces of the Fuel Cavity are defined by a stainless steel ‘W’-shaped plate that accommodates two fuel assemblies side-by-side in the package. The Fuel Cavity is designed to retain its original dimensions (i.e. dimensions important for criticality safety) when subjected to the HAC tests.

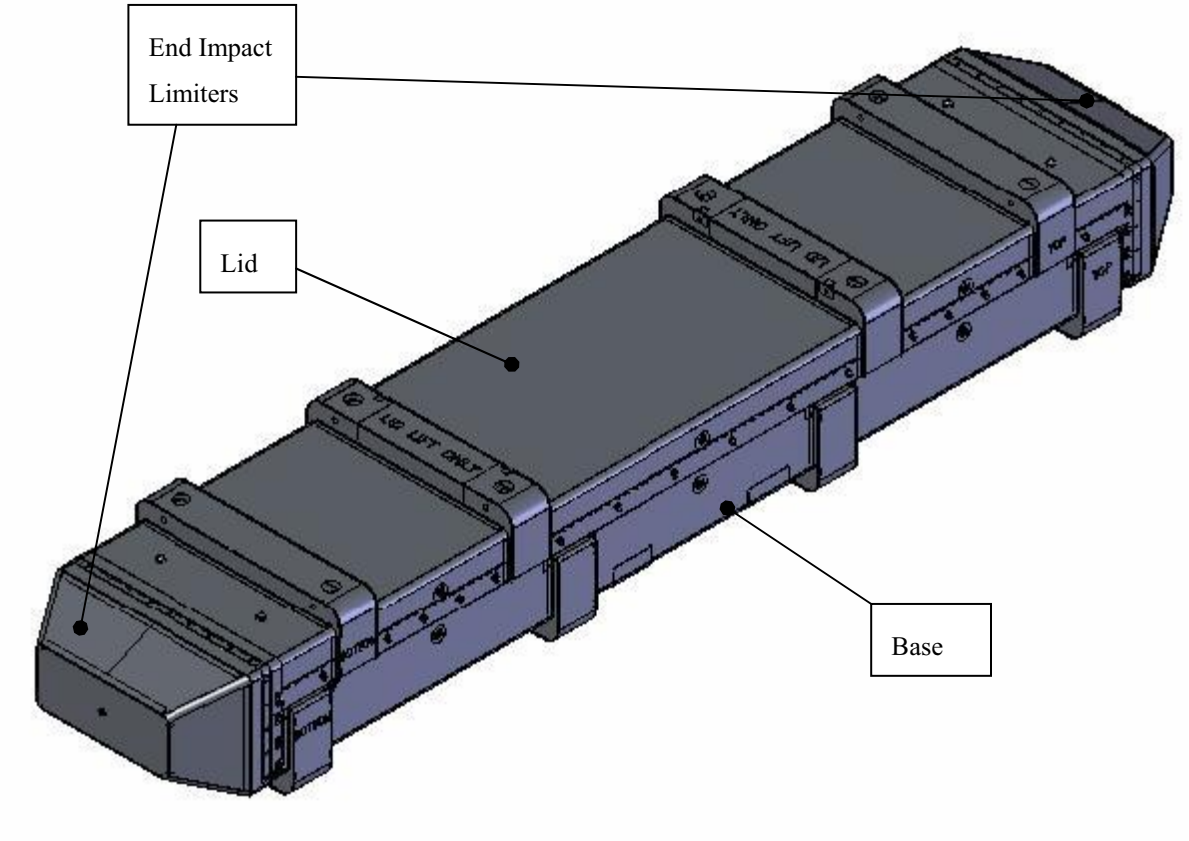

Figure 6-1 MAP Package – Isometric View

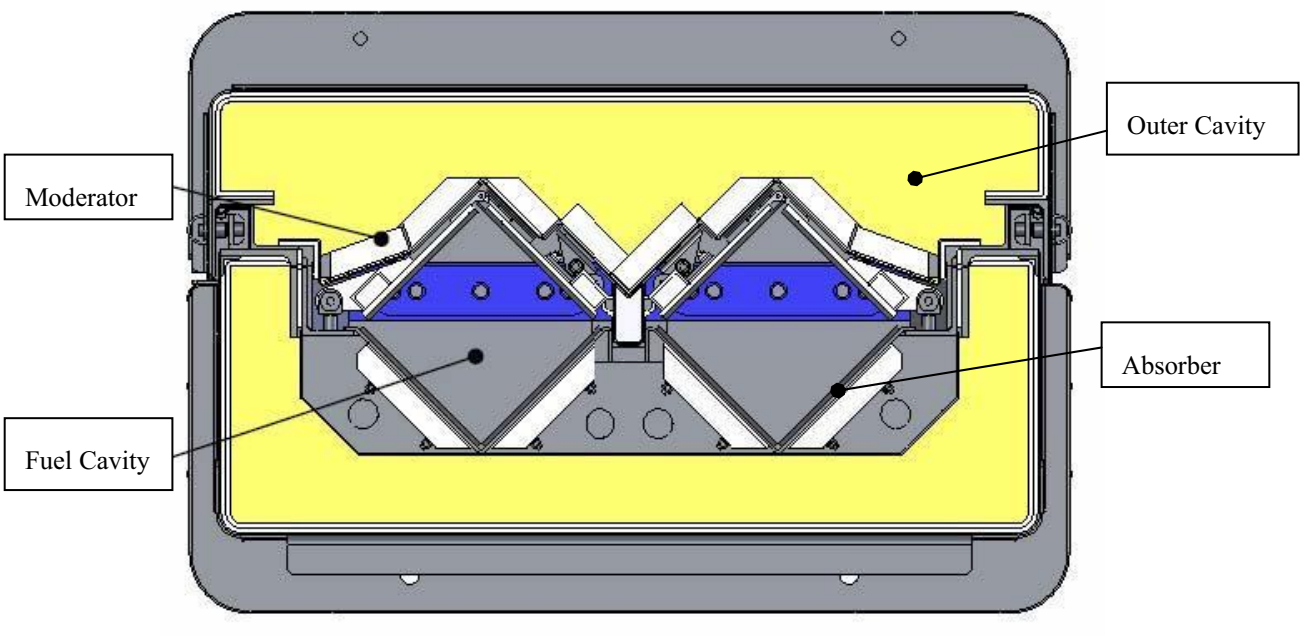

Figure 6-2 MAP Package – Cross Sectional View

6.2.1.1 Containment System

The Containment System is described in 10CFR71 as, "the assembly of components of the packaging intended to retain the radioactive material during transport." The Containment System for the MAP consists of the fuel rod cladding.

6.2.1.2 Flux Trap

The MAP package features a unique flux trap system which does not require an accident condition (i.e., flooding) in order to function. The system was designed to ensure an acceptable subcritical margin for the unlikely but most conservative flooding scenario, described in Section 6.7.2. The flux trap system consists of neutron absorber plates and moderator blocks mounted to the angled stainless steel plates that define the top and bottom surfaces of the Fuel Cavity. Note that the absorber plates and moderator blocks are all considered as part of the Outer Cavity. The majority

of neutrons escaping from one fuel assembly would pass through two moderator blocks prior to encountering the absorber of a neighboring package.

Interior top and bottom stiffening brackets divide the flux trap into 11 axial sections. The flux trap components in a given axial section all have the same axial length. The nine middle sections have the same length while the outer axial sections have shorter and unequal lengths.

The nylon blocks ensure that there will be neutron moderation for any condition ranging from low density interspersed moderation to fully flooded. The flux trap components and those package components which would enhance neutron absorption during a significant hypothetical accident condition (i.e., flooding) are described in the following sections. Figure 6-3 illustrates the flux trap system.

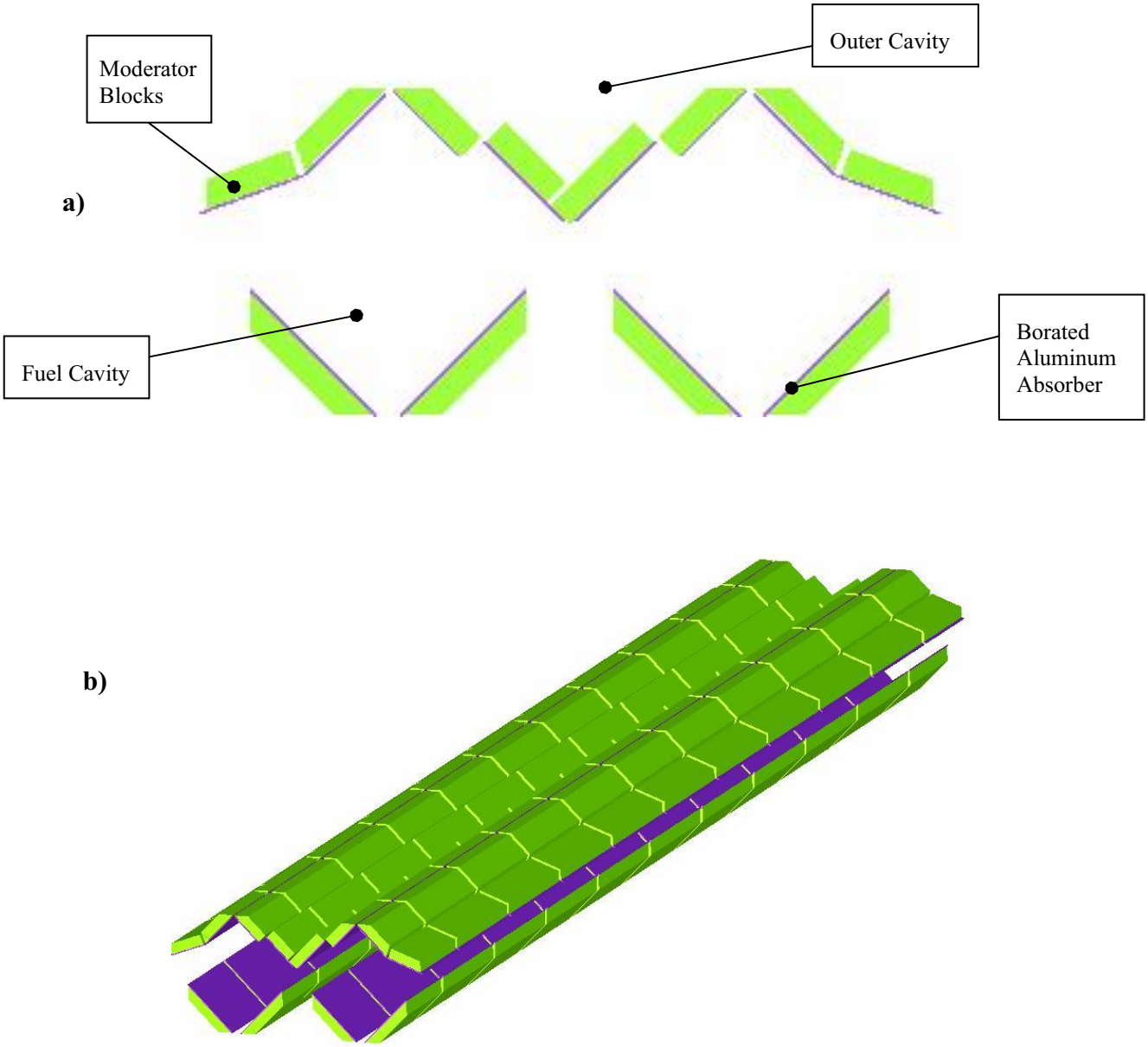

Figure 6-3 Flux Trap System – a) Shows Cross-Sectional View, b) Shows Isometric View

6.2.1.3 Neutron-Absorbing Materials

Neutron absorbing materials are present in the MAP in two forms: materials of construction and the neutron absorber in the flux trap.

6.2.1.3.1 Materials of Construction

Materials of construction include those materials normally present. Note that the only materials mentioned here are those that exist within the axial bounds of the flux trap system. These materials include the stainless steel defining the Outer Cavity and the outer stiffeners (or spacers) on the lid and base; the 'W' stainless steel plates defining the top and bottom of the Fuel Cavity; aluminum door panels and associated components above the assembly envelope; stainless steel bar in the center; lateral stainless steel baffle/stiffener plates within the Outer Cavity; neoprene padding present on the inner surfaces of the lower 'W' plates and the aluminum door panels; polyurethane foam in the Outer Cavity; fiberglass material present at some of the metal-metal interfaces.

6.2.1.3.2 Neutron Absorbers

Neutron absorbers have been added to the MAP specifically to limit reactivity during hypothetical accident conditions. The neutron absorbers used in the MAP are borated plates in the Outer Cavity. These panels are permanently fixed to the upper and lower stainless steel plates defining the Fuel Cavity.

6.2.1.3.2.1 Borated Plates

The borated plates are composed of boron carbide (B_4C) and aluminum. Boron carbide is a compound having high boron content in a physically stable and chemically inert form. The two materials (boron carbide and aluminum) are chemically compatible and ideally suited for long-term use. Acceptance testing, described in Section 8, is used to ensure an effective minimum ^{10}B areal density of 0.024 g/cm^2. BORAL® is the form of borated plate used in the packaging, as discussed in Section 8.1.5.2.

6.2.1.4 Neutron-Moderating Materials

Neutron-moderating materials in the MAP include materials of construction and moderator blocks that are part of the flux trap system and enhance the effectiveness of the borated plates.

6.2.1.4.1 Materials of Construction

6.2.1.4.1.1 Polyurethane Foam

Polyurethane foam has potential to act as a neutron moderator/reflector due to its hydrogen and carbon content. Chemically, polyurethane reduces to $C_3H_8(NO)_2$ and has a density of approximately 6 lbs/ft^3 (0.096 g/cm^3).

6.2.1.4.1.2 Neoprene

As a protective padding, neoprene is affixed to the bottom 'W' plate where the fuel assembly rests and on the aluminum door panels that keep the assembly firmly in place. Neoprene has a chemical formula for the monomer unit of C_4H_5Cl and a density of approximately 1.28 g/cm^3. The presence of chlorine indicates that neoprene will act as a slight absorber rather than a moderator.

6.2.1.4.1.3 Nylon in Spacers

There are small beveled nylon spacer blocks that reside within stainless steel carriers that extend downward from the inner part of the lid where the lid stainless steel 'W' plates meet in the lateral center of the container. There are 5 of these blocks spaced incrementally over the axial length of the package.

6.2.1.4.2 Moderator in Flux Trap

The Nylon used in the MAP series of packagings consists of Nylon 6,6. Nylon 6,6 is a polymer consisting of a series of bonded chains with a simplified compound structure of $C_6H_{11}NO$. It is widely used in commercial structural applications including automotive, furniture, power tool housings, and lawn and garden equipment. The term polymer means "many parts" and refers to a molecule formed from many smaller molecules, called monomers, which are linked together into

large molecules. Nylon 6,6 is so named because it is synthesized from two different organic compounds, each containing six carbon atoms.

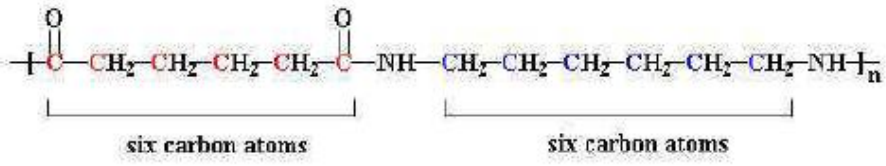

Moderator blocks are attached to the outer surfaces of the borated plates and reside within the top and bottom portions of the Outer Cavity. The minimum thickness of the blocks (i.e. portions that are not beveled) is 1.25 inches (3.18 cm). The moderator is fixed in place with the neutron absorber to form the flux trap system. Many portions of the blocks have bevels at one or more surfaces. Therefore, some parts of the borated plates are not covered by the maximum thickness of moderator. Nylon 6,6 is modeled at a nominal density of 1.14 g/cm^3.

Nylon 6,6 has a manufactured density ranging from 1.13 to 1.15 g/cc. The minimum thickness (1.25") used in the MAP package is not influenced by manufacturing tolerances. Typical manufactured thicknesses range from 1.26" to 1.28". The material is a thermal-plastic with a very high melting temperature ranging from 482 to 509 ^{o}F. The flash ignition temperature for the material is about 752 ^{o}F.[3]

Nylon 6,6 is suitable for packaging applications due to it hardness, abrasion resistance, self-extinguishing ability, and high melting and flash ignition temperatures.

6.2.1.5 Floodable Void Spaces

The MAP packaging and contents contain four floodable regions. These regions have been modeled in various flooding combinations in order to determine the most conservative accident configuration. The floodable regions are shown in Figure 6-4. Flooding is specifically addressed in Section 6.7.1. Note that the fuel-clad gap within the fuel rods in the fuel assembly is <u>not</u> considered as floodable, per the actual as-found condition after HAC testing, which is discussed in

[3] Nylon Plastics Handbook, Melvin I Kohan, 1995, Hanser Gardner Publications.

Section 6.4.5.4. However, in the HAC array size calculations of Section 6.7.7.2, the fuel-clad gap was assumed flooded, and therefore the CSI is conservatively based on the assumption of flooded fuel-clad gap.

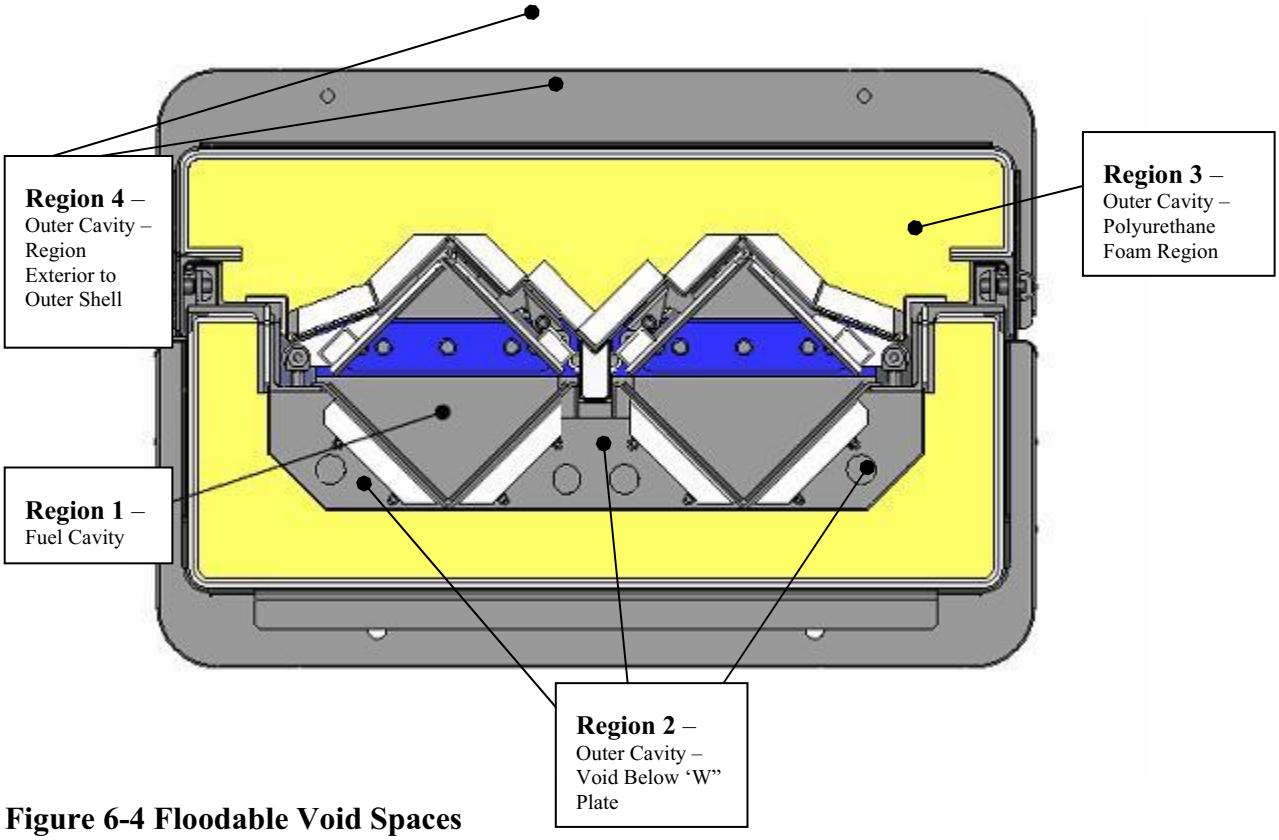

Figure 6-4 Floodable Void Spaces

6.2.1.5.1 Region 1 – Fuel Cavity

The Fuel Cavity includes the region between the angled stainless steel plates defining the bottom surface of the top portion of the Outer Cavity, i.e. lid, and the stainless steel 'W' plates that support the fuel. The Fuel Cavity includes the fuel assembly envelope/inside of rod container. The Fuel Cavity will fill and drain uniformly. Therefore, it is unlikely for areas to be preferentially flooded (i.e. the fuel assembly envelope or rod array) within the Fuel Cavity in a realistic accident condition.

6.2.1.5.2 Region 2 – Outer Cavity – Void Below 'W' Plate

The region below the lower 'W' plates and above the stainless steel liner defining the inner boundary of the polyurethane region for the Outer Cavity is an additional floodable region.

6.2.1.5.3 Region 3 – Outer Cavity – Polyurethane Foam Region

The polyurethane foam region is considered to be a floodable void space under accident conditions. In the analysis, no credit is taken for the presence of the foam under any conditions (normal and accident). It is assumed that this region can contain partial to full density water (0 – 1 g/cc). This will bound the effects of all foam being present, partial amounts of foam being present, or no foam being present with the available space either flooded or dry. The partial water density chosen for license-basis calculations will be the most conservative for the condition under consideration.

6.2.1.5.4 Region 4 – Outer Cavity – Region Exterior to Outer Shell

The region outside the package outer shell, which is defined by the dimensions of the stiffening brackets on the outside of the lid and base of the package, is also considered a floodable void space. This is grouped in the modeling nomenclature as part of the package Outer Cavity, although in reality the region exists outside of the container.

6.2.2 Summary Tables of Criticality Evaluation

Sensitivity studies were performed by evaluating the MAP and determining the most conservative configurations for the normal and hypothetical accident conditions for an individual package and package arrays. The results for the worst cases defined through the sensitivity studies, rounded to four decimal places, are shown in Table 6-1. The results show that the Upper Safety Limit (USL) of 0.94 discussed in Section 6.8.2 is satisfied.

Table 6-1 Summary Table for MAP with PWR Fuel Assembly

	k_{eff} + 2σ
Single Package	
Normal	0.2206
HAC	0.8823
Package Array	
Normal	0.2127
HAC	0.9398

6.2.3 Criticality Safety Index (CSI)

6.2.3.1 PWR Fuel Transport Index

The Criticality Safety Index when transporting PWR fuel assemblies is calculated as follows:

2 * N = Array Size

Array Size = 36

N= 36/2 = 18

Therefore, CSI = 50/18 = 2.8

6.3 FISSILE MATERIAL CONTENTS

The package will be used to carry heterogeneous uranium compounds in the form of fuel rods. These rods will be transported as PWR fuel assemblies. The uranium enrichment shall not be greater than 5.0 wt% ^{235}U. The uranium isotopic distribution considered in the models for this evaluation is shown in Table 6-2.

Table 6-2 Modeled uranium isotopic distribution within uranium material specification

Isotope	Modeled Wt%
^{235}U	5.0
^{238}U	95.0

6.3.1 PWR Fuel Assemblies

The fuel assembly types to be transported in the MAP belong to the 14x14, 15x15, 16x16, and 17x17 families. The specific products covered within these families are not named in this report, but the parameters used for criticality modeling are provided in Appendix 6.9.1.

The MAP-12 will carry assemblies with active fuel lengths up to 12-ft. long (nominal), while the MAP-13 will carry assemblies with active fuel lengths up to 12½ - ft. long (nominal).

The parameters for the fuel assembly types to be allowed for transport in the MAP are summarized in Table 6-3.

Table 6-3 Fuel assembly parameters for Certificate of Compliance

Fuel Rod Array	14x14 (Figure 6-33)		15x15 (Figure 6-34)					16x16 (Figure 6-35)	17x17 (Figure 6-36)	
Assy Type	1	2	1			2	3	1	1	2
# Fuel Rods	176	179	208			216	204	236	264	264
# Non-Fuel Cells	20	17	17			9	21	20	25	25
Nominal Fuel Rod Pitch (inches)	0.580	0.556	0.568			0.550	0.563	0.506	0.502	0.496
Maximum Pellet OD (inches)	0.3812	0.3682	0.3622	0.3707	0.3742	0.3617	0.3682	0.3282	0.3252	0.3232
Minimum Pellet OD (inches)	0.3758	0.3568	0.3608	0.3693	0.3728	0.3593	0.3558	0.3268	0.3238	0.3188
Minimum Fuel Rod OD (inches)	0.438	0.422	0.414	0.428	0.428	0.414	0.422	0.380	0.377	0.372
Minimum Clad Wall Thickness (inches)	0.0245	0.0230	0.0220	0.0245	0.0230	0.0220	0.0230	0.0220	0.0220	0.0205

Fuel Rod Array	14x14 (Figure 6-33)		15x15 (Figure 6-34)					16x16 (Figure 6-35)	17x17 (Figure 6-36)	
Maximum Guide Tube ID (inches)	N/A	N/A	0.500	N/A	N/A	N/A	N/A	N/A	N/A	N/A
Minimum Guide Tube OD (inches)	N/A	N/A	0.528	N/A	N/A	N/A	N/A	N/A	N/A	N/A
Number of Guide Tubes per Assembly	N/A	N/A	16	N/A	N/A	N/A	N/A	N/A	N/A	N/A
Maximum Instrument Tube ID (inches)	N/A	N/A	0.443	N/A	N/A	N/A	N/A	N/A	N/A	N/A
Minimum Instrument Tube OD (inches)	N/A	N/A	0.491	N/A	N/A	N/A	N/A	N/A	N/A	N/A
Number of Instrument Tubes per Assembly	N/A	N/A	1	N/A	N/A	N/A	N/A	N/A	N/A	N/A
Max ^{235}U Loading (kg)	25.44	24.14	27.14	28.43	28.97	28.11	27.51	25.28	27.77	27.43
Clad/Tube Material Type	Zr Alloy	Zr Alloy	Zr Alloy			Zr Alloy	Zr Alloy	Zr Alloy	Zr Alloy	Zr Alloy
Maximum Active Length (inches)	160	160	160			160	160	160	160	160

6.4 MODELING CONSIDERATIONS

The models developed for these calculations are conservative representations of the package that include all of the physical features that are important to criticality safety. This section describes the packaging with contents models.

6.4.1 Model Orientation

Geometry input dimensions are taken directly from design drawings and are derived by stacking dimensions using geometric relationships and dimensions shown on the drawings. Longitudinal dimensions in the model are oriented along the z-axis, and the lateral dimensions are oriented in the x-y plane. The origin of the individual package unit is at the center of the package along the z-axis, at the center of the package along the x-axis, and about 7.3 inches below the center of the package along the y-axis. The positive z direction is from bottom to top of the package along the z-axis; the positive x direction is from left to right along the x-axis when viewed from the top of the package; and the positive y direction is from bottom to top of the lateral cross section along the y-axis when viewed from the top of the package.

6.4.2 Package Model

The package model (contents and packaging) are described in this section.

6.4.2.1 Contents Model

6.4.2.1.1 PWR Fuel Assembly Model: 15 Type 1a

As demonstrated in Section 6.7.1, the 15 Type 1a is the bounding fuel assembly. Therefore, it is used as the base assembly in all single container and package array calculations. The fuel assembly was modeled with an active length (pellet stack length) equivalent to the length of the Fuel Cavity region covered by the Flux Trap (modeled as 163 inches). This is greater than the 150 inch actual maximum active fuel length over all fuel assembly types. No structural components, such as the top and bottom nozzles, rod end caps, or grids were modeled.

The fuel rod clad inner diameter was maximized and the fuel rod clad outer diameter was minimized. This produces the smallest clad wall thickness and maximizes the amount of water in the lattice. The clad material is modeled as pure zirconium to bound any zirconium alloy clad material.

The fuel-clad gap is modeled as void to represent a dry gap. The fuel-clad gap within the fuel rods in the fuel assembly is not considered as floodable based upon the HAC testing and results

presented in Section 2.12.1 as further discussed in Section 6.4.5.4. However, in the HAC array size calculations of Section 6.7.7.2, the fuel-clad gap was assumed flooded, and therefore the CSI is conservatively based on the assumption of flooded fuel-clad gap.

As mentioned in Section 6.7.1, the single container sensitivity studies include minimum GT/IT tube thicknesses in the water holes. However, for the licensing evaluations, the tubes are not modeled, with the exception of the HAC array size licensing evaluations for the most reactive assembly (Section 6.7.7.2), which is due to the fact that the fuel-clad gap was assumed flooded for these evaluations. In addition, these evaluations minimized the pellet diameter since this approach maximizes reactivity when the fuel-clad gap is flooded. Therefore, the pertinent GT/IT parameters as well as the minimum pellet diameter are included here.

Table 6-4 summarizes the most conservative parameters for the 15 Type 1a fuel assembly model used in the evaluation. As in all models for the evaluation, the fuel is modeled at an enrichment of 5.0 wt% ^{235}U and pellet (UO_2) density at 100% Theoretical Density (TD), or 10.96 g/cc.

Table 6-4 Conservative modeling parameters for the 15 Type 1a fuel assembly model

Parameter	Conservative Value (Maximum Tolerances Included)
Maximum Pellet Diameter	0.3622 in (0.91999 cm)
Minimum Pellet Diameter	0.3608 in (0.91643 cm)
Fuel Rod Pitch	0.568 in (1.44272 cm)
Minimum Fuel Rod Clad Outer Diameter	0.414 in (1.05156 cm)
Maximum Fuel Rod Clad Inner Diameter	0.370 in (0.93980 cm)
Minimum Guide Tube Outer Diameter	0.528 in (1.34112 cm)
Maximum Guide Tube Inner Diameter	0.500 in (1.27000 cm)
Minimum Instrument Tube Outer Diameter	0.491 in (1.24714 cm)
Maximum Instrument Tube Inner Diameter	0.443 in (1.12522 cm)
Fuel Rod Clad Material	Zr (bounds any zirconium alloy)
Fuel Rod Active Length	163 inches (414.02 cm)

Enrichment	5.0 wt% ^{235}U
Pellet Density (UO_2 Density)	100% TD (10.96 g/cc)

6.4.2.2 Packaging Model

The packaging model only considers the length of the package that includes the flux trap. The axial end portions of the package are cut off, so that the length modeled is open on either end.

6.4.2.2.1 Fuel Cavity and Flux Trap Model

The actual MAP-13 and MAP-12 flux trap regions are identical except that the axial bottom and top sections of the MAP-12 are 6.38 and 6.53 inches shorter (nominal) than the MAP-12. This gives the MAP-12 a total flux trap length of about 150 inches. In addition, the inside spacer blocks (incrementally spaced over the length of the container) have different axial (z-direction) lengths and the axial spacing between the blocks is different. The blocks for the MAP-12 are 2.5 inches shorter and the center-to-center spacing between blocks reduced by 2.5 inches. The criticality evaluations employ models consistent with the MAP-13. However, one calculation is performed for the bounding HAC array in which the lengths of the bottom and top axial sections are reduced to give a total flux trap length of 150 inches, and the spacer blocks are reduced in length by 2.5 inches and are placed 2.5 inches closer together, to demonstrate that both package designs are bounded by the MAP-13 model (see Appendix 6.9.2). Figure 6-5 shows the Fuel Cavity model with the flux trap surrounding it, and Figure 6-6 shows the flux trap removed.

a)

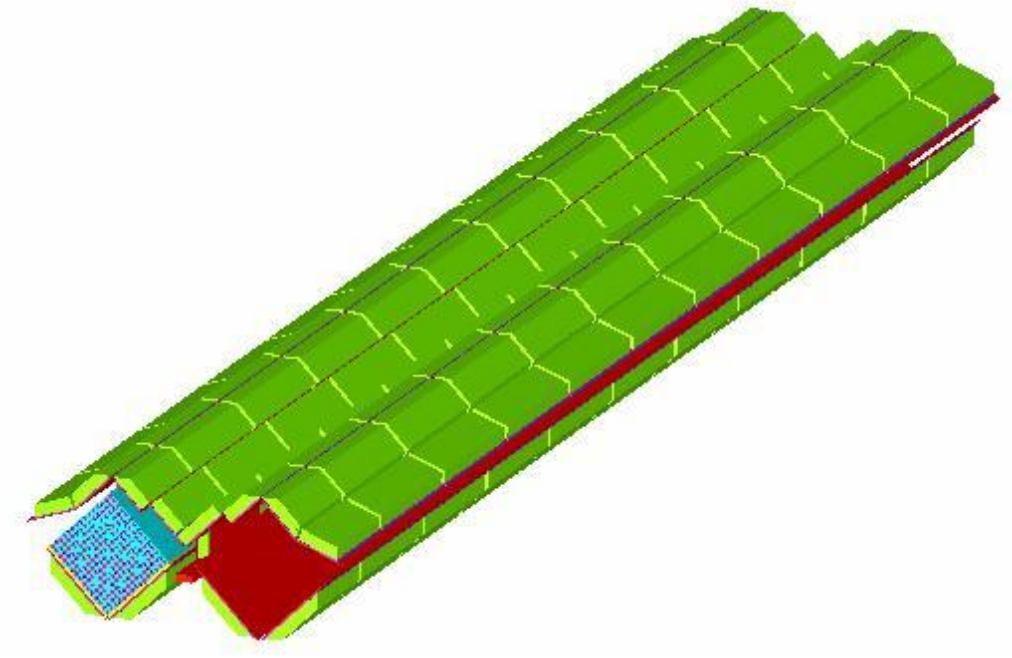

b)

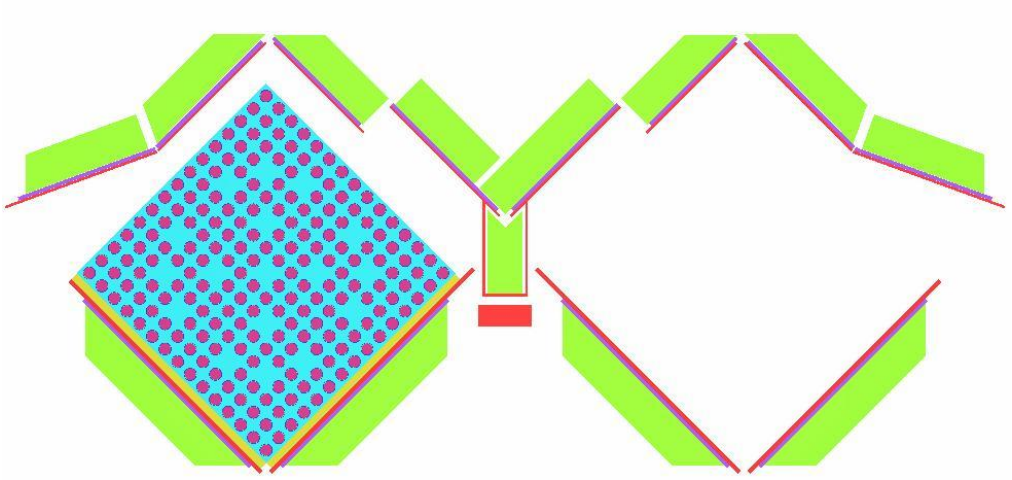

Figure 6-5 Fuel Cavity with surrounding flux trap, fuel assembly placed on one side to illustrate loaded and empty Fuel Cavity; a) is an isometric view, and b) is a lateral cross-sectional view; green=nylon, purple=Boral, red=steel, yellow=neoprene (water), remainder is within fuel assembly envelope

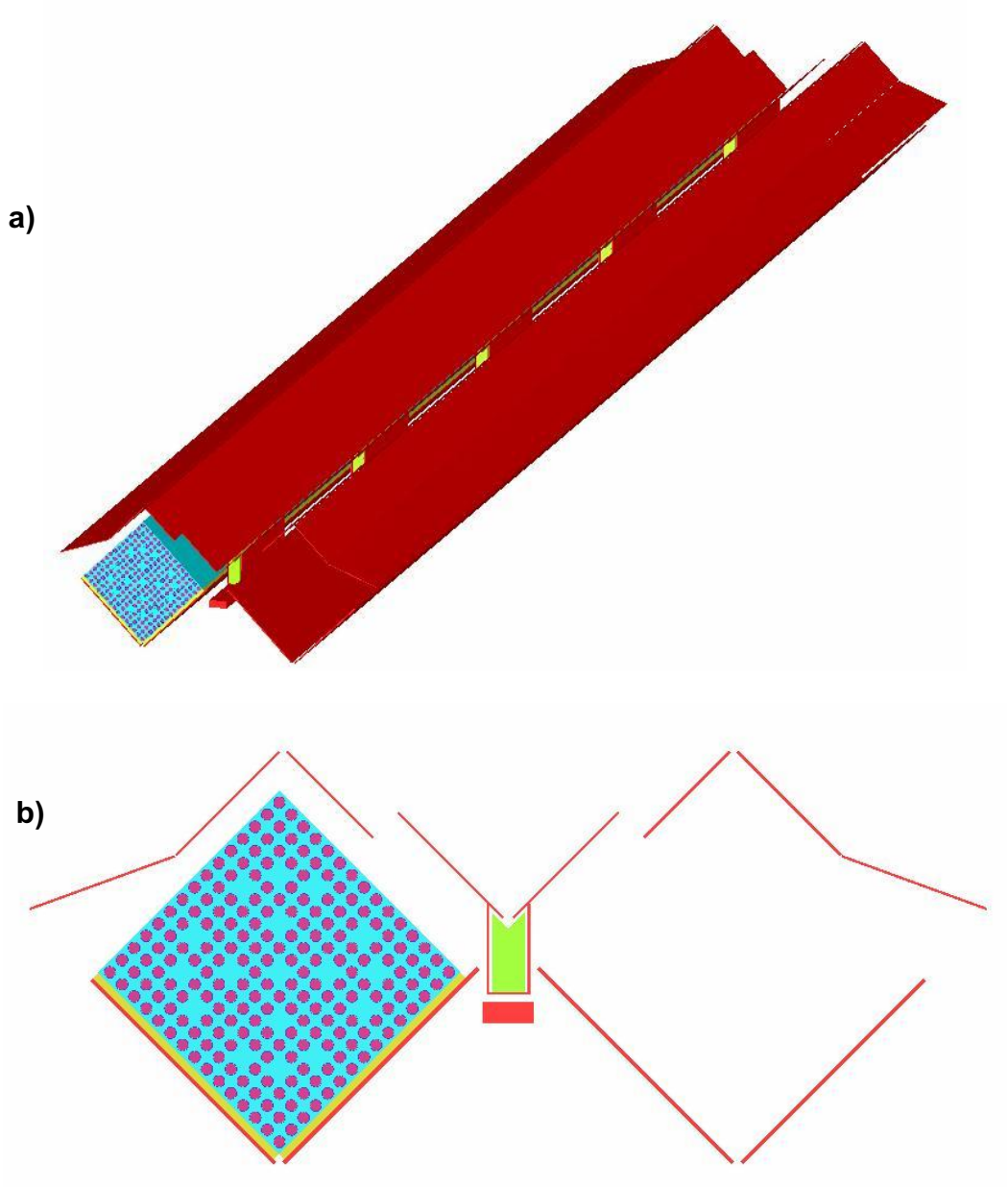

Figure 6-6 Fuel Cavity with surrounding flux trap removed; a) is an isometric view, and b) is a lateral cross-sectional view; green=nylon (only in central blocks), red=steel, yellow=neoprene (water), remainder is within fuel assembly envelope

6.4.2.2.2 Outer Cavity Model

The Outer Cavity is modeled as the packaging components surrounding those shown in Figure 66. This includes the region exterior to the outer steel shell enveloped by the outer stiffeners; however, the outer stiffener structural materials are not modeled. Since the regions occupied by the

polyurethane foam are considered as floodable void spaces, the only additional component added to the portion of the model illustrated in Figure 6-5 is the stainless steel shell, completing the package model. To bound the effects from container crushing, two inches have been conservatively removed from the package envelope width and height. This modeling approach is used for all calculational models employed in the evaluation (even normal conditions). Figure 6-7 shows the Outer Cavity model.

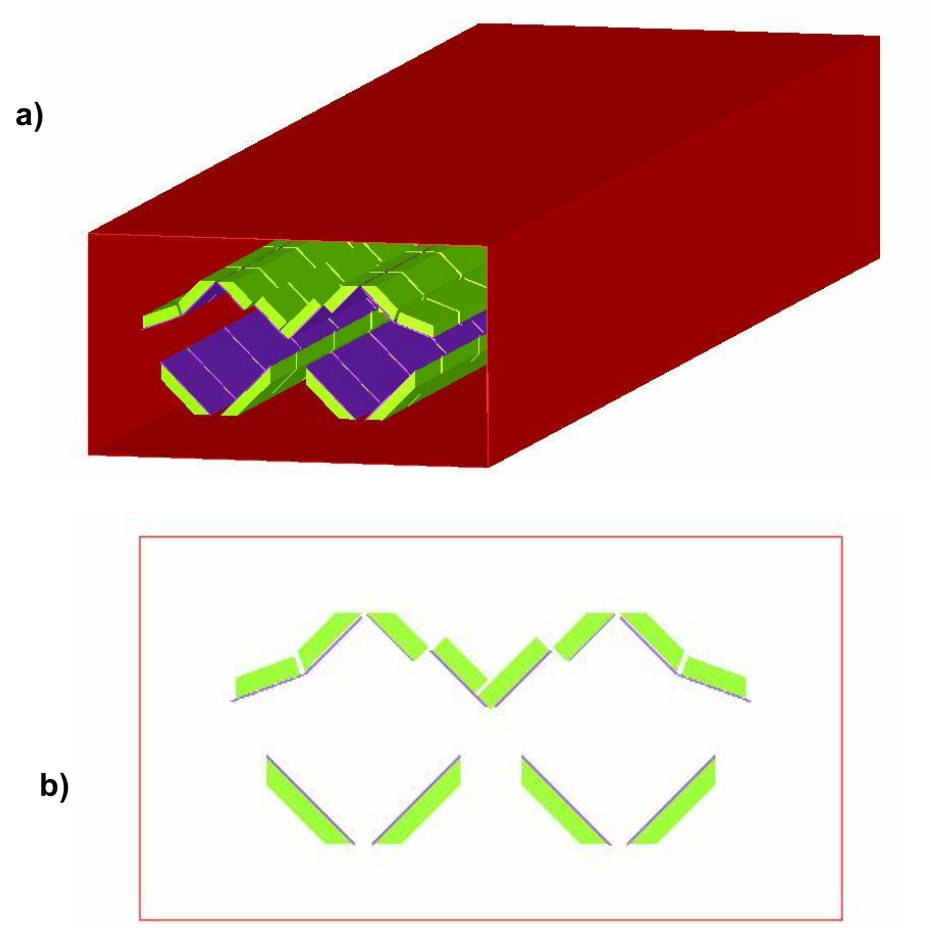

Figure 6-7 Outer Cavity; a) is an isometric view, and b) is a lateral cross-sectional view; green=nylon, red=steel, purple=Boral

6.4.3 Material Properties for Package Model

The Standard Composition Library was used to specify material and mixtures. Those mixtures not found in the library are specified using the procedures for arbitrary mixtures described in the SCALE manual. Table 6-5 illustrates the material specification in a typical input file. The

technique used for modeling certain materials as a void was to replace the material with water at a density of 0.9982×10^{-8} g/cm^3.

Table 6-5 Excerpt from an input deck showing material properties description

```
238g     latticecell
'100% td and 5.0 w/o
uo2  1   1.0 293 92235 5 92238 95 end
'zirc
zr  2   1.0 293 end
'water in assy lattice
h2o  3   1.0 293 end
'volume in container external to bundles
h2o  4   1.0e-8   293 end
'rubber
h2o  5 1.0 293 end
' ss plate, 0.13" thick
ss304  6   1.0   293 end
'  boral, minimum areal density(at min thk)=0.0240 gm b-10/sqcm
' min thk = 0.119" = 0.30226cm
' vol dens = 0.0240/(0.30226*0.18431) =0.4308 gm natural b/cucm
' we use only 75%, 0.75 * 0.4308 = 0.3231 gm natural b/cucm
b  7   den=0.3231 1 293 end
'nylon 66
arbmnyl 1.14 4 0 1 0 6012 6 7014 1 8016 1 1001 11 8 1.0 293 end
'reflector water
h2o  9   1.0 293 end
' ss plate, 0.085" thick
ss304  10   1.0   293 end
' ss plate, 0.115" thick
ss304  11   1.0   293 end
' gap water
h2o  12   1.0 293 end
' ss bar at center
ss304  14   1.0   293 end
end comp
```

To more fully document the composition of each compound and/or document the assumptions used in producing the associated cross-section data, a brief description of each material is given in Table 6-6.

Table 6-6 Material Descriptions

UO2: Uranium dioxide (UO_2) – 10.96 g/cm^3	**ZR:** Zirconium (Zr) – 6.49 g/cm^3
H2O : Water (H_2O) – Varying densities from 0–0.9982 g/cm^3 This also represents: • Polyurethane foam, chemical formula is $C_3H_8(NO)_2$, and uncrushed density is approximately 0.096 g/cm^3 • Neoprene, chemical formula is C_4H_5Cl, and density is approximately 1.28 g/cm^3	**SS304:** Stainless Steel-304 – 7.94 g/cm^3 • 68.375 wt% iron • 19 wt% chromium • 9.5 wt% nickel • 2 wt% manganese • 1 wt% silicon • 0.08 wt% carbon • 0.045 wt% phosphorus
B: Boron (B) – 0.3231 g/cm^3 • 0.0180 g/cm^2 ^{10}B areal density (0.0240 g/cm^2 minimum ^{10}B areal density with 75% ^{10}B credited) • Volumetric B density calculated from ^{10}B areal density smeared over 0.119 inch minimum total borated plate thickness, and 18.431 wt% ^{10}B in natural B	**ARBMNYL:** Nylon 6,6 – 1.14 g/cm^3 • Reduced chemical formula is $C_6H_{11}NO$

6.4.3.1 Package to Model Comparison

The masses of the materials in the packaging model were obtained using the volume option with Monte Carlo sampling in KENO-VI. The model volume is multiplied by the material density to obtain the model mass for each material. There are some materials in the actual package that are not included in the package model. Tables 6-7 – 6-8 compare the model mass quantities to the actual for the packaging and contents, respectively. The actual mass of materials is obtained from design drawings for the package.

Note that boron is not included in Table 6-7. The model credits 75% of the minimum ^{10}B areal density of 0.0240 g/cm^2, which equates to 0.0180 g/cm^2, modeled areal density. Natural boron (B) is smeared over the minimum plate thickness of 0.119 inch (0.125 inch minus 0.006 inch tolerance, see Section 8). The lateral borated plate dimensions were modeled at nominal values. Note that the aluminum in the BORAL® absorber material as well as the carbon in B_4C are excluded from the model.

Table 6-7 Actual Mass versus Modeled Mass – Packaging

Material	Density	Approx. Modeled Mass		Approx. Actual Mass	Approx. Percent of Actual Mass
SS-304	7.94 g/cc (496 lb/ft^3)	485 kg (1070 lb)		1,635 kg (3605 lb)	30%
Nylon	1.14 g/cc (71.2 lb/ft^3)	*Flux Trap – Lid*	103 kg (227 lb)	121 kg (267 lb)	85%
		Flux Trap – Base	83.8 kg (185 lb)	92.8 kg (205 lb)	90%
		Flux Trap – Total	187 kg (412 lb)	214 kg (471 lb)	87%
		Spacer Blocks	2.91 kg (6.41 lb)	3.81 kg (8.39 lb)	76%
		Total	190 kg (419 lb)	218 kg (480 lb)	87%

None of the materials in the fuel assembly other than the zirconium (bounds zirconium alloy) cladding and the uranium dioxide pellet stack are included in the model. The uranium dioxide actual mass is less than the model mass because the theoretical density of sintered uranium dioxide is used in the model (10.96 g/cc); however, the actual density is not expected to exceed 98 percent of the theoretical density. Additionally, the fuel rod pellet stack (active length) is modeled much longer than in reality (modeled as 163 inches, whereas actual active lengths do not exceed 150

inches). The zirconium mass is less in the model because the spacer grids and any other components containing zirconium, other than rod cladding, are not included.

Zirconium is not included in Table 6-8 since the modeling practice was to minimize the cladding outer diameter and thickness in the fuel assembly model per the specifications in Appendix 6.9.1. This ensures a conservative modeling approach since the floodable volume within the fuel assembly envelope is maximized.

Table 6-8 Actual Mass versus Modeled Mass – Contents

Material or Isotope	Density	Approx. Modeled Mass	Approx. Actual Mass (Maximum)	Approx. Percent of Actual Mass
UO_2	10.96 g/cc (Theoretical Density)	1,336 kg (2,945 lb)	1,148 kg (2,531 lb)	116%
^{235}U	0.4831 g/cc (for 100% UO_2 TD and 5.0 wt% ^{235}U)	59 kg (130 lb)	51 kg (112 lb)	116%

6.4.4 Computer Codes and Cross-Section Libraries

The 238-group ENDF/B-V library was utilized in this analysis with the CSAS26 code option of SCALE4.4a. The use of this cross-section library and code option was validated against 55 critical benchmark experiments with adequate similarities to the MAP package. Section 6.8 describes the code validation and determination of the Upper Safety Limit (USL) for this evaluation.

Table 6-26 in Section 6.8 verifies that the validation benchmarks adequately represent the range of parameters for the MAP package.

6.4.5 Demonstration of Maximum Package Reactivity

This section summarizes the features of the licensing-basis models that represent the most reactive configurations for a single package, an array of undamaged packages, and an array of damaged packages. The evaluations of these configurations with the appropriate licensing-basis models are discussed in Sections 6.5 and 6.6.

The licensing-basis models implement modifications to the as-built MAP configuration to enhance the reactivity of the MAP configuration relative to contents, moderation, materials of construction, and package condition. This section describes modeling of the most reactive fuel assembly, flooding conditions, conservative material assumptions, as well as the package configuration based upon pre-test (normal) and post-test information. Table 6-9 itemizes the differences between the as-built package, the normal condition model, and the HAC model with the as-found test results that form the bases for the models.

6.4.5.1 Assumptions for Maximizing Reactivity

This section summarizes the modeling assumptions that maximize reactivity. These assumptions relate to the package contents, flooding, and materials.

6.4.5.1.1 Most Reactive Fuel Assembly Type (Contents)

The most reactive fuel assembly type was determined by comparing all PWR fuel assemblies to be transported in the MAP. The results of this analysis are presented in Section 6.7.1. The assumptions and conservatisms are summarized below:

- Assumed 100% TD
- Assumed dry pin-gap (fuel-clad gap) for all calculations except the HAC array size licensing evaluations of Section 6.7.7.2, in which it was assumed that the fuel-clad gap was flooded, which maximizes reactivity
- Ignored burnable poisons (e.g. Gd, boron)
- Minimized fuel cladding outer diameter (maximizes amount of space available for water in lattice)

- Minimized fuel cladding thickness
- Guide or instrument tubing not credited (in water holes) to maximize amount of water for all calculations except for the HAC array size licensing evaluations of Section 6.7.7.2 for the most reactive assembly type (for these calculations, it was necessary to credit minimum GT/IT volumes within the assembly lattice due to the fact that the fuel-clad gap was assumed floodable)
- 163 inch active fuel length modeled (150 inch actual maximum)
- No additional fuel assembly structures

6.4.5.1.2 Most Reactive Flooding Configurations

The most reactive flooding configurations are defined for a single package and a package array. The respective configurations were determined by modeling the floodable void spaces (see Section 6.2.1.5) in different combinations to determine which combination produces the highest k_{eff}. The combinations considered water immersion (full density water) or low density moderation (such as burial in snow). The flooding scenarios are discussed in Section 6.7.2. The most reactive flooding configuration for a single package is described in Section 6.5.1.2. The most reactive flooding configuration for a package array is described in Section 6.6.1.2. The most reactive flooding cases for the individual package and package array cases are summarized in Table 6-9.

6.4.5.1.3 Conservative Material Assumptions

The following conservative material assumptions, which are demonstrated through sensitivity studies in Section 6.7, are used in the package model:

Metals (stainless steel and aluminum)

- The MAP outer stainless steel shell is conservatively modeled with lateral outer dimensions to bound one inch of crushing on all x-z and y-z faces for both normal and HAC conditions. The 11GA ASTM A240 Type 304 sheet is modeled with a thickness of 0.115 inch, rather than 0.12 inch nominal thickness for 11GA sheet.

- The lower and upper stainless steel 'W' plates (boundaries of the Fuel Cavity) are modeled at 0.13 and 0.085 inch, respectively, rather than nominal thicknesses of 0.14 inch (10GA sheet) and 0.09 inch (13GA sheet).
- The stainless steel bar running along the container length is modeled with a width (x) and height (y) of 1.70 and 0.70 inch, respectively. This represents dimensional reductions of 0.05 inch which covers tolerances.
- The stainless steel 'shell' for the central spacer blocks attached to the top 'W' plate is modeled with thickness of 0.085 inch, rather than the nominal thickness of 0.09 inch for 13GA sheet. The steel sheet material for the axial ends of the individual spacers is not modeled.
- No other metal component of the packaging are modeled, such as aluminum (for the doors and latching mechanisms), or any other components containing stainless steel. The latter would include the axial end regions beyond the length covered by the flux trap (impact limiters, sheet material at the axial ends of the base and lid weldments, and associated angles, supports, welds, etc.), the outer stiffener spacers (two on lid and two on base), the inner stiffeners, and any other structural materials within the container itself (radial baffle plates, lid and base rails/supports, angles, supports, welds, bolts, nuts, washers, etc.).

Nylon

- The moderator blocks for the flux trap system are modeled with a uniform dimensional reduction that results in ~87% (see Tables 6-7 and 6-9) of the total moderator block volume for the flux trap being modeled. The method was to remove 0.0781 inch from all block faces with the exception of the faces contacting the absorber plates. The faces created due to the axial gaps between blocks are included. This resulted in a reduction in the lid moderator blocks of ~85% due to the larger surface area (bevels) as compared to the base moderator blocks that were reduced ~90%. The moderator material is modeled at full nominal theoretical density for Nylon 6,6 (1.14 g/cc).

  The thickness reduction bounds any effective loss of the nylon resulting from the thermal test (see Section 2.12.1) and due to any density variations.

The criticality assessment considered both dimensional and density reductions with dimensional reductions leading to higher k_{eff} results. The most reactive modeled condition involved a Nylon 6,6 density of 1.14 g/cc with thicknesses reduced by 10%. Nylon 6,6 at a density of 1.14 g/cc has a Hydrogen density of 11.1%. Reducing the Nylon 6,6 density to 1.13 g/cc reduces the Hydrogen density to 11.0%. Variations in the Nylon 6,6 density within the manufactured range have negligible effect on Hydrogen density of the compound. The manufactured thicknesses of 1.26" to 1.28" (1.25" minimum) for moderator blocks used in the MAP package more than off-sets this negligible variation.

This variation in density will have a negligible effect on the modeled ~87% credit for the Nylon 6,6 thickness. Modeled as a reduced thickness, the reduction was used to bound minor melting experienced during the HAC fire test and not to bound dimensional manufacturing tolerances. Based on the results of the fire test, the modeled 87% credit for the Nylon 6,6 moderator blocks bounds the loss experienced in a single section. The modeled configuration is therefore very conservative with respect to the HAC test results.

- The beveled nylon blocks, which comprise the volume of the central spacer blocks, are included in the models. Each face of the nylon blocks had 0.0781 inch removed. This results in more moderator being removed in the lid as opposed to the base.

Boron

- The ^{10}B content in the borated absorber plates is modeled at 75% of the minimum areal density for BORAL® (0.0180 g/cm^2) as specified in Section 8.

Neoprene

- The neoprene padding on the bottom (base) 'W' plates is represented by full density water in the model. This is conservative because neoprene contains chlorine (chemical formula C_4H_5Cl) which is a relatively effective neutron absorber.

Polyurethane Foam

- The polyurethane is not modeled explicitly. Rather, the region it would normally occupy is interpreted as a floodable void space in which partial water densities are possible.

Because the void space is optimized, this approach bounds the moderating effects of the foam under all conditions.

Other Materials

- No other materials present in the container are included in the models. The materials in the actual container that are not modeled are replaced by floodable void space.

6.4.5.2 As-Built Packaging

The as-built data represents the routine configuration for the MAP package. The as-built packaging is not modeled; however, it is summarized in order to show the inherent conservatism that exists in the normal condition of transport models. The as-built packaging is bounded by the normal condition of transport model.

6.4.5.3 Normal Condition of Transport

The MAP model under normal condition of transport is described as follows:

- The outer shell, the 'W' plates, the 'shell' for the spacer blocks, and the steel bar are modeled as in Section 6.4.5.1.3.
- Fuel assembly is modeled as in Section 6.4.5.1.1, except that it is dry rather than flooded.
- The moderator blocks (in flux trap and spacer blocks) are modeled as in Section 6.4.5.1.3.
- The neutron absorber is modeled as in Section 6.4.5.1.3.
- The polyurethane foam is modeled as a floodable void space, as described in Section 6.4.5.1.3.
- The floodable void spaces that reside within the Outer Cavity are modeled with the worst case partial or full water density (single container or container array, in which worst case Outer Cavity water densities are different), see Table 6-9.
- The floodable void space that resides within the Fuel Cavity is modeled dry.
- The single container and container array are both reflected by 30 cm close-fitting water.

The MAP shipping package has been designed and constructed such that under the tests specified for normal conditions of transport:

- The contents are subcritical.
- The geometric forms of the package contents are not altered.
- There is no inleakage of water.
- There is no reduction in effectiveness of the packaging.

Section 2.12.1 describes the Certification Test Unit (CTU) following the normal condition tests.

6.4.5.4 As-Found Condition after HAC Testing

The condition of the MAP package after HAC testing is described in Section 2.12.1. The as-found condition is described so comparisons can be made between it and the licensing-basis models.

The key features of the as-found condition after HAC testing with respect to criticality are as follows:

- Fuel rod cladding did not crack or rupture – This allows the licensing-basis assumption that the fuel-clad gap is dry under the worst-case HAC condition. However, in the HAC array size calculations of Section 6.7.7.2, the fuel-clad gap was assumed flooded.
- No fuel assembly lattice expansion was observed. The worst case damaged test assembly had a maximum envelope that fit within the original undamaged envelope. In fact, lattice compression was observed, which diminishes the fuel assembly reactivity, so the nominal lattice remains bounding – This allows the licensing-basis assumption that lattice expansion does not occur under the worst-case HAC condition.
- Fuel Cavity geometry was maintained. The fuel assembly did not laterally shift outside of the original envelope placement on the strong-back nor did it axially shift outside of the flux trap region. No change in the geometric placement of the surrounding flux trap components occurred – This allows the licensing-basis assumption that no geometric modeling deviations need to be made from the normal Fuel Cavity and surrounding flux trap specifications or fuel assembly placements.

- Minor melting of the moderator blocks in the flux trap occurred. The most affected axial section of moderator blocks occurred in the lid (see Table 2.12.1-4 of Section 2.12.1). For this entire section, the average nylon loss was ~2.1% of the original weight, so it would be conservative to assume that all nylon within the flux trap (lid and base) lost ~2.1%. The two most heavily affected blocks (B4/(6) and B6/(5), as defined in Figure 2.12.1-70 and shown in Table 2.12.1-5) which melted together lost ~8.6% of their original combined weight. As shown in Table 6-7, the models for the moderator blocks credited ~85% of the lid block mass, ~90% for the base block mass, and ~87% combined – This validates the approach for the licensing-basis models for the moderator blocks.

- The lid drop test resulted in crushing of its outer stiffeners which provide spacing between containers in an array – Thus, the licensing-basis models remove the spacing provided by the lid outer stiffeners for array cases. A sensitivity study in Section 6.7.8 confirms that the loss of spacing is conservative.

- The drop tests resulted in a ½ inch to 1½ inch reduction of the outer shell height due to lid compression. The global modeling approach reduced the package envelope width and height dimensions by 2 inches for both normal and HAC conditions – This validates the approach for the licensing-basis models for the outer shell.

6.4.5.5 Licensing-Basis Models

The licensing-basis models bound the as-found condition of the MAP by combining the most reactive flooding configuration, the conservative material assumptions of Section 6.4.5.1.3, the worst case fuel assembly of Section 6.4.5.1.1, and the as-found condition after HAC testing described in Section 6.4.5.4. The licensing-basis models are summarized in Table 6-9 and described below:

- The outer shell, the 'W' plates, the 'shell' for the spacer blocks, and the steel bar are modeled as in Section 6.4.5.1.3. The spacing provided by the lid stiffeners is eliminated per the as-found condition described in Section 6.4.5.4.

- Fuel assembly is modeled as in Section 6.4.5.1.1.

- The nylon blocks are modeled as in Section 6.4.5.1.3.
- The neutron absorber is modeled as in Section 6.4.5.1.3.
- The polyurethane foam is modeled as a floodable void space as in Section 6.4.5.1.3.
- The floodable void spaces that reside within the Outer Cavity are modeled with the worst case partial or full water density, see Table 6-9.
- The floodable void space that resides within the Fuel Cavity is modeled with the worst case flooding configuration, see Table 6-9.
- The single container and container array are both reflected by 30 cm close-fitting water.

Table 6-9 Summary of Packaging Modeling and Conservatisms

Parameter	**As-Built**	**Normal Condition Model**	**As-Found Condition After HAC Testing**	**HAC Condition Model**
Package Dimensional/Material Characteristics				
^{10}B Density in absorber	Minimum density (0.0240 g/cm^2)	75% of minimum (0.0180 g/cm^2)	No damage observed	75% of minimum (0.0180 g/cm^2)
Nylon Weight in Flux Trap	Nominal weight	~87% of nominal overall (~85% in Lid, ~90% in Base)	Two Lid blocks lost 6.6% (2.1% average loss in Lid, no loss in Base)[4]	~87% of nominal overall (~85% in Lid, ~90% in Base)
Mass of structural stainless steel	~1,635 kg (3605 lb)	~485 kg (1070 lb) (~30% of as-built)	N/A	~485 kg (1070 lb) (~30% of as-built)
Outer Shell Thickness	Nominal thickness (0.12 inch)	0.115 inch	N/A	0.115 inch

[4] See Table 2.12.1-5 – Post Burn Test Characterization of Moderator in Segment #5 and Figure 2.12.1-70.

Parameter	As-Built	Normal Condition Model	As-Found Condition After HAC Testing	HAC Condition Model
Outer Stiffener Dimensions	Nominal dimensions (44.98 inches wide x 30.78 inches high)	2 inch reduction from nominal width and height	½ – 1½ inch compression in lid height reduces the package envelope; significant damage to lid stiffeners in the form of buckling, but spacing was not completely lost	2 inch reduction from nominal width and height plus complete removal of lid stiffener spacing
Outer Stiffener Materials	Stainless steel	Not modeled	Stainless steel	Not modeled
Fuel Assembly Lattice Pitch Expansion	None	None	Envelope compression, but no lattice expansion	None
'W' plate protective pads	Neoprene	Water at 0.9982 g/cm^3	No damage observed	Water at 0.9982 g/cm^3
Fuel Rod Fuel-Clad Gap	Dry	Dry	No rod cracking/failure	Dry or flooded, CSI based on flooded gap
Moderator Characteristics of Floodable Spaces (Excluding Nylon)				
Fuel Cavity	No moderator ingress	No moderator ingress	N/A	Fully flooded
Outer Cavity	Polyurethane at 6 lbs/ft^3 (0.096 g/cm^3)	Void (H2O at 0.9982×10^{-8} g/cm^3) to fully flooded (H2O at 0.9982 g/cm^3)	Significant charring, loss of material	Void (H2O at 0.9982×10^{-8} g/cm^3) to fully flooded (H2O at 0.9982 g/cm^3)

6.5 SINGLE PACKAGE EVALUATION

Calculations were performed to determine the most reactive configuration for a single package in isolation under normal and hypothetical accident conditions of transport. The configurations and results are described below.

6.5.1 Configuration for MAP Package with Fuel Assemblies

6.5.1.1 Normal Conditions of Transport

For normal conditions of transport, 10CFR71 requires that the contents be subcritical. The individual package evaluation includes 30 cm close-fitting water reflection around the Outer Cavity. The parameters for the normal condition of transport are summarized in Table 6-9.

6.5.1.2 Hypothetical Accident Conditions

The hypothetical accident condition requires that the most reactive flooding configuration be considered. Generally, the most reactive configuration for an individual package would be that in which the neutrons are moderated as close to the fuel as possible and reflected back into the fuel assembly region. They should not be allowed to escape or to reach the neutron absorber where they could be absorbed. Calculations have shown that this is the case for the MAP. Therefore, all floodable void spaces in the package are modeled as fully flooded with the package close-reflected by 30 cm full density water. The remaining parameters for the licensing-basis case for the MAP are summarized in Table 6-9.

6.5.2 Deleted

6.5.3 Results for MAP Package with Fuel Assemblies

The results for the single package with fuel assemblies are presented in Table 6-10. They include results for normal conditions of transport and hypothetical accident conditions and show that the 0.94 USL is satisfied.

Table 6-10 Results for Single Package with Fuel Assemblies

Configuration	Calculated k_{eff}	Uncertainty (σ)	$k_{eff} + 2\sigma$
MAP with Fuel Assembly			
Normal	0.2192	0.0007	0.2206
HAC	0.8791	0.0016	0.8823

6.6 PACKAGE ARRAY EVALUATION

Calculations were performed to determine the most reactive configuration for a package array under normal and hypothetical accident conditions of transport. The configurations are described below.

6.6.1 Configuration for MAP Package with Fuel Assemblies

6.6.1.1 Normal Conditions of Transport

The package model for the normal condition of transport is summarized in Table 6-9. For this analysis the package was modeled in an infinite array which bounds the 5N array.

6.6.1.2 Hypothetical Accident Conditions

The most reactive configuration for the package array under HAC conditions (licensing-basis case), in contrast to a single package, is the one that maximizes neutron interaction between the fuel regions. Thus, the Fuel Cavity is fully flooded while the Outer Cavity is voided, maximizing neutron interaction between fuel regions. The configurations for the Outer Cavity, Fuel Cavity, and contents under hypothetical accident condition models for the MAP are summarized in Table 6-9. The package was modeled in a 2N array (2N=36 packages).

6.6.2 Deleted

6.6.3 Results for MAP Package with Fuel Assemblies

The results for package arrays under normal conditions of transport and hypothetical accident conditions are presented in Table 6-11 and satisfy the USL.

The results for package arrays under hypothetical accident conditions provide the basis for a Criticality Safety Index (CSI) of 2.8.

Table 6-11 Results for Package Array with Fuel Assemblies

Configuration	Calculated k_{eff}	Uncertainty (σ)	$k_{eff} + 2\sigma$
MAP with Fuel Assembly			
Normal (Infinite Array)	0.2113	0.0007	0.2127
HAC (Maximum k for ≤ 2N Array)	0.9380	0.0009	0.9398

6.7 SENSITIVITY STUDIES

This section discusses sensitivity studies performed to ensure that the normal and licensing-basis models provide bounding results relative to fabrication tolerances, package conditions, and HAC. The following sensitivity studies were performed:

- Fuel Assembly optimization: this determines the most reactive fuel assembly based on optimized specification parameters.
- Flooding in the package: this addresses both preferential flooding of the fuel assembly envelope, non-preferential flooding of the Fuel Cavity floodable void space, partial flooding (variable flooding height) of the Fuel Cavity, and interspersed moderation water density variation in the Fuel Cavity and Outer Cavity floodable void spaces.
- Flux trap effectiveness: fixed moderator density, ^{10}B density in absorber, and removal of various flux trap components.

- Non-flux trap packaging material modeling: neoprene and minimum structural materials.
- Variations on the degree of interaction between assemblies in the same container.
- Shifting of the assemblies laterally along lower 'W' plates (x-y directions) and axially relative to flux trap region.
- Package array size and orientation.
- Lid stiffener spacing removal.

6.7.1 Fuel Assembly Optimization

The fuel assembly types to be transported in the MAP belong to the 14x14, 15x15, 16x16, and 17x17 families. While the specific products covered within these families are not listed in this report, the parameters important to criticality are described in Appendix 6.9.1. Note that all fuel assembly types were modeled with a 163-inch active length to conform to the package model. The MAP-12 will carry assemblies with active fuel lengths up to 12-ft. long (nominal), while the MAP-13 will carry assemblies with active fuel lengths up to 12½ - ft. long (nominal).

Since this evaluation covers both package lengths without providing limitations to the types of fuel that can be carried in either package, the calculations performed are not specific to the fuel assembly lengths. The fuel type is defined by the fuel pin layout which depends on the array size (e.g. '15x15', or just '15' for simplicity), the location of water holes (non-fueled cells), and the fuel rod pitch (unit cell dimension). For each fuel assembly type, the worst case is determined. The analysis compares the bounding k_{eff} values for each fuel assembly type, fully flooded and 30 cm water-reflected, with flooded or non-flooded fuel-clad gap, and either the minimum or maximum pellet diameter. The analysis shows that the bounding fuel assembly type is the 15 Type 1 (15 Type 1a which bounds Types 1b and 1c) so this was used in all package calculations with fuel assemblies.

- The worst cases for all assembly types have a minimum pellet diameter for a flooded fuel-clad gap, and with a maximum pellet diameter for a dry fuel-clad gap. The calculated values for maximum pellet diameter and dry gap are either greater than those for the minimum pellet diameter and dry gap, or are well within statistical uncertainty. Likewise,

the same is true for flooded gap cases with minimum pellet diameter. For a flooded fuel-clad gap, the reason is that minimizing the pellet diameter maximizes the amount of water within the assembly lattice, which maximizes reactivity since PWR fuel assemblies are inherently undermoderated (by design). For a dry fuel-clad gap minimizing the pellet diameter has no effect on the amount of water within the assembly lattice; rather, maximizing the pellet diameter also maximizes the amount of fuel in the assembly while having insignificant effect on the thermal neutron flux at the outer pellet surface. Table 6-12 provides the results. The table shows the results for maximum pellet diameter, minimum pellet diameter, and a third result for only the 15 Type 1 (worst case assembly) with minimum thickness guide tube/instrument tubes added to the water holes. The latter calculation was performed because the single container sensitivity studies included this tubing in the water holes, and the result demonstrates that 1) having no guide tube/instrument tubes present in the water holes is conservative, and 2) the effect produced by the tubes in the water holes is small ($\leq$ 0.7 %Δk). All bounding single container or package array (normal condition or HAC) cases in this evaluation exclude this tubing in the models, with the exception of the HAC array size licensing evaluations of Section 6.7.7.2 for the most reactive assembly type (for these calculations, it was necessary to credit minimum GT/IT volumes within the assembly lattice due to the fact that the fuel-clad gap was assumed flooded).

Note that the HAC testing showed no fuel assembly lattice expansion or rod cracking (see Table 6-9). Therefore, no lattice pitch increase or flooding of the fuel-clad gap is necessarily assumed in the evaluation. However, the HAC array size licensing evaluations of Section 6.7.7.2 do assume that the fuel-clad gap is flooded. Table 6-12 shows flooded fuel-clad gap results for comparison.

Table 6-12 Key results for single PWR fuel assembly calculations

Array Size	Type	$k_{eff} + 2\sigma$		
		Max Pellet Diameter	**Min Pellet Diameter**	**Most Reactive Pellet Diameter – GT/IT Clad Added to Water Holes**
Dry Fuel-Clad Gap				
14x14	1	0.9196	0.9200	–
	2	0.9068	0.9035	–
15x15	**1**	**0.9605**	0.9549	0.9535
	2	0.9124	0.9124	–
	3	0.9459	0.9406	–
16x16	1	0.9243	0.9206	–
17x17	1	0.9543	0.9512	–
	2	0.9477	0.9482	–
Flooded Fuel-Clad Gap				
14x14	1	0.9290	0.9316	–
	2	0.9152	0.9175	–
15x15	**1**	0.9644	**0.9661**	0.9628
	2	0.9232	0.9264	–
	3	0.9538	0.9624	–
16x16	1	0.9301	0.9285	–
17x17	1	0.9616	0.9614	–
	2	0.9540	0.9581	–

6.7.2 Package Moderation Studies

The MAP package has been designed to prevent water intrusion into the package. However, because immersion tests have not been performed, it is necessary to optimize moderation within the package during normal and HAC conditions. The sensitivity evaluation considers the MAP under various moderator densities and flooding schemes to determine the most reactive flooding combinations for both the individual package and the array. The analysis assumes the fuel assembly is moderated with full density water in all cases to optimize the system reactivity. Thus, the moderator density variations only consider areas external to the fuel assembly envelope in the Fuel Cavity and in the Outer Cavity for a single package or a package array. A minor modeling difference from the licensing-basis models is the introduction of water into the pellet-clad gap. As illustrated in Table 6-12 this provides a slight increase in reactivity that will not affect the conclusions of this sensitivity study.

6.7.2.1 Single Package Evaluation

The sensitivity studies for as single package consider reactivity effects related to the flooding height (partial flooding) within the Fuel Cavity and interspersed moderator density effects within the package. The models all assume a 30 cm reflector around the package shell and full flooding within the fuel assembly envelope.

The results of these studies show that full flooding in the Fuel Cavity and voiding of the Outer Cavity represents the most reactive package configuration. This validates the use of these conditions in the single container licensing-basis model.

6.7.2.1.1 Partial Flooding

Partial flooding represents a change in the water level in void spaces of the package. Calculations were performed to evaluate two partial flooding scenarios: variable water level heights in the Fuel Cavity for a single container with the container upright, i.e., top facing up, and with the container inverted with top facing down. In the first scenario, the water level rises from the bottom of the Fuel Cavity toward the top. In the second scenario, the water level rises from the top toward the bottom. Figures 6-8 and 6-9 illustrate the modeling for the partial flooding evaluation.

The results shown in Figure 6-10 illustrate the relationship between reactivity (k_{eff}) and incremental addition of water from the bottom to the top of the Fuel Cavity and from the top to the bottom. When water is added to the top of the Fuel Cavity (scenario 2), k_{eff} immediately begins to increase as the top half of fuel assembly envelope is covered by water (~ 80–90% of the assembly half-diagonal measured from the center of the assembly) and levels off as the remainder of the Fuel Cavity is fully flooded. When water is added to the bottom of the Fuel Cavity (scenario 1), k_{eff} does not begin to increase until a small portion of the fuel assembly envelope is covered (~ 10–20% of the assembly half-diagonal). This likely occurs because covering the small portion of the envelope at the bottom (lower portion) of the Fuel Cavity has little impact on neutron leakage from the fuel assemblies, while covering the remaining upper portion significantly reduces leakage due to the gap between the assembly and the upper 'W' plate.

As the 2σ error bars indicate in Figure 6-10 there is no statistically significant difference between k_{eff} for the 80% case of scenario 2 and the fully flooded Fuel Cavity. The difference between k_{eff} + 2σ for the peaks is ~ 0.32% Δk with a propagated 2σ uncertainty of ~ 0.45% Δk*. The results demonstrate that full flooding in the Fuel Cavity maximizes the reactivity of the single container.

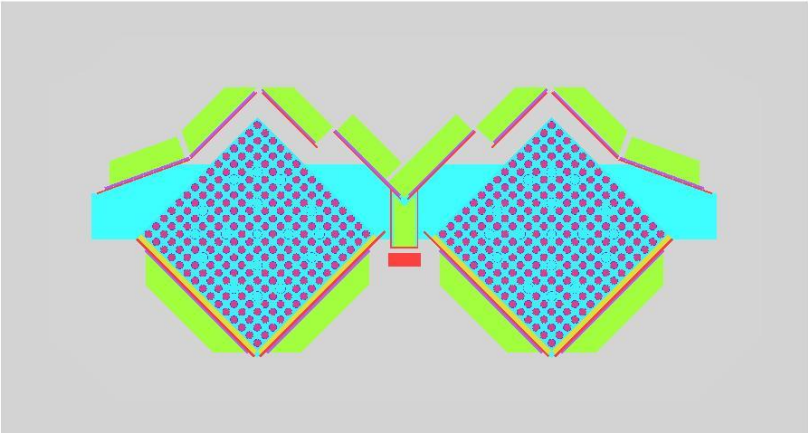

Figure 6-8 View of lateral cross section for one case from partial flooding scenario #1

* From evaluating propagation of error for the difference between two values, each with associated uncertainties, commonly referred to as "square root of the sum of the squares" of the individual 1σ values. This is a general result of the classic error propagation formula when applied to a quantity which is derived from the sum or difference of two or more quantities with associated uncertainties.

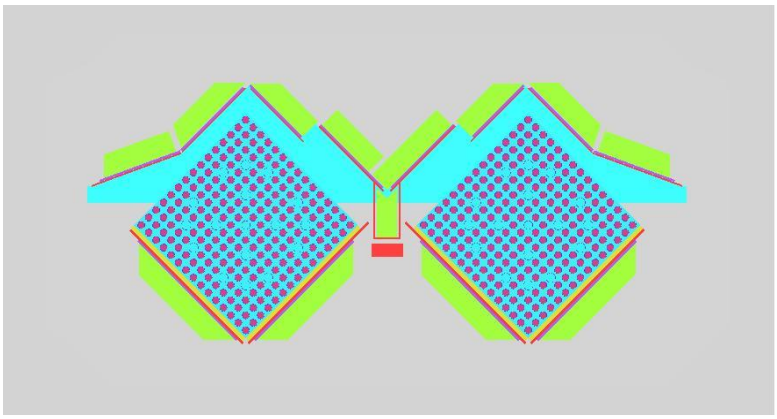

Figure 6-9 View of lateral cross section for one case from partial flooding scenario #2

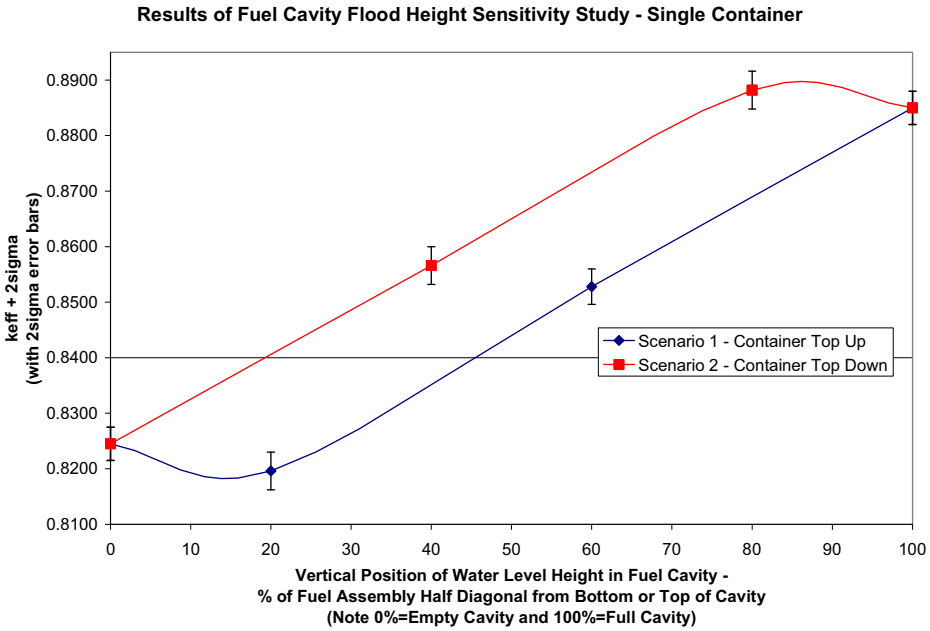

Figure 6-10 Results of Fuel Cavity flood height sensitivity study; shows relationships between reactivity (k_{eff}) and incremental addition of water from the bottom to the top (container top up), and from the top to the bottom (container top down)

6.7.2.1.2 Partial Density Interspersed Moderation

The reactivity effect of moderator density variation in the Fuel Cavity and the Outer Cavity is also evaluated. Preferential flooding (also called selective flooding) represents the scenario in which

one or more discrete volume(s) of the package/cavity remain(s) flooded while the remaining volumes of the package/cavities drain completely. For this evaluation, preferential flooding refers to full flooding of the fuel assembly envelope (or rod array) and void elsewhere in the Fuel Cavity. The Outer Cavity may contain void or water.

The interspersed moderation study adds partial to full density water to the Fuel Cavity void spaces of the preferentially flooded case and to the Outer Cavity. Figure 6-11 illustrates the modeling used to evaluate partial density moderation in the Outer Cavity and the Fuel Cavity.

The results for Outer Cavity partial density moderation in the single container model are shown in Figure 6-12 for both preferential and non-preferential (full) flooding of the Fuel Cavity. The results for Fuel Cavity partial density moderation in the region outside the fuel assembly envelope are shown in Figure 6-13. This series assumes that a void fills the Outer Cavity. This study parallels the results of the partial flooding cases in the previous section that illustrate full density water, especially at the top portion of the container, provides the highest reactivity. A comparison of the 100% moderator density k_{eff} values in Figures 6-12 and 6-13 shows that a fully flooded Fuel and Outer Cavity provides the highest reactivity. This validates the single package licensing-basis model with full flooding of both the Fuel and Outer Cavities. The model with full flooding of Fuel and Outer Cavities is illustrated in Figure 6-14.

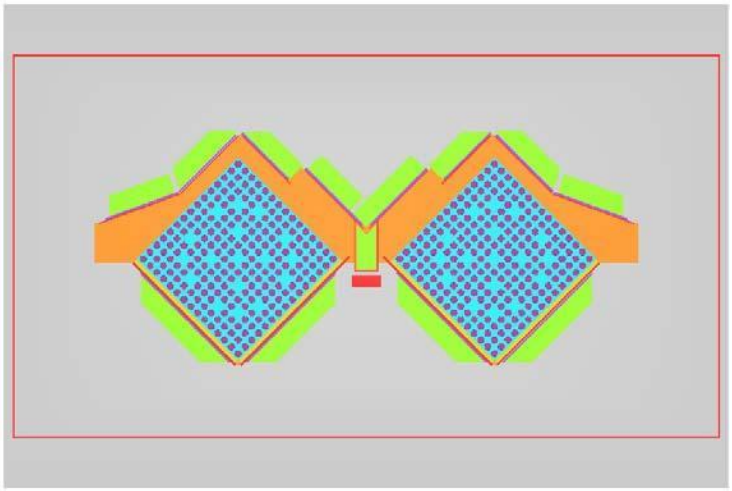

Figure 6-11 View of lateral cross section for model used to evaluate partial density moderation in the Fuel Cavity and Outer Cavity; blue=full density water (in fuel assembly envelope), orange=partial density water in remainder of Fuel Cavity, grey=partial density water in Outer Cavity

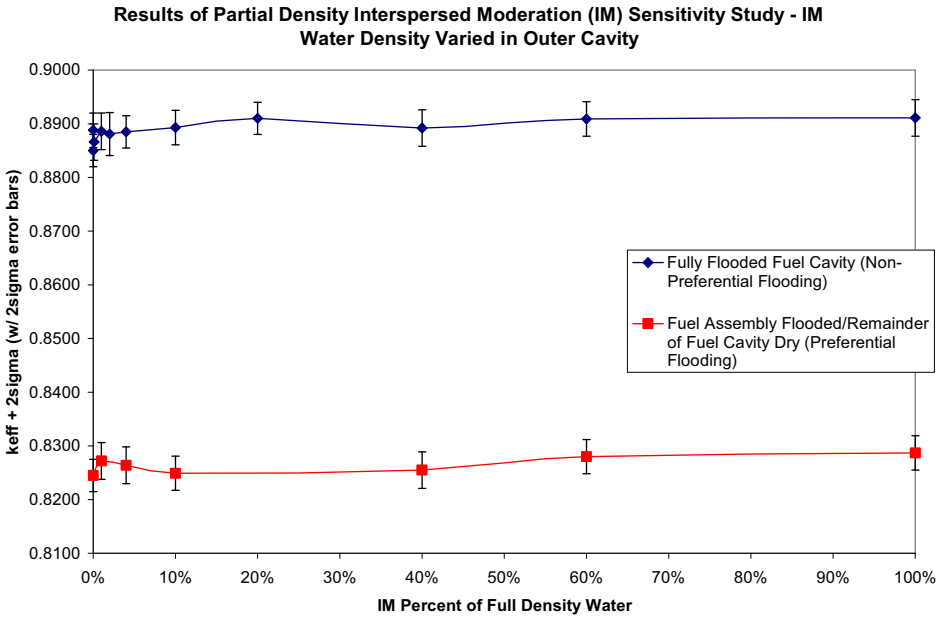

Figure 6-12 Results of partial density moderation study for the Outer Cavity, single container

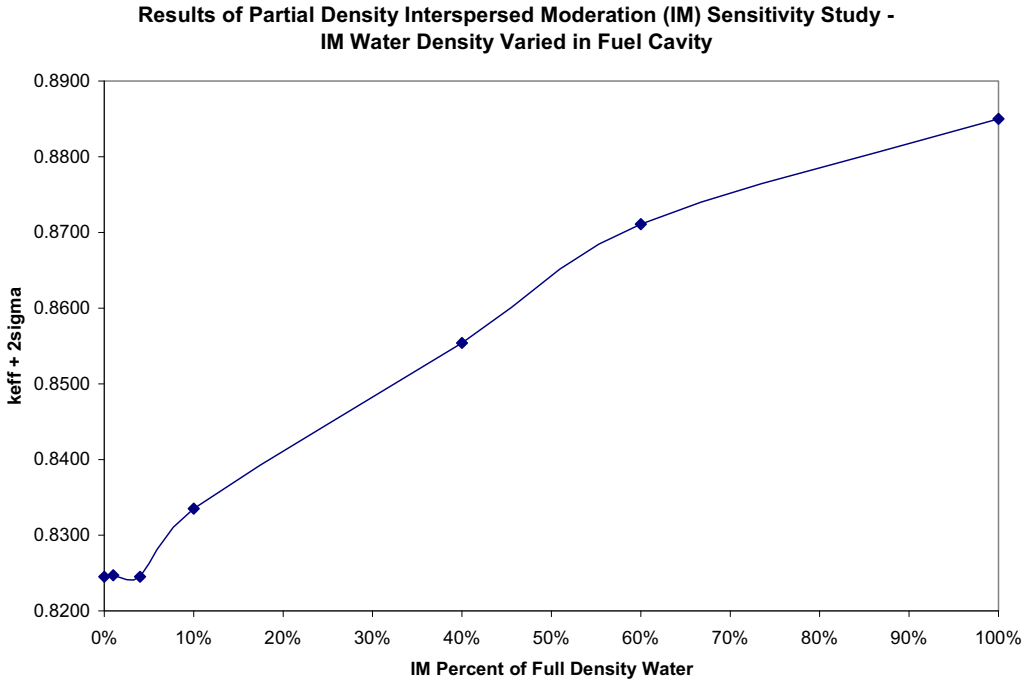

Figure 6-13 Results of partial density moderation study for the Fuel Cavity, single container

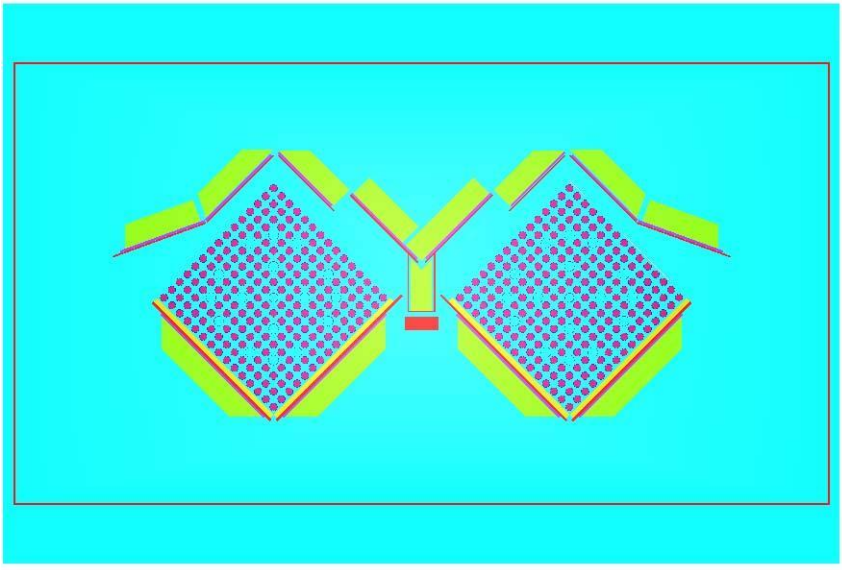

Figure 6-14 View of lateral cross section for package under most reactive flooding condition for a single container – fully flooded Fuel Cavity and in Outer Cavity; blue=full density water

6.7.2.2 Package Array Evaluation

The sensitivity of k_{eff} to moderation introduced to a package array is evaluated in this section. Partial flooding of the Fuel Cavity is not reexamined for the array configuration. This is due to the statistically equal results obtained for the reactivity of a partially and fully flooded single container from Figure 6-12 in Section 6.7.2.1.1. This evaluation is only concerned with partial to full density interspersed moderation within and between packages in an array.

The Outer Cavity includes the region surrounding the Fuel Cavity within the package and the spacing between packages. The outer stiffeners maintain void regions between the packages in an array in which environmental factors (snow, rain, ice, and immersion) may provide moderation. The spacing is assumed to be equivalent to that provided by the lid and base outer stiffeners; however, the package envelope is reduced by 2 inches in width and 2 inches in height, see Table 6-9. Therefore, the sensitivity studies related to moderator density in the Outer Cavity consider the void spaces within and between packages in an array.

Partial density interspersed moderation within the Fuel Cavity is also evaluated. This is analogous to the study performed for the single package.

Figure 6-15 illustrates the individual package modeling used to evaluate partial density moderation in the Outer Cavity and the Fuel Cavity. This is used to create the array model consisting of a 4 wide by 6 high by 1 deep array of containers. The array is surrounded by a 30 cm water reflector to simulate close reflection at the array boundary.

The first series of cases examines the reactivity effect of varying the moderator density within the Fuel Cavity without moderation in the Outer Cavity of the array packages. The results for the evaluation are shown in Figure 6-16. These results follow the same trend as Figure 6-13 for the single package and show a positive trend in reactivity with increasing moderator density. The significant difference is the increased reactivity due to the interaction between packages within the array.

The next sets of cases examine the effect of moderator density variations in the Outer Cavity for both preferential and non-preferential flooding of the Fuel Cavity. The results for each set shown in Figure 6-17 exhibit the same decreasing trend versus increasing moderator density. The voided

Outer Cavity provides the maximum reactivity for both sets with the non-preferential Fuel Cavity flooding model providing higher values over the range of moderator densities.

The increased reactivity of the non-preferential flooding was explained for the single package by reduced leakage of neutrons from the Fuel Cavity region. A comparison of the reactivity increase going from 100% to 0% moderation for the non-preferential and preferential flooding at in Figure 6-17 illustrates the validity of this explanation. The Δk_{eff} between 100% to 0% density for preferential flooding is ~ 7%Δk versus ~ 4%Δk for non-preferential flooding. This indicates more interaction between packages within the preferentially flooded array due to increased leakage for that Fuel Cavity configuration. The higher k_{eff} for the non-preferentially flooded Fuel Cavity is due to less leakage in the individual package which increases the k_{eff} of each package. Although the increased leakage for preferential flooding reduces the reactivity differences between the two models as moderator density decreases (causing increased package interaction), it is not enough to offset the lower leakage within the Fuel Cavity for the non-preferential flooding model with a higher single package k_{eff}.

A comparison between the 100% moderation (Fuel and Outer Cavities fully flooded) case k_{eff} in Figures 6-13 and 6-17 shows that the array results are slightly higher. This indicates that there is still some interaction between packages even with a fully flooded Outer Cavity (full density water between packages).

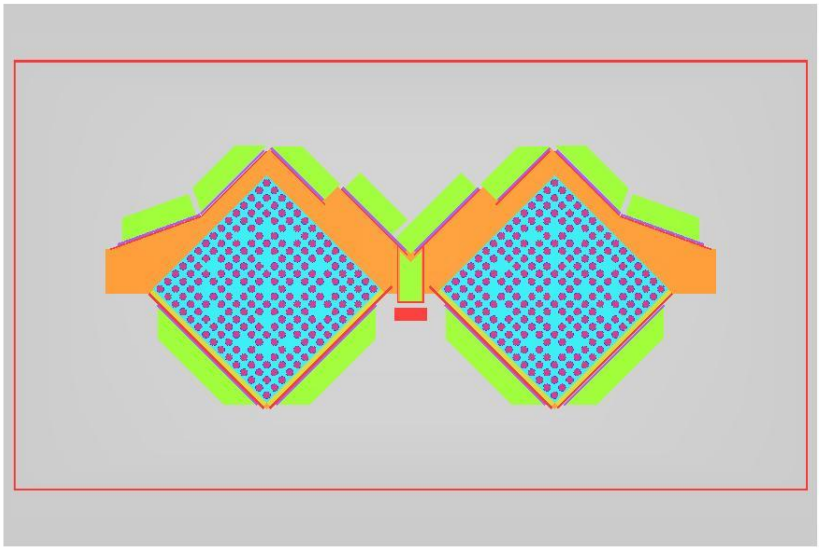

Figure 6-15 View of lateral cross section for model used to evaluate partial density moderation in the Fuel Cavity and Outer Cavity; blue=full density water (in fuel assembly envelope), orange=partial density water in remainder of Fuel Cavity, grey=partial density water in Outer Cavity

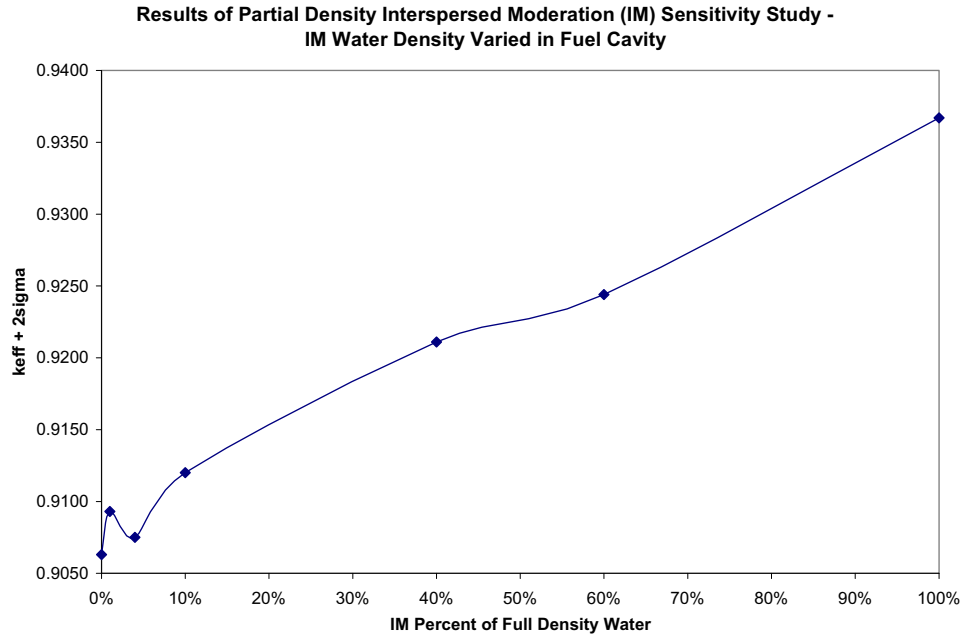

Figure 6-16 Results of partial density moderation study for the Fuel Cavity, package array evaluated

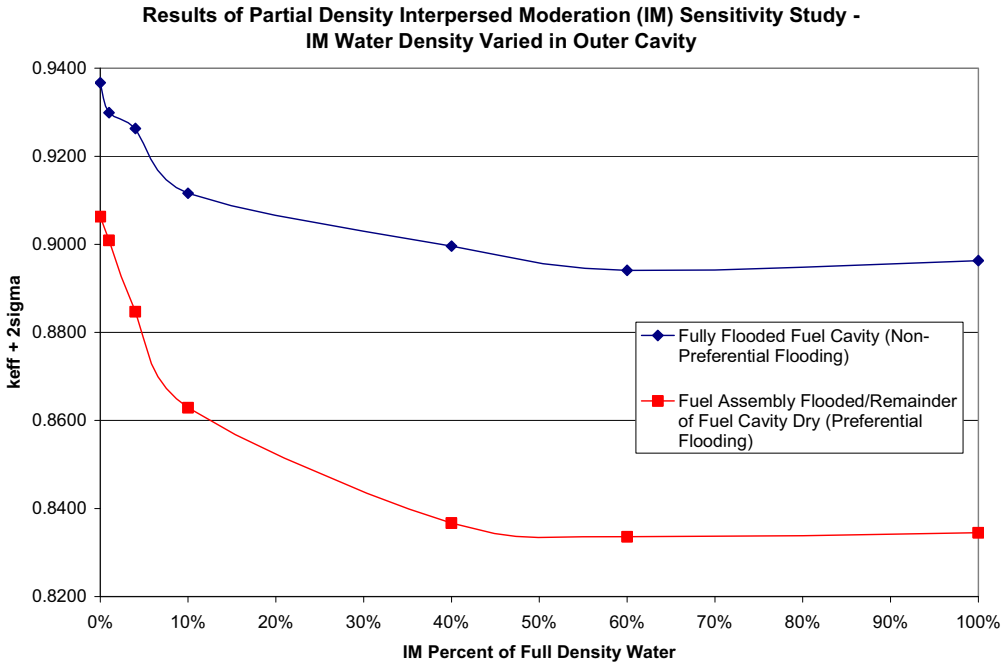

Figure 6-17 Results of partial density moderation study for the Outer Cavity, package array

6.7.2.3 Polyurethane Foam Moderating Effect

The polyurethane foam has a hydrogen weight percent less than full density water and a material density significantly less than full density water (0.096 g/cm^3) for the normal condition of transport. For HAC conditions, the amount of foam and the hydrogen content is significantly reduced. Thus, the sensitivity studies that evaluate partial density moderation in the Outer Cavity bound the effects of polyurethane foam and validate the replacement of this material with either void or full density water, as appropriate in the licensing-basis or normal models.

6.7.3 Flux Trap Effectiveness

This section examines the effect of density variations in the moderator and absorber materials of the flux trap, as well as the importance of individual portions of the flux trap attached to the outer surfaces of the Fuel Cavity.

6.7.3.1 Moderator Density in Flux Trap

The MAP packaging contains a flux trap system that effectively reduces the interaction between packages by providing fixed neutron moderation and absorber materials within each package. The Nylon blocks are the component of the flux trap that maintains a fixed amount of moderation within and between packages. The sensitivity of the flux trap to nylon density is evaluated for both a single package and package array for models of the fuel cavity with both non-preferential and preferential flooding of the fuel assembly envelope. For this evaluation the nylon block dimensions are reduced such that the block density is ~87% of the as-built density (see Table 6-9).

The results for the single container model are shown in Table 6-13 and are based upon a fully flooded single package. The results demonstrate that the presence of fixed moderator in the single container increases reactivity of the single container. This indicates that the fixed moderator serves more as a reflector than a moderator for a fully flooded package.

The results for a 4x6x1 package array model with a voided Outer Cavity are shown in Table 6-14. For the package array, the importance of the fixed moderator for the flux trap is clearly illustrated by the significant reduction in the array reactivity due to the fixed moderator. Furthermore, these results indicate that the fixed moderator has been included in the flux trap solely to ensure criticality safety for package array HAC.

These results validate that the ~10% reduction in fixed moderator mass is conservative.

Table 6-13 Single Package Results for the sensitivity study for variation of nylon density in Flux Trap– preferentially and non-preferentially flooded Fuel Cavity evaluated

% Full Nylon Density	Calculated k_{eff}	Uncertainty (σ)	k_{eff} + 2σ	% Δk from 100% Case
Fully Flooded Fuel Cavity (Non-Preferential Flooding)				
100%	0.8820	0.0015	0.8850	–
50%	0.8786	0.0016	0.8818	-0.32%
0%	0.8705	0.0016	0.8737	-1.13%
Fuel Assembly Flooded/Remainder of Fuel Cavity Dry (Preferential Flooding)				
100%	0.8215	0.0015	0.8245	–
50%	0.8184	0.0018	0.8220	-0.25%
0%	0.8031	0.0016	0.8063	-1.82%

Table 6-14 Package array results for the sensitivity study for variation of nylon density in Flux Trap– preferentially and non-preferentially flooded Fuel Cavity evaluated

% Full Nylon Density	Calculated k_{eff}	Uncertainty (σ)	k_{eff} + 2σ	% Δk from 100% Case
Fully Flooded Fuel Cavity (Non-Preferential Flooding)				
100%	0.9335	0.0016	0.9367	–
50%	0.9625	0.0016	0.9657	2.90%
0%	0.9935	0.0015	0.9965	5.98%
Fuel Assembly Flooded/Remainder of Fuel Cavity Dry (Preferential Flooding)				
100%	0.9031	0.0016	0.9063	–
50%	0.9461	0.0017	0.9495	4.32%
0%	1.0118	0.0015	1.0148	10.85%

6.7.3.2 ^{10}B Density in Absorber Plates

The previous section evaluated the reactivity effect of the fixed moderator in the flux trap. This section performs a similar evaluation for the fixed absorber. The ^{10}B density was varied for a

single container. No evaluation for the package array was performed here because the sensitivities on moderator density (previous section) within the flux trap and removal of various flux trap components (following section) were performed for the package array. The calculations for this section were performed for a fully flooded Fuel Cavity (non-preferential flooding).

The results in Table 6-15 show that removal of boron neutron absorber increases the package reactivity by allowing more neutron reflection toward the Fuel Cavity from the Outer Cavity.

These results validate that the 25% reduction in boron density is conservative.

Table 6-15 Results of the sensitivity study for variation of ^{10}B arial density in Flux Trap for the package array model – non-preferentially flooded Fuel Cavity/single container evaluated

% Minimum ^{10}B Arial Density (0.0180 g/cm^2)	Calculated k_{eff}	Uncertainty (σ)	k_{eff} + 2σ	% Δk from 100% Case
100%	0.8820	0.0015	0.8850	–
75%	0.8884	0.0015	0.8914	0.64%
50%	0.8908	0.0015	0.8938	0.88%
25%	0.8981	0.0015	0.9011	1.61%
0%	0.9299	0.0015	0.9329	4.79%

6.7.3.3 Removal of Various Flux Trap Components

This section evaluates the relative importance of the various flux trap components (moderator + absorber). The evaluation is performed for a single container and a package array, with preferential and non-preferential flooding. For this evaluation water replaces the component removed.

The results in Tables 6-16 and 6-17 show that under conditions of non-preferential flooding, the lower (base) flux trap components appear to be slightly more important than the upper (lid) components. Under conditions of preferential flooding, however, the lid components appear to be

more important. For the single container, the inner sections seem to have highest importance. For the container array, the results do not show a preference between the inner or outer sections.

In all cases, the flux trap as a whole is most important for preferentially flooding conditions. This is because the effect of neutron interaction is more prevalent.

Table 6-16 Results of the sensitivity study for removal of various flux trap (FT) components from the single container model – preferentially and non-preferentially flooded Fuel Cavity evaluated

Description	Calculated k_{eff}	Uncertainty (σ)	$k_{eff} + 2\sigma$	% Δk from No Removal Case
Fully Flooded Fuel Cavity (Non-Preferential Flooding)				
No FT Components Removed	0.8820	0.0015	0.8850	–
Lower-Inner FT Removed	0.8925	0.0016	0.8957	1.07%
Lower-Outer FT Removed	0.8864	0.0016	0.8896	0.46%
Upper-Inner FT Removed	0.8904	0.0016	0.8936	0.86%
Upper-Outer FT Removed	0.8822	0.0015	0.8852	0.02%
All FT Components Removed	0.9058	0.0016	0.9090	2.40%
All FT Components Removed – 100% IM in Outer Cavity	0.9427	0.0016	0.9459	6.09%
Fuel Assembly Flooded/Remainder of Fuel Cavity Dry (Preferential Flooding)				
No FT Components Removed	0.8215	0.0015	0.8245	–
Lower-Inner FT Removed	0.8292	0.0015	0.8322	0.77%
Lower-Outer FT Removed	0.8236	0.0016	0.8268	0.23%
Upper-Inner FT Removed	0.8320	0.0019	0.8358	1.13%
Upper-Outer FT Removed	0.8263	0.0014	0.8291	0.46%
All FT Components Removed	0.8556	0.0016	0.8588	3.43%
All FT Components Removed – 100% IM in Outer Cavity	0.9238	0.0016	0.9270	10.25%

Table 6-17 Results of the sensitivity study for removal of various flux trap (FT) components from the package array model – preferentially and non-preferentially flooded Fuel Cavity evaluated

Description	Calculated k_{eff}	Uncertainty (σ)	k_{eff} + 2σ	% Δk from No Removal Case
Fully Flooded Fuel Cavity (Non-Preferential Flooding)				
No FT Components Removed	0.9335	0.0016	0.9367	–
Lower-Inner FT Removed	0.9546	0.0016	0.9578	2.11%
Lower-Outer FT Removed	0.9546	0.0016	0.9578	2.11%
Upper-Inner FT Removed	0.9460	0.0018	0.9496	1.29%
Upper-Outer FT Removed	0.9566	0.0018	0.9602	2.35%
All FT Components Removed	1.0449	0.0017	1.0483	11.16%
Fuel Assembly Flooded/Remainder of Fuel Cavity Dry (Preferential Flooding)				
No FT Components Removed	0.9031	0.0016	0.9063	–
Lower-Inner FT Removed	0.9418	0.0017	0.9452	3.89%
Lower-Outer FT Removed	0.9351	0.0016	0.9383	3.20%
Upper-Inner FT Removed	0.9459	0.0017	0.9493	4.30%
Upper-Outer FT Removed	0.9443	0.0016	0.9475	4.12%
All FT Components Removed	1.1156	0.0015	1.1186	21.23%

6.7.4 Non-Flux Trap Packaging Material Property Modeling

This section examines in the reactivity effects of the remaining non-flux trap packaging material specifications. This includes the modeling of neoprene and stainless steel.

6.7.4.1 Material Specification for Neoprene Padding

Neoprene is represented in the models by full density water. The actual chemical formula for neoprene is C_4H_5Cl and has a nominal density of 1.23 g/cc. Chlorine is a relatively effective neutron absorber, so some built-in margin exists by representing neoprene by water. This evaluation considers neoprene specified as C_4H_5Cl (1.23 g/cc) and as C_4H_5, where the Cl is simply

removed from the mixture, i.e. no change in atom density for C and H so the material mass density goes down. This is evaluated for a single package and demonstrates that representing neoprene by water is conservative. The reactivity worth of the chlorine is also estimated from this evaluation.

The results in Table 6-18 demonstrate that chlorine acts as a weak neutron absorber and validate modeling neoprene as full density water.

Table 6-18 Results for neoprene material specification sensitivity study – non-preferentially flooded Fuel Cavity/single container evaluated

Description	Calculated k_{eff}	Uncertainty (σ)	$k_{eff} + 2\sigma$	% Δk from Base Case
Neoprene Modeled as H_2O	0.8820	0.0015	0.8850	–
Neoprene Modeled as C_4H_5 (without Cl)	0.8825	0.0017	0.8859	0.09%
Neoprene Modeled as C_4H_5Cl (with Cl)	0.8782	0.0016	0.8814	-0.36%

6.7.4.2 Elimination of Structural Stainless Steel

Neutron absorption occurs to a relatively small degree in the stainless steel of the package due primarily to its chromium content. The modeling credits ~30% of the stainless steel in the package, see Table 6-9. Single container calculations with non-preferential flooding were performed to determine the effect on k_{eff} due to removal of steel in different areas of the package.

The results in Table 6-19 demonstrate a relatively weak effect due to the stainless steel in the package, but do suggest that the steel acts as a weak neutron absorber.

The results show that a slight decrease from removal of the steel 'W' plates nearest the fuel assembly due to reduced reflection. However, for the other steel components modeled their removal resulted in an equivalent increase due to reduced absorption. The non-'W' plate components comprise the vast majority of the ~70% of steel not included in the model. Therefore, results validate that the ~30% credit for stainless steel in the package is conservative.

Table 6-19 Results of the sensitivity study for removal of various stainless steel components in the base models – non-preferentially flooded Fuel Cavity/single container evaluated

Description	Calculated k_{eff}	Uncertainty (σ)	$k_{eff} + 2\sigma$	% Δk from No Removal Case
No Steel Removed	0.8820	0.0015	0.8850	–
Lower W Plate Removed	0.8739	0.0016	0.8771	-0.79%
Upper W Plate Removed	0.8811	0.0016	0.8843	-0.07%
Lower & Upper W Plates Removed	0.8748	0.0017	0.8782	-0.68%
Steel Bar (Rail) Removed	0.8881	0.0017	0.8915	0.65%
Container Shell Removed	0.8848	0.0016	0.8880	0.30%
All Steel in Container Removed	0.8770	0.0017	0.8804	-0.46%

6.7.5 Variations on the Degree of Interaction between Assemblies in the Same Container

Stainless steel and aluminum associated with the doors (latches, hinges, etc.) between assembly locations have been neglected in the models. This study examines the importance of these materials relative to neutron interaction between fuel assemblies in the same container. Calculations were performed for a single container with non-preferential flooding. The model for this evaluation assumed an aluminum or stainless steel slab running the entire package length with variable thickness. The slab was placed at the lateral center of the package between the two fuel assemblies. Figure 6-18 illustrates the steel/aluminum slab modeling for this study.

The results in Figures 6-19 and 6-20 demonstrate that the effect associated with aluminum or stainless steel components existing between the fuel assemblies in the actual package is insignificant. The results suggest a slightly higher neutron transmittance through the aluminum versus the stainless steel which is expected due to the higher thermal neutron absorption properties for stainless steel. However, the results also show that the effect of displacing water with either of the two is statistically insignificant.

The results validate the modeling of the space between assemblies as a fully floodable region.

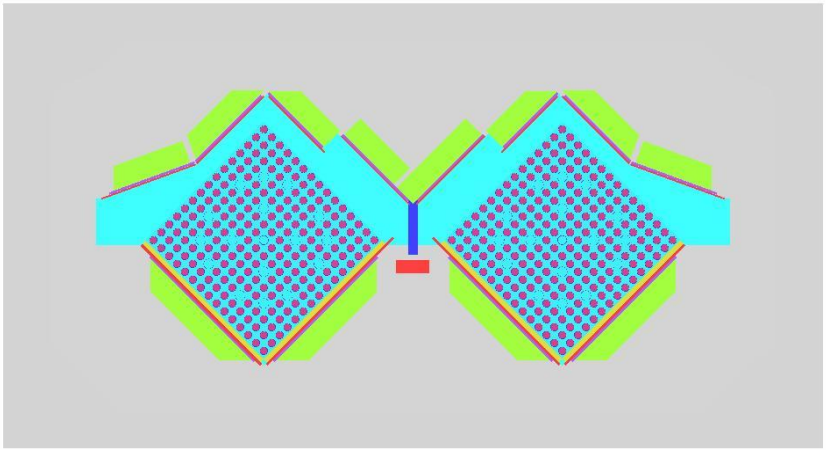

Figure 6-18 View of lateral cross section for model used to evaluate interaction between fuel assemblies in the same container with aluminum/stainless steel slabs; shows the aluminum or stainless steel slab between the assemblies

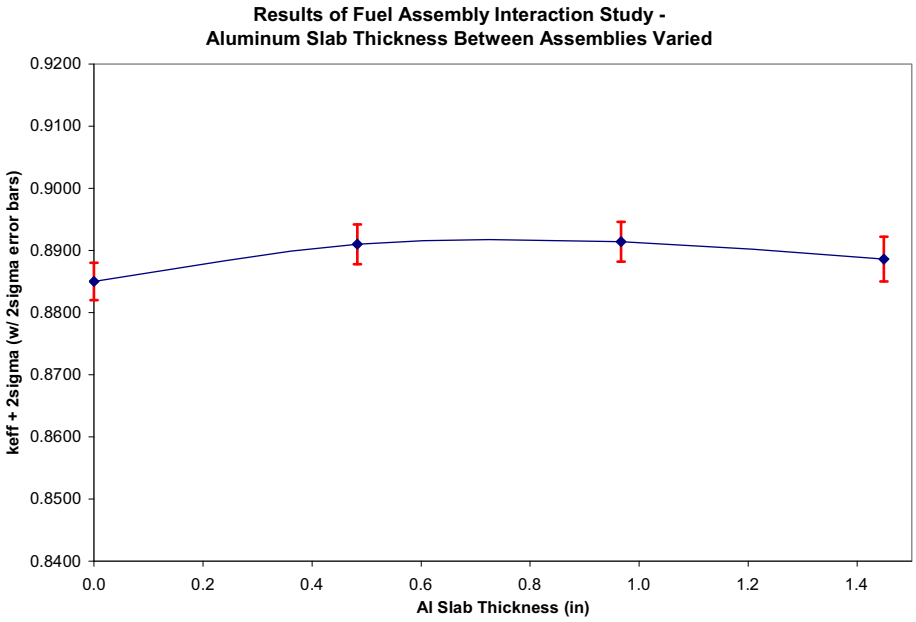

Figure 6-19 Results of fuel assembly interaction study for variable aluminum slab thickness between assemblies in the same container

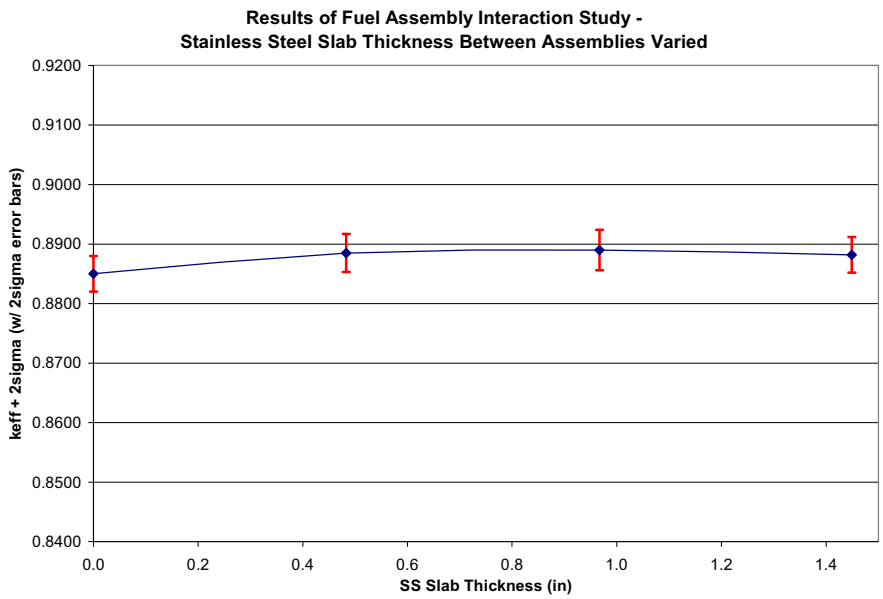

Figure 6-20 Results of fuel assembly interaction study for variable stainless steel slab thickness between assemblies in the same container

6.7.6 Fuel Assembly Shifting within Container

This section examines lateral and axial shifting of the fuel assemblies within the container. Note that the HAC test results showed that the assemblies did not shift laterally or axially.

6.7.6.1 Lateral Shifting of Fuel Assemblies

This section evaluates the effect on k_{eff} resulting from the fuel assemblies shifting laterally within the Fuel Cavity. The model considers both assemblies shifted laterally along the lower 'W' plates (x-y directions) toward the center (+x direction for left assembly, –x direction for right assembly) and the top (+y direction) of the container. The assemblies were shifted so that the corner of the envelope pointing to the lateral center of the package was aligned with the corresponding corner of the lower-inner 'W' plate, which represents the closest approach between assemblies within the package. Each assembly was moved ~ 0.396 inch horizontally (+/–x direction) and vertically (+y direction), for a total movement along the lower-inner 'W' plate (which is at a 45° angle) of ~ 0.560 inch. The calculation was performed for a single container under conditions of non-preferential flooding, as illustrated in Figure 6-21.

The results in Table 6-20 show that the effect on fuel assembly interaction due to a significant lateral shift is small.

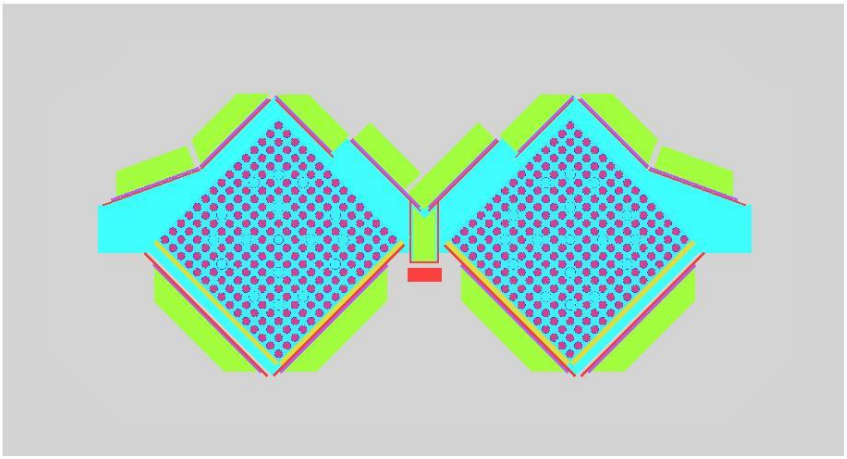

Figure 6-21 View of lateral cross section for model used to evaluate lateral shifting of fuel assemblies within a container

Table 6-20 Results for lateral assembly shift sensitivity study – non-preferentially flooded Fuel Cavity/single container evaluated

Description	Calculated k_{eff}	Uncertainty (σ)	$k_{eff} + 2\sigma$	% Δk from Base Case
No Shift	0.8820	0.0015	0.8850	–
Assys Shifted Along Lower – Inner W Plates Toward Center/Lid, 0.396" Horizontal/Vertical, for 0.560" Along W at 45°	0.8896	0.0018	0.8932	0.82%

6.7.6.2 Axial Shifting of Fuel Assemblies in a Container

This section evaluates the effect of the fuel assemblies shifting axially (longitudinally) at various distances outside of the flux trap region. The evaluation demonstrates that a significant axial shift outside the flux trap region has a small effect. Also note that each fuel assembly is shimmed

within the fuel cavity with rigid supports to prevent movement and HAC testing demonstrates that axial shifting of the payload does not occur.

In the calculational model, both assemblies are shifted along the z axis while maintaining their normal x-y positions. The calculation was performed for a single container under conditions of non-preferential flooding, as illustrated in Figure 6-22 provides an illustration of the modeling for this study.

The results shown in Figure 6-23 demonstrate that even a significant axial shift outside the flux trap region has a small effect (~ < 0.5%Δk).

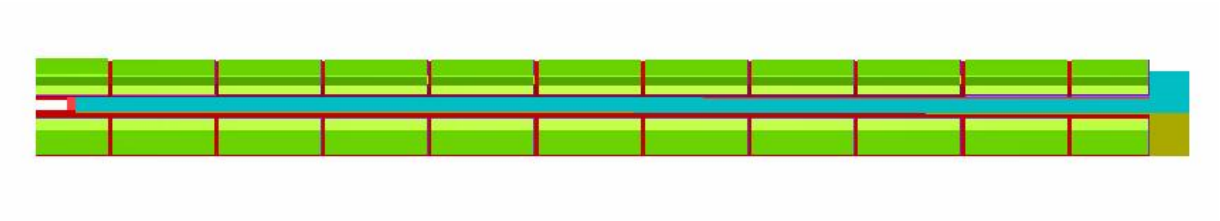

Figure 6-22 View of the side of the package (y-z plane) where assemblies have been shifted axially where 15 cm (5.906 inches) of the assemblies are outside of the flux trap region

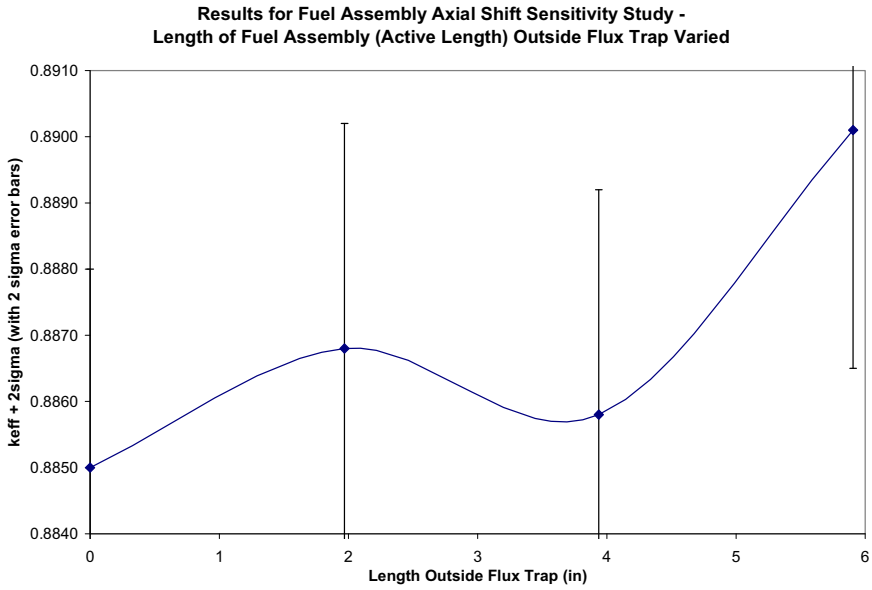

Figure 6-23 Results of fuel assembly axial shift sensitivity study (variable active length shifted outside flux trap region) – non-preferentially flooded Fuel Cavity/single container evaluated

6.7.7 Variations on Package Orientations within Array and Package Array Size

This section examines the effect of variable package orientations within an array and the package array size. The package array size evaluation provides the basis for the 2N array size of 36 packages that supports a CSI of 2.8.

6.7.7.1 Orientations of Packages within Array

This section evaluates package arrays with regular package orientations (package top-up), as well as irregular orientation patterns within a 4x6x1 array. The irregular orientation patterns considered are as follows:

1. The packages in every other package row, or layer, (in y directions) 'flipped'; this scenario is denoted by 'FLIP1'; note that for package arrays with an odd number of rows (in y directions), there are two possibilities within this scenario:
    a. FLIP1a – Normally oriented (top side up) containers (designated as 'unit 1000') at the +/–y boundaries of the array, or
    b. FLIP1b – Flipped (top side down) containers (designated as 'unit 1001') at the +/–y boundaries of the array.
        – Figure 6-24 illustrates units 1000 and 1001
        – Figure 6-25 illustrates different FLIP1 configurations
        – The conclusion from this study (see Table 6-21) is that the FLIP1 scenario is the worst case for irregular stacking; however, but the FLIP1a and FLIP1b scenarios are still evaluated in the array size section in which the 2N array size is established
2. The packages in every other package column (in x directions) 'flipped'; this scenario is denoted by 'FLIP2'. As in the FLIP1 scenario, there are two possibilities for this scenario with an odd number of columns, but only one is evaluated in this section because this sensitivity shows that this scenario can be removed from further consideration.
        – Figure 6-26 illustrates the FLIP2 configuration

3. The packages in every other diagonal across the x-y face of the array 'flipped'; this scenario is denoted by 'FLIP3'. As in the other two scenarios there are multiple possibilities for this scenario, but only one is evaluated in this section because this sensitivity shows that this scenario can be removed from further consideration.

   – Figure 6-27 illustrates the FLIP3 configuration

The results in Table 6-21 demonstrate that the FLIP1 configuration results in a slight increase in k_{eff} from a regular stacking configuration. For the non-preferential flooding condition, FLIP1 resulted in an increase of ~ 0.10 %Δk with propagated 2σ uncertainty of ~ 0.50 %Δk. For the preferential flooding condition, FLIP1 resulted in an increase of ~ 0.25 %Δk with propagated 2σ uncertainty of ~ 0.50 %Δk. The corresponding changes in reactivity for FLIP2 and FLIP3 were less with comparable uncertainties. These changes in reactivity are not statistically significant. However, for the purpose of completeness and conservatism, the FLIP1 configurations are evaluated in the array size evaluation in addition to the regular stacking configurations of the base case. Had the changes in reactivity all been negative and statistically significant, none would have been included in the array size sensitivity study.

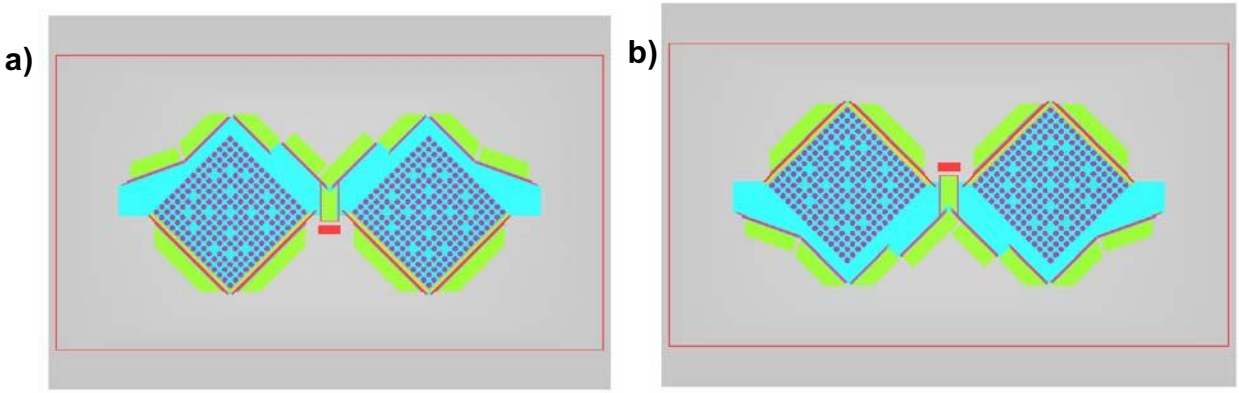

Figure 6-24 a) View of lateral cross section for unit 1000: package under most reactive flooding condition for a container array – fully flooded Fuel Cavity, void in Outer Cavity, blue=full density water, grey=void; b) view of lateral cross section for unit 1001: unit 1000 flipped upside down (rotated 180° about the z-axis)

a)

1000	1000	1000	1000
1001	1001	1001	1001
1000	1000	1000	1000
1001	1001	1001	1001
1000	1000	1000	1000
1001	1001	1001	1001

y

x

b)

1000	1000	1000
1001	1001	1001
1000	1000	1000
1001	1001	1001
1000	1000	1000
1001	1001	1001
1000	1000	1000
1001	1001	1001
1000	1000	1000

c)

1001	1001	1001
1000	1000	1000
1001	1001	1001
1000	1000	1000
1001	1001	1001
1000	1000	1000
1001	1001	1001
1000	1000	1000
1001	1001	1001

Figure 6-25 Illustrations of the FLIP1 configuration; a) illustrates a 4x6x1 array with only one possibility for the FLIP1 configuration; b) illustrates a 3x9x1 array with the FLIP1a configuration; c) illustrates a 3x9x1 array with the FLIP1b configuration

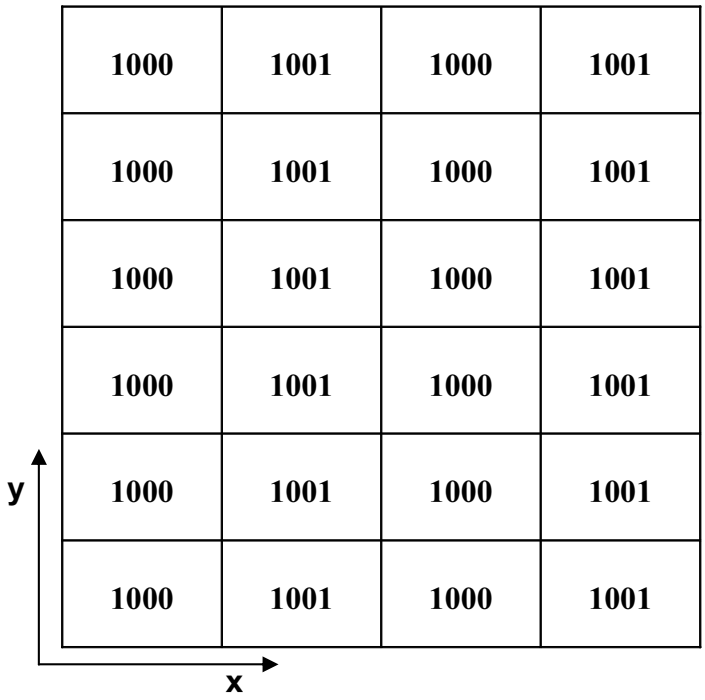

Figure 6-26 Illustration of the FLIP2 configuration; shows 4x6x1 array

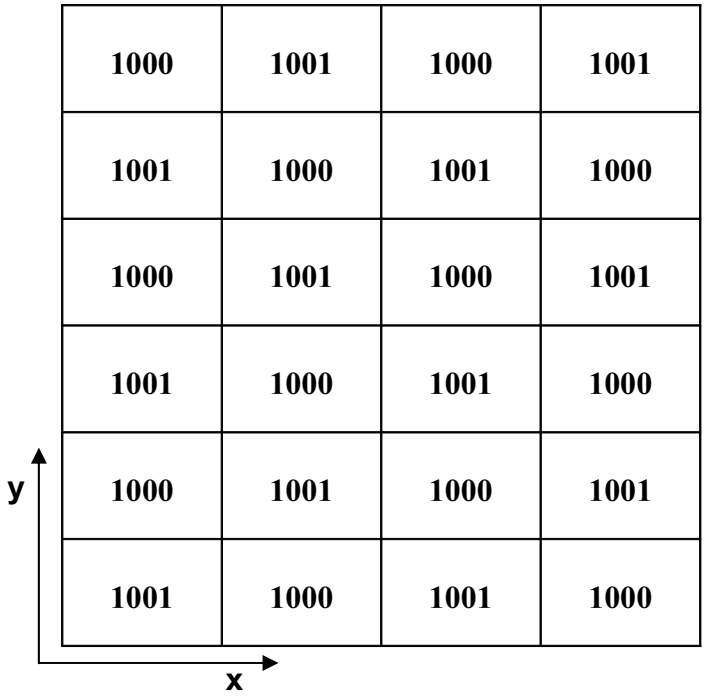

Figure 6-27 Illustration of the FLIP3 configuration; shows 4x6x1 array

Table 6-21 Results for study evaluating different configurations of flipped packages within a package array

Description	Calculated k_{eff}	Uncertainty (σ)	$k_{eff} + 2\sigma$
Fully Flooded Fuel Cavity (Non-Preferentially Flooded)			
4x6x1 Array – No Packages Flipped	0.9335	0.0016	0.9367
FLIP1 Configuration	0.9354	0.0019	0.9392
FLIP2 Configuration	0.9319	0.0015	0.9349
FLIP3 Configuration	0.9340	0.0017	0.9374
Fuel Assembly Flooded/Remainder of Fuel Cavity Dry (Preferential Flooding)			
4x6x1 Array – No Packages Flipped	0.9031	0.0016	0.9063
FLIP1 Configuration	0.9035	0.0019	0.9073
FLIP2 Configuration	0.9019	0.0016	0.9051
FLIP3 Configuration	0.9017	0.0016	0.9049

6.7.7.2 Package Array Size

This section evaluates variable package array sizes under conditions of non-preferential flooding. Both the regular stacking configurations (no 'flipped' containers in the array) and the FLIP1 stacking configurations (described in the previous section) are considered in this evaluation. The results in Figure 6-28 show that the FLIP1 configuration (irregular stacking) remains the most reactive for the range of array sizes examined. The results also show that stacking a given array size one deep in the z-direction is most reactive.

Additional array size cases with FLIP1 configurations were performed in which the fuel-clad gap is dry or flooded, and the spacing provided by the lid outer stiffeners has been removed. These cases have all the characteristics of the licensing-basis models for a package array, see Table 6-9. The results are shown in Figures 6-29 and 6-30. The results shown in Figure 6-29 demonstrate that the package array with a dry fuel-clad gap is acceptable for sizes less than or equal to 40

packages. This supports a 2N array size of at least 36 packages and Criticality Safety Index (CSI) of 2.8.

The results in Figure 6-30 shows that the 2N array size of 36 is unacceptable for a flooded fuel-clad gap (and pellet diameter minimized) if no guide or instrument tube cladding is credited. In order for the 2N array size of 36 to remain acceptable under these conditions, both guide and instrument tubes must be credited for the most reactive (15 Type 1a) assembly design. Because of the fact that the flooded fuel-clad gap without guide or instrument tubes was unacceptable at the 2N array size of 36 packages, the other possible fuel assembly designs were inserted into a bounding 40 package array with flooded fuel-clad gap (and pellet diameter minimized) These results are shown in Table 6-22.

The results in Table 6-22 show that all other assembly designs with flooded fuel-clad gap and with no guide or instrument tubes credited are acceptable at the 40 package array size, and hence at or below the 36 package array size, with the exception of the 15 Type 3 assembly design. Therefore, this design was evaluated at the smaller package array sizes to demonstrate that the 36 package array size is acceptable. The results of this study are shown in Figure 6-31, which demonstrates that this assembly design is acceptable at or below a 2N array size of 36 packages with flooded fuel-clad gap and no guide or instrument tubes credited.

Table 6-23 shows the data used to generate the figures.

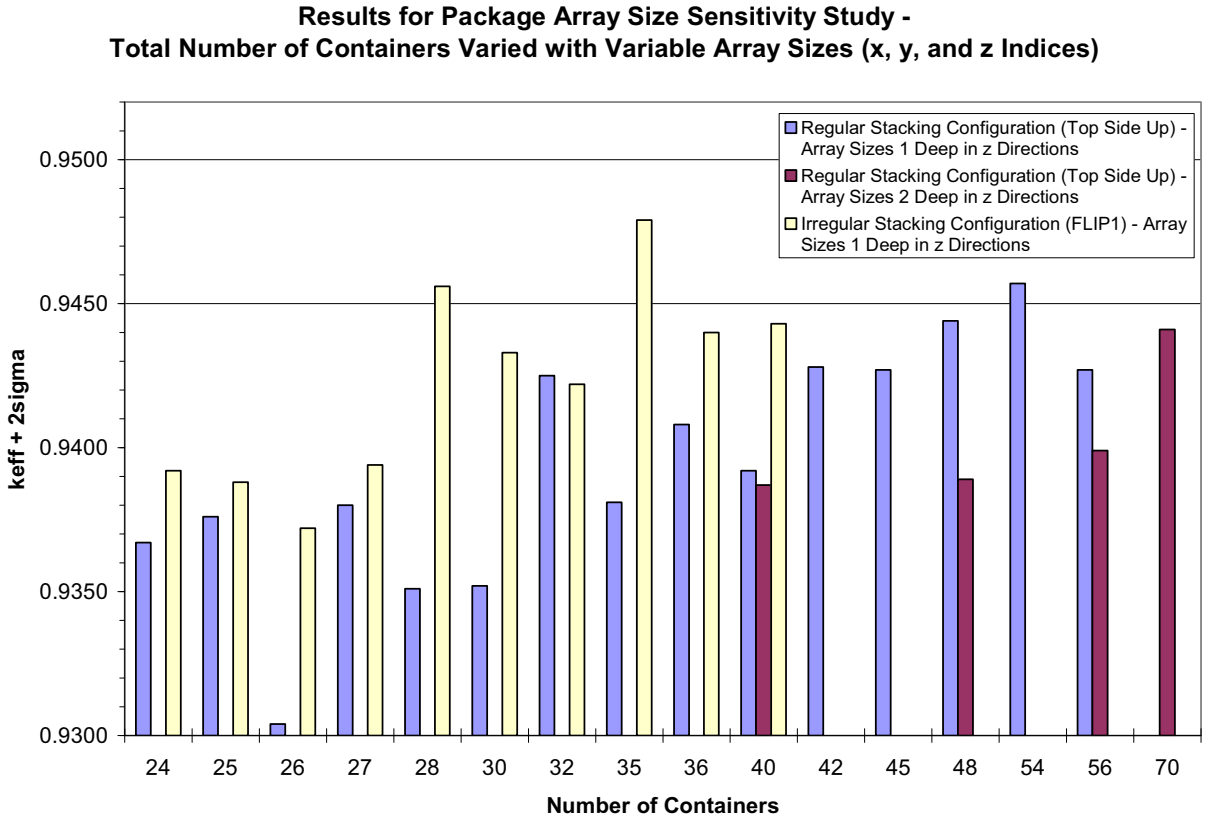

Figure 6-28 Results for package array size sensitivity study; shows k_{eff} versus number of containers for three array configurations – regular stacking/one container deep in z direction, regular stacking/two containers deep in z direction, FLIP1 stacking/one container deep in z direction

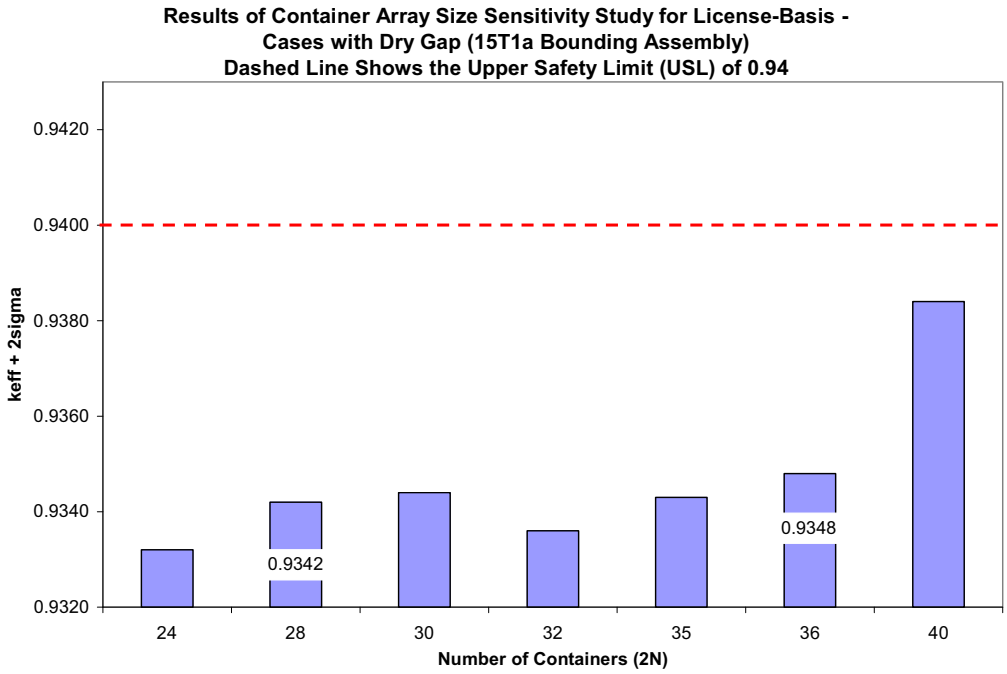

Figure 6-29 Results for final package array size sensitivity study; FLIP1 configurations with fuel-clad gap dry and spacing provided by lid stiffeners removed; 2N = 36 supports the licensing-basis case for the array

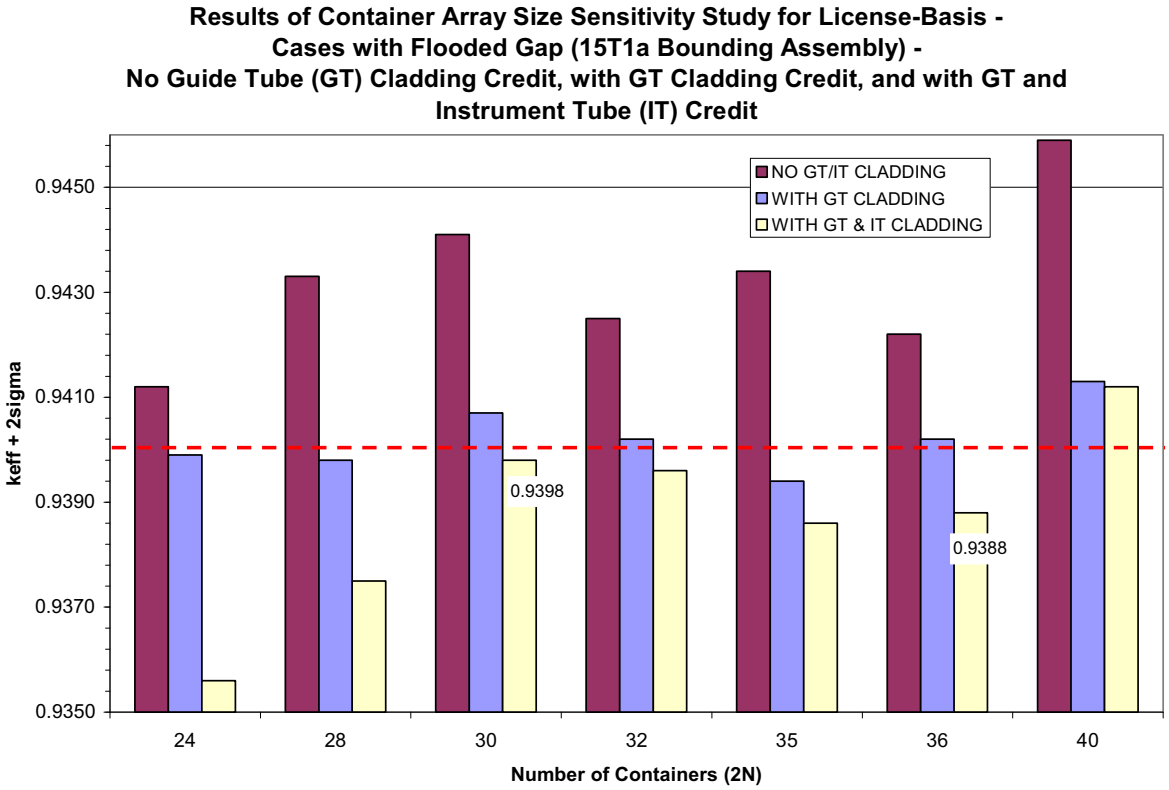

Figure 6-30 Results for final package array size sensitivity study; FLIP1 configurations with fuel-clad gap flooded (and pellet diameter minimized) and spacing provided by lid stiffeners removed; 2N = 36 supports the licensing-basis case for the array with guide and instrument tube cladding credited for the bounding 15 Type 1a assembly

Table 6-22 Results for final package array size sensitivity study; FLIP1 configurations with fuel-clad gap flooded (and pellet diameter mimimized) and spacing provided by lid stiffeners removed; remaining 9 fuel assembly designs evaluated at a package array size 2N = 40 with no guide or instrument tube cladding credited; supports licensing-basis of 2N = 36 for all remaining designs except for the 15 Type 3 assembly

Assembly Type	Calculated k_{eff}	Uncertainty (σ)	$k_{eff} + 2\sigma$
14 Type 1	0.9038	0.0008	0.9054
14 Type 2	0.8889	0.0008	0.8905
15 Type 1b	0.9311	0.0008	0.9327

15 Type 1c	0.9341	0.0008	0.9357
15 Type 2	0.8984	0.0009	0.9002
15 Type 3	0.9388	0.0009	**0.9406**
16 Type 1	0.9046	0.0009	0.9064
17 Type 1	0.9368	0.0008	0.9384
17 Type 2	0.9348	0.0009	0.9366

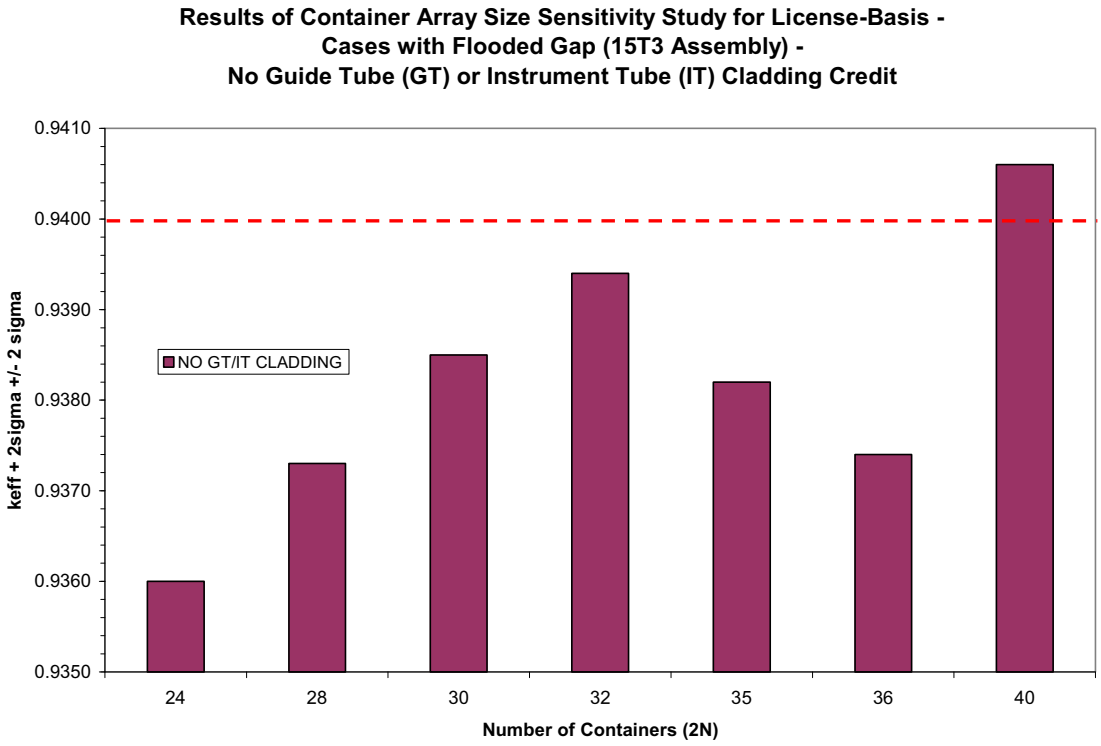

Figure 6-31 Results for final package array size sensitivity study; FLIP1 configurations with fuel-clad gap flooded (and pellet diameter minimized) and spacing provided by lid stiffeners removed; 2N = 36 supports the licensing-basis case for the array with guide and instrument tube cladding credited for the 15 Type 3 assembly

Table 6-23 Data used to create plots

Number of Containers	Array Size	Calculated k_{eff}	Uncertainty (σ)	$k_{eff} + 2\sigma$
Regular Stacking Configuration – Array Sizes 1 Deep in z Direction				
24	4x6x1	0.9335	0.0016	0.9367
25	5x5x1	0.9346	0.0015	0.9376
26	2x13x1	0.9274	0.0015	0.9304
27	3x9x1	0.9346	0.0017	0.9380
28	4x7x1	0.9317	0.0017	0.9351
30	5x6x1	0.9320	0.0016	0.9352
32	4x8x1	0.9393	0.0016	0.9425
35	5x7x1	0.9349	0.0016	0.9381
36	4x9x1	0.9378	0.0015	0.9408
40	5x8x1	0.9358	0.0017	0.9392
42	6x7x1	0.9398	0.0015	0.9428
45	5x9x1	0.9397	0.0015	0.9427
48	6x8x1	0.9412	0.0016	0.9444
54	6x9x1	0.9425	0.0016	0.9457
56	7x8x1	0.9397	0.0015	0.9427
Regular Stacking Configuration – Array Sizes 2 Deep in z Direction				
40	4x5x2	0.9355	0.0016	0.9387
48	4x6x2	0.9353	0.0018	0.9389
56	4x7x2	0.9371	0.0014	0.9399
70	5x7x2	0.9411	0.0015	0.9441

Number of Containers	Array Size	Calculated k_{eff}	Uncertainty (σ)	k_{eff} + 2σ
Irregular Stacking Configuration (FLIP1) – Array Sizes 1 Deep in z Direction				
24	4x6x1	0.9354	0.0019	0.9392
25	5x5x1	0.9358	0.0015	0.9388
	5x5x1	0.9350	0.0016	0.9382
26	2x13x1	0.9344	0.0014	0.9372
	2x13x1	0.9304	0.0017	0.9338
27	3x9x1	0.9364	0.0015	0.9394
	3x9x1	0.9341	0.0017	0.9375
28	4x7x1	0.9372	0.0015	0.9402
	4x7x1	0.9426	0.0015	0.9456
30	5x6x1	0.9397	0.0018	0.9433
32	4x8x1	0.9386	0.0018	0.9422
35	5x7x1	0.9447	0.0016	0.9479
	5x7x1	0.9374	0.0015	0.9404
36	4x9x1	0.9402	0.0019	0.9440
	4x9x1	0.9402	0.0016	0.9434
40	5x8x1	0.9409	0.0017	0.9443
FLIP1 with Dry Fuel-Clad Gap and Spacing from Lid Stiffeners Eliminated (for Licensing-Basis Models)				
24	4x6x1	0.9314	0.0009	0.9332
28	4x7x1	0.9324	0.0009	0.9342
30	5x6x1	0.9326	0.0009	0.9344
32	4x8x1	0.9318	0.0009	0.9336
35	5x7x1	0.9327	0.0008	0.9343

36	4x9x1	0.9332	0.0008	0.9348
40	5x8x1	0.9366	0.0009	0.9384
FLIP1 with Flooded Fuel-Clad Gap and Spacing from Lid Stiffeners Eliminated (for Licensing-Basis Models), and Bounding 15 Type 1a Assembly with no Guide or Instrument Tube Cladding Credited				
24	4x6x1	0.9396	0.0008	0.9412
28	4x7x1	0.9415	0.0009	0.9433
30	5x6x1	0.9421	0.0010	0.9441
32	4x8x1	0.9405	0.0010	0.9425
35	5x7x1	0.9418	0.0008	0.9434
36	4x9x1	0.9404	0.0009	0.9422
40	5x8x1	0.9439	0.0010	0.9459
FLIP1 with Flooded Fuel-Clad Gap and Spacing from Lid Stiffeners Eliminated (for Licensing-Basis Models), and Bounding 15 Type 1a Assembly with Guide Tube Cladding Credited				
24	4x6x1	0.9381	0.0009	0.9399
28	4x7x1	0.9380	0.0009	0.9398
30	5x6x1	0.9391	0.0008	0.9407
32	4x8x1	0.9384	0.0009	0.9402
35	5x7x1	0.9376	0.0009	0.9394
36	4x9x1	0.9384	0.0009	0.9402
40	5x8x1	0.9397	0.0008	0.9413
FLIP1 with Flooded Fuel-Clad Gap and Spacing from Lid Stiffeners Eliminated (for Licensing-Basis Models), and Bounding 15 Type 1a Assembly with Guide and Instrument Tube Cladding Credited				
24	4x6x1	0.9338	0.0009	0.9356
28	4x7x1	0.9357	0.0009	0.9375
30	5x6x1	0.9380	0.0009	0.9398

32	4x8x1	0.9378	0.0009	0.9396
35	5x7x1	0.9366	0.0010	0.9386
36	4x9x1	0.9372	0.0008	0.9388
40	5x8x1	0.9394	0.0009	0.9412
FLIP1 with Flooded Fuel-Clad Gap and Spacing from Lid Stiffeners Eliminated (for Licensing-Basis Models), and 15 Type 3 Assembly with no Guide and Instrument Tube Cladding Credited				
24	4x6x1	0.9344	0.0008	0.9360
28	4x7x1	0.9357	0.0008	0.9373
30	5x6x1	0.9367	0.0009	0.9385
32	4x8x1	0.9374	0.0010	0.9394
35	5x7x1	0.9364	0.0009	0.9382
36	4x9x1	0.9356	0.0009	0.9374
40	5x8x1	0.9388	0.0009	0.9406

6.7.8 Removal of Spacing Provided by Lid Stiffeners

This section evaluates elimination of the spacing provided by the lid stiffeners to show the effect on the array k_{eff}. This was done to confirm the licensing-basis models which eliminate this spacing per the as-found condition after HAC testing. The perturbation was made on the FLIP1 4x6x1 base case with the fuel-clad gap flooded.

The results shown in Table 6-24 demonstrate that removal of the spacing is conservative or statistically insignificant.

Table 6-24 Results for sensitivity on container array for removal of spacing provided by lid spacers

Description	Calculated k_{eff}	Uncertainty (σ)	$k_{eff} + 2\sigma$
FLIP1 Configuration (spacing included)	0.9354	0.0019	0.9392
FLIP1 Configuration (spacing eliminated)	0.9361	0.0017	0.9395

6.8 BENCHMARK EVALUATIONS

The computer code used for these criticality calculations has been benchmarked against applicable criticality experiments.

6.8.1 Applicability of Benchmark Experiments

There are 55 critical benchmark experiments selected for MAP benchmarking from a larger group applicable to transportation and storage packages[5]. The larger group consisted of 180 experiments, 173 of which are LWR-type fuel pin lattice experiments (remaining 7 are homogeneous uranium experiments). The 55 experiments for the MAP package were selected based on their material, geometry, absorber, and overall spectral similarities to the MAP package. Table 6-25 provides a listing of the benchmark experiment groups from which the MAP experiments were selected and the number within groups that were selected for MAP benchmarking.

To understand how the selected experiments relate to the features important to criticality for the MAP package, the selected set was subdivided into four groups: Poison Plate Separation, Non-Poison Plate Separation, Water Hole Separation, and Simple Rod Lattice. These categories are specific to materials, absorbers, geometry, and moderation. These criticality parameters imply spectral similarities with the MAP which is verified through the calculations of Energy of the

[5] NUREG/CR-6361 (ORNL/TM-13211): Criticality Benchmark Guide for Light-Water-Reactor Fuel in Transportation and Storage Packages.

Average Lethargy Causing Fission (EALF). This provides a measure of the degree of neutron thermalization for a given experiment, and allows a simple, direct, and quantitative comparison to the MAP spectrum. There were 7 experiments grouped into Poison Plate Separation, 27 in Non-Poison Plate Separation, 6 in Water Hole Separation, and 15 in Simple Rod Lattice. Table 6-26 lists the grouping of the experiments.

The experiments within the larger group were rejected as non applicable to the MAP based on the following criteria:

1) No hexagonal fuel rod lattices, i.e. only square-pitch lattices;

2) Fixed poisons only in a plate-type geometric form (no soluble poison or poison rods) and contain only boron as the poison material;

3) No thick-wall reflectors (no lead, steel, or uranium thick-wall reflectors).

From the 180 experiments, 55 experiments were accepted and analyzed for applicability of key parameters to those for the MAP package. This analysis is summarized in Table 6-27. The KENOV input decks available from Reference 3 were converted to KENOVI format and run locally to provide the necessary calculated parameters for benchmarking. Appendix 6.9.3 provides a comparison between the calculated k_{eff} values for the original KENOV cases and those for the converted KENOVI cases to verify the conversion process.

The comparison provided in Table 6-27 shows that the selected benchmark set bounds the important characteristics of the MAP.

Table 6-25 Listing and descriptions of benchmark experiment groups that MAP benchmarks were selected from (reports referenced in Ref. 3), and number of experiments selected from each group

Report	No. of Available Experiments in Report	No. of Selected Experiments for MAP/ No. Listed in Ref. 3	Description of Full Set of Experiments in Report
ANS Transactions, Vol. 33, p. 362 (Ref. 4)	25	9/9	4.74 wt% ^{235}U UO_2 fuel rods in square lattices of 1.35 cm pitch; fuel rod clusters separated by air, polystyrene, polyethylene, or water; fuel clusters submersed in aqueous $NaNO_3$ solution
BAW-1484 (Ref. 5)	37	1/10	2.46 wt% ^{235}U UO_2 fuel rods in square lattices of 1.636 cm pitch; the spacing between 3 x 3 array of LWR-type fuel assemblies is filled with water and B_4C pins, stainless steel sheets, or borated stainless steel sheets; lattices with borated moderator
EPRI-NP-196 (Ref. 6)	6	3/6	2.35 wt% ^{235}U UO_2 fuel rods in square lattices of 1.562, 1.905, and 2.210 cm pitch; lattices with borated moderator
NS&E, Vol. 71 (Ref. 7)	26	3/6	4.74 wt% ^{235}U UO_2 fuel rods in square lattices of 1.26, 1.60, 2.10, and 2.52 cm pitch; triangular and triangular with pseudo-cylindrical shaped lattices of 1.35, 1.72, and 2.26 cm pitch; irregular hexagonal lattices of 1.35 cm pitch; lattices with water holes
PNL-2438 (Ref. 8)	48	4/6	2.35 wt% ^{235}U UO_2 fuel rods in square lattices of 2.032 cm pitch; Cd, Al, Cu, stainless steel, borated stainless steel, BORAL®, and Zircaloy separator plates between assemblies

Report	No. of Available Experiments in Report	No. of Selected Experiments for MAP/ No. Listed in Ref. 3	Description of Full Set of Experiments in Report
PNL-2615 (Ref. 9)	32	3/7	4.31 wt% ^{235}U UO_2 fuel rods in square lattices of 2.540 cm pitch; Cd, Al, Cu, stainless steel, borated stainless steel, BORAL®, and Zircaloy separator plates between assemblies
PNL-2827 (Ref. 10)	23	1/9	2.35 and 4.31 wt% ^{235}U UO_2 fuel rods in square lattices of 2.032 and 2.540 cm pitch; reflecting walls of Pb or depleted uranium
PNL-3314 (Ref. 11)	142	18/27	2.35 and 4.31 wt% ^{235}U UO_2 fuel rods in square lattices of 1.684 and 1.892 cm pitch; stainless steel, borated stainless steel, Cd, Al, Cu, BORAL®, Boroflex, and Zircaloy separator plates between assemblies; lattices with water holes and voids
PNL-3926 (Ref. 12)	22	2/14	2.35 and 4.31 wt% ^{235}U UO_2 fuel rods in square lattices of 1.684 and 1.892 cm pitch; reflecting walls of Pb or depleted uranium
PNL-6205 (Ref. 13)	19	1/1	4.31 wt% ^{235}U UO_2 fuel rods in square lattices of 1.891 cm pitch; BORAL® absorber plates
PNL-7167 (Ref. 14)	9	4/4	4.31 wt% ^{235}U UO_2 fuel rods in square lattices of 1.891 cm pitch; BORAL® absorber plates, with adjacent voids filled with Al plates, Al rods, or UO_2 fuel rods
WCAP-3269 (Ref. 15)	157	4/9	2.7, 3.7, and 5.7 wt% ^{235}U UO_2 fuel rods in square lattices of 1.029, 1.105, and 1.422 cm pitch; lattices with Ag-In-Cd absorber rods, water holes, and void tubes

Report	No. of Available Experiments in Report	No. of Selected Experiments for MAP/ No. Listed in Ref. 3	Description of Full Set of Experiments in Report
WCAP-3385 (Ref. 16)	3	2/2	5.74 wt% ^{235}U UO_2 fuel rods in square lattices of 1.321, 1.422, and 2.012 cm pitch

Table 6-26 Listing of MAP critical benchmark cases by report and by group

	MAP Critical Benchmark Experiment Group								
	Poison Plate Separation		Non-Poison Plate Separation		Water Hole Separation		Simple Rod Lattice		
Report	Case IDs	No. of Exp.	Case IDs	No. of Exp.	Case IDs	No. of Exp.	Case IDs	No. of Exp.	Total
ANS Transactions, Vol. 33, p. 362 (Ref. 4)			ANS33EB1 ANS33EB2 ANS33EP1 ANS33EP2 ANS33STY ANS33AL1 ANS33AL2 ANS33AL3	8			ANS33SLG	1	9
BAW-1484 (Ref. 5)							BW1484SL	1	1
EPRI-NP-196 (Ref. 6)							EPRU65 EPRU75 EPRU87	3	3
NS&E, Vol. 71 (Ref. 7)					NSE71W1 NSE71W2	2	NSE71SQ	1	3
PNL-2438 (Ref. 8)	P2438BA	1	P2438AL P2438SS	2			P2438SLG	1	4
PNL-2615	P2615BA	1	P2615AL	2					3

(Ref. 9)			P2615SS						
PNL-2827 (Ref. 10)							P2827SLG	1	1
PNL-3314 (Ref. 11)			P3314AL P3314BA P3314BC P3314BF1 P3314BF2 P3314BS1 P3314BS2 P3314BS3 P3314BS4 P3314SS1 P3314SS2 P3314SS3 P3314SS4 P3314SS5 P3314SS6	15	P3314W1 P3314W2	2	P3314SLG	1	18
PNL-3926 (Ref. 12)							P3926L1 P3926L2	2	2
PNL-6205 (Ref. 13)	P62FT231	1							1
PNL-7167 (Ref. 14)	P71F214R P71F14F3 P71F14V3 P71F14V5	4							4
WCAP-3269					W3269W1	2	W3269SL1	2	4

(Ref. 15)					W3269W2		W3269SL2		
WCAP-3385 (Ref. 16)							W3385SL1 W3385SL2	2	2
Total		7		27		6		15	**55**

Table 6-27 Comparison of critical benchmark experiment properties to MAP

	Critical Benchmark Experiments					
	All	**Poison Plate Separation**	**Non-Poison Plate Separation**	**Water Hole Separation**	**Simple Rod Lattice**	**MAP Package**
Number of benchmark cases	55	7	27	6	15	N/A
Geometric Properties of Lattice						
Water-to-fuel volume ratio	1.19 – 5.07	1.59 – 3.88	1.60 – 3.88	1.50 – 1.93	1.19 – 5.07	1.56 – 1.84
Lattice pitch (cm)	1.260 – 2.540	1.891 – 2.540	1.350 – 2.540	1.260 – 1.892	1.260 – 2.210	1.259 – 1.474
Properties of UO_2 Fuel Rods						
Clad OD (cm)	0.940 – 1.415	1.270 – 1.415	0.940 – 1.415	0.940 – 1.415	0.940 – 1.415	0.944 – 1.123
Pellet OD (cm)	0.790 – 1.265	1.118 – 1.265	0.790 – 1.265	0.790 – 1.265	0.790 – 1.265	0.817 – 0.969
Clad Wall Thickness (cm)	0.038 – 0.081	0.066 – 0.076	0.060 – 0.076	0.038 – 0.080	0.038 – 0.081	0.052 – 0.073
^{235}U Density in Fuel (g/cc)	0.191 – 0.516	0.191 – 0.395	0.191 – 0.434	0.191 – 0.512	0.191 – 0.516	0.272 – 0.474 (typically)
^{235}U Enrichment (wt% $^{235}U/U$)	2.350 – 5.742	2.350 – 4.310	2.350 – 4.742	2.350 – 5.700	2.350 – 5.742	3.000 – 5.000 (typically)
Borated Plate Properties						

Borated Plate Thickness (cm)	0 – 0.509	0.470 – 0.509	0	N/A	N/A	0.3175 (nom)
^{10}B Areal Density (g/cm^2)	0 – 0.0832	0.0668 – 0.0832	0	N/A	N/A	0.0240 (min)
Neutron Spectrum Properties						
EALF (eV)	0.0823 – 0.3730	0.0972 – 0.3730	0.0944 – 0.3229	0.1486 – 0.3087	0.0823 – 0.3236	0.2749 – 0.2831 (for License-Basis Single Container and Array Cases)

6.8.2 Determination of the Upper Safety Limit (USL)

The methodology employed for determination of the USL was consistent with that described in Reference 3. Calculation of k_{eff} was performed for each benchmark case described in Section 6.8.1 (modeled in KENOVI and utilizing the CSAS26 option of SCALE4.4a). These calculated values were then compared (statistically) with the experimental k_{eff} values through the use of the USLSTATS application. The results are shown in Figure 6-32, where the USL-1 and USL-2 plots are for the entire set of 55 experiments.

The minimum values for USL-1 and USL-2 were calculated to be 0.9405 and 0.9866, respectively (at the lower bound of EALF for the benchmark set). The administrative margin of 0.05 is supported by the statistically based minimum margin of subcriticality that was calculated to be 0.0039, and also that USL-2 is greater than USL-1, which is required. The results support an overall USL of 0.94 to be applied to the calculated values for cases presented in this analysis.

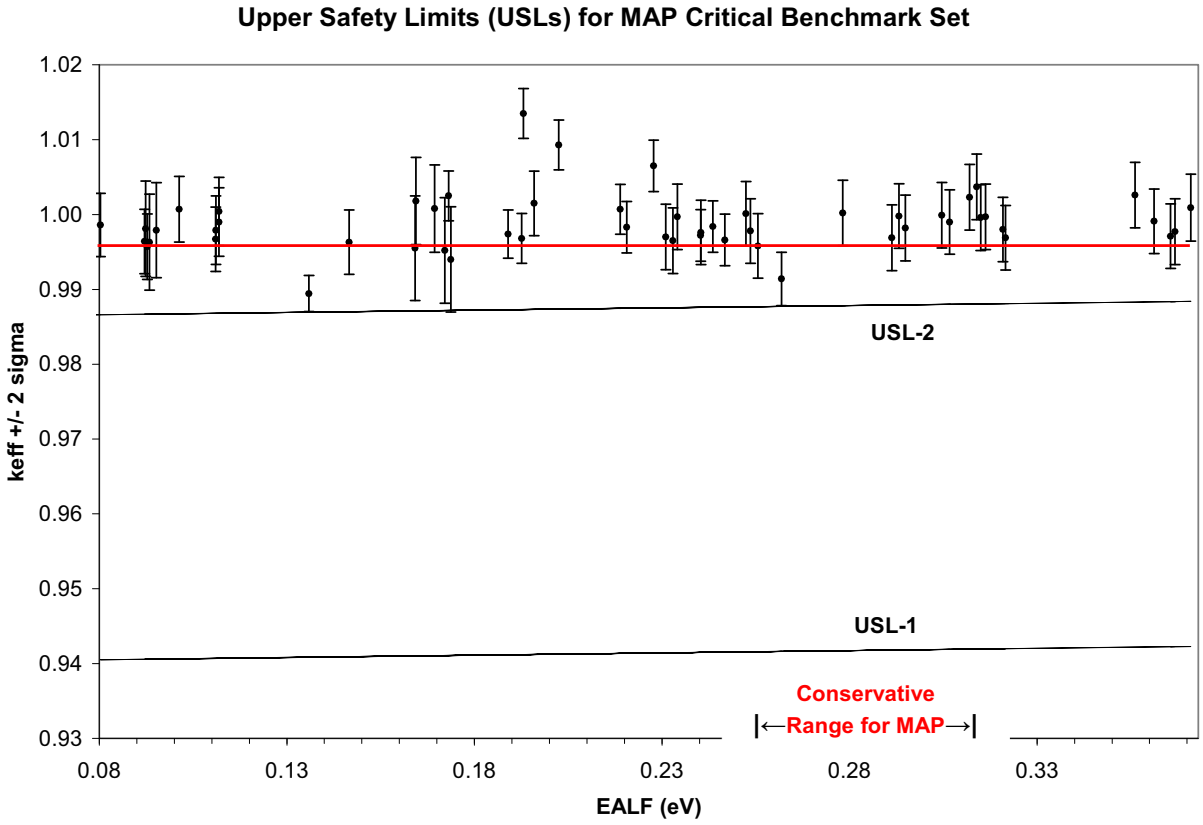

Figure 6-32 Critical benchmark experiment calculational results; shows USL-1 and USL-2 plots over range of EALF values for benchmark set

6.9 APPENDICES

This appendix provides additional information relevant to material contained in Section 6. These include the fuel assembly design parameters, the MAP-12 calculation, the KENOVI conversion verification, and sample licensing-basis cases for the package array and the single container.

6.9.1 Fuel Assembly Design Parameters and Pin Layouts

Tables 6-28 – 6-37 and Figures 6-33 – 6-36 provide the relevant design information used to create the fuel assembly models.

Table 6-28 Design parameters for the 14 Type 1 assembly

Dimension	Lengths in inches		
	Nominal	Tolerance	Bounding (Modeled)
Pellet OD	≤ 0.3805	0.0007	0.3812
Minimum Pellet OD	N/A	N/A	0.3758
Clad ID	≤ 0.387	0.002	0.389
Clad OD	≥ 0.440	0.002	0.438
Pitch	0.580	-	0.580
Active Fuel Length	144	-	163

Table 6-29 Design parameters for the 14 Type 2 assembly

Dimension	Lengths in inches		
	Nominal	Tolerance	Bounding (Modeled)
Pellet OD	≤ 0.3675	0.0007	0.3682
Minimum Pellet OD	N/A	N/A	0.3568
Clad ID	≤ 0.374	0.002	0.376
Clad OD	≥ 0.424	0.002	0.422
Pitch	0.556	-	0.556
Active Fuel Length	144	-	163

Table 6-30 Design parameters for the 15 Type 1a assembly

Dimension	Lengths in inches		
	Nominal	Tolerance	Bounding (Modeled)
Pellet OD	≤ 0.3615	0.0007	0.3622
Minimum Pellet OD	N/A	N/A	0.3608
Clad ID	≤ 0.368	0.002	0.37
Clad OD	≥ 0.416	0.002	0.414
Guide Tube ID	≤ 0.498	0.002	0.500
Guide Tube OD	≥ 0.530	0.002	0.528
Instrument Tube ID	≤ 0.441	0.002	0.443
Instrument Tube OD	≥ 0.493	0.002	0.491
Pitch	0.568	-	0.568
Active Fuel Length	144	-	163

Table 6-31 Design parameters for the 15 Type 1b assembly

Dimension	Lengths in inches		
	Nominal	Tolerance	Bounding (Modeled)
Pellet OD	≤ 0.3700	0.0007	0.3707
Minimum Pellet OD	N/A	N/A	0.3693
Clad ID	≤ 0.377	0.002	0.379
Clad OD	≥ 0.430	0.002	0.428
Pitch	0.568	-	0.568
Active Fuel Length	144	-	163

Table 6-32 Design parameters for the 15 Type 1c assembly

Dimension	Lengths in inches		
	Nominal	**Tolerance**	**Bounding (Modeled)**
Pellet OD	≤ 0.3735	0.0007	0.3742
Minimum Pellet OD	N/A	N/A	0.3728
Clad ID	≤ 0.380	0.002	0.382
Clad OD	≥ 0.430	0.002	0.428
Pitch	0.568	-	0.568
Active Fuel Length	144	-	163

Table 6-33 Design parameters for the 15 Type 2 assembly

Dimension	Lengths in inches		
	Nominal	**Tolerance**	**Bounding (Modeled)**
Pellet OD	≤ 0.3610	0.0007	0.3617
Minimum Pellet OD	N/A	N/A	0.3593
Clad ID	≤ 0.368	0.002	0.37
Clad OD	≥ 0.416	0.002	0.414
Pitch	0.550	-	0.550
Active Fuel Length	144	-	163

Table 6-34 Design parameters for the 15 Type 3 assembly

Dimension	Lengths in inches		
	Nominal	**Tolerance**	**Bounding (Modeled)**
Pellet OD	≤ 0.3675	0.0007	0.3682
Minimum Pellet OD	N/A	N/A	0.3558
Clad ID	≤ 0.374	0.002	0.376
Clad OD	≥ 0.424	0.002	0.422
Pitch	0.563	-	0.563
Active Fuel Length	144	-	163

Table 6-35 Design parameters for the 16 Type 1 assembly

Dimension	Lengths in inches		
	Nominal	**Tolerance**	**Bounding (Modeled)**
Pellet OD	≤ 0.3275	0.0007	0.3282
Minimum Pellet OD	N/A	N/A	0.3268
Clad ID	≤ 0.334	0.002	0.336
Clad OD	≥ 0.382	0.002	0.38
Pitch	0.506	-	0.506
Active Fuel Length	150	-	163

Table 6-36 Design parameters for the 17 Type 1 assembly

Dimension	Lengths in inches		
	Nominal	**Tolerance**	**Bounding (Modeled)**
Pellet OD	≤ 0.3245	0.0007	0.3252
Minimum Pellet OD	N/A	N/A	0.3238
Clad ID	≤ 0.331	0.002	0.333
Clad OD	≥ 0.379	0.002	0.377
Pitch	0.502	-	0.502
Active Fuel Length	144	-	163

Table 6-37 Design parameters for the 17 Type 2 assembly

Dimension	Lengths in inches		
	Nominal	**Tolerance**	**Bounding (Modeled)**
Pellet OD	≤ 0.3225	0.0007	0.3232
Minimum Pellet OD	N/A	N/A	0.3188
Clad ID	≤ 0.329	0.002	0.331
Clad OD	≥ 0.374	0.002	0.372
Pitch	0.496	-	0.496
Active Fuel Length	144	-	163

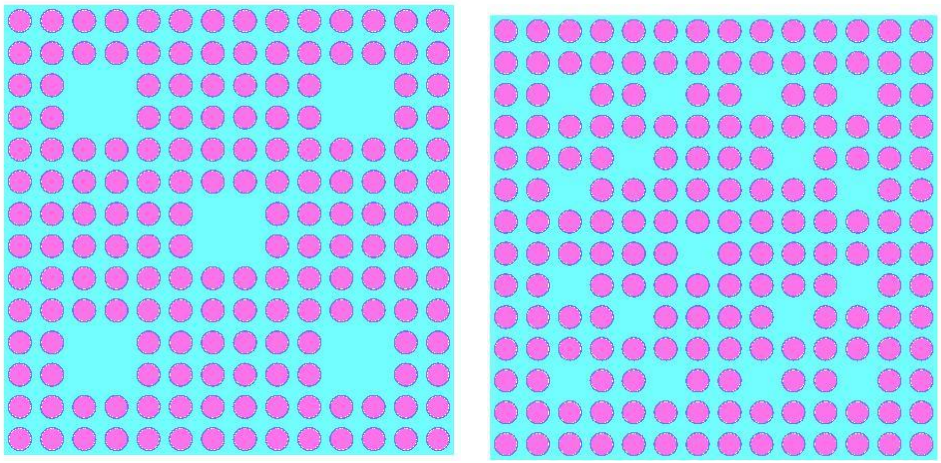

Figure 6-33 Pin layouts for 14x14 assemblies; 14 Type 1 (left – 20 non-fueled locations) and 14 Type 2 (right – 17 non-fueled locations)

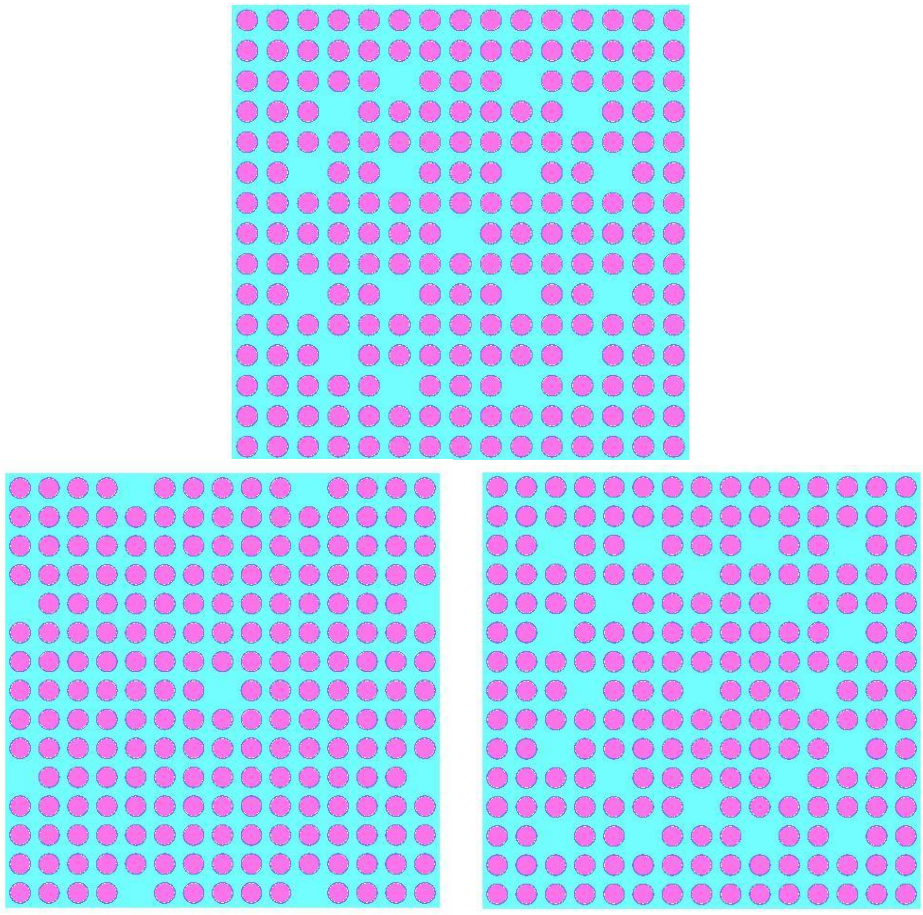

Figure 6-34 Pin layouts for 15x15 assemblies; 15 Type 1 (top – 17 non-fueled locations, note that center location is for instrument tube, and remaining 16 are for guide tubes), 15 Type 2 (bottom-left – 9 non-fueled locations), and 15 Type 3 (bottom-right – 21 non-fueled locations)

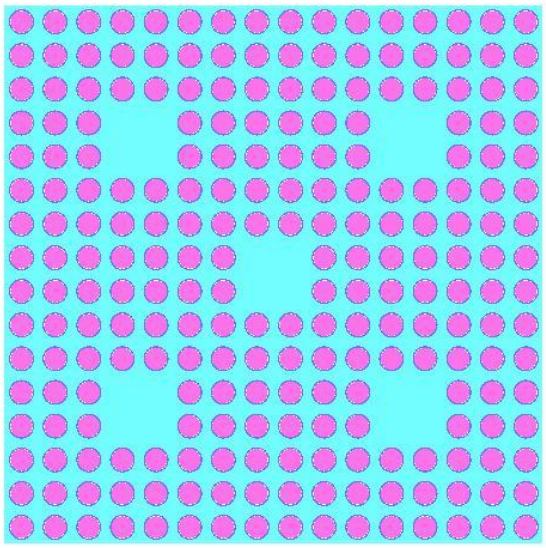

Figure 6-35 Pin layout for 16x16 assembly; 16 Type 1 (20 non-fueled locations)

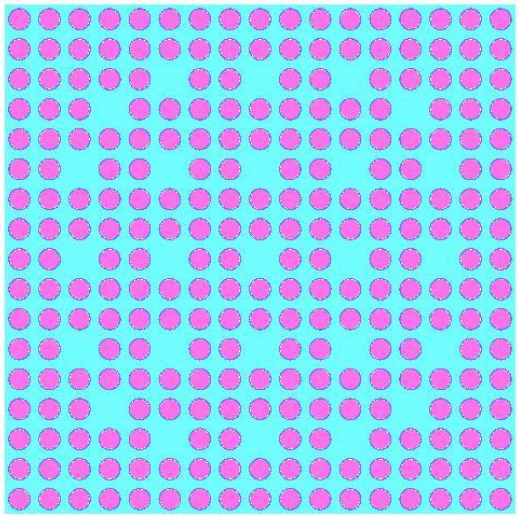

Figure 6-36 Pin layout for 17x17 assembly; 17 Type 1 and 17 Type 2 (25 non-fueled locations)

6.9.2 Explicit MAP-12 Calculation

An additional case was run to provide an explicit comparison between the modeling used in this analysis based on the MAP-13 package and one based on the MAP-12 package design. The intent is to demonstrate that the calculations presented in this analysis bound both package designs.

The only differences between the two designs that may affect the criticality analysis are those differences that exist in the flux trap (axial) region. The MAP-13 and MAP-12 flux trap regions are identical except that the axial bottom and top sections are 6.38 and 6.53 inches shorter (nominal) for the MAP-12. This gives a total flux trap length of about 150 inches for the MAP-12 (there are 11 axial sections, with the inner 9 being identical; these inner sections are the same for both the MAP-12 and MAP-13) versus 163 inches for the MAP-13. In addition, the inside spacer blocks (incrementally spaced over the length of the container) have different axial (z-direction) lengths and the axial spacing between the blocks is different. The blocks for the MAP-12 are 2.5 inches shorter and are spaced 2.5 inches closer together (center-to-center).

These modifications were made to the license-basis case for the package array, to evaluate the same condition with the MAP-12. The results are shown in Table 6-38. The results show that the difference is statistically insignificant, although the MAP-12 has a slightly lower calculated k_{eff}. This confirms that the criticality analysis bounds both the MAP-13 and MAP-12 designs.

Table 6-38 Comparison between the MAP-13 and MAP-12

Description	Calculated k_{eff}	Uncertainty (σ)	$k_{eff} + 2\sigma$
Array licensing-basis case with dry fuel-clad gap (MAP-13)	0.9324	0.0016	0.9356
Array licensing-basis case with dry-fuel clad gap (MAP-12)	0.9313	0.0016	0.9345

6.9.3 Comparison between KENOV and KENOVI Versions of Benchmarks

Table 6-39 shows the comparison between results from the original KENOV versions of the benchmark input cases and the converted KENOVI cases used for benchmarking in this analysis. There are differences in calculated k_{eff}, as expected from the Monte Carlo method. However, the majority of the differences are within 1 sigma, and all are within 2 sigma statistical uncertainty. Therefore, it is concluded that the differences between the original KENOV and the converted KENOVI cases are statistically insignificant and the converted KENOVI cases are valid for benchmarking.

Table 6-39 Comparison between the benchmark cases in KENOV (original verified cases) and KENOVI (converted cases) formats

	KENOV		KENOVI		KENOV – KENOVI	
Case ID	**Calculated k_{eff}**	**Uncertainty (σ)**	**Calculated k_{eff}**	**Uncertainty (σ)**	**Δk_{eff}**	**Combined Uncertainty (1σ)**
P2438BA	0.9975	0.0008	0.9979	0.0007	0.0004	0.0011
P2615BA	0.9988	0.0008	1.0004	0.0009	0.0016	0.0012
P62FT231	1.0003	0.0010	1.0026	0.0009	0.0023	0.0013
P71F214R	0.9983	0.0009	0.9991	0.0008	0.0008	0.0012
P71F14F3	0.9998	0.0009	1.0009	0.0010	0.0011	0.0013
P71F14V3	0.9982	0.0008	0.9971	0.0008	-0.0011	0.0011
P71F14V5	0.9985	0.0009	0.9977	0.0009	-0.0008	0.0013
ANS33EB1	0.9970	0.0009	0.9972	0.0010	0.0002	0.0013
ANS33EB2	1.0084	0.0010	1.0093	0.0009	0.0009	0.0013
ANS33EP1	0.9966	0.0008	0.9966	0.0010	0.0000	0.0013
ANS33EP2	0.9991	0.0008	1.0007	0.0009	0.0016	0.0012
ANS33STY	0.9918	0.0011	0.9914	0.0011	-0.0004	0.0016
ANS33AL1	1.0082	0.0008	1.0065	0.0010	-0.0017	0.0013

ANS33AL2	1.0109	0.0009	1.0135	0.0009	0.0026	0.0013	
ANS33AL3	1.0016	0.0010	1.0025	0.0009	0.0009	0.0013	
P2438AL	0.9969	0.0007	0.9981	0.0007	0.0012	0.0010	
P2438SS	0.9968	0.0008	0.9963	0.0008	-0.0005	0.0011	
P2615AL	0.9979	0.0009	0.9979	0.0009	0.0000	0.0013	
P2615SS	0.9985	0.0008	0.9990	0.0009	0.0005	0.0012	
P3314AL	0.9954	0.0008	0.9965	0.0009	0.0011	0.0012	
P3314BA	0.9998	0.0009	0.9980	0.0008	-0.0018	0.0012	
P3314BC	1.0003	0.0009	0.9996	0.0009	-0.0007	0.0013	
P3314BF1	1.0011	0.0009	1.0023	0.0009	0.0012	0.0013	
P3314BF2	1.0003	0.0009	0.9997	0.0009	-0.0006	0.0013	
P3314BS1	0.9965	0.0008	0.9952	0.0009	-0.0013	0.0012	
P3314BS2	0.9940	0.0008	0.9940	0.0009	0.0000	0.0012	
P3314BS3	0.9984	0.0008	0.9969	0.0009	-0.0015	0.0012	
P3314BS4	1.0008	0.0008	0.9998	0.0008	-0.0010	0.0011	
P3314SS1	0.9995	0.0008	0.9997	0.0009	0.0002	0.0012	
P3314SS2	0.9993	0.0008	1.0001	0.0008	0.0008	0.0011	
P3314SS3	0.9982	0.0008	0.9976	0.0008	-0.0006	0.0011	
P3314SS4	0.9976	0.0008	0.9978	0.0008	0.0002	0.0011	
P3314SS5	0.9940	0.0009	0.9955	0.0008	0.0015	0.0012	
P3314SS6	0.9994	0.0008	1.0002	0.0009	0.0008	0.0012	
NSE71W1	0.9965	0.0010	0.9983	0.0010	0.0018	0.0014	
NSE71W2	0.9979	0.0008	0.9974	0.0008	-0.0005	0.0011	
P3314W1	1.0018	0.0010	1.0015	0.0008	-0.0003	0.0013	
P3314W2	0.9965	0.0009	0.9963	0.0008	-0.0002	0.0012	
W3269W1	0.9981	0.0008	0.9990	0.0008	0.0009	0.0011	

W3269W2	0.9996	0.0010	0.9999	0.0009	0.0003	0.0013	
ANS33SLG	0.9975	0.0008	0.9968	0.0009	-0.0007	0.0012	
BW1484SL	0.9940	0.0008	0.9924	0.0008	-0.0016	0.0011	
EPRU65	0.9967	0.0008	0.9958	0.0008	-0.0009	0.0011	
EPRU75	0.9971	0.0009	0.9967	0.0008	-0.0004	0.0012	
EPRU87	0.9981	0.0008	0.9986	0.0007	0.0005	0.0011	
NSE71SQ	0.9977	0.0010	0.9984	0.0010	0.0007	0.0014	
P2438SLG	0.9961	0.0007	0.9957	0.0009	-0.0004	0.0011	
P2827SLG	0.9962	0.0008	0.9964	0.0008	0.0002	0.0011	
P3314SLG	0.9974	0.0009	0.9970	0.0009	-0.0004	0.0013	
P3926L1	1.0013	0.0007	1.0008	0.0008	-0.0005	0.0011	
P3926L2	1.0008	0.0007	1.0018	0.0008	0.0010	0.0011	
W3269SL1	0.9973	0.0009	0.9969	0.0008	-0.0004	0.0012	
W3269SL2	1.0029	0.0008	1.0037	0.0009	0.0008	0.0012	
W3385SL1	0.9963	0.0009	0.9982	0.0009	0.0019	0.0013	
W3385SL2	1.0005	0.0009	1.0007	0.0009	0.0002	0.0013	

6.9.4 Sample Input Cases

6.9.4.1 Input for Licensing-Basis Case for Package Array with Dry Fuel-Clad Gap

```
=csas26     parm='size=900000'
15type1 fa in shipping container
238g     latticecell
'100% td and 5.0 w/o
uo2  1   1.0 293 92235 5 92238 95 end
'zirc
zr  2   1.0 293 end
'water in assy lattice
h2o  3   1.0 293 end

'volume in container external to bundles
h2o  4   1.0e-8   293 end

'rubber
h2o  5 1.0 293 end

' ss plate, 0.13" thick
ss304  6   1.0   293 end

'  boral, minimum areal density(at min thk)=0.0240 gm b-10/sqcm
' min thk = 0.119" = 0.30226cm
' vol dens = 0.0240/(0.30226*0.18431) =0.4308 gm natural b/cucm
' we use only 75%, 0.75 * 0.4308 = 0.3231 gm natural b/cucm
b  7   den=0.3231 1 293 end

'nylon 66
arbmnyl 1.14 4 0 1 0 6012 6 7014 1 8016 1 1001 11 8 1.0 293 end

'reflector water
h2o  9   1.0 293 end

' ss plate, 0.085" thick
ss304  10   1.0   293 end

' ss plate, 0.115" thick
ss304  11   1.0   293 end

' gap water
h2o  12   1.0 293 end
```

```
' aluminum for doors
al  13 1 293 end

' ss bar at center
ss304  14   1.0   293 end
end comp
squarepitch 1.44272 0.91999 1 3 1.05156 2 0.93980 0 end

more data
dab=2000
res=6 slab 0.3302
res=10 slab 0.2159
res=11 slab 0.2921
res=14 cyli 1.563
end more

read parm tme=120 gen=280 nsk=3 run=yes npg=1000 far=yes plt=yes
lng=3000000 nb8=1200
end parm
read geometry

unit  10
com='wet fuel pin cell'

' fuel stack
cyli  10 0.45999 2p207.01

' clad inner surface
cyli  20 0.46990 2p207.01

' clad outer surface
cyli  30 0.52578 2p207.01

' unit cell
cubo  40 4p0.72136 2p207.01

' fuel
media  1 1 10

' fuel-clad gap (void)
media  0 1 20 -10
```

```
' clad
media  2 1 30 -20

' water or whatever is external to clad
media  3 1 40 -30

boundary  40

unit  20
com='wet guidetube cell-no clad'

' guide tube inner surface
cyli  10 0.63500 2p207.01

' guide tube outer surface
cyli  20 0.67056 2p207.01

' unit cell
cubo  40 4p0.72136 2p207.01

' water or whatever is internal to clad
media  3 1 10

' clad
media  3 1 20 -10

' water or whatever is external to clad
media  3 1 40 -20

boundary  40

unit  30
com='wet instrument tube cell-no clad'

' instrument tube inner surface
cyli  10 0.56261 2p207.01

' instrument tube outer surface
cyli  20 0.62357 2p207.01

' unit cell
cubo  40 4p0.72136 2p207.01
```

```
' water or whatever is internal to clad
media  3 1 10

' clad-water
media  3 1 20 -10

' water or whatever is external to clad
media  3 1 40 -20

boundary  40

' region type=pad
' edge type=base_inner_full
unit 200

cubo 100  10.79500 -10.79500 0.31750 -0.31750 207.01000 -207.01000

media 5 1 100

boundary 100

' region type=pad
' edge type=base_outer_full
unit 210

cubo 100  10.79500 -10.79500 0.31750 -0.31750 207.01000 -207.01000


media 5 1 100

boundary 100

' region type=steel
' edge type=base_inner_full
unit 300

cubo 100  11.60249 -11.60249 0.16510 -0.16510 207.01000 -207.01000


media 6 1 100

boundary 100
```

```
' region type=steel
' edge type=base_outer_full
unit 310

cubo 100  10.91999 -10.91999 0.16510 -0.16510 207.01000 -207.01000

media 6 1 100

boundary 100

' region type=steel
' edge type=lid_inner_lower
unit 320

cubo 100  6.27380 -6.27380 0.10795 -0.10795 207.01000 -207.01000

media 10 1 100

boundary 100

' region type=steel
' edge type=lid_inner_upper
unit 330

cubo 100  5.13080 -5.13080 0.10795 -0.10795 207.01000 -207.01000

media 10 1 100

boundary 100

' region type=steel
' edge type=lid_outer_upper
unit 340

cubo 100  6.15950 -6.15950 0.10795 -0.10795 207.01000 -207.01000


media 10 1 100

boundary 100

' region type=steel
```

```
' edge type=lid_outer_lower
unit 350

cubo 100  6.51510 -6.51510 0.10795 -0.10795 207.01000 -207.01000



media 10 1 100

boundary 100

' region type=boral
' edge type=base_inner_full
' axial part type=lower(1)
unit 400

cubo 100 9.52500 -9.52500 0.15113 -0.15113 14.42720 -14.42720

cubo 200 9.52500 -9.52500 0.15113 -0.15113 15.07490 -14.42720

media 7 1 100



media  4 1 -100 200

boundary  200

' region type=boral
' edge type=base_inner_full
' axial part type=main(9)
unit 402

cubo 100 9.52500 -9.52500 0.15113 -0.15113 19.17700 -19.17700

cubo 200 9.52500 -9.52500 0.15113 -0.15113 19.82470 -19.82470



media 7 1 100



media  4 1 -100 200

boundary  200
```

```
' region type=boral
' edge type=base_inner_full
' axial part type=upper(1)
unit 404

cubo 100 9.52500 -9.52500 0.15113 -0.15113 13.51280 -13.51280

cubo 200 9.52500 -9.52500 0.15113 -0.15113 13.51280 -14.16050

media 7 1 100
media  4 1 -100 200

boundary  200

' region type=boral
' edge type=base_inner_full
' axial array
unit 406

cubo 10 9.52500 -9.52500 0.15113 -0.15113 207.01000 -207.01000

array 406 10  place  1 1 1  0 0 -192.58280

boundary  10

' region type=boral
' edge type=base_outer_full
' axial part type=lower(1)
unit 410

cubo 100 9.52500 -9.52500 0.15113 -0.15113 14.42720 -14.42720

cubo 200 9.52500 -9.52500 0.15113 -0.15113 15.07490 -14.42720

media 7 1 100


media  4 1 -100 200

boundary  200

' region type=boral
' edge type=base_outer_full
```

```
' axial part type=main(9)
unit 412

cubo 100 9.52500 -9.52500 0.15113 -0.15113 19.17700 -19.17700

cubo 200 9.52500 -9.52500 0.15113 -0.15113 19.82470 -19.82470

media 7 1 100

media  4 1 -100 200

boundary  200

' region type=boral
' edge type=base_outer_full
' axial part type=upper(1)
unit 414

cubo 100 9.52500 -9.52500 0.15113 -0.15113 13.51280 -13.51280

cubo 200 9.52500 -9.52500 0.15113 -0.15113 13.51280 -14.16050

media 7 1 100

media  4 1 -100 200

boundary  200

' region type=boral
' edge type=base_outer_full
' axial array
unit 416

cubo 10 9.52500 -9.52500 0.15113 -0.15113 207.01000 -207.01000

array 416 10  place  1 1 1  0 0 -192.58280

boundary  10

' region type=boral
' edge type=lid_inner_lower
' axial part type=lower(1)
unit 420
```

```
cubo 100 6.03250 -6.03250 0.15113 -0.15113 14.42720 -14.42720

cubo 200 6.03250 -6.03250 0.15113 -0.15113 15.07490 -14.42720

media 7 1 100

media  4 1 -100 200

boundary  200

' region type=boral
' edge type=lid_inner_lower
' axial part type=main(9)
unit 422

cubo 100 6.03250 -6.03250 0.15113 -0.15113 19.17700 -19.17700

cubo 200 6.03250 -6.03250 0.15113 -0.15113 19.82470 -19.82470

media 7 1 100

media  4 1 -100 200

boundary  200

' region type=boral
' edge type=lid_inner_lower
' axial part type=upper(1)
unit 424

cubo 100 6.03250 -6.03250 0.15113 -0.15113 13.51280 -13.51280

cubo 200 6.03250 -6.03250 0.15113 -0.15113 13.51280 -14.16050


media 7 1 100

media  4 1 -100 200

boundary  200

' region type=boral
```

```
' edge type=lid_inner_lower
' axial array
unit 426

cubo 10 6.03250 -6.03250 0.15113 -0.15113 207.01000 -207.01000

array 426 10  place  1 1 1  0 0 -192.58280

boundary  10

' region type=boral
' edge type=lid_inner_upper
' axial part type=lower(1)
unit 430

cubo 100 4.95300 -4.95300 0.15113 -0.15113 14.42720 -14.42720

cubo 200 4.95300 -4.95300 0.15113 -0.15113 15.07490 -14.42720

media 7 1 100

media  4 1 -100 200

boundary  200

' region type=boral
' edge type=lid_inner_upper
' axial part type=main(9)
unit 432

cubo 100 4.95300 -4.95300 0.15113 -0.15113 19.17700 -19.17700

cubo 200 4.95300 -4.95300 0.15113 -0.15113 19.82470 -19.82470

media 7 1 100

media  4 1 -100 200

boundary  200

' region type=boral
' edge type=lid_inner_upper
' axial part type=upper(1)
```

```
unit 434

cubo 100 4.95300 -4.95300 0.15113 -0.15113 13.51280 -13.51280

cubo 200 4.95300 -4.95300 0.15113 -0.15113 13.51280 -14.16050

media 7 1 100

media  4 1 -100 200

boundary  200

' region type=boral
' edge type=lid_inner_upper
' axial array
unit 436

cubo 10 4.95300 -4.95300 0.15113 -0.15113 207.01000 -207.01000

array 436 10  place  1 1 1  0 0 -192.58280

boundary  10

' region type=boral
' edge type=lid_outer_upper
' axial part type=lower(1)
unit 440

cubo 100 6.03250 -6.03250 0.15113 -0.15113 14.42720 -14.42720

cubo 200 6.03250 -6.03250 0.15113 -0.15113 15.07490 -14.42720



media 7 1 100

media  4 1 -100 200

boundary  200

' region type=boral
' edge type=lid_outer_upper
' axial part type=main(9)
unit 442
```

```
cubo 100 6.03250 -6.03250 0.15113 -0.15113 19.17700 -19.17700

cubo 200 6.03250 -6.03250 0.15113 -0.15113 19.82470 -19.82470

media 7 1 100

media  4 1 -100 200

boundary  200

' region type=boral
' edge type=lid_outer_upper
' axial part type=upper(1)
unit 444

cubo 100 6.03250 -6.03250 0.15113 -0.15113 13.51280 -13.51280

cubo 200 6.03250 -6.03250 0.15113 -0.15113 13.51280 -14.16050

media 7 1 100

media  4 1 -100 200

boundary  200

' region type=boral
' edge type=lid_outer_upper
' axial array
unit 446

cubo 10 6.03250 -6.03250 0.15113 -0.15113 207.01000 -207.01000

array 446 10  place  1 1 1  0 0 -192.58280

boundary  10

' region type=boral
' edge type=lid_outer_lower
' axial part type=lower(1)
unit 450

cubo 100 5.88010 -5.88010 0.15113 -0.15113 14.42720 -14.42720
```

```
cubo 200 5.88010 -5.88010 0.15113 -0.15113 15.07490 -14.42720

media 7 1 100
media  4 1 -100 200

boundary  200

' region type=boral
' edge type=lid_outer_lower
' axial part type=main(9)
unit 452

cubo 100 5.88010 -5.88010 0.15113 -0.15113 19.17700 -19.17700

cubo 200 5.88010 -5.88010 0.15113 -0.15113 19.82470 -19.82470

media 7 1 100

media  4 1 -100 200

boundary  200

' region type=boral
' edge type=lid_outer_lower
' axial part type=upper(1)
unit 454

cubo 100 5.88010 -5.88010 0.15113 -0.15113 13.51280 -13.51280

cubo 200 5.88010 -5.88010 0.15113 -0.15113 13.51280 -14.16050

media 7 1 100

media  4 1 -100 200

boundary  200

' region type=boral
' edge type=lid_outer_lower
' axial array
unit 456
```

```
cubo 10 5.88010 -5.88010 0.15113 -0.15113 207.01000 -207.01000

array 456 10  place  1 1 1  0 0 -192.58280

boundary  10

' region type=plastic
' edge type=base_inner_full
' axial part type=lower(1)
unit 1160
com=' part 16 plastic block'
' plastic thickness removed=0.0781 inch =0.19844 cm

' bevel surface at -x
plane  10 xpl=1 origin x=-9.24437 y=1.48828 rotate a3=45

' bevel surface at +x
plane  20 xpl=1 origin x=9.24437 y=1.48828 rotate a3=-45
' thinned block without bevels, without axial gaps
cubo 100 9.24437 -9.24437 1.48828 -1.48828 2p14.22876

' thinned block without bevels, with axial gaps
cubo 200 9.24437 -9.24437 1.48828 -1.48828 15.07490 -14.42720

media  8 1 10 -20 100

media  4 1 -10 100
media  4 1 20 100

media  4 1 -100 200
boundary  200

' region type=plastic
' edge type=base_inner_full
' axial part type=main(9)
unit 1162
com=' part 16 plastic block'
' plastic thickness removed=0.0781 inch =0.19844 cm

' bevel surface at -x
plane  10 xpl=1 origin x=-9.24437 y=1.48828 rotate a3=45

' bevel surface at +x
```

```
plane  20 xpl=1 origin x=9.24437 y=1.48828 rotate a3=-45
' thinned block without bevels, without axial gaps
cubo 100 9.24437 -9.24437 1.48828 -1.48828 2p18.97856

' thinned block without bevels, with axial gaps
cubo 200 9.24437 -9.24437 1.48828 -1.48828 2p19.82470

media  8 1 10 -20 100

media  4 1 -10 100
media  4 1 20 100

media  4 1 -100 200
boundary  200

' region type=plastic
' edge type=base_inner_full
' axial part type=upper(1)
unit 1164
com=' part 16 plastic block'
' plastic thickness removed=0.0781 inch =0.19844 cm

' bevel surface at -x
plane  10 xpl=1 origin x=-9.24437 y=1.48828 rotate a3=45

' bevel surface at +x
plane  20 xpl=1 origin x=9.24437 y=1.48828 rotate a3=-45
' thinned block without bevels, without axial gaps
cubo 100 9.24437 -9.24437 1.48828 -1.48828 2p13.31436

' thinned block without bevels, with axial gaps
cubo 200 9.24437 -9.24437 1.48828 -1.48828 13.51280 -14.16050

media  8 1 10 -20 100

media  4 1 -10 100
media  4 1 20 100

media  4 1 -100 200
boundary  200

' region type=plastic
' edge type=base_inner_full
```

```
' axial array
unit 1166

cubo 10 9.24437 -9.24437 1.48828 -1.48828 206.81156 -206.81156

array 1166 10  place  1 1 1  0 0 -192.38436

boundary  10

' region type=plastic
' edge type=base_inner_full
' axial part type=lower(1)
unit 2160
com=' part 16 plastic block (right)'
' plastic thickness removed=0.0781 inch =0.19844 cm

' bevel surface at -x
plane  10 xpl=1 origin x=-9.24437 y=1.48828 rotate a3=45

' bevel surface at +x
plane  20 xpl=1 origin x=9.24437 y=1.48828 rotate a3=-45
' thinned block without bevels, without axial gaps
cubo 100 9.24437 -9.24437 1.48828 -1.48828 2p14.22876

' thinned block without bevels, with axial gaps
cubo 200 9.24437 -9.24437 1.48828 -1.48828 15.07490 -14.42720

media  8 1 10 -20 100



media  4 1 -10 100
media  4 1 20 100

media  4 1 -100 200
boundary  200

' region type=plastic
' edge type=base_inner_full
' axial part type=main(9)
unit 2162
com=' part 16 plastic block (right)'
' plastic thickness removed=0.0781 inch =0.19844 cm
```

```
' bevel surface at -x
plane  10 xpl=1 origin x=-9.24437 y=1.48828 rotate a3=45

' bevel surface at +x
plane  20 xpl=1 origin x=9.24437 y=1.48828 rotate a3=-45
' thinned block without bevels, without axial gaps
cubo 100 9.24437 -9.24437 1.48828 -1.48828 2p18.97856

' thinned block without bevels, with axial gaps
cubo 200 9.24437 -9.24437 1.48828 -1.48828 2p19.82470

media  8 1 10 -20 100

media  4 1 -10 100
media  4 1 20 100

media  4 1 -100 200
boundary  200

' region type=plastic
' edge type=base_inner_full
' axial part type=upper(1)
unit 2164
com=' part 16 plastic block (right)'
' plastic thickness removed=0.0781 inch =0.19844 cm

' bevel surface at -x
plane  10 xpl=1 origin x=-9.24437 y=1.48828 rotate a3=45

' bevel surface at +x
plane  20 xpl=1 origin x=9.24437 y=1.48828 rotate a3=-45
' thinned block without bevels, without axial gaps
cubo 100 9.24437 -9.24437 1.48828 -1.48828 2p13.31436

' thinned block without bevels, with axial gaps
cubo 200 9.24437 -9.24437 1.48828 -1.48828 13.51280 -14.16050

media  8 1 10 -20 100

media  4 1 -10 100
media  4 1 20 100

media  4 1 -100 200
```

```
boundary  200

' region type=plastic
' edge type=base_inner_full  (right)
' axial array
unit 2166

cubo 10 9.24437 -9.24437 1.48828 -1.48828 206.78366 -206.78366

array 2166 10  place  1 1 1  0 0 -192.38436

boundary 10

' region type=plastic
' edge type=base_outer_full
' axial part type=lower(1)
unit 1170
com=' part 17l plastic block'
' plastic thickness removed=0.0781 inch =0.19844 cm

' bevel surface at -x
plane  10 xpl=1 origin x=-9.24437 y=.31512 rotate a3=45

' bevel surface at +x
plane  20 xpl=1 origin x=9.24437 y=1.48828 rotate a3=-45
' thinned block without bevels, without axial gaps
cubo 100 9.24437 -9.24437 1.48828 -1.48828 2p14.22876

' thinned block without bevels, with axial gaps
cubo 200 9.24437 -9.24437 1.48828 -1.48828 15.07490 -14.42720

media  8 1 10 -20 100

media  4 1 -10 100
media  4 1 20 100

media  4 1 -100 200
boundary  200

' region type=plastic
' edge type=base_outer_full
' axial part type=main(9)
unit 1172
```

```
com=' part 17l plastic block'
' plastic thickness removed=0.0781 inch =0.19844 cm

' bevel surface at -x
plane  10 xpl=1 origin x=-9.24437 y=.31512 rotate a3=45

' bevel surface at +x
plane  20 xpl=1 origin x=9.24437 y=1.48828 rotate a3=-45
' thinned block without bevels, without axial gaps
cubo 100 9.24437 -9.24437 1.48828 -1.48828 2p18.97856

' thinned block without bevels, with axial gaps
cubo 200 9.24437 -9.24437 1.48828 -1.48828 2p19.82470

media  8 1 10 -20 100

media  4 1 -10 100
media  4 1 20 100

media  4 1 -100 200
boundary  200

' region type=plastic
' edge type=base_outer_full
' axial part type=upper(1)
unit 1174
com=' part 17l plastic block'
' plastic thickness removed=0.0781 inch =0.19844 cm

' bevel surface at -x
plane  10 xpl=1 origin x=-9.24437 y=.31512 rotate a3=45

' bevel surface at +x
plane  20 xpl=1 origin x=9.24437 y=1.48828 rotate a3=-45
' thinned block without bevels, without axial gaps
cubo 100 9.24437 -9.24437 1.48828 -1.48828 2p13.31436

' thinned block without bevels, with axial gaps
cubo 200 9.24437 -9.24437 1.48828 -1.48828 13.51280 -14.16050

media  8 1 10 -20 100
media  4 1 -10 100
media  4 1 20 100
```

```
media  4 1 -100 200
boundary  200

' region type=plastic
' edge type=base_outer_full
' axial array
unit 1176

cubo 10 9.24437 -9.24437 1.48828 -1.48828 206.81156 -206.81156

array 1176 10  place  1 1 1  0 0 -192.38436

boundary  10

' region type=plastic
' edge type=base_outer_full
' axial part type=lower(1)
unit 2170
com=' part 17r plastic block'
' plastic thickness removed=0.0781 inch =0.19844 cm

' bevel surface at -x
plane  10 xpl=1 origin x=-9.24437 y=1.48828 rotate a3=45

' bevel surface at +x
plane  20 xpl=1 origin x=9.24437 y=.31512 rotate a3=-45
' thinned block without bevels, without axial gaps
cubo 100 9.24437 -9.24437 1.48828 -1.48828 2p14.22876

' thinned block without bevels, with axial gaps
cubo 200 9.24437 -9.24437 1.48828 -1.48828 15.07490 -14.42720

media  8 1 10 -20 100

media  4 1 -10 100
media  4 1 20 100

media  4 1 -100 200
boundary  200

' region type=plastic
' edge type=base_outer_full
```

```
' axial part type=main(9)
unit 2172
com=' part 17r plastic block'
' plastic thickness removed=0.0781 inch =0.19844 cm

' bevel surface at -x
plane  10 xpl=1 origin x=-9.24437 y=1.48828 rotate a3=45

' bevel surface at +x
plane  20 xpl=1 origin x=9.24437 y=.31512 rotate a3=-45
' thinned block without bevels, without axial gaps
cubo 100 9.24437 -9.24437 1.48828 -1.48828 2p18.97856

' thinned block without bevels, with axial gaps
cubo 200 9.24437 -9.24437 1.48828 -1.48828 2p19.82470

media  8 1 10 -20 100

media  4 1 -10 100
media  4 1 20 100

media  4 1 -100 200
boundary  200

' region type=plastic
' edge type=base_outer_full
' axial part type=upper(1)
unit 2174
com=' part 17r plastic block'
' plastic thickness removed=0.0781 inch =0.19844 cm

' bevel surface at -x
plane  10 xpl=1 origin x=-9.24437 y=1.48828 rotate a3=45

' bevel surface at +x
plane  20 xpl=1 origin x=9.24437 y=.31512 rotate a3=-45
' thinned block without bevels, without axial gaps
cubo 100 9.24437 -9.24437 1.48828 -1.48828 2p13.31436

' thinned block without bevels, with axial gaps
cubo 200 9.24437 -9.24437 1.48828 -1.48828 13.51280 -14.16050

media  8 1 10 -20 100
```

```
media  4 1 -10 100
media  4 1 20 100

media  4 1 -100 200
boundary  200

' region type=plastic
' edge type=base_outer_full
' axial array
unit 2176

cubo 10 9.24437 -9.24437 1.48828 -1.48828 206.81156 -206.81156

array 2176 10  place  1 1 1  0 0 -192.38436

boundary  10

' region type=plastic
' edge type=lid_inner_lower
' axial part type=lower(1)
unit 1550
com=' part 55l plastic block'
' plastic thickness removed=0.0781 inch =0.19844 cm
' thinned block without bevels, without axial gaps
cubo 100 4.51326 -4.51326 1.48828 -1.48828 2p14.22876

' thinned block without bevels, with axial gaps
cubo 200 4.51326 -4.51326 1.48828 -1.48828 15.07490 -14.42720

media  8 1 100

media  4 1 -100 200
boundary  200

' region type=plastic
' edge type=lid_inner_lower
' axial part type=main(9)
unit 1552
com=' part 55l plastic block'
' plastic thickness removed=0.0781 inch =0.19844 cm
' thinned block without bevels, without axial gaps
cubo 100 4.51326 -4.51326 1.48828 -1.48828 2p18.97856
```

```
' thinned block without bevels, with axial gaps
cubo 200 4.51326 -4.51326 1.48828 -1.48828 2p19.82470

media  8 1 100

media  4 1 -100 200
boundary  200

' region type=plastic
' edge type=lid_inner_lower
' axial part type=upper(1)
unit 1554
com=' part 55l plastic block'
' plastic thickness removed=0.0781 inch =0.19844 cm
' thinned block without bevels, without axial gaps
cubo 100 4.51326 -4.51326 1.48828 -1.48828 2p13.31436

' thinned block without bevels, with axial gaps
cubo 200 4.51326 -4.51326 1.48828 -1.48828 13.51280 -14.16050

media  8 1 100

media  4 1 -100 200
boundary  200

' region type=plastic
' edge type=lid_inner_lower
' axial array
unit 1556

cubo 10 4.51326 -4.51326 1.48828 -1.48828 206.81156 -206.81156

array 1556 10  place  1 1 1  0 0 -192.38436

boundary  10

' region type=plastic
' edge type=lid_inner_lower
' axial part type=lower(1)
unit 2550
com=' part 55r plastic block'
' plastic thickness removed=0.0781 inch =0.19844 cm
```

```
' thinned block without bevels, without axial gaps
cubo 100 6.16426 -6.36270 1.48828 -1.48828 2p14.22876

' thinned block without bevels, with axial gaps
cubo 200 6.16426 -6.36270 1.48828 -1.48828 15.07490 -14.42720

media  8 1 100

media  4 1 -100 200
boundary  200

' region type=plastic
' edge type=lid_inner_lower
' axial part type=main(9)
unit 2552
com=' part 55r plastic block'
' plastic thickness removed=0.0781 inch =0.19844 cm
' thinned block without bevels, without axial gaps
cubo 100 6.16426 -6.36270 1.48828 -1.48828 2p18.97856

' thinned block without bevels, with axial gaps
cubo 200 6.16426 -6.36270 1.48828 -1.48828 2p19.82470

media  8 1 100

media  4 1 -100 200
boundary  200

' region type=plastic
' edge type=lid_inner_lower
' axial part type=upper(1)
unit 2554
com=' part 55r plastic block'
' plastic thickness removed=0.0781 inch =0.19844 cm
' thinned block without bevels, without axial gaps
cubo 100 6.16426 -6.36270 1.48828 -1.48828 2p13.31436

' thinned block without bevels, with axial gaps
cubo 200 6.16426 -6.36270 1.48828 -1.48828 13.51280 -14.16050

media  8 1 100

media  4 1 -100 200
```

```
boundary  200

' region type=plastic
' edge type=lid_inner_lower
' axial array
unit 2556

cubo 10 6.16426 -6.36270 1.48828 -1.48828 206.81156 -206.81156

array 2556 10  place  1 1 1  0 0 -192.38436

boundary  10

' region type=plastic
' edge type=lid_inner_upper
' axial part type=lower(1)
unit 1570
com=' part 57l plastic block'
' plastic thickness removed=0.0781 inch =0.19844 cm

' bevel surface at -x
plane  10 xpl=1 origin x=.28063 y=-1.48828 rotate a3=-45
' thinned block without bevels, without axial gaps
cubo 100 10.49496 .28063 1.48828 -1.48828 2p14.22876

' thinned block without bevels, with axial gaps
cubo 200 10.49496 .28063 1.48828 -1.48828 15.07490 -14.42720

media  8 1 10 100



media  4 1 -10 100
media  4 1 -100 200
boundary  200

' region type=plastic
' edge type=lid_inner_upper
' axial part type=main(9)
unit 1572
com=' part 57l plastic block'
' plastic thickness removed=0.0781 inch =0.19844 cm

' bevel surface at -x
```

```
plane  10 xpl=1 origin x=.28063 y=-1.48828 rotate a3=-45
' thinned block without bevels, without axial gaps
cubo 100 10.49496 .28063 1.48828 -1.48828 2p18.97856

' thinned block without bevels, with axial gaps
cubo 200 10.49496 .28063 1.48828 -1.48828 2p19.82470

media  8 1 10 100

media  4 1 -10 100
media  4 1 -100 200
boundary  200

' region type=plastic
' edge type=lid_inner_upper
' axial part type=upper(1)
unit 1574
com=' part 57l plastic block'
' plastic thickness removed=0.0781 inch =0.19844 cm

' bevel surface at -x
plane  10 xpl=1 origin x=.28063 y=-1.48828 rotate a3=-45
' thinned block without bevels, without axial gaps
cubo 100 10.49496 .28063 1.48828 -1.48828 2p13.31436

' thinned block without bevels, with axial gaps
cubo 200 10.49496 .28063 1.48828 -1.48828 13.51280 -14.16050

media  8 1 10 100

media  4 1 -10 100
media  4 1 -100 200
boundary  200

' region type=plastic
' edge type=lid_inner_upper
' axial array
unit 1576

cubo 10 10.49496 0.28063 1.48828 -1.48828 206.81156 -206.81156

array 1576 10  place  1 1 1  0 0 -192.38436
```

```
boundary  10

' region type=plastic
' edge type=lid_inner_upper
' axial part type=lower(1)
unit 2570
com=' part 57r plastic block'
' plastic thickness removed=0.0781 inch =0.19844 cm

' bevel surface at +x
plane  10 xpl=1 origin x=-.28063 y=-1.48828 rotate a3=45
' thinned block without bevels, without axial gaps
cubo 100 -.28063 -10.49496 1.48828 -1.48828 2p14.22876

' thinned block without bevels, with axial gaps
cubo 200 -.28063 -10.49496 1.48828 -1.48828 15.07490 -14.42720

media  8 1 -10 100

media  4 1 10 100
media  4 1 -100 200
boundary  200

' region type=plastic
' edge type=lid_inner_upper
' axial part type=main(9)
unit 2572
com=' part 57r plastic block'
' plastic thickness removed=0.0781 inch =0.19844 cm

' bevel surface at +x
plane  10 xpl=1 origin x=-.28063 y=-1.48828 rotate a3=45
' thinned block without bevels, without axial gaps
cubo 100 -.28063 -10.49496 1.48828 -1.48828 2p18.97856

' thinned block without bevels, with axial gaps
cubo 200 -.28063 -10.49496 1.48828 -1.48828 2p19.82470

media  8 1 -10 100

media  4 1 10 100
media  4 1 -100 200
boundary  200
```

```
' region type=plastic
' edge type=lid_inner_upper
' axial part type=upper(1)
unit 2574
com=' part 57r plastic block'
' plastic thickness removed=0.0781 inch =0.19844 cm

' bevel surface at +x
plane  10 xpl=1 origin x=-.28063 y=-1.48828 rotate a3=45
' thinned block without bevels, without axial gaps
cubo 100 -.28063 -10.49496 1.48828 -1.48828 2p13.31436

' thinned block without bevels, with axial gaps
cubo 200 -.28063 -10.49496 1.48828 -1.48828 13.51280 -14.16050

media  8 1 -10 100

media  4 1 10 100
media  4 1 -100 200
boundary  200

' region type=plastic
' edge type=lid_inner_upper
' axial array
unit 2576

cubo 10 -0.28063 -10.49496 1.48828 -1.48828 206.81156 -206.81156

array 2576 10  place  1 1 1  0 0 -192.38436

boundary  10

' region type=plastic
' edge type=lid_outer_upper
unit 1598
com=' part 59lw plastic block'
' plastic thickness removed=0.0781 inch =0.19844 cm

wedge 10 1.38799 1.38799 2.97656 28.45753 origin z=0.19844
media 8 1 10

wedge 20 1.38799 1.38799 2.97656 37.95713 origin z=30.34824
media 8 1 20
```

```
wedge 30 1.38799 1.38799 2.97656 37.95713 origin z=69.99764
media 8 1 30

wedge 40 1.38799 1.38799 2.97656 37.95713 origin z=109.64704
media 8 1 40

wedge 50 1.38799 1.38799 2.97656 37.95713 origin z=149.29644
media 8 1 50

wedge 60 1.38799 1.38799 2.97656 37.95713 origin z=188.94584
media 8 1 60

wedge 70 1.38799 1.38799 2.97656 37.95713 origin z=228.59524
media 8 1 70

wedge 80 1.38799 1.38799 2.97656 37.95713 origin z=268.24464
media 8 1 80

wedge 90 1.38799 1.38799 2.97656 37.95713 origin z=307.89404
media 8 1 90

wedge 100 1.38799 1.38799 2.97656 37.95713 origin z=347.54344
media 8 1 100

wedge 110 1.38799 1.38799 2.97656 26.62873 origin z=387.19284
media 8 1 110

wedge 120 1.38799 1.38799 2.97656 414.02000 origin z=0.00000
media  4 1  -10 -20 -30 -40 -50 -60 -70 -80 -90 -100 -110 120
boundary 120

' region type=plastic
' edge type=lid_outer_upper
unit 2598
com=' part 59rw plastic block'
' plastic thickness removed=0.0781 inch =0.19844 cm

wedge 10 1.38799 0.00000 2.97656 28.45753 origin z=0.19844
media 8 1 10

wedge 20 1.38799 0.00000 2.97656 37.95713 origin z=30.34824
media 8 1 20
```

```
wedge 30 1.38799 0.00000 2.97656 37.95713 origin z=69.99764
media 8 1 30

wedge 40 1.38799 0.00000 2.97656 37.95713 origin z=109.64704
media 8 1 40

wedge 50 1.38799 0.00000 2.97656 37.95713 origin z=149.29644
media 8 1 50

wedge 60 1.38799 0.00000 2.97656 37.95713 origin z=188.94584
media 8 1 60

wedge 70 1.38799 0.00000 2.97656 37.95713 origin z=228.59524
media 8 1 70

wedge 80 1.38799 0.00000 2.97656 37.95713 origin z=268.24464
media 8 1 80

wedge 90 1.38799 0.00000 2.97656 37.95713 origin z=307.89404
media 8 1 90

wedge 100 1.38799 0.00000 2.97656 37.95713 origin z=347.54344
media 8 1 100

wedge 110 1.38799 0.00000 2.97656 26.62873 origin z=387.19284
media 8 1 110

wedge 120 1.38799 0.00000 2.97656 414.02000 origin z=0.00000
media  4 1  -10 -20 -30 -40 -50 -60 -70 -80 -90 -100 -110 120
boundary 120

' region type=plastic
' edge type=lid_outer_upper
' axial part type=lower(1)
unit 1590
com=' part 59l plastic block'
' plastic thickness removed=0.0781 inch =0.19844 cm

' bevel surface at +x
plane  10 xpl=1 origin x=-.28063 y=-1.48828 rotate a3=45
' thinned block without bevels, without axial gaps
cubo 100 -.28063 -11.37245 1.48828 -1.48828 2p14.22876
```

```
' thinned block without bevels, with axial gaps
cubo 200 -.28063 -11.37245 1.48828 -1.48828 15.07490 -14.42720

media  8 1 -10 100

media  4 1 10 100
media  4 1 -100 200
boundary  200

' region type=plastic
' edge type=lid_outer_upper
' axial part type=main(9)
unit 1592
com=' part 59l plastic block'
' plastic thickness removed=0.0781 inch =0.19844 cm

' bevel surface at +x
plane  10 xpl=1 origin x=-.28063 y=-1.48828 rotate a3=45
' thinned block without bevels, without axial gaps
cubo 100 -.28063 -11.37245 1.48828 -1.48828 2p18.97856

' thinned block without bevels, with axial gaps
cubo 200 -.28063 -11.37245 1.48828 -1.48828 2p19.82470

media  8 1 -10 100

media  4 1 10 100
media  4 1 -100 200
boundary  200

' region type=plastic
' edge type=lid_outer_upper
' axial part type=upper(1)
unit 1594
com=' part 59l plastic block'
' plastic thickness removed=0.0781 inch =0.19844 cm

' bevel surface at +x
plane  10 xpl=1 origin x=-.28063 y=-1.48828 rotate a3=45
' thinned block without bevels, without axial gaps
cubo 100 -.28063 -11.37245 1.48828 -1.48828 2p13.31436
```

```
' thinned block without bevels, with axial gaps
cubo 200 -.28063 -11.37245 1.48828 -1.48828 13.51280 -14.16050

media  8 1 -10 100

media  4 1 10 100
media  4 1 -100 200
boundary  200

' region type=plastic
' edge type=lid_outer_upper
' axial array
unit 1596

cubo 10 -0.28063 -11.37245 1.48828 -1.48828 206.81156 -206.81156

array 1596 10  place  1 1 1  0 0 -192.38436

boundary  10

' region type=plastic
' edge type=lid_outer_upper
' axial part type=lower(1)
unit 2590
com=' part 59r plastic block'
' plastic thickness removed=0.0781 inch =0.19844 cm

' bevel surface at -x
plane  10 xpl=1 origin x=.28063 y=-1.48828 rotate a3=-45
' thinned block without bevels, without axial gaps
cubo 100 11.37245 .28063 1.48828 -1.48828 2p14.22876

' thinned block without bevels, with axial gaps
cubo 200 11.37245 .28063 1.48828 -1.48828 15.07490 -14.42720

media  8 1 10 100
media  4 1 -10 100
media  4 1 -100 200
boundary  200

' region type=plastic
' edge type=lid_outer_upper
' axial part type=main(9)
```

```
unit 2592
com=' part 59r plastic block'
' plastic thickness removed=0.0781 inch =0.19844 cm

' bevel surface at -x
plane  10 xpl=1 origin x=.28063 y=-1.48828 rotate a3=-45
' thinned block without bevels, without axial gaps
cubo 100 11.37245 .28063 1.48828 -1.48828 2p18.97856

' thinned block without bevels, with axial gaps
cubo 200 11.37245 .28063 1.48828 -1.48828 2p19.82470

media  8 1 10 100

media  4 1 -10 100
media  4 1 -100 200
boundary  200

' region type=plastic
' edge type=lid_outer_upper
' axial part type=upper(1)
unit 2594
com=' part 59r plastic block'
' plastic thickness removed=0.0781 inch =0.19844 cm

' bevel surface at -x
plane  10 xpl=1 origin x=.28063 y=-1.48828 rotate a3=-45
' thinned block without bevels, without axial gaps
cubo 100 11.37245 .28063 1.48828 -1.48828 2p13.31436

' thinned block without bevels, with axial gaps
cubo 200 11.37245 .28063 1.48828 -1.48828 13.51280 -14.16050

media  8 1 10 100

media  4 1 -10 100
media  4 1 -100 200
boundary  200

' region type=plastic
' edge type=lid_outer_upper
' axial array
unit 2596
```

```
cubo 10 11.37245 0.28063 1.48828 -1.48828 206.81156 -206.81156

array 2596 10  place  1 1 1  0 0 -192.38436

boundary  10

' region type=plastic
' edge type=lid_outer_lower
' axial part type=lower(1)
unit 1610
com=' part 611 plastic block'
' plastic thickness removed=0.0781 inch =0.19844 cm

' bevel surface at -x
plane  10 xpl=1 origin x=-10.71083 y=-1.48828 rotate a3=-20
' thinned block without bevels, without axial gaps
cubo 100 -.19844 -10.71083 1.48828 -1.48828 2p14.22876

' thinned block without bevels, with axial gaps
cubo 200 -.19844 -10.71083 1.48828 -1.48828 15.07490 -14.42720

media  8 1 10 100

media  4 1 -10 100
media  4 1 -100 200
boundary  200

' region type=plastic
' edge type=lid_outer_lower
' axial part type=main(9)
unit 1612
com=' part 611 plastic block'
' plastic thickness removed=0.0781 inch =0.19844 cm

' bevel surface at -x
plane  10 xpl=1 origin x=-10.71083 y=-1.48828 rotate a3=-20
' thinned block without bevels, without axial gaps
cubo 100 -.19844 -10.71083 1.48828 -1.48828 2p18.97856

' thinned block without bevels, with axial gaps
cubo 200 -.19844 -10.71083 1.48828 -1.48828 2p19.82470

media  8 1 10 100
```

```
media  4 1 -10 100
media  4 1 -100 200
boundary  200

' region type=plastic
' edge type=lid_outer_lower
' axial part type=upper(1)
unit 1614
com=' part 61l plastic block'
' plastic thickness removed=0.0781 inch =0.19844 cm

' bevel surface at -x
plane  10 xpl=1 origin x=-10.71083 y=-1.48828 rotate a3=-20
' thinned block without bevels, without axial gaps
cubo 100 -.19844 -10.71083 1.48828 -1.48828 2p13.31436

' thinned block without bevels, with axial gaps
cubo 200 -.19844 -10.71083 1.48828 -1.48828 13.51280 -14.16050

media  8 1 10 100

media  4 1 -10 100
media  4 1 -100 200
boundary  200

' region type=plastic
' edge type=lid_outer_lower
' axial array
unit 1616

cubo 10 -0.19844 -10.71083 1.48828 -1.48828 206.81156 -206.81156

array 1616 10  place  1 1 1  0 0 -192.38436

boundary  10

' region type=plastic
' edge type=lid_outer_lower
' axial part type=lower(1)
unit 2610
com=' part 61r plastic block'
' plastic thickness removed=0.0781 inch =0.19844 cm
```

```
' bevel surface at +x
plane  10 xpl=1 origin x=10.71083 y=-1.48828 rotate a3=20
' thinned block without bevels, without axial gaps
cubo 100 10.71083 .19844 1.48828 -1.48828 2p14.22876

' thinned block without bevels, with axial gaps
cubo 200 10.71083 .19844 1.48828 -1.48828 15.07490 -14.42720

media  8 1 -10 100

media  4 1 10 100
media  4 1 -100 200
boundary  200

' region type=plastic
' edge type=lid_outer_lower
' axial part type=main(9)
unit 2612
com=' part 61r plastic block'
' plastic thickness removed=0.0781 inch =0.19844 cm

' bevel surface at +x
plane  10 xpl=1 origin x=10.71083 y=-1.48828 rotate a3=20
' thinned block without bevels, without axial gaps
cubo 100 10.71083 .19844 1.48828 -1.48828 2p18.97856

' thinned block without bevels, with axial gaps
cubo 200 10.71083 .19844 1.48828 -1.48828 2p19.82470

media  8 1 -10 100
media  4 1 10 100
media  4 1 -100 200
boundary  200

' region type=plastic
' edge type=lid_outer_lower
' axial part type=upper(1)
unit 2614
com=' part 61r plastic block'
' plastic thickness removed=0.0781 inch =0.19844 cm

' bevel surface at +x
plane  10 xpl=1 origin x=10.71083 y=-1.48828 rotate a3=20
```

```
' thinned block without bevels, without axial gaps
cubo 100 10.71083 .19844 1.48828 -1.48828 2p13.31436

' thinned block without bevels, with axial gaps
cubo 200 10.71083 .19844 1.48828 -1.48828 13.51280 -14.16050

media  8 1 -10 100

media  4 1 10 100
media  4 1 -100 200
boundary  200

' region type=plastic
' edge type=lid_outer_lower
' axial array
unit 2616

cubo 10 10.71083 0.19844 1.48828 -1.48828 206.81156 -206.81156

array 2616 10  place  1 1 1  0 0 -192.38436

boundary  10

unit 810
com='aluminum door and rubber at upper edge of assy'
' nominal aluminum dims: 0.25" thk by 7.9" wide by 35.0" long
' tolerances: 0.03" by 0.1" by 0.1"
' dimensions modeled: 0.22" by 7.8" by 34.9"
' there is a nominal 0.25" axial gap, modeled as 0.25 + 0.03(gap tol) + .1 (half of alum length tol times two)
' axial gap modeled as 0.38"

' this is a rubber layer, modeled as same width and length as alum and 0.22" thk
cubo  20 2p9.906 0.5588 0 2p44.323
' this is aluminum
cubo  40 2p9.906 1.1176 0 2p44.323
' gap
cubo  60 2p9.906 1.1176 0 2p44.8056

media  5 1 20
media  13 1 40 -20
media  9 1 60 -40

boundary 60
```

```
unit 820
com='aluminum door and rubber at upper edge of assy'
' there are 4 units 810, unit 820 is at -z end
' 4 * 44.8056 = 179.2224
' total length here is 207.01 - 179.2224 = 27.7876
' gap is final 0.19" (0.4826 cm) of the length

' this is a rubber layer, modeled as same width and length as alum and 0.22" thk
cubo  20 2p9.906 0.5588 0 27.305 0
' this is aluminum
cubo  40 2p9.906 1.1176 0 27.305 0
' gap
cubo  60 2p9.906 1.1176 0 27.7876 0

media  5 1 20
media  13 1 40 -20
media  9 1 60 -40

boundary 60

unit 830
com="same as unit 820 except gap at -z end"

' this is a rubber layer, modeled as same width and length as alum and 0.22" thk
cubo  20 2p9.906 0.5588 0 27.7876 0.4846
' this is aluminum
cubo  40 2p9.906 1.1176 0 27.7876 0.4846
' gap
cubo  60 2p9.906 1.1176 0 27.7876 0

media  5 1 20
media  13 1 40 -20
media  9 1 60 -40

boundary 60

unit 840
com='axial array of doors'
cubo  10 2p9.906 1.1176 0 2p207.01
array  2 10  place  1 1 1 0 0 -207.01

boundary 10
```

```
unit 860
com='steel bar at center of package'
' nominal 0.75" high by 1.75" wide, use 0.70 x 1.70

cubo  20 2p2.159 1.778 0 2p207.01

media  14 1 20
boundary 20

unit 900
com='fuel assembly, not rotated'

cubo  10 21.640800 0 21.640800 0 2p207.01
array  1 10  place  1 1 1 0.721360 0.721360 0

' water layer around assy
cubo  20 23.8633 -0.635 23.8633 -0.635 2p207.01

'hole 840 origin x=11.73480 y=21.64080
'hole 840 origin x=21.64080 y=11.73480 rotate a3=-90

hole  200 origin x=10.795 y=-0.3175
hole  200 origin x=-0.3175 y=10.795 rotate a3=90
media  9 1 20 -10
boundary 20

unit 1000
com='one package'
' bundle c-c spacing is 15.2"
' diamond is 10.03" x 9.86" (across outer steel surfaces)
' diamond diagonal is 14.0649"
' distance to spacers from diagonal: 8.10" (lower) and 8.62" (upper)
'  vertical sum is 30.78"

' distance to outer surface of steel wall is 4.10" (lower) and 4.62" (upper)
' horizontal span across outer steel surfaces: 41.95"
' model steel as 0.115" thick

' base is 21.5" tall, including spacer height (54.61 cm)
' top of base is at y= 54.61 - 20.574 = 34.036 cm

' hanging central blocks with steel carriers
' inner steel surface
```

```
cubo  2 2p1.6256 22.45 14.9866 2p207.01
' outer steel surface
cubo  4 2p1.8415 22.45 14.7707 2p207.01

wedge 6 1.4018 0 1.4018 414.02 origin x=-1.4018 y=20.3255 z=-207.01

wedge 8 1.4018 1.4018 1.4018 414.02 origin x=0 y=20.3255 z=-207.01

cubo  10 2p1.4018 20.3255 14.9866 2p207.01

plane  11 zpl=1 origin z=-195.41973
plane  12 zpl=1 origin z=-164.04107
plane  13 zpl=1 origin z=-105.55453
plane  14 zpl=1 origin z=-74.17587
plane  15 zpl=1 origin z=-15.68933

plane  16 zpl=1 origin z=15.68933
plane  17 zpl=1 origin z=74.17587
plane  18 zpl=1 origin z=105.55453
plane  19 zpl=1 origin z=164.04107
plane  20 zpl=1 origin z=195.41973



' flooded regions
plane 31 ypl=1 origin y=16
cubo  32 -17 -30.5 34.5 26 2p207.01 rotate a3=20
cubo  33 30.5 17 34.5 26 2p207.01 rotate a3=-20
cubo  34 3.2 -5 24.5 0 2p207.01 origin x=-1.828 y=17.942 rotate a3=45
cubo  35 5 -3.2 24.5 0 2p207.01 origin x=1.828 y=17.942 rotate a3=-45
cubo  36 2p41 22 16 2p207.01
media  9 1  32 31
media  9 1  33 31
media  4 1  32 -31
media  4 1  33 -31

media  9 1  34 -4
media  9 1  35 -34 -4
media  9 1  36 -35 -34 -33 -32 -4

media  9 1 4 -11 31
media  4 1 4 -11 -31

' steel
```

```
media  10 1 4 -2 11 -12

' nylon
media  8 1 6 11 -12
media  8 1 8 11 -12
media  8 1 10 11 -12

' water
media  9 1 2 -6 -8 -10 11 -12

media  9 1 4 12 -13 31
media  4 1 4 12 -13 -31

' steel
media  10 1 4 -2 13 -14

' nylon
media  8 1 6 13 -14
media  8 1 8 13 -14
media  8 1 10 13 -14

' water
media  9 1 2 -6 -8 -10 13 -14

media  9 1 4 14 -15 31
media  4 1 4 14 -15 -31

' steel
media  10 1 4 -2 15 -16

' nylon
media  8 1 6 15 -16
media  8 1 8 15 -16
media  8 1 10 15 -16

' water
media  9 1 2 -6 -8 -10 15 -16

media  9 1 4 16 -17 31
media  4 1 4 16 -17 -31



' steel
```

```
media  10 1 4 -2 17 -18

' nylon
media  8 1 6 17 -18
media  8 1 8 17 -18
media  8 1 10 17 -18

' water
media  9 1 2 -6 -8 -10 17 -18

media  9 1 4 18 -19 31
media  4 1 4 18 -19 -31

' steel
media  10 1 4 -2 19 -20

' nylon
media  8 1 6 19 -20
media  8 1 8 19 -20
media  8 1 10 19 -20

' water
media  9 1 2 -6 -8 -10 19 -20

media  9 1 4 20 31
media  4 1 4 20 -31

'  inner surface of steel
cubo  580  2p52.9844 47.1675 -10.1981 2p207.01

media  4 1  580 -32 -33 -34 -35 -36 -4

'  outer surface of steel
cubo  590  2p53.2765 47.4596 -10.4140 2p207.01

media  11 1 -580 590

' package is 44.98" wide by 30.78" high by 207.98" long
'  modeled as 42.98" by 28.78" by 163"
cubo  600  2p54.5846 47.4596 -18.034 2p207.01

media  4 1 -590 600
```

```
' top of bar is 0.25" below bottom of steel carrier
' 14.7707 - 0.25 * 2.54 - 0.7 * 2.54 = 12.3577
hole  860 origin x=0 y=12.3577 z=0

hole 900  origin x=19.304 y=1.36500 z=0 rotate a3=45

hole 900  origin x=-19.304 y=1.36500 z=0  rotate a3=45

' region type=steel
' edge type=base_inner_full
hole 300 origin x=-10.73161 y=8.80588 rotate a3=45.0

hole 300 origin x=10.73161 y=8.80588 rotate a3=-45.0

' region type=steel
' edge type=base_outer_full
hole 310 origin x=-27.39379 y=8.32328 rotate a3=-45.0

hole 310 origin x=27.39379 y=8.32328 rotate a3=45.0

' region type=steel
' edge type=lid_inner_lower
hole 320 origin x=-4.86824 y=25.67904 rotate a3=-45.0

hole 320 origin x=4.86824 y=25.67904 rotate a3=45.0
' region type=steel
' edge type=lid_inner_upper
hole 330 origin x=-15.05185 y=31.62397 rotate a3=-45.0

hole 330 origin x=15.05185 y=31.62397 rotate a3=45.0

' region type=steel
' edge type=lid_outer_upper
hole 340 origin x=-23.67289 y=30.89657 rotate a3=45.0

hole 340 origin x=23.67289 y=30.89657 rotate a3=-45.0

' region type=steel
' edge type=lid_outer_lower
hole 350 origin x=-34.23368 y=24.21537 rotate a3=20

hole 350 origin x=34.23368 y=24.21537 rotate a3=-20
```

```
' region type=boral
' edge type=base_inner_full
hole 406 origin x=-11.31247 y=7.77780 rotate a3=45.0

hole 406 origin x=11.31247 y=7.77780 rotate a3=-45.0

' region type=boral
' edge type=base_outer_full
hole 416 origin x=-27.29553 y=7.77780 rotate a3=-45.0

hole 416 origin x=27.29553 y=7.77780 rotate a3=45.0

' region type=boral
' edge type=lid_inner_lower
hole 426 origin x=-4.85567 y=26.03286 rotate a3=-45.0

hole 426 origin x=4.85567 y=26.03286 rotate a1=180 a3=45.0

' region type=boral
' edge type=lid_inner_upper
hole 436 origin x=-15.20990 y=32.14842 rotate a3=-45.0

hole 436 origin x=15.20990 y=32.14842 rotate a1=180 a3=45.0

' region type=boral
' edge type=lid_outer_upper
hole 446 origin x=-23.87405 y=31.06181 rotate a3=45.0

hole 446 origin x=23.87405 y=31.06181 rotate a1=180 a3=-45.0

' region type=boral
' edge type=lid_outer_lower
hole 456 origin x=-33.78217 y=24.66807 rotate a3=20

hole 456 origin x=33.78217 y=24.66807 rotate a1=180 a3=-20

' region type=plastic
' edge type=base_inner_full
hole 1166 origin x=-10.15323 y=6.61856 rotate a3=45.0
hole 2166 origin x=10.15323 y=6.61856 rotate a3=-45.0



' region type=plastic
```

```
' edge type=base_outer_full

hole 1166 origin x=-28.45477 y=6.61856 rotate a3=-45.0
hole 2166 origin x=28.45477 y=6.61856 rotate a3=45.0

' region type=plastic
' edge type=lid_inner_lower

hole 1556 origin x=-4.63037 y=28.12605 rotate a3=-45.0
hole 2556 origin x=3.46294 y=26.95862 rotate a3=45.0

' region type=plastic
' edge type=lid_inner_upper

hole 1576 origin x=-17.87625 y=37.13325 rotate a3=-45.0
hole 2576 origin x=17.87625 y=37.13325 rotate a3=45.0

' region type=plastic
' edge type=lid_outer_upper

hole 1596 origin x=-20.19180 y=37.20396 rotate a3=45.0
hole 2596 origin x=20.19180 y=37.20396 rotate a3=-45.0

' region type=plastic
' edge type=lid_outer_upper (wedge)

hole 1598 origin x=-28.09172 y=27.05787 z=-207.01 rotate a3=45.0
hole 2598 origin x=27.11026 y=28.03933 z=-207.01 rotate a3=-45.0

' region type=plastic
' edge type=lid_outer_lower
hole 1616 origin x=-29.12357 y=28.13077 rotate a3=20
hole 2616 origin x=29.12357 y=28.13077 rotate a3=-20

boundary 600

unit 1001
com='single container flipped'
cubo  600  2p54.5846 47.4596 -18.034 2p207.01
hole 1000 origin x=0 y=29.4256 rotate a3=180
boundary 600

global
```

```
unit 2000
com='4x9x1 array of damaged packages'
cubo  10 436.6768 0 589.4424 0 414.02 0
array 2000 10  place  1 1 1  54.58460 18.03400 207.01000
cubo  20 466.6768 -30 619.4424 -30 444.02 -30
media  9 1 -10 20
boundary  20
end geometry

read array

' doors
ara=2 nux=1 nuy=1 nuz=6
fill 820 4r810 830 end fill

'assy lattice
ara=1  nux=15 nuy=15 nuz=1
fill
10 10 10 10 10 10 10 10 10 10 10 10 10 10 10
10 10 10 10 10 10 10 10 10 10 10 10 10 10 10
10 10 10 10 10 20 10 10 10 20 10 10 10 10 10
10 10 10 20 10 10 10 10 10 10 10 20 10 10 10
10 10 10 10 10 10 10 10 10 10 10 10 10 10 10
10 10 20 10 10 20 10 10 10 20 10 10 20 10 10
10 10 10 10 10 10 10 10 10 10 10 10 10 10 10
10 10 10 10 10 10 10 30 10 10 10 10 10 10 10
10 10 10 10 10 10 10 10 10 10 10 10 10 10 10
10 10 20 10 10 20 10 10 10 20 10 10 20 10 10
10 10 10 10 10 10 10 10 10 10 10 10 10 10 10
10 10 10 20 10 10 10 10 10 10 10 20 10 10 10
10 10 10 10 10 20 10 10 10 20 10 10 10 10 10
10 10 10 10 10 10 10 10 10 10 10 10 10 10 10
10 10 10 10 10 10 10 10 10 10 10 10 10 10 10
end fill

' region type=boral
' edge type=base_inner_full
ara=406 nux=1 nuy=1 nuz=11
fill 400 9r402 404 end fill

' region type=boral
' edge type=base_outer_full
ara=416 nux=1 nuy=1 nuz=11
```

```
fill 410 9r412 414 end fill

' region type=boral
' edge type=lid_inner_lower
ara=426 nux=1 nuy=1 nuz=11
fill 420 9r422 424 end fill

' region type=boral
' edge type=lid_inner_upper
ara=436 nux=1 nuy=1 nuz=11
fill 430 9r432 434 end fill

' region type=boral
' edge type=lid_outer_upper
ara=446 nux=1 nuy=1 nuz=11
fill 440 9r442 444 end fill

' region type=boral
' edge type=lid_outer_lower
ara=456 nux=1 nuy=1 nuz=11
fill 450 9r452 454 end fill

' region type=plastic
' edge type=base_inner_full
ara=1166 nux=1 nuy=1 nuz=11
fill 1160 9r1162 1164 end fill

' region type=plastic
' edge type=base_inner_full
ara=2166 nux=1 nuy=1 nuz=11
fill 2160 9r2162 2164 end fill

' region type=plastic
' edge type=base_outer_full
ara=1176 nux=1 nuy=1 nuz=11
fill 1170 9r1172 1174 end fill

' region type=plastic
' edge type=base_outer_full
ara=2176 nux=1 nuy=1 nuz=11
fill 2170 9r2172 2174 end fill

' region type=plastic
```

```
' edge type=lid_inner_lower
ara=1556 nux=1 nuy=1 nuz=11
fill 1550 9r1552 1554 end fill

' region type=plastic
' edge type=lid_inner_lower
ara=2556 nux=1 nuy=1 nuz=11
fill 2550 9r2552 2554 end fill

' region type=plastic
' edge type=base_outer_full
ara=1576 nux=1 nuy=1 nuz=11
fill 1570 9r1572 1574 end fill

' region type=plastic
' edge type=base_outer_full
ara=2576 nux=1 nuy=1 nuz=11
fill 2570 9r2572 2574 end fill

' region type=plastic
' edge type=lid_outer_upper
ara=1596 nux=1 nuy=1 nuz=11
fill 1590 9r1592 1594 end fill

' region type=plastic
' edge type=lid_outer_upper
ara=2596 nux=1 nuy=1 nuz=11
fill 2590 9r2592 2594 end fill

' region type=plastic
' edge type=lid_outer_lower
ara=1616 nux=1 nuy=1 nuz=11
fill 1610 9r1612 1614 end fill

' region type=plastic
' edge type=lid_outer_lower
ara=2616 nux=1 nuy=1 nuz=11
fill 2610 9r2612 2614 end fill

ara=2000 nux=4 nuy=9 nuz=1
fill 4r1000
     4r1001
     4r1000
```

```
     4r1001
     4r1000
     4r1001
     4r1000
     4r1001
     4r1000 end fill
end array

read bounds all=vacu end bounds
read start
nst=1
end start
end data
end
```

6.9.4.2 Input for Licensing-Basis Model for Single Container

```
=csas26     parm='size=900000'
15type1 fa in shipping container
238g     latticecell
'100% td and 5.0 w/o
uo2  1   1.0 293 92235 5 92238 95 end
'zirc
zr  2   1.0 293 end
'water in assy lattice
h2o  3   1.0 293 end

'volume in container external to bundles
h2o  4   1.0   293 end

'rubber
h2o  5 1.0 293 end

' ss plate, 0.13" thick
ss304  6   1.0   293 end

'  boral, minimum areal density(at min thk)=0.0240 gm b-10/sqcm
' min thk = 0.119" = 0.30226cm
' vol dens = 0.0240/(0.30226*0.18431) =0.4308 gm natural b/cucm
' we use only 75%, 0.75 * 0.4308 = 0.3231 gm natural b/cucm
b  7   den=0.3231 1 293 end

'nylon 66
arbmnyl 1.14 4 0 1 0 6012 6 7014 1 8016 1 1001 11 8 1.0 293 end

'reflector water
h2o  9   1.0 293 end

' ss plate, 0.085" thick
ss304  10   1.0   293 end

' ss plate, 0.115" thick
ss304  11   1.0   293 end

' gap water
h2o  12   1.0 293 end

' aluminum for doors
al  13 1 293 end
```

```
' ss bar at center
ss304  14   1.0   293 end
end comp
squarepitch 1.44272 0.91999 1 3 1.05156 2 0.93980 0 end

more data
dab=2000
res=6 slab 0.3302
res=10 slab 0.2159
res=11 slab 0.2921
res=14 cyli 1.563
end more

read parm tme=120 gen=280 nsk=3 run=yes npg=1000 far=yes plt=yes
lng=3000000 nb8=1200
end parm
read geometry

unit  10
com='wet fuel pin cell'

' fuel stack
cyli  10 0.45999 2p207.01

' clad inner surface
cyli  20 0.46990 2p207.01

' clad outer surface
cyli  30 0.52578 2p207.01

' unit cell
cubo  40 4p0.72136 2p207.01

' fuel
media  1 1 10

' fuel-clad gap (void)
media  0 1 20 -10

' clad
media  2 1 30 -20
```

```
' water or whatever is external to clad
media  3 1 40 -30

boundary  40

unit  20
com='wet guidetube cell-no clad'

' guide tube inner surface
cyli  10 0.63500 2p207.01

' guide tube outer surface
cyli  20 0.67056 2p207.01

' unit cell
cubo  40 4p0.72136 2p207.01

' water or whatever is internal to clad
media  3 1 10

' clad
media  3 1 20 -10

' water or whatever is external to clad
media  3 1 40 -20

boundary  40

unit  30
com='wet instrument tube cell-no clad'

' instrument tube inner surface
cyli  10 0.56261 2p207.01

' instrument tube outer surface
cyli  20 0.62357 2p207.01

' unit cell
cubo  40 4p0.72136 2p207.01

' water or whatever is internal to clad
media  3 1 10
```

```
' clad-water
media  3 1 20 -10

' water or whatever is external to clad
media  3 1 40 -20

boundary  40

' region type=pad
' edge type=base_inner_full
unit 200

cubo 100  10.79500 -10.79500 0.31750 -0.31750 207.01000 -207.01000



media 5 1 100

boundary 100

' region type=pad
' edge type=base_outer_full
unit 210

cubo 100  10.79500 -10.79500 0.31750 -0.31750 207.01000 -207.01000

media 5 1 100

boundary 100

' region type=steel
' edge type=base_inner_full
unit 300

cubo 100  11.60249 -11.60249 0.16510 -0.16510 207.01000 -207.01000

media 6 1 100

boundary 100

' region type=steel
' edge type=base_outer_full
unit 310
```

```
cubo 100  10.91999 -10.91999 0.16510 -0.16510 207.01000 -207.01000

media 6 1 100

boundary 100

' region type=steel
' edge type=lid_inner_lower
unit 320

cubo 100  6.27380 -6.27380 0.10795 -0.10795 207.01000 -207.01000

media 10 1 100

boundary 100

' region type=steel
' edge type=lid_inner_upper
unit 330

cubo 100  5.13080 -5.13080 0.10795 -0.10795 207.01000 -207.01000

media 10 1 100

boundary 100

' region type=steel
' edge type=lid_outer_upper
unit 340

cubo 100  6.15950 -6.15950 0.10795 -0.10795 207.01000 -207.01000

media 10 1 100

boundary 100

' region type=steel
' edge type=lid_outer_lower
unit 350

cubo 100  6.51510 -6.51510 0.10795 -0.10795 207.01000 -207.01000

media 10 1 100
```

```
boundary 100

' region type=boral
' edge type=base_inner_full
' axial part type=lower(1)
unit 400

cubo 100 9.52500 -9.52500 0.15113 -0.15113 14.42720 -14.42720

cubo 200 9.52500 -9.52500 0.15113 -0.15113 15.07490 -14.42720

media 7 1 100

media  4 1 -100 200

boundary  200

' region type=boral
' edge type=base_inner_full
' axial part type=main(9)
unit 402

cubo 100 9.52500 -9.52500 0.15113 -0.15113 19.17700 -19.17700

cubo 200 9.52500 -9.52500 0.15113 -0.15113 19.82470 -19.82470

media 7 1 100

media  4 1 -100 200

boundary  200

' region type=boral
' edge type=base_inner_full
' axial part type=upper(1)
unit 404

cubo 100 9.52500 -9.52500 0.15113 -0.15113 13.51280 -13.51280

cubo 200 9.52500 -9.52500 0.15113 -0.15113 13.51280 -14.16050

media 7 1 100
```

```
media  4 1 -100 200

boundary  200

' region type=boral
' edge type=base_inner_full
' axial array
unit 406

cubo 10 9.52500 -9.52500 0.15113 -0.15113 207.01000 -207.01000

array 406 10  place  1 1 1  0 0 -192.58280

boundary  10

' region type=boral
' edge type=base_outer_full
' axial part type=lower(1)
unit 410

cubo 100 9.52500 -9.52500 0.15113 -0.15113 14.42720 -14.42720

cubo 200 9.52500 -9.52500 0.15113 -0.15113 15.07490 -14.42720

media 7 1 100

media  4 1 -100 200

boundary  200

' region type=boral
' edge type=base_outer_full
' axial part type=main(9)
unit 412

cubo 100 9.52500 -9.52500 0.15113 -0.15113 19.17700 -19.17700

cubo 200 9.52500 -9.52500 0.15113 -0.15113 19.82470 -19.82470

media 7 1 100

media  4 1 -100 200
```

```
boundary  200

' region type=boral
' edge type=base_outer_full
' axial part type=upper(1)
unit 414

cubo 100 9.52500 -9.52500 0.15113 -0.15113 13.51280 -13.51280

cubo 200 9.52500 -9.52500 0.15113 -0.15113 13.51280 -14.16050

media 7 1 100

media  4 1 -100 200

boundary  200

' region type=boral
' edge type=base_outer_full
' axial array
unit 416

cubo 10 9.52500 -9.52500 0.15113 -0.15113 207.01000 -207.01000

array 416 10  place  1 1 1  0 0 -192.58280

boundary  10

' region type=boral
' edge type=lid_inner_lower
' axial part type=lower(1)
unit 420

cubo 100 6.03250 -6.03250 0.15113 -0.15113 14.42720 -14.42720

cubo 200 6.03250 -6.03250 0.15113 -0.15113 15.07490 -14.42720

media 7 1 100

media  4 1 -100 200

boundary  200
```

```
' region type=boral
' edge type=lid_inner_lower
' axial part type=main(9)
unit 422

cubo 100 6.03250 -6.03250 0.15113 -0.15113 19.17700 -19.17700

cubo 200 6.03250 -6.03250 0.15113 -0.15113 19.82470 -19.82470

media 7 1 100

media  4 1 -100 200

boundary  200

' region type=boral
' edge type=lid_inner_lower
' axial part type=upper(1)
unit 424

cubo 100 6.03250 -6.03250 0.15113 -0.15113 13.51280 -13.51280

cubo 200 6.03250 -6.03250 0.15113 -0.15113 13.51280 -14.16050

media 7 1 100

media  4 1 -100 200

boundary  200

' region type=boral
' edge type=lid_inner_lower
' axial array
unit 426

cubo 10 6.03250 -6.03250 0.15113 -0.15113 207.01000 -207.01000

array 426 10  place  1 1 1  0 0 -192.58280

boundary  10

' region type=boral
```

```
' edge type=lid_inner_upper
' axial part type=lower(1)
unit 430

cubo 100 4.95300 -4.95300 0.15113 -0.15113 14.42720 -14.42720

cubo 200 4.95300 -4.95300 0.15113 -0.15113 15.07490 -14.42720

media 7 1 100

media  4 1 -100 200

boundary  200

' region type=boral
' edge type=lid_inner_upper
' axial part type=main(9)
unit 432

cubo 100 4.95300 -4.95300 0.15113 -0.15113 19.17700 -19.17700

cubo 200 4.95300 -4.95300 0.15113 -0.15113 19.82470 -19.82470

media 7 1 100

media  4 1 -100 200

boundary  200

' region type=boral
' edge type=lid_inner_upper
' axial part type=upper(1)
unit 434

cubo 100 4.95300 -4.95300 0.15113 -0.15113 13.51280 -13.51280

cubo 200 4.95300 -4.95300 0.15113 -0.15113 13.51280 -14.16050

media 7 1 100

media  4 1 -100 200

boundary  200
```

```
' region type=boral
' edge type=lid_inner_upper
' axial array
unit 436

cubo 10 4.95300 -4.95300 0.15113 -0.15113 207.01000 -207.01000

array 436 10  place  1 1 1  0 0 -192.58280

boundary  10

' region type=boral
' edge type=lid_outer_upper
' axial part type=lower(1)
unit 440

cubo 100 6.03250 -6.03250 0.15113 -0.15113 14.42720 -14.42720

cubo 200 6.03250 -6.03250 0.15113 -0.15113 15.07490 -14.42720

media 7 1 100

media  4 1 -100 200

boundary  200

' region type=boral
' edge type=lid_outer_upper
' axial part type=main(9)
unit 442

cubo 100 6.03250 -6.03250 0.15113 -0.15113 19.17700 -19.17700

cubo 200 6.03250 -6.03250 0.15113 -0.15113 19.82470 -19.82470

media 7 1 100

media  4 1 -100 200

boundary  200

' region type=boral
' edge type=lid_outer_upper
```

```
' axial part type=upper(1)
unit 444

cubo 100 6.03250 -6.03250 0.15113 -0.15113 13.51280 -13.51280

cubo 200 6.03250 -6.03250 0.15113 -0.15113 13.51280 -14.16050

media 7 1 100

media  4 1 -100 200

boundary  200

' region type=boral
' edge type=lid_outer_upper
' axial array
unit 446

cubo 10 6.03250 -6.03250 0.15113 -0.15113 207.01000 -207.01000

array 446 10  place  1 1 1  0 0 -192.58280

boundary  10

' region type=boral
' edge type=lid_outer_lower
' axial part type=lower(1)
unit 450

cubo 100 5.88010 -5.88010 0.15113 -0.15113 14.42720 -14.42720

cubo 200 5.88010 -5.88010 0.15113 -0.15113 15.07490 -14.42720

media 7 1 100

media  4 1 -100 200

boundary  200

' region type=boral
' edge type=lid_outer_lower
' axial part type=main(9)
unit 452
```

```
cubo 100 5.88010 -5.88010 0.15113 -0.15113 19.17700 -19.17700

cubo 200 5.88010 -5.88010 0.15113 -0.15113 19.82470 -19.82470

media 7 1 100

media  4 1 -100 200

boundary  200

' region type=boral
' edge type=lid_outer_lower
' axial part type=upper(1)
unit 454

cubo 100 5.88010 -5.88010 0.15113 -0.15113 13.51280 -13.51280

cubo 200 5.88010 -5.88010 0.15113 -0.15113 13.51280 -14.16050

media 7 1 100

media  4 1 -100 200

boundary  200

' region type=boral
' edge type=lid_outer_lower
' axial array
unit 456

cubo 10 5.88010 -5.88010 0.15113 -0.15113 207.01000 -207.01000

array 456 10  place  1 1 1  0 0 -192.58280

boundary  10

' region type=plastic
' edge type=base_inner_full
' axial part type=lower(1)
unit 1160
com=' part 16 plastic block'
' plastic thickness removed=0.0781 inch =0.19844 cm
```

```
' bevel surface at -x
plane  10 xpl=1 origin x=-9.24437 y=1.48828 rotate a3=45

' bevel surface at +x
plane  20 xpl=1 origin x=9.24437 y=1.48828 rotate a3=-45
' thinned block without bevels, without axial gaps
cubo 100 9.24437 -9.24437 1.48828 -1.48828 2p14.22876

' thinned block without bevels, with axial gaps
cubo 200 9.24437 -9.24437 1.48828 -1.48828 15.07490 -14.42720

media  8 1 10 -20 100

media  4 1 -10 100
media  4 1 20 100

media  4 1 -100 200
boundary  200

' region type=plastic
' edge type=base_inner_full
' axial part type=main(9)
unit 1162
com=' part 16 plastic block'
' plastic thickness removed=0.0781 inch =0.19844 cm

' bevel surface at -x
plane  10 xpl=1 origin x=-9.24437 y=1.48828 rotate a3=45

' bevel surface at +x
plane  20 xpl=1 origin x=9.24437 y=1.48828 rotate a3=-45
' thinned block without bevels, without axial gaps
cubo 100 9.24437 -9.24437 1.48828 -1.48828 2p18.97856

' thinned block without bevels, with axial gaps
cubo 200 9.24437 -9.24437 1.48828 -1.48828 2p19.82470

media  8 1 10 -20 100

media  4 1 -10 100
media  4 1 20 100

media  4 1 -100 200
```

```
boundary  200

' region type=plastic
' edge type=base_inner_full
' axial part type=upper(1)
unit 1164
com=' part 16 plastic block'
' plastic thickness removed=0.0781 inch =0.19844 cm

' bevel surface at -x
plane  10 xpl=1 origin x=-9.24437 y=1.48828 rotate a3=45

' bevel surface at +x
plane  20 xpl=1 origin x=9.24437 y=1.48828 rotate a3=-45
' thinned block without bevels, without axial gaps
cubo 100 9.24437 -9.24437 1.48828 -1.48828 2p13.31436

' thinned block without bevels, with axial gaps
cubo 200 9.24437 -9.24437 1.48828 -1.48828 13.51280 -14.16050

media  8 1 10 -20 100

media  4 1 -10 100
media  4 1 20 100

media  4 1 -100 200
boundary  200

' region type=plastic
' edge type=base_inner_full
' axial array
unit 1166

cubo 10 9.24437 -9.24437 1.48828 -1.48828 206.81156 -206.81156

array 1166 10  place  1 1 1  0 0 -192.38436

boundary  10

' region type=plastic
' edge type=base_inner_full
' axial part type=lower(1)
unit 2160
```

```
com=' part 16 plastic block (right)'
' plastic thickness removed=0.0781 inch =0.19844 cm

' bevel surface at -x
plane  10 xpl=1 origin x=-9.24437 y=1.48828 rotate a3=45

' bevel surface at +x
plane  20 xpl=1 origin x=9.24437 y=1.48828 rotate a3=-45
' thinned block without bevels, without axial gaps
cubo 100 9.24437 -9.24437 1.48828 -1.48828 2p14.22876

' thinned block without bevels, with axial gaps
cubo 200 9.24437 -9.24437 1.48828 -1.48828 15.07490 -14.42720

media  8 1 10 -20 100

media  4 1 -10 100
media  4 1 20 100

media  4 1 -100 200
boundary  200

' region type=plastic
' edge type=base_inner_full
' axial part type=main(9)
unit 2162
com=' part 16 plastic block (right)'
' plastic thickness removed=0.0781 inch =0.19844 cm

' bevel surface at -x
plane  10 xpl=1 origin x=-9.24437 y=1.48828 rotate a3=45

' bevel surface at +x
plane  20 xpl=1 origin x=9.24437 y=1.48828 rotate a3=-45
' thinned block without bevels, without axial gaps
cubo 100 9.24437 -9.24437 1.48828 -1.48828 2p18.97856

' thinned block without bevels, with axial gaps
cubo 200 9.24437 -9.24437 1.48828 -1.48828 2p19.82470

media  8 1 10 -20 100

media  4 1 -10 100
```

```
media  4 1 20 100

media  4 1 -100 200
boundary  200

' region type=plastic
' edge type=base_inner_full
' axial part type=upper(1)
unit 2164
com=' part 16 plastic block (right)'
' plastic thickness removed=0.0781 inch =0.19844 cm

' bevel surface at -x
plane  10 xpl=1 origin x=-9.24437 y=1.48828 rotate a3=45

' bevel surface at +x
plane  20 xpl=1 origin x=9.24437 y=1.48828 rotate a3=-45
' thinned block without bevels, without axial gaps
cubo 100 9.24437 -9.24437 1.48828 -1.48828 2p13.31436

' thinned block without bevels, with axial gaps
cubo 200 9.24437 -9.24437 1.48828 -1.48828 13.51280 -14.16050

media  8 1 10 -20 100

media  4 1 -10 100
media  4 1 20 100

media  4 1 -100 200
boundary  200

' region type=plastic
' edge type=base_inner_full  (right)
' axial array
unit 2166

cubo 10 9.24437 -9.24437 1.48828 -1.48828 206.78366 -206.78366

array 2166 10  place  1 1 1  0 0 -192.38436

boundary 10

' region type=plastic
```

```
' edge type=base_outer_full
' axial part type=lower(1)
unit 1170
com=' part 17l plastic block'
' plastic thickness removed=0.0781 inch =0.19844 cm

' bevel surface at -x
plane  10 xpl=1 origin x=-9.24437 y=.31512 rotate a3=45

' bevel surface at +x
plane  20 xpl=1 origin x=9.24437 y=1.48828 rotate a3=-45
' thinned block without bevels, without axial gaps
cubo 100 9.24437 -9.24437 1.48828 -1.48828 2p14.22876

' thinned block without bevels, with axial gaps
cubo 200 9.24437 -9.24437 1.48828 -1.48828 15.07490 -14.42720

media  8 1 10 -20 100

media  4 1 -10 100
media  4 1 20 100

media  4 1 -100 200
boundary  200

' region type=plastic
' edge type=base_outer_full
' axial part type=main(9)
unit 1172
com=' part 17l plastic block'
' plastic thickness removed=0.0781 inch =0.19844 cm

' bevel surface at -x
plane  10 xpl=1 origin x=-9.24437 y=.31512 rotate a3=45

' bevel surface at +x
plane  20 xpl=1 origin x=9.24437 y=1.48828 rotate a3=-45
' thinned block without bevels, without axial gaps
cubo 100 9.24437 -9.24437 1.48828 -1.48828 2p18.97856

' thinned block without bevels, with axial gaps
cubo 200 9.24437 -9.24437 1.48828 -1.48828 2p19.82470
```

```
media  8 1 10 -20 100

media  4 1 -10 100
media  4 1 20 100

media  4 1 -100 200
boundary  200

' region type=plastic
' edge type=base_outer_full
' axial part type=upper(1)
unit 1174
com=' part 17l plastic block'
' plastic thickness removed=0.0781 inch =0.19844 cm

' bevel surface at -x
plane  10 xpl=1 origin x=-9.24437 y=.31512 rotate a3=45

' bevel surface at +x
plane  20 xpl=1 origin x=9.24437 y=1.48828 rotate a3=-45
' thinned block without bevels, without axial gaps
cubo 100 9.24437 -9.24437 1.48828 -1.48828 2p13.31436

' thinned block without bevels, with axial gaps
cubo 200 9.24437 -9.24437 1.48828 -1.48828 13.51280 -14.16050

media  8 1 10 -20 100

media  4 1 -10 100
media  4 1 20 100

media  4 1 -100 200
boundary  200

' region type=plastic
' edge type=base_outer_full
' axial array
unit 1176

cubo 10 9.24437 -9.24437 1.48828 -1.48828 206.81156 -206.81156

array 1176 10  place  1 1 1  0 0 -192.38436
boundary  10
```

```
' region type=plastic
' edge type=base_outer_full
' axial part type=lower(1)
unit 2170
com=' part 17r plastic block'
' plastic thickness removed=0.0781 inch =0.19844 cm

' bevel surface at -x
plane  10 xpl=1 origin x=-9.24437 y=1.48828 rotate a3=45

' bevel surface at +x
plane  20 xpl=1 origin x=9.24437 y=.31512 rotate a3=-45
' thinned block without bevels, without axial gaps
cubo 100 9.24437 -9.24437 1.48828 -1.48828 2p14.22876

' thinned block without bevels, with axial gaps
cubo 200 9.24437 -9.24437 1.48828 -1.48828 15.07490 -14.42720

media  8 1 10 -20 100

media  4 1 -10 100
media  4 1 20 100

media  4 1 -100 200
boundary  200

' region type=plastic
' edge type=base_outer_full
' axial part type=main(9)
unit 2172
com=' part 17r plastic block'
' plastic thickness removed=0.0781 inch =0.19844 cm

' bevel surface at -x
plane  10 xpl=1 origin x=-9.24437 y=1.48828 rotate a3=45

' bevel surface at +x
plane  20 xpl=1 origin x=9.24437 y=.31512 rotate a3=-45
' thinned block without bevels, without axial gaps
cubo 100 9.24437 -9.24437 1.48828 -1.48828 2p18.97856

' thinned block without bevels, with axial gaps
cubo 200 9.24437 -9.24437 1.48828 -1.48828 2p19.82470
```

```
media  8 1 10 -20 100

media  4 1 -10 100
media  4 1 20 100

media  4 1 -100 200
boundary  200

' region type=plastic
' edge type=base_outer_full
' axial part type=upper(1)
unit 2174
com=' part 17r plastic block'
' plastic thickness removed=0.0781 inch =0.19844 cm

' bevel surface at -x
plane  10 xpl=1 origin x=-9.24437 y=1.48828 rotate a3=45

' bevel surface at +x
plane  20 xpl=1 origin x=9.24437 y=.31512 rotate a3=-45
' thinned block without bevels, without axial gaps
cubo 100 9.24437 -9.24437 1.48828 -1.48828 2p13.31436

' thinned block without bevels, with axial gaps
cubo 200 9.24437 -9.24437 1.48828 -1.48828 13.51280 -14.16050

media  8 1 10 -20 100

media  4 1 -10 100
media  4 1 20 100

media  4 1 -100 200
boundary  200

' region type=plastic
' edge type=base_outer_full
' axial array
unit 2176

cubo 10 9.24437 -9.24437 1.48828 -1.48828 206.81156 -206.81156

array 2176 10  place  1 1 1  0 0 -192.38436
```

```
boundary  10

' region type=plastic
' edge type=lid_inner_lower
' axial part type=lower(1)
unit 1550
com=' part 55l plastic block'
' plastic thickness removed=0.0781 inch =0.19844 cm
' thinned block without bevels, without axial gaps
cubo 100 4.51326 -4.51326 1.48828 -1.48828 2p14.22876

' thinned block without bevels, with axial gaps
cubo 200 4.51326 -4.51326 1.48828 -1.48828 15.07490 -14.42720

media  8 1 100

media  4 1 -100 200
boundary  200

' region type=plastic
' edge type=lid_inner_lower
' axial part type=main(9)
unit 1552
com=' part 55l plastic block'
' plastic thickness removed=0.0781 inch =0.19844 cm
' thinned block without bevels, without axial gaps
cubo 100 4.51326 -4.51326 1.48828 -1.48828 2p18.97856

' thinned block without bevels, with axial gaps
cubo 200 4.51326 -4.51326 1.48828 -1.48828 2p19.82470

media  8 1 100

media  4 1 -100 200
boundary  200

' region type=plastic
' edge type=lid_inner_lower
' axial part type=upper(1)
unit 1554
com=' part 55l plastic block'
' plastic thickness removed=0.0781 inch =0.19844 cm
```

```
' thinned block without bevels, without axial gaps
cubo 100 4.51326 -4.51326 1.48828 -1.48828 2p13.31436

' thinned block without bevels, with axial gaps
cubo 200 4.51326 -4.51326 1.48828 -1.48828 13.51280 -14.16050

media  8 1 100

media  4 1 -100 200
boundary  200

' region type=plastic
' edge type=lid_inner_lower
' axial array
unit 1556

cubo 10 4.51326 -4.51326 1.48828 -1.48828 206.81156 -206.81156

array 1556 10  place  1 1 1  0 0 -192.38436

boundary  10

' region type=plastic
' edge type=lid_inner_lower
' axial part type=lower(1)
unit 2550
com=' part 55r plastic block'
' plastic thickness removed=0.0781 inch =0.19844 cm
' thinned block without bevels, without axial gaps
cubo 100 6.16426 -6.36270 1.48828 -1.48828 2p14.22876

' thinned block without bevels, with axial gaps
cubo 200 6.16426 -6.36270 1.48828 -1.48828 15.07490 -14.42720

media  8 1 100

media  4 1 -100 200
boundary  200

' region type=plastic
' edge type=lid_inner_lower
' axial part type=main(9)
unit 2552
```

```
com=' part 55r plastic block'
' plastic thickness removed=0.0781 inch =0.19844 cm
' thinned block without bevels, without axial gaps
cubo 100 6.16426 -6.36270 1.48828 -1.48828 2p18.97856

' thinned block without bevels, with axial gaps
cubo 200 6.16426 -6.36270 1.48828 -1.48828 2p19.82470

media  8 1 100

media  4 1 -100 200
boundary  200

' region type=plastic
' edge type=lid_inner_lower
' axial part type=upper(1)
unit 2554
com=' part 55r plastic block'
' plastic thickness removed=0.0781 inch =0.19844 cm
' thinned block without bevels, without axial gaps
cubo 100 6.16426 -6.36270 1.48828 -1.48828 2p13.31436

' thinned block without bevels, with axial gaps
cubo 200 6.16426 -6.36270 1.48828 -1.48828 13.51280 -14.16050

media  8 1 100

media  4 1 -100 200
boundary  200

' region type=plastic
' edge type=lid_inner_lower
' axial array
unit 2556

cubo 10 6.16426 -6.36270 1.48828 -1.48828 206.81156 -206.81156

array 2556 10  place  1 1 1  0 0 -192.38436

boundary  10

' region type=plastic
' edge type=lid_inner_upper
```

```
' axial part type=lower(1)
unit 1570
com=' part 57l plastic block'
' plastic thickness removed=0.0781 inch =0.19844 cm

' bevel surface at -x
plane  10 xpl=1 origin x=.28063 y=-1.48828 rotate a3=-45
' thinned block without bevels, without axial gaps
cubo 100 10.49496 .28063 1.48828 -1.48828 2p14.22876

' thinned block without bevels, with axial gaps
cubo 200 10.49496 .28063 1.48828 -1.48828 15.07490 -14.42720

media  8 1 10 100

media  4 1 -10 100
media  4 1 -100 200
boundary  200

' region type=plastic
' edge type=lid_inner_upper
' axial part type=main(9)
unit 1572
com=' part 57l plastic block'
' plastic thickness removed=0.0781 inch =0.19844 cm

' bevel surface at -x
plane  10 xpl=1 origin x=.28063 y=-1.48828 rotate a3=-45
' thinned block without bevels, without axial gaps
cubo 100 10.49496 .28063 1.48828 -1.48828 2p18.97856

' thinned block without bevels, with axial gaps
cubo 200 10.49496 .28063 1.48828 -1.48828 2p19.82470

media  8 1 10 100

media  4 1 -10 100
media  4 1 -100 200
boundary  200

' region type=plastic
' edge type=lid_inner_upper
' axial part type=upper(1)
```

```
unit 1574
com=' part 57l plastic block'
' plastic thickness removed=0.0781 inch =0.19844 cm

' bevel surface at -x
plane  10 xpl=1 origin x=.28063 y=-1.48828 rotate a3=-45
' thinned block without bevels, without axial gaps
cubo 100 10.49496 .28063 1.48828 -1.48828 2p13.31436

' thinned block without bevels, with axial gaps
cubo 200 10.49496 .28063 1.48828 -1.48828 13.51280 -14.16050

media  8 1 10 100

media  4 1 -10 100
media  4 1 -100 200
boundary  200

' region type=plastic
' edge type=lid_inner_upper
' axial array
unit 1576

cubo 10 10.49496 0.28063 1.48828 -1.48828 206.81156 -206.81156

array 1576 10  place  1 1 1  0 0 -192.38436

boundary  10

' region type=plastic
' edge type=lid_inner_upper
' axial part type=lower(1)
unit 2570
com=' part 57r plastic block'
' plastic thickness removed=0.0781 inch =0.19844 cm

' bevel surface at +x
plane  10 xpl=1 origin x=-.28063 y=-1.48828 rotate a3=45
' thinned block without bevels, without axial gaps
cubo 100 -.28063 -10.49496 1.48828 -1.48828 2p14.22876

' thinned block without bevels, with axial gaps
cubo 200 -.28063 -10.49496 1.48828 -1.48828 15.07490 -14.42720
```

```
media  8 1 -10 100

media  4 1 10 100
media  4 1 -100 200
boundary  200

' region type=plastic
' edge type=lid_inner_upper
' axial part type=main(9)
unit 2572
com=' part 57r plastic block'
' plastic thickness removed=0.0781 inch =0.19844 cm

' bevel surface at +x
plane  10 xpl=1 origin x=-.28063 y=-1.48828 rotate a3=45
' thinned block without bevels, without axial gaps
cubo 100 -.28063 -10.49496 1.48828 -1.48828 2p18.97856

' thinned block without bevels, with axial gaps
cubo 200 -.28063 -10.49496 1.48828 -1.48828 2p19.82470

media  8 1 -10 100

media  4 1 10 100
media  4 1 -100 200
boundary  200

' region type=plastic
' edge type=lid_inner_upper
' axial part type=upper(1)
unit 2574
com=' part 57r plastic block'
' plastic thickness removed=0.0781 inch =0.19844 cm

' bevel surface at +x
plane  10 xpl=1 origin x=-.28063 y=-1.48828 rotate a3=45
' thinned block without bevels, without axial gaps
cubo 100 -.28063 -10.49496 1.48828 -1.48828 2p13.31436

' thinned block without bevels, with axial gaps
cubo 200 -.28063 -10.49496 1.48828 -1.48828 13.51280 -14.16050
```

```
media  8 1 -10 100

media  4 1 10 100
media  4 1 -100 200
boundary  200

' region type=plastic
' edge type=lid_inner_upper
' axial array
unit 2576

cubo 10 -0.28063 -10.49496 1.48828 -1.48828 206.81156 -206.81156

array 2576 10  place  1 1 1  0 0 -192.38436

boundary  10

' region type=plastic
' edge type=lid_outer_upper
unit 1598
com=' part 59lw plastic block'
' plastic thickness removed=0.0781 inch =0.19844 cm

wedge 10 1.38799 1.38799 2.97656 28.45753 origin z=0.19844
media 8 1 10

wedge 20 1.38799 1.38799 2.97656 37.95713 origin z=30.34824
media 8 1 20

wedge 30 1.38799 1.38799 2.97656 37.95713 origin z=69.99764
media 8 1 30

wedge 40 1.38799 1.38799 2.97656 37.95713 origin z=109.64704
media 8 1 40

wedge 50 1.38799 1.38799 2.97656 37.95713 origin z=149.29644
media 8 1 50

wedge 60 1.38799 1.38799 2.97656 37.95713 origin z=188.94584
media 8 1 60

wedge 70 1.38799 1.38799 2.97656 37.95713 origin z=228.59524
media 8 1 70
```

```
wedge 80 1.38799 1.38799 2.97656 37.95713 origin z=268.24464
media 8 1 80

wedge 90 1.38799 1.38799 2.97656 37.95713 origin z=307.89404
media 8 1 90

wedge 100 1.38799 1.38799 2.97656 37.95713 origin z=347.54344
media 8 1 100

wedge 110 1.38799 1.38799 2.97656 26.62873 origin z=387.19284
media 8 1 110

wedge 120 1.38799 1.38799 2.97656 414.02000 origin z=0.00000
media  4 1  -10 -20 -30 -40 -50 -60 -70 -80 -90 -100 -110 120
boundary 120

' region type=plastic
' edge type=lid_outer_upper
unit 2598
com=' part 59rw plastic block'
' plastic thickness removed=0.0781 inch =0.19844 cm

wedge 10 1.38799 0.00000 2.97656 28.45753 origin z=0.19844
media 8 1 10

wedge 20 1.38799 0.00000 2.97656 37.95713 origin z=30.34824
media 8 1 20

wedge 30 1.38799 0.00000 2.97656 37.95713 origin z=69.99764
media 8 1 30

wedge 40 1.38799 0.00000 2.97656 37.95713 origin z=109.64704
media 8 1 40

wedge 50 1.38799 0.00000 2.97656 37.95713 origin z=149.29644
media 8 1 50

wedge 60 1.38799 0.00000 2.97656 37.95713 origin z=188.94584
media 8 1 60

wedge 70 1.38799 0.00000 2.97656 37.95713 origin z=228.59524
media 8 1 70
```

```
wedge 80 1.38799 0.00000 2.97656 37.95713 origin z=268.24464
media 8 1 80

wedge 90 1.38799 0.00000 2.97656 37.95713 origin z=307.89404
media 8 1 90

wedge 100 1.38799 0.00000 2.97656 37.95713 origin z=347.54344
media 8 1 100

wedge 110 1.38799 0.00000 2.97656 26.62873 origin z=387.19284
media 8 1 110

wedge 120 1.38799 0.00000 2.97656 414.02000 origin z=0.00000
media  4 1  -10 -20 -30 -40 -50 -60 -70 -80 -90 -100 -110 120
boundary 120

' region type=plastic
' edge type=lid_outer_upper
' axial part type=lower(1)
unit 1590
com=' part 59l plastic block'
' plastic thickness removed=0.0781 inch =0.19844 cm

' bevel surface at +x
plane  10 xpl=1 origin x=-.28063 y=-1.48828 rotate a3=45
' thinned block without bevels, without axial gaps
cubo 100 -.28063 -11.37245 1.48828 -1.48828 2p14.22876

' thinned block without bevels, with axial gaps
cubo 200 -.28063 -11.37245 1.48828 -1.48828 15.07490 -14.42720

media  8 1 -10 100

media  4 1 10 100
media  4 1 -100 200
boundary  200

' region type=plastic
' edge type=lid_outer_upper
' axial part type=main(9)
unit 1592
com=' part 59l plastic block'
```

```
' plastic thickness removed=0.0781 inch =0.19844 cm

' bevel surface at +x
plane  10 xpl=1 origin x=-.28063 y=-1.48828 rotate a3=45
' thinned block without bevels, without axial gaps
cubo 100 -.28063 -11.37245 1.48828 -1.48828 2p18.97856

' thinned block without bevels, with axial gaps
cubo 200 -.28063 -11.37245 1.48828 -1.48828 2p19.82470

media  8 1 -10 100

media  4 1 10 100
media  4 1 -100 200
boundary  200

' region type=plastic
' edge type=lid_outer_upper
' axial part type=upper(1)
unit 1594
com=' part 59l plastic block'
' plastic thickness removed=0.0781 inch =0.19844 cm

' bevel surface at +x
plane  10 xpl=1 origin x=-.28063 y=-1.48828 rotate a3=45
' thinned block without bevels, without axial gaps
cubo 100 -.28063 -11.37245 1.48828 -1.48828 2p13.31436

' thinned block without bevels, with axial gaps
cubo 200 -.28063 -11.37245 1.48828 -1.48828 13.51280 -14.16050

media  8 1 -10 100

media  4 1 10 100
media  4 1 -100 200
boundary  200

' region type=plastic
' edge type=lid_outer_upper
' axial array
unit 1596

cubo 10 -0.28063 -11.37245 1.48828 -1.48828 206.81156 -206.81156
```

```
array 1596 10  place  1 1 1  0 0 -192.38436

boundary  10

' region type=plastic
' edge type=lid_outer_upper
' axial part type=lower(1)
unit 2590
com=' part 59r plastic block'
' plastic thickness removed=0.0781 inch =0.19844 cm

' bevel surface at -x
plane  10 xpl=1 origin x=.28063 y=-1.48828 rotate a3=-45
' thinned block without bevels, without axial gaps
cubo 100 11.37245 .28063 1.48828 -1.48828 2p14.22876

' thinned block without bevels, with axial gaps
cubo 200 11.37245 .28063 1.48828 -1.48828 15.07490 -14.42720

media  8 1 10 100

media  4 1 -10 100
media  4 1 -100 200
boundary  200

' region type=plastic
' edge type=lid_outer_upper
' axial part type=main(9)
unit 2592
com=' part 59r plastic block'
' plastic thickness removed=0.0781 inch =0.19844 cm

' bevel surface at -x
plane  10 xpl=1 origin x=.28063 y=-1.48828 rotate a3=-45
' thinned block without bevels, without axial gaps
cubo 100 11.37245 .28063 1.48828 -1.48828 2p18.97856

' thinned block without bevels, with axial gaps
cubo 200 11.37245 .28063 1.48828 -1.48828 2p19.82470

media  8 1 10 100
```

```
media  4 1 -10 100
media  4 1 -100 200
boundary  200

' region type=plastic
' edge type=lid_outer_upper
' axial part type=upper(1)
unit 2594
com=' part 59r plastic block'
' plastic thickness removed=0.0781 inch =0.19844 cm

' bevel surface at -x
plane  10 xpl=1 origin x=.28063 y=-1.48828 rotate a3=-45
' thinned block without bevels, without axial gaps
cubo 100 11.37245 .28063 1.48828 -1.48828 2p13.31436

' thinned block without bevels, with axial gaps
cubo 200 11.37245 .28063 1.48828 -1.48828 13.51280 -14.16050

media  8 1 10 100

media  4 1 -10 100
media  4 1 -100 200
boundary  200

' region type=plastic
' edge type=lid_outer_upper
' axial array
unit 2596

cubo 10 11.37245 0.28063 1.48828 -1.48828 206.81156 -206.81156

array 2596 10  place  1 1 1  0 0 -192.38436

boundary  10

' region type=plastic
' edge type=lid_outer_lower
' axial part type=lower(1)
unit 1610
com=' part 61l plastic block'
' plastic thickness removed=0.0781 inch =0.19844 cm
```

```
' bevel surface at -x
plane  10 xpl=1 origin x=-10.71083 y=-1.48828 rotate a3=-20
' thinned block without bevels, without axial gaps
cubo 100 -.19844 -10.71083 1.48828 -1.48828 2p14.22876

' thinned block without bevels, with axial gaps
cubo 200 -.19844 -10.71083 1.48828 -1.48828 15.07490 -14.42720

media  8 1 10 100

media  4 1 -10 100
media  4 1 -100 200
boundary  200

' region type=plastic
' edge type=lid_outer_lower
' axial part type=main(9)
unit 1612
com=' part 61l plastic block'
' plastic thickness removed=0.0781 inch =0.19844 cm

' bevel surface at -x
plane  10 xpl=1 origin x=-10.71083 y=-1.48828 rotate a3=-20
' thinned block without bevels, without axial gaps
cubo 100 -.19844 -10.71083 1.48828 -1.48828 2p18.97856

' thinned block without bevels, with axial gaps
cubo 200 -.19844 -10.71083 1.48828 -1.48828 2p19.82470

media  8 1 10 100

media  4 1 -10 100
media  4 1 -100 200
boundary  200

' region type=plastic
' edge type=lid_outer_lower
' axial part type=upper(1)
unit 1614
com=' part 61l plastic block'
' plastic thickness removed=0.0781 inch =0.19844 cm

' bevel surface at -x
```

```
plane  10 xpl=1 origin x=-10.71083 y=-1.48828 rotate a3=-20
' thinned block without bevels, without axial gaps
cubo 100 -.19844 -10.71083 1.48828 -1.48828 2p13.31436

' thinned block without bevels, with axial gaps
cubo 200 -.19844 -10.71083 1.48828 -1.48828 13.51280 -14.16050

media  8 1 10 100

media  4 1 -10 100
media  4 1 -100 200
boundary  200

' region type=plastic
' edge type=lid_outer_lower
' axial array
unit 1616

cubo 10 -0.19844 -10.71083 1.48828 -1.48828 206.81156 -206.81156

array 1616 10  place  1 1 1  0 0 -192.38436

boundary  10

' region type=plastic
' edge type=lid_outer_lower
' axial part type=lower(1)
unit 2610
com=' part 61r plastic block'
' plastic thickness removed=0.0781 inch =0.19844 cm

' bevel surface at +x
plane  10 xpl=1 origin x=10.71083 y=-1.48828 rotate a3=20
' thinned block without bevels, without axial gaps
cubo 100 10.71083 .19844 1.48828 -1.48828 2p14.22876

' thinned block without bevels, with axial gaps
cubo 200 10.71083 .19844 1.48828 -1.48828 15.07490 -14.42720

media  8 1 -10 100

media  4 1 10 100
media  4 1 -100 200
```

```
boundary  200

' region type=plastic
' edge type=lid_outer_lower
' axial part type=main(9)
unit 2612
com=' part 61r plastic block'
' plastic thickness removed=0.0781 inch =0.19844 cm

' bevel surface at +x
plane  10 xpl=1 origin x=10.71083 y=-1.48828 rotate a3=20
' thinned block without bevels, without axial gaps
cubo 100 10.71083 .19844 1.48828 -1.48828 2p18.97856

' thinned block without bevels, with axial gaps
cubo 200 10.71083 .19844 1.48828 -1.48828 2p19.82470

media  8 1 -10 100

media  4 1 10 100
media  4 1 -100 200
boundary  200

' region type=plastic
' edge type=lid_outer_lower
' axial part type=upper(1)
unit 2614
com=' part 61r plastic block'
' plastic thickness removed=0.0781 inch =0.19844 cm

' bevel surface at +x
plane  10 xpl=1 origin x=10.71083 y=-1.48828 rotate a3=20
' thinned block without bevels, without axial gaps
cubo 100 10.71083 .19844 1.48828 -1.48828 2p13.31436

' thinned block without bevels, with axial gaps
cubo 200 10.71083 .19844 1.48828 -1.48828 13.51280 -14.16050

media  8 1 -10 100

media  4 1 10 100
media  4 1 -100 200
boundary  200
```

```
' region type=plastic
' edge type=lid_outer_lower
' axial array
unit 2616

cubo 10 10.71083 0.19844 1.48828 -1.48828 206.81156 -206.81156

array 2616 10  place  1 1 1  0 0 -192.38436

boundary  10

unit 810
com='aluminum door and rubber at upper edge of assy'
' nominal aluminum dims: 0.25" thk by 7.9" wide by 35.0" long
' tolerances: 0.03" by 0.1" by 0.1"
' dimensions modeled: 0.22" by 7.8" by 34.9"
' there is a nominal 0.25" axial gap, modeled as 0.25 + 0.03(gap tol) + .1 (half of alum length tol times two)
' axial gap modeled as 0.38"

' this is a rubber layer, modeled as same width and length as alum and 0.22" thk
cubo  20 2p9.906 0.5588 0 2p44.323
' this is aluminum
cubo  40 2p9.906 1.1176 0 2p44.323
' gap
cubo  60 2p9.906 1.1176 0 2p44.8056

media  5 1 20
media  13 1 40 -20
media  9 1 60 -40

boundary 60

unit 820
com='aluminum door and rubber at upper edge of assy'
' there are 4 units 810, unit 820 is at -z end
' 4 * 44.8056 = 179.2224
' total length here is 207.01 - 179.2224 = 27.7876
' gap is final 0.19" (0.4826 cm) of the length

' this is a rubber layer, modeled as same width and length as alum and 0.22" thk
cubo  20 2p9.906 0.5588 0 27.305 0
' this is aluminum
cubo  40 2p9.906 1.1176 0 27.305 0
```

```
' gap
cubo  60 2p9.906 1.1176 0 27.7876 0

media  5 1 20
media  13 1 40 -20
media  9 1 60 -40

boundary 60

unit 830
com="same as unit 820 except gap at -z end"

' this is a rubber layer, modeled as same width and length as alum and 0.22" thk
cubo  20 2p9.906 0.5588 0 27.7876 0.4846
' this is aluminum
cubo  40 2p9.906 1.1176 0 27.7876 0.4846
' gap
cubo  60 2p9.906 1.1176 0 27.7876 0

media  5 1 20
media  13 1 40 -20
media  9 1 60 -40

boundary 60

unit 840
com='axial array of doors'
cubo  10 2p9.906 1.1176 0 2p207.01
array  2 10  place  1 1 1 0 0 -207.01

boundary 10

unit 860
com='steel bar at center of package'
' nominal 0.75" high by 1.75" wide, use 0.70 x 1.70

cubo  20 2p2.159 1.778 0 2p207.01

media  14 1 20
boundary 20

unit 900
com='fuel assembly, not rotated'
```

```
cubo  10 21.640800 0 21.640800 0 2p207.01
array  1 10  place  1 1 1 0.721360 0.721360 0

' water layer around assy

cubo  20 23.8633 -0.635 23.8633 -0.635 2p207.01

'hole 840 origin x=11.73480 y=21.64080
'hole 840 origin x=21.64080 y=11.73480 rotate a3=-90

hole  200 origin x=10.795 y=-0.3175
hole  200 origin x=-0.3175 y=10.795 rotate a3=90
media  9 1 20 -10
boundary 20

global
unit 1000
com='one package'
' bundle c-c spacing is 15.2"
' diamond is 10.03" x 9.86" (across outer steel surfaces)
' diamond diagonal is 14.0649"
' distance to spacers from diagonal: 8.10" (lower) and 8.62" (upper)
'  vertical sum is 30.78"

' distance to outer surface of steel wall is 4.10" (lower) and 4.62" (upper)
' horizontal span across outer steel surfaces: 41.95"
' model steel as 0.115" thick

' base is 21.5" tall, including spacer height (54.61 cm)
' top of base is at y= 54.61 - 20.574 = 34.036 cm

' hanging central blocks with steel carriers
' inner steel surface
cubo  2 2p1.6256 22.45 14.9866 2p207.01
' outer steel surface
cubo  4 2p1.8415 22.45 14.7707 2p207.01

wedge 6 1.4018 0 1.4018 414.02 origin x=-1.4018 y=20.3255 z=-207.01

wedge 8 1.4018 1.4018 1.4018 414.02 origin x=0 y=20.3255 z=-207.01

cubo  10 2p1.4018 20.3255 14.9866 2p207.01
```

```
plane  11 zpl=1 origin z=-195.41973
plane  12 zpl=1 origin z=-164.04107
plane  13 zpl=1 origin z=-105.55453
plane  14 zpl=1 origin z=-74.17587
plane  15 zpl=1 origin z=-15.68933

plane  16 zpl=1 origin z=15.68933
plane  17 zpl=1 origin z=74.17587
plane  18 zpl=1 origin z=105.55453
plane  19 zpl=1 origin z=164.04107
plane  20 zpl=1 origin z=195.41973

' flooded regions
plane 31 ypl=1 origin y=16
cubo  32 -17 -30.5 34.5 26 2p207.01 rotate a3=20
cubo  33 30.5 17 34.5 26 2p207.01 rotate a3=-20
cubo  34 3.2 -5 24.5 0 2p207.01 origin x=-1.828 y=17.942 rotate a3=45
cubo  35 5 -3.2 24.5 0 2p207.01 origin x=1.828 y=17.942 rotate a3=-45
cubo  36 2p41 22 16 2p207.01
media  9 1  32 31
media  9 1  33 31
media  4 1  32 -31
media  4 1  33 -31

media  9 1  34 -4
media  9 1  35 -34 -4
media  9 1  36 -35 -34 -33 -32 -4

media  9 1 4 -11 31
media  4 1 4 -11 -31

' steel
media  10 1 4 -2 11 -12

' nylon
media  8 1 6 11 -12
media  8 1 8 11 -12
media  8 1 10 11 -12

' water
media  9 1 2 -6 -8 -10 11 -12
```

```
media  9 1 4 12 -13 31
media  4 1 4 12 -13 -31

' steel
media  10 1 4 -2 13 -14

' nylon
media  8 1 6 13 -14
media  8 1 8 13 -14
media  8 1 10 13 -14

' water
media  9 1 2 -6 -8 -10 13 -14

media  9 1 4 14 -15 31
media  4 1 4 14 -15 -31

' steel
media  10 1 4 -2 15 -16

' nylon
media  8 1 6 15 -16
media  8 1 8 15 -16
media  8 1 10 15 -16

' water
media  9 1 2 -6 -8 -10 15 -16

media  9 1 4 16 -17 31
media  4 1 4 16 -17 -31

' steel
media  10 1 4 -2 17 -18

' nylon
media  8 1 6 17 -18
media  8 1 8 17 -18
media  8 1 10 17 -18

' water
media  9 1 2 -6 -8 -10 17 -18
```

```
media  9 1 4 18 -19 31
media  4 1 4 18 -19 -31

' steel
media  10 1 4 -2 19 -20

' nylon
media  8 1 6 19 -20
media  8 1 8 19 -20
media  8 1 10 19 -20

' water
media  9 1 2 -6 -8 -10 19 -20

media  9 1 4 20 31
media  4 1 4 20 -31

'  inner surface of steel
cubo  580  2p52.9844 47.1675 -10.1981 2p207.01

media  4 1  580 -32 -33 -34 -35 -36 -4

'  outer surface of steel
cubo  590  2p53.2765 47.4596 -10.4140 2p207.01

media  11 1 -580 590

' package is 44.98" wide by 30.78" high by 207.98" long
'  modeled as 42.98" by 28.78" by 163"
cubo  600  2p54.5846 47.4596 -18.034 2p207.01

media  4 1 -590 600

'water reflector
cubo  601  2p84.5846 77.4596 -48.034 2p237.01

media  9 1 -600 601

' top of bar is 0.25" below bottom of steel carrier
' 14.7707 - 0.25 * 2.54 - 0.7 * 2.54 = 12.3577
hole  860 origin x=0 y=12.3577 z=0

hole 900  origin x=19.304 y=1.36500 z=0 rotate a3=45
```

```
hole 900  origin x=-19.304 y=1.36500 z=0  rotate a3=45

' region type=steel
' edge type=base_inner_full
hole 300 origin x=-10.73161 y=8.80588 rotate a3=45.0

hole 300 origin x=10.73161 y=8.80588 rotate a3=-45.0

' region type=steel
' edge type=base_outer_full
hole 310 origin x=-27.39379 y=8.32328 rotate a3=-45.0

hole 310 origin x=27.39379 y=8.32328 rotate a3=45.0

' region type=steel
' edge type=lid_inner_lower
hole 320 origin x=-4.86824 y=25.67904 rotate a3=-45.0

hole 320 origin x=4.86824 y=25.67904 rotate a3=45.0

' region type=steel
' edge type=lid_inner_upper
hole 330 origin x=-15.05185 y=31.62397 rotate a3=-45.0

hole 330 origin x=15.05185 y=31.62397 rotate a3=45.0

' region type=steel
' edge type=lid_outer_upper
hole 340 origin x=-23.67289 y=30.89657 rotate a3=45.0

hole 340 origin x=23.67289 y=30.89657 rotate a3=-45.0

' region type=steel
' edge type=lid_outer_lower
hole 350 origin x=-34.23368 y=24.21537 rotate a3=20

hole 350 origin x=34.23368 y=24.21537 rotate a3=-20

' region type=boral
' edge type=base_inner_full
hole 406 origin x=-11.31247 y=7.77780 rotate a3=45.0
```

```
hole 406 origin x=11.31247 y=7.77780 rotate a3=-45.0

' region type=boral
' edge type=base_outer_full
hole 416 origin x=-27.29553 y=7.77780 rotate a3=-45.0

hole 416 origin x=27.29553 y=7.77780 rotate a3=45.0

' region type=boral
' edge type=lid_inner_lower
hole 426 origin x=-4.85567 y=26.03286 rotate a3=-45.0

hole 426 origin x=4.85567 y=26.03286 rotate a1=180 a3=45.0

' region type=boral
' edge type=lid_inner_upper
hole 436 origin x=-15.20990 y=32.14842 rotate a3=-45.0

hole 436 origin x=15.20990 y=32.14842 rotate a1=180 a3=45.0

' region type=boral
' edge type=lid_outer_upper
hole 446 origin x=-23.87405 y=31.06181 rotate a3=45.0

hole 446 origin x=23.87405 y=31.06181 rotate a1=180 a3=-45.0

' region type=boral
' edge type=lid_outer_lower
hole 456 origin x=-33.78217 y=24.66807 rotate a3=20

hole 456 origin x=33.78217 y=24.66807 rotate a1=180 a3=-20

' region type=plastic
' edge type=base_inner_full
hole 1166 origin x=-10.15323 y=6.61856 rotate a3=45.0
hole 2166 origin x=10.15323 y=6.61856 rotate a3=-45.0

' region type=plastic
' edge type=base_outer_full

hole 1166 origin x=-28.45477 y=6.61856 rotate a3=-45.0
hole 2166 origin x=28.45477 y=6.61856 rotate a3=45.0
```

```
' region type=plastic
' edge type=lid_inner_lower

hole 1556 origin x=-4.63037 y=28.12605 rotate a3=-45.0
hole 2556 origin x=3.46294 y=26.95862 rotate a3=45.0

' region type=plastic
' edge type=lid_inner_upper

hole 1576 origin x=-17.87625 y=37.13325 rotate a3=-45.0
hole 2576 origin x=17.87625 y=37.13325 rotate a3=45.0

' region type=plastic
' edge type=lid_outer_upper

hole 1596 origin x=-20.19180 y=37.20396 rotate a3=45.0
hole 2596 origin x=20.19180 y=37.20396 rotate a3=-45.0

' region type=plastic
' edge type=lid_outer_upper (wedge)

hole 1598 origin x=-28.09172 y=27.05787 z=-207.01 rotate a3=45.0
hole 2598 origin x=27.11026 y=28.03933 z=-207.01 rotate a3=-45.0

' region type=plastic
' edge type=lid_outer_lower
hole 1616 origin x=-29.12357 y=28.13077 rotate a3=20
hole 2616 origin x=29.12357 y=28.13077 rotate a3=-20

boundary 601

end geometry

read array

' doors
ara=2 nux=1 nuy=1 nuz=6
fill 820 4r810 830 end fill

'assy lattice
ara=1  nux=15 nuy=15 nuz=1
fill
```

```
10 10 10 10 10 10 10 10 10 10 10 10 10 10
10 10 10 10 10 10 10 10 10 10 10 10 10 10
10 10 10 10 10 20 10 10 10 20 10 10 10 10
10 10 10 20 10 10 10 10 10 10 10 20 10 10
10 10 10 10 10 10 10 10 10 10 10 10 10 10
10 10 20 10 10 20 10 10 10 20 10 10 20 10
10 10 10 10 10 10 10 10 10 10 10 10 10 10
10 10 10 10 10 10 10 30 10 10 10 10 10 10
10 10 10 10 10 10 10 10 10 10 10 10 10 10
10 10 20 10 10 20 10 10 10 20 10 10 20 10
10 10 10 10 10 10 10 10 10 10 10 10 10 10
10 10 10 20 10 10 10 10 10 10 20 10 10 10
10 10 10 10 10 20 10 10 10 20 10 10 10 10
10 10 10 10 10 10 10 10 10 10 10 10 10 10
10 10 10 10 10 10 10 10 10 10 10 10 10 10
end fill

' region type=boral
' edge type=base_inner_full
ara=406 nux=1 nuy=1 nuz=11
fill 400 9r402 404 end fill

' region type=boral
' edge type=base_outer_full
ara=416 nux=1 nuy=1 nuz=11
fill 410 9r412 414 end fill

' region type=boral
' edge type=lid_inner_lower
ara=426 nux=1 nuy=1 nuz=11
fill 420 9r422 424 end fill

' region type=boral
' edge type=lid_inner_upper
ara=436 nux=1 nuy=1 nuz=11
fill 430 9r432 434 end fill

' region type=boral
' edge type=lid_outer_upper
ara=446 nux=1 nuy=1 nuz=11
fill 440 9r442 444 end fill
```

```
' region type=boral
' edge type=lid_outer_lower
ara=456 nux=1 nuy=1 nuz=11
fill 450 9r452 454 end fill

' region type=plastic
' edge type=base_inner_full
ara=1166 nux=1 nuy=1 nuz=11
fill 1160 9r1162 1164 end fill

' region type=plastic
' edge type=base_inner_full
ara=2166 nux=1 nuy=1 nuz=11
fill 2160 9r2162 2164 end fill

' region type=plastic
' edge type=base_outer_full
ara=1176 nux=1 nuy=1 nuz=11
fill 1170 9r1172 1174 end fill

' region type=plastic
' edge type=base_outer_full
ara=2176 nux=1 nuy=1 nuz=11
fill 2170 9r2172 2174 end fill

' region type=plastic
' edge type=lid_inner_lower
ara=1556 nux=1 nuy=1 nuz=11
fill 1550 9r1552 1554 end fill

' region type=plastic
' edge type=lid_inner_lower
ara=2556 nux=1 nuy=1 nuz=11
fill 2550 9r2552 2554 end fill

' region type=plastic
' edge type=base_outer_full
ara=1576 nux=1 nuy=1 nuz=11
fill 1570 9r1572 1574 end fill

' region type=plastic
' edge type=base_outer_full
ara=2576 nux=1 nuy=1 nuz=11
```

```
fill 2570 9r2572 2574 end fill

' region type=plastic
' edge type=lid_outer_upper
ara=1596 nux=1 nuy=1 nuz=11
fill 1590 9r1592 1594 end fill

' region type=plastic
' edge type=lid_outer_upper
ara=2596 nux=1 nuy=1 nuz=11
fill 2590 9r2592 2594 end fill

' region type=plastic
' edge type=lid_outer_lower
ara=1616 nux=1 nuy=1 nuz=11
fill 1610 9r1612 1614 end fill

' region type=plastic
' edge type=lid_outer_lower
ara=2616 nux=1 nuy=1 nuz=11
fill 2610 9r2612 2614 end fill

end array

read bounds all=vacu end bounds
read start
nst=1
end start

end data
end
```

6.10 REFERENCES

1) Title 10, Code of Federal Regulations, Part 71 (10CFR71), Packaging and Transportation of Radioactive Material, edition effective Oct 2004.

2) "Recommendations for Preparing the Criticality Safety Evaluation of Transport Packages," NUREG/CR-5661.

3) Criticality Benchmark Guide for Light-Water-Reactor Fuel in Transportation and Storage Packages," NUREG/CR-6361 (ORNL/TM-13211).

4) J.C. Manaranche, D. Mangin, L. Maubert, G. Colomb, and G. Poullot, "Dissolution and Storage Experimental Program with U[4.75]O_2 Rods," Trans. Am. Nucl. Soc., Vol. 33, pp. 362-364, November 1979.

5) M.N. Baldwin, G.S. Hoovler, R.L. Eng, and F.G. Welfare, "Critical Experiments Supporting Close Proximity Water Storage of Power Reactor Fuel," BAW-1484-7, Babcock & Wilcox Company, July 1979.

6) R.I. Smith and G.J. Konzek, "Clean Critical Experiment Benchmarks for Plutonium Recycle in LWR's, Volume I," EPRI-NP-196, Electric Power Research Institute, April 1976.

7) J.C. Manaranche, D. Mangin, L. Maubert, G. Colomb, and G. Poullot, "Critical Experiments with Lattices of 4.75-wt%-^{235}U-Enriched UO_2 Rods in Water," Nucl. Sci. Eng., Vol. 71, pp. 154-163, 1979.

8) S.R. Bierman, E.D. Clayton, and B.M. Durst, "Critical Separation Between Subcritical Clusters of 2.35 wt% ^{235}U Enriched UO_2 Rods in Water with Fixed Neutron Poisons," PNL-2438, Pacific Northwest Laboratories, October 1977.

9) "Critical Separation Between Subcritical Clusters of 4.31 wt % ^{235}U Enriched UO_2 Rods in Water with Fixed Neutron Poisons," NUREG/CR-0079 (PNL-2615), U.S. Nuclear Regulatory Commission, March 1978.

10) S.R. Bierman, B.M. Durst, and E.D. Clayton, "Critical Experiments with Subcritical Clusters of 2.35 wt % and 4.31 wt % ^{235}U Enriched UO_2 Rods in Water with Uranium or Lead Reflecting Walls," NUREG/CR-0796, Vol. 1 (PNL-2827), U.S. Nuclear Regulatory Commission, April 1979.

11) S.R. Bierman and E.D. Clayton, "Critical Experiments with Subcritical Clusters of 2.35 wt % and 4.31 wt % ^{235}U Enriched UO_2 Rods in Water at a Water-to-Fuel Volume Ratio of 1.6," NUREG/CR-1547 (PNL-3314), U.S. Nuclear Regulatory Commission, July 1980.

12) S.R. Bierman, B.M. Durst, and E.D. Clayton, "Critical Experiments with Subcritical Clusters of 2.35 wt % and 4.31 wt % ^{235}U Enriched UO_2 Rods in Water with Uranium or Lead Reflecting Walls," NUREG/CR-0796, Vol. 2 (PNL-3926), U.S. Nuclear Regulatory Commission, December 1981.

13) S.R. Bierman, "Criticality Experiments to Provide Benchmark Data on Neutron Flux Traps," PNL-6205, Pacific Northwest Laboratory, June 1988.

14) S.R. Bierman, "Criticality Experiments with Neutron Flux Traps Containing Voids," PNL-7167, Pacific Northwest Laboratory, April 1990.

15) R.D. Leamer, D.F. Hanlen, G.N. Hamilton, and E.G. Taylor, "Critical Experiments Performed with Clustered and Uniform Arrays of Rodded Absorbers," WCAP-3269-39, Westinghouse Electric Corp., November 1965.

16) E.G. Taylor, "Saxton Plutonium Program, Critical Experiments for the Saxton Partial Plutonium Core," EURAEC-1493 (WCAP-3385-54), U.S. Atomic Energy Commission, December 1965.

Exhibited foam compressive strength for 10% strain perpendicular to foam rise shall fall within the following range of values:

1.	Impact Limiter	317 psi min	384 psi max
2.	Package Body	132 psi min	160 psi max

8.1.5.1.3 Flame Retardant Characteristics

Flame retardant characteristics shall be qualified by demonstrating compliance with the following requirements. Position test samples for approximately 60 seconds above a sufficiently sized burner with a flame temperature of a least 1,500°F. Immediately after removal of the test sample from the burner flame, measure and record the elapsed time until flames from the test sample extinguish. The average flame extinguishment time shall not exceed fifteen (15) seconds.

8.1.5.1.4 Thermal Proprieties

The 6 and 10 lb/ft^3 nominal density foam shall exhibit the following thermal characteristics:

1. Thermal Conductivity: 0.17 to 0.30 BTU-in/hr-ft^2-°F.
2. Specific Heat: 0.28 to 0.42 BTU/lb_m-°F

8.1.5.1.5 Chemical Composition

The foam will be a rigid polyether polyurethane formed as reaction product of the primary chemicals: polyphenylene, polymethylene, polyisocyanate (polymeric isocyanate) and polyoxypropylene glycols (polyether polyols). These materials react to produce a rigid, polyether, polyurethane foam. The foam will not contain halogen containing flame retardant or trichloromonoflouromethane (Freon 11).

Leachable chloride testing is required when using stainless steel as the container structure because free chloride ions in contact with the container sides have been faulted as a contributor to stress corrosion cracking. Leachable chlorides will not be greater than 1 ppm when tested in accordance with GP-TM9510: Method for Sample Preparation and Determination of Leachable Chlorides in

Attachment B

Response to NRC Request for Additional Information
for Review of the Model No. MAP-12 and MAP-13 Packages,
dated September 6, 2007

AREVA NP INC.
An AREVA and Siemens company

3315 Old Forest Road, P.O. Box 10935, Lynchburg, VA 24506-0935
Tel.: (434) 832-3000 - Fax: (434) 832-3840

AREVA NP Inc Response to NRC Request for Additional Information
Docket No. 71-9319
Certificate of Compliance No. 9319
Model No. MAP-12 and MAP-13 Packages

Chapter 1.0 General Information

NRC Question 1-1:

Clarify the discrepancy between the cover letter and Section 1.2.2.2, page 1-10, of the SAR regarding the justification for a "Type B" classification of the MAP-12/MAP- 13 packages.

The cover letter of the application states: "Since this material constitutes Type B material due to the U-236 content, the shipment and use of this fuel is directly dependant upon the implementation of the MAP shipping package ...[.] "Section 1.2.2.2 of the SAR states: "The increase in 234U causes the contents to fall under the Type B requirements." It is not clear as to the reason AREVA is requesting a "Type B" classification for the Model No. MAP-12/MAP-13.

AREVA Response to Question 1-1:

The text in Section 1.2.2.2 has been revised to be consistent with the cover letter. U-234 is attributed to the bulk of the radioactivity of the material however the increase in U-236 causes the contents to fall under the Type B requirements.

Section 1.2.2.2 of the SAR has been changed to clarify the discrepancy between the cover letter.

NRC Question 1-2:

Confirm that AREVA is not seeking approval for the transportation of loose fuel rods per the current version of the application. Section 1 .I, Page 1-1, of the SAR states: "The MAP package is designed to transport both Type A and Type B fissile material in the form of unirradiated nuclear fuel assemblies or loose rods containing sintered uranium dioxide fuel pellets enriched up to 5.0 weight percent 235U." Chapter 6 of the SAR, however, does not provide a criticality evaluation for the loose fuel rod contents in the MAP-12/MAP-I3 packages. This information is needed to determine compliance with 10 CFR 71.35. 1-3 Explain how the CSI value of 2.8 was obtained. Also explain the application of the CSI value to the loose fuel rod contents in the MAP package.

Section 1.1, page 1-1, of the application states the MAP'S CSI is 2.8 for fuel assemblies and loose fuel rods; however there is no criticality evaluation provided in the SAR for the loose fuel rods in the MAP package.

AREVA Response to Question 1-2:

AREVA is not seeking approval for the transportation of loose fuel rods.

The SAR sections identifying loose fuel rods have been deleted.

NRC Question 1-3:

Explain how the CSI value of 2.8 was obtained. Also explain the application of the CSI value to the loose fuel rod contents in the MAP package.

Section 1 .I, page 1-1, of the application states the MAP'S CSI is 2.8 for fuel assemblies and loose fuel rods; however there is no criticality evaluation provided in the SAR for the loose fuel rods in the MAP package.

AREVA Response to Question 1-3:

The CSI value of 2.8 was based on the criticality assessment performed in Section 6. For a 36 package array, 2N=36, N=18, 50/18 = 2.77778, which is rounded to 2.8.

Section 1 of the SAR has been revised to include this description.

Chapter 2.0 Structural Evaluation

NRC Question 2-1:

Provide the discussion and/or analysis to demonstrate the structural integrity of the cladding during hypothetical accident conditions (HAC).

The fuel rod cladding is considered to provide containment of radioactive material under both normal conditions of transport (NCT) and HAG. Section 2.11 states that the discussion of cladding and its ability to maintain sufficient mechanical integrity to provide such containment is described in Section 1.2.2 and Chapter 4.0 of the SAR. No such discussions were found to verify the structural integrity of the cladding during HAC.

AREVA Response to Question 2-1:

Section 2.12.1 has been revised to include a more detailed description of the cladding following the drop and fire tests.

Visual inspections of the fuel rods in each CTU did not identify any bent or damaged rods. The test assemblies were removed from each CTU and further inspected, and no cracked or breached rods were identified visually. A random sample of rods was removed from the most damaged assembly and checked for pressurization. All were found to be pressurized. Therefore, no leakage or breach of the rods occurred as a result of the performance tests. The interior of the CTU3 was coated with tars as a result of the condensation of foam off-gas; however the fuel rods, being covered by a thin sheet of polypropylene, remained in their as fabricated bright condition. The HAC fire test had no further effect on the cladding.

Chapter 3.0 Thermal Evaluation

NRC Question 3-1:

Revise the following pages to incorporate omitted references: 3-16, 3-25, 3-46, 3-47, 3-48.

The sources referenced in the above listed pages are omitted and instead show the following text: "Error! Reference source not found." In some instance a figure number is referenced and the source can be identified within the application, in other instances there is no identifiable information with regards to the reference.

AREVA Response to Question 3-1:

The identified pages have been revised to indicate the correct references as indicated below:

Page 3-16 – Figure 3-1

Page 3-25, first instance – Figures 2.12.1-62 through 2.12.1-65 and Table 2.12.1-4.

Page 3-25, second instance – Figures 2.12.1-69 and 2.12.1-70.

Page 3-46 – Figure 3-22.

Page 3-47 – Figure 3-22.

Page 3-48, first instance – Delete text, no further reference needed.

Page 3-48, second instance – Delete text, no further reference needed.

NRC Question 3-2:

Provide a figure that reports steady-state temperatures for the MAP-12/MAP-13 packages under NCT hot conditions with insolation. Justify that the method used to apply solar insolation (assuming a diurnal cycle as opposed to a constant heat flux) provides a conservative result.

Figure 3-1 of the SAR shows the time evolution of NCT temperatures under hot conditions with solar insolation. It is not clear from the figure that the package reaches steady state temperatures for the time scale presented.

AREVA Response to Question 3-2:

The diurnal cycle provides the §10 CFR 71.71 (c)(1) specified insolation over a 12 hour period. Per IAEA Safety Guide TS-G-1.1, §654.4, time dependant sinusoidal heat flux is the more precise way to model insolation.

The peak and average foam temperatures achieved with the diurnal cycle are 201 and 144°F, respectively, versus 174 and 142°F, respectively, for a steady-state analysis using 24-hour average solar. As such, the two methodologies provide essentially the same average foam temp., but the diurnal cycle yields a higher peak foam temperature and a higher thermal gradient.

The change in component temperatures over the last 24 hours of the 10 day heatup period depicted in Figure 3-1 is 0.5°F, or less – indicating that steady-state conditions are essentially attained. An enlarged plot of the transient heat up plus a figure depicting the alternative steady-state temperature distribution is provided to demonstrate these facts.

Page changes provide for Sections 3.3, 3.3.1.1, and 3.5.2 and a new Figure 3-2 have been added to the SAR to present an enlarged view of the transient shown in Figure 3-1

NRC Question 3-3:

Provide a description of how the solar absorptivity values listed in Table 3-6 of the SAR were actually applied to the thermal model. Application of solar absorptivity values to the package surfaces can serve to decrease the amount of energy absorbed by a package, thereby, reducing the intended values for insolation as outlined in 10 CFR 71.71(c)(l).

AREVA Response to Question 3-3:

The details of the solar modeling are provided in Section 3.5.2 of the SAR. The solar absorptivity value in Table 3-6 was applied by multiplying the incident insolation value at the package surface for the given time of the day by the Table 3-6 value to yield the amount of solar energy actually absorbed by the package. This approach is consistent with NUREG-1609, §3.5.2.1 which indicates that the thermal absorptivities and emissivities are to be appropriate for the package surface conditions. Similar directions are provided in RegGuide 7.9, Rev. 2, §3.2.1.

Page changes have been provided for Sections 3.2.1 and 3.5.2 to indicate the above.

NRC Question 3-4:

Provide a clarification of the sequence of events related to the fire test of the MAP certified testing unit (CTU), with particular attention to when the test was concluded and what means were used to extinguish the pool fire. It is not clear from the description provided in Section 3.4.2, page 3-22, of the SAR what the actual sequence of events was related to the end of the fire test of the MAP CTU. The regulation in 10 CFR 71.73 clearly prohibits the use of fire suppressants to stop any combustion that may occur on or in a package that is being tested following the conclusion of the fire test. The SAR states that a fire suppressant foam was used to attempt to suppress the fire, but it is not clear if this foam served to provide cooling to the CTU as well.

AREVA Response to Question 3-4:

The fire suppressant was introduced to the test setup approximately 31 minutes after the fire was ignited. The fire suppressant was introduced to the test setup via piping below the surface of the fuel pool. At no time did the fire suppressant make contact with any portion of the package or serve to cool the package, nor did the suppressant stop any combustion occurring in or on the package.

Sections 2.12.1 and 3.4.2 of the SAR have been revised to include this clarification.

NRC Question 3-5:

Justify the claim that the test fire generated twice the heat input to the package than the regulatory 800°C 30 minute fire. Section 3.4.2, page 3-23, estimated the fire had twice the heat input of a regulatory fire due to the higher temperature and longer duration, as radiative heat transfer scales as absolute temperature to the fourth power. However, only the heat transfer due to radiation would be two times larger than a regulatory fire, not the total heat flux. Further justification of this statement is needed. If AREVA believes the fire test exceeded the regulatory requirements, then a clear, quantitative discussion of the conservatisms present in the fire test should be presented.

AREVA Response to Question 3-5:

The intent of the statement was to simply state that the fire test resulted in the package being exposed to a higher heat input to the package than the regulatory 800°C 30 minute fire. While an accurate determination would involve a complex computation of the transient temperatures of all components, etc., the estimate of twice the heat input was based on heat transfer between an assumed package skin temperature of 1475°F for a regulatory fire and 1746°F for the fire test, a foam char temperature of approximately 650°F, an effective emissivity exchange factor of 0.9, and a convection coef. of 3.5 Btuh/sq. ft-F.

As such, the heat input per hour for a regulatory fire would be on the order of ((1475+460)^4 – (650+460)^4)*0.9*1.714e-9 + (1475-650)*3.5 = 22,172 Btuh/sq-ft. The equivalent heat input for the observed fire test would be on the order of ((1746+460)^4 – (650+460)^4)*0.9*1.714e-9 + (1746-650)*3.5 = 38,026 Btuh/sq-ft. The ratio of heat input would then be (38,026*38 minutes)/(22,172*30 minutes) = 2.2. Excluding the additional burn time the ratio of heat input (38,026/22,172) is 1.72 or 72% higher than the minimum regulatory fire.

Since this heat input ratio is only an estimate and its exact level is not important to the safety evaluation, the SAR text has been revised to simply state that the heat input to the package as a result of the fire test exceeded the regulatory requirements.

Page changes have been provided for Section 3.4.2 to include a justification for the heat input ratio between the regulatory and fire test results.

NRC Question 3-6:

Provide a detailed description of the temperature sensitive strips used during thermal testing and a rationale for their use over other methods of measuring temperatures inside the package during the HAC fire test. Provide additional justification for the accuracy of predicted temperatures for components internal to the package.

Section 3.4.3.1, page 3-23, of the SAR states that temperatures inside the package were to be measured with temperature sensitive strips, which were unreadable due to condensation from foam out-gassing, causing the temperatures to be estimated from the extent of damage to each package component. Given this, temperature sensitive strips appear to be a less than ideal choice for this application. The temperatures reported in the SAR need to be more accurate in order to make a safety finding.

AREVA Response to Question 3-6:

The temperature indicating strips used were Tempil Thermax THE06S-8. Temperature indicating strips were used because the expected peak temperatures inside the package were relatively low and since the use of thermocouples would have required altering the package design to accommodate the routing the T/C leads. Further, since the CTU's were to be dropped prior the fire test, there was no way of protecting the T/C leads that extended beyond the surface of the package without risking the integrity of the drop test results due to the protective covers required for the leads. Adding the T/C's after the drop tests was not an option since the packages could not be opened and re-closed to their post-drop configuration.

Estimating peak temperatures attained in a fire based on the condition of components is a standard fire investigation technique. The fuel assembly has an accident temperature limit of 1,058°F (570°C) or higher, whereas the polypropylene sheet surrounding the fuel assembly has a melting point of 275 to 330 °F. Given that the polypropylene sheet was essentially un-damaged and the large thermal margin between 1,058°F and 275 °F, the accuracy of the predicted temperatures is sufficient to assess the safety of the package design.

The maximum potential temperature achieved within the Fuel Cavity during the fire has been revised up from 225°F to 275°F due to understanding that the plastic wrap is polypropylene and not polyethylene. For further conservatism, a bounding fuel rod temperature of 300°F is assumed.

Page changes in Sections 3.2.2 and 3.4.3 provide clarification of the basis for the estimated temperatures reached during the fire.

NRC Question 3-7:

Provide a complete description of the physical state of the neutron moderator components after the HAC fire test. Include photographs of those components if available (reference Section 3.4.3.1 of the SAR).

One of the criteria by which the package design is to be evaluated is how the neutron moderator components survive the HAC fire test. Therefore, the staff requires all possible information relating to their condition after the fire.

AREVA Response to Question 3-7:

Section 2.12.1 was revised to include a more complete description of the physical state of the neutron moderator after the HAC fire test for each segment.

Specifically, Figure 2.12.1-69 was added to identify the segment descriptions for blocks from segment #1 in the Forward to segment #11 in the package Aft locations. Figure 2.12.1-70 was modified to provide block identification consistency with license drawing 9045399. Table 2.12.1-4 was added to identify the physical state of each neutron moderator block based on visual examinations. Table 2.12.1-5 was further modified to identify the physical state of the neutron moderator blocks in the segment (#5) that showed slight melting with material loss in the peak of one block. The table was further modified to change the pretest characterization of the moderator from a volume basis to a mass basis

for consistency with the post test mass measurement results. Figures 2.12.1-71 through 2.12.1-74 were added to visually show the state of the majority of moderator blocks in the Lid and Figures 2.12.1-81 through 2.12.1-83 were added to visually show the state of selected moderator blocks in the Base.

Sections 3 and 6 were also modified for consistency with the reported test results in Section 2.12.1.

NRC Question 3-8:

Provide a detailed description of the behavior of the intumescent char layer of polyurethane foam described in Section 3.5.3 of the SAR, specifically with regards to its expansion, and the structural stresses it may incur in the package shell.

A property of intumescent polyurethane foam is expansion to seal any holes in the outer shell caused by puncture damage during the fire exposure. However, according to design drawings, it appears that in certain areas of the package, the foam has no room to expand. Depending on the amount of expansion the foam undergoes as it decomposes, it could cause additional structural stresses.

AREVA Response to Question 3-8:

The char has no appreciable structural capacity and will not develop unless there is already space available. Without available space the pyrolysis gases developed as a result of the charring process will move the char mass out through the vent ports and prevent its buildup. Only as the charring process continues and space becomes available will char be retained, filling the available space.

The foam char has no appreciable structural capacity and can not produce stress in the package shell.

Page changes are provided for Section 3.5.3 for clarification.

NRC Question 3-9:

Provide a comparison of the NCT analysis conducted in SINDA/FLUINT and the observations of NCT (pre-fire) temperatures of the actual MAP CTU (reference Section 3.5.2.1 of the SAR). Typically, when analytical (computer based) models are presented for a package design, there is some comparison made between the analysis model results and any experimental results, if physical testing was conducted, in order to validate the predications of the analytical model. The applicant has provided an analysis to predict NCT temperatures as well as test results for HAC. There is no nexus drawn between the analytical modeling and the experimental test results. Comparisons of this type serve to strengthen the demonstration of thermal performance of the package when they are presented.

AREVA Response to Question 3-9:

As stated in Section 3.4 of the SAR, the test results for the HAC condition is via physical testing and not by analytical modeling. The only use of the analytical model for the HAC event was as a test planning tool to predict how long it would take to cool or heat the package to the drop test conditions. Verification of the test article's condition prior to the drop test is based on physical measurements via temperature probes inserted into the package vent ports and not by the analytical predictions. As such, no part of the safety basis for the package under HAC conditions used the analytical model of the package.

None of the physical testing was conducted to validate the predictions of the analytical model. Further, the thermal conditioning prior to the physical testing was not conducted in a manner that would permit its use in validating the analytical model.

Given that the package has essentially no decay heat, the need to validate the analytical model is not deem critical to the safety analysis since the peak temperatures of the components under NCT conditions can not exceed the local ambient-solar temperature.

NRC Question 3-10:

Provide a summary in Section 3.5.3 of the SAR of the physical properties of charred/decomposed polyurethane foam (e.g., specific heat, thermal conductivity, density, etc.). If these properties are not available, provide a justification for the exclusion of these properties from the SAR. Include a discussion of the intumescence of the foam and what effects the foam material reaction could have on the other materials of the package.

Information about the decomposed foam is necessary for confirmatory analyses of the performance of the package in response to HAC conditions. References for this information should be cited in the SAR.

AREVA Response to Question 3-10:

The physical properties of charred/decomposed polyurethane foam are not available. The non-availability is due to a charred foam structure that is too fragile to permit consistent testing of samples and the fact that the exact makeup of char is not repeatable between test setups.

Since the confirmation of the package design is by test and not by analysis (as allowed by §10 CFR 71.73 (c)(4) and NUREG-1609, §3.5.3), the properties of the charred foam are not needed nor required for the safety determination. The demonstration of the safety of the package design is evidenced by the condition of the safety critical components of the package (i.e., the nylon moderator and the fuel assemblies) after fire.

The foam material reaction during charring has not been observed having an effect on other materials in the package for this application nor for any of the numerous other packages in which it is used.

Page changes are provided for Section 3.5.3.

NRC Question 3-11:

Provide the rationale for conducting the "bucket tests" (mentioned in Section 3.5.3) as a means to determine the correlation between foam recession depth and density. Discuss how the bucket tests influenced the testing and evaluation of the MAP 12fMAP-13 packages, and provide justification of the applicability of the bucket tests to the foam as it was used in the package.

The value of the bucket tests that were conducted on the foam is not clearly described in the SAR. Additionally, this relationship of foam density to recession rate only applies when the fire conditions (heat, duration, etc.) and material configuration (surface area, depth, etc., of each material) are reasonably close to the bucket test, which may not be the case for the fire test. It appears that measuring the amount of decomposition (which could be easily correlated to the recession depth) as a function of heat input, or temperature, could provide more useful information. This could be used to estimate the heat input or highest temperatures seen during the fire test by examining the recession depth of the charred foam.

AREVA Response to Question 3-11:

The "bucket tests" described in Section 3.5.3 were not conducted to determine the correlation between foam recession depth and density. The correlation of foam recession was provided by foam vendor (see footnotes 10 & 11). The bucket tests were conducted as a design verification process prior to proceeding to full scale test unit fabrication. The reason for mentioning the bucket tests was simply to indicate that the results seen from the full scale fire test were viewed as consistent to what was expected based on the bucket tests. This consistency of results can be taken to demonstrate that the observed performance of the package design under the full scale testing was not abnormal, but would be repeatable for a similar setup. This discussion is consistent with the last sentence in NUREG-1609, §3.5.3.3.

Page changes are provided for Section 3.5.3 to clarify the purpose of these tests.

Chapter 4.0 Containment

NRC Question 4-1:

Correct the inconsistency for the cladding leakage rate mentioned in Section 4.2.3, page 4-3, and in Section 8.1.4, page 8-2. Also specify the type of gas used for the leak test.

Section 4.2.3, says that "the containment boundary is less than 3E-08 ref-cc/sec." Section 8.1.4 says, "the leak rate is typically less than 1 E-7 atm-cm3/sec." The post fabrication leakage test for the fuel rods should be clearly and unambiguously stated in both sections.

AREVA Response to Question 4-1:

The text in Section 4 has been revised to be consistent with Section 8.

NRC Question 4-2:

Provide justification in the SAR that the cladding can withstand HAC in the form of drop test and fire test results, such that the containment boundary remains unbreached. Also, describe the condition of the cladding after being subjected to HAC.

Section 4.3.2.2 states: "The performance tests documented in Section 2 [of the SARI demonstrates that no pellets are released from the cladding as a result of the postulated hypothetical accident conditions." Contrary to this statement no material could be identified in the SAR that describes the condition of the cladding after being subjected to HAC.

AREVA Response to Question 4-2:

Section 2.12.1 has been revised to include a description of the cladding following the HAC drop and fire tests:

A visual inspection of the fuel rods in the CTU did not identify any bent or damaged rods. The test assemblies were removed from the CTU and further inspected, and no cracked or breached rods were identified visually. A random sample of rods was removed from the most damaged assembly and checked for pressurization. All were found to be pressurized. Therefore, no leakage or breach of the rods occurred as a result of the performance tests. The interior of the package was coated with tars as a result of the condensation of foam off-gas; however the fuel rods, being covered by a thin sheet of polyethylene, remained in their as fabricated bright condition. The HAC fire test had no further effect on the cladding

NRC Question 4-3:

a) State in the SAR whether or not the dummy fuel assembly in the CTUs had the fuel tubes pressurized. Also, if the CTUS rods were not pressurized, explain what effect pressurized rods would have on cladding integrity resulting from HAC.

b) Explain how the CTUs with a dummy fuel assembly bound the case of shipment of loose rods in a container for the HAC tests. Also, evaluate any additional effect on the loose rod cladding integrity resulting from the HAC tests.

The staff needs this information to ascertain whether or not the dummy fuel assembly adequately represents the fuel being shipped in the drop tests. For example, the drop tests only include a dummy assembly which would tend to reduce bending forces on an individual rod by reinforcing it with the combined strength of the assembly.

AREVA Response to Question 4-3:

Section 2.12 1 has been revised to include the rod pressure information. The CTU rods were pressurized to the maximum design pressure for current assembly designs, 225 +0/-15 psig.

AREVA is not seeking approval for the transportation of loose fuel rods.

NRC Question 4-4:

Include in the SAR the weight of fuel that is equivalent to an A, quantity and the likelihood of it escaping from the post-HAC of the cladding.

This information is needed to clarify exactly how much fuel could be released after a postulated accident and still be below an A, value.

AREVA Response to Question 4-4:

For assemblies containing low-enriched commercial grade uranium dioxide, the A_2 value is unlimited; therefore, there is no corresponding limiting weight. For assemblies containing blended low-enriched (BLEU) uranium dioxide, from Section 4 the mixture A_2 value is 0.175 Ci and the specific activity of the material is 0.0143 Ci/kg. Thus, the limiting mass for Type A shipment of BLEU material is 0.175/0.0143=12.2 kg (~ 2,000 pellets).

The packaging used for low-enriched commercial grade uranium dioxide is the same as the packaging used for the BLEU material. Additionally, the leak tests used to confirm the integrity of the BLEU fuel rods to a rate less than 1E-7 ref-cc/sec is the same as the leak tests used for the low-enriched commercial grade rods. Thus, the leakage rate of the low enriched commercial grade material following the 10CFR71.73 HAC sequence of tests is expected to be the same as that demonstrated for the BLEU material in Section 4. Since the leakage requirement for low enriched uranium dioxide is no dispersal, the limit established for the package based on BLEU material bounds the limit for the low-enriched commercial grade material.

Section 4 has been revised to add the above information.

NRC Question 4-5:

State the initial pressure in the fuel rods in the SAR. It is suggested to include this as an addition to Table 1-1 or 1-3.

This information is needed to provide an accurate description of the fuel being shipped and it provides a mechanism for propelling particulates from a failed fuel rod, or in this application, the containment boundary.

AREVA Response to Question 4-5:

The CTU rods were pressurized to the maximum design pressure for current assembly designs, 225 +0/-15 psig. This information has been added to the performance test discussion in Section 2.12.1 per RAI question 4-3. Typical rod pressures have been listed in Table 1-3.

The pressure of the rods used in the CTU is the highest rod pressure currently manufactured by AREVA. Following the 10CFR71 HAC performance tests, no leakage was observed. Thus, the post-test leakage rate is the same as the pre-test leakage rate (on the order of 1E-7 ref-cc/sec) and the expected leakage rate is much less than the allowable post-HAC leakage rate (2.25E+3 ref-cc/sec assuming aerosol leakage). Thus, there is significant margin to the allowable leakage rate.

Note that the assumption that aerosol leakage occurs is conservative, since there was essentially no damage to the fuel rods resulting from the HAC tests and past experience with handling pellets indicates that sintered pellets do not readily release particulates.

Additionally, the mass density used to calculate the allowable leakage rate for the BLEU material (9E-6 g/cc) is a reasonable bounding assessment per ANSI N14.5-1997 for powder materials. Since only sintered pellets will be used in the assemblies, the use of this value is extremely conservative and adds additional margin to the evaluation.

Thus, the margin to the allowable is significant (more than 1,000 times less than the allowable) and differential leakage due to the initial differential rod pressure is considered negligible

Chapter 6.0 Criticality

NRC Question 6-1:

Justify the statement: "any form of borated aluminum that satisfies the ^{10}B areal density requirement is acceptable," in Section 6.2.1.3.2.1, page 6-8, of the SAR.

It has been NRC practice for approved containers to permit only absorber materials that have been properly qualified, have sufficient durability for the application, and require acceptance standards on fabricated neutron absorber plates to be used in casks licensed under 10 CFR Part 71. Qualification and acceptance tests of the material are comparatively few when only 75% credit for ^{10}B is to be taken but "any material that contains a boron absorber" would not be suitable.

AREVA Response to Question 6-1:

The criticality model represented a borated plate at the minimum B-10 areal density with a further 75% reduction of the B-10 content. Other non-boron constituent materials were not included in the criticality model. Therefore, any borated plate satisfying the minimum B-10 areal density would, in principle, be considered adequate. In addition, Section 8.1.5.2 "Neutron Absorber Plates" commits to the use of the BORAL absorber with minimum B-10 areal density, which is clearly bounded by the criticality model.

Section 6.2.1.3.2.1 of the SAR has been revised to clarify the model and intended use of Boral as the as specified in Section 8.1.5.2.

NRC Question 6-2:

Justify the nomenclature "borated aluminum" as used to represent the commercial product BORAL®.

Traditionally, the term "borated aluminum" has been used to represent a solid solution containing boron. It has not been used to represent a composite of powders that are formed into an absorber material. The description given for BORAL® is the type expected for a composite material.

AREVA Response to Question 6-2:

The SAR has been revised to replace the use of "borated aluminum" with either "borated metal matrix composite" or BORAL.

NRC Question 6-3:

Justify the use of 90% credit given to the moderator block, and 100% theoretical density for the moderator nylon materials.

Section 6.4.5.1.3, states, "The moderator blocks for the flux trap system are modeled with a uniform dimensional reduction that results in 90% of the total moderator block volume for the flux trap being modeled." The staff is not familiar with the nylon in question. For example, helpful information would be the data source and how manufacturing tolerances and other variables would be expected to influence pertinent properties of moderator materials.

AREVA Response to Question 6-3:

The Nylon used in the MAP series of packagings consists of Nylon 6,6. Nylon 6,6 is a polymer consisting of a series of bonded chains with a simplified compound structure of C6H11NO. It is widely used in commercial structural applications including automotive, furniture, power tool housings, and lawn and garden equipment. The term polymer means "many parts" and refers to a molecule formed from many smaller molecules, called monomers, which are linked together into large molecules. Nylon 6,6 is so named because it is synthesized from two different organic compounds, each containing six carbon atoms.

Nylon 6,6 has a manufactured density ranging from 1.13 to 1.15 g/cc. The minimum thickness (1.25") used in the MAP package is not influenced by manufacturing tolerances. Typical manufactured thicknesses range from 1.26" to 1.28". The material is a thermal-plastic with a very high melting temperature ranging from 482 to 509 F. The flash ignition temperature for the material is about 752 F.

Nylon 6,6 is suitable for packaging applications due to it hardness, abrasion resistance, self-extinguishing ability, and high melting and flash ignition temperatures.

Additional information on Nylon can be found in the Nylon Plastics Handbook, Melvin I Kohan, 1995, Hanser Gardner Publications. Manufacturing data sheets are also available that describe commercially available Nylon. Additional information can also be found via internet search.

The criticality assessment considered both dimensional and density reductions with dimensional reductions leading to higher k_{eff} results. The most reactive modeled condition involved a Nylon 6,6 density of 1.14 g/cc with thicknesses reduced by 10%. Nylon 6,6 at a density of 1.14 g/cc has a Hydrogen density of 11.1%. Reducing the Nylon 6,6 density to 1.13 g/cc reduces the Hydrogen density to 11.0%. Variations in the Nylon 6,6 density within the manufactured range have negligible effect on Hydrogen density of the compound. The manufactured thicknesses in the range from 1.26" to 1.28" more than off-sets this negligible variation.

This variation in density will have a negligible effect on the modeled 90% (actually 85% for the Lid and 90% for the Base) credit for the Nylon 6,6 thickness. Modeled as a reduced thickness, the reduction was used to bound minor melting experienced during the HAC fire test and not to bound dimensional manufacturing tolerances. Based on the results of the fire test, the minimum modeled 90% credit for the Nylon 6,6 moderator blocks bounds the

loss experienced in a single section. The modeled configuration is therefore very conservative with respect to the HAC test results.

NRC Question 6-4:

a) Explain the basis of the criticality safety evaluation under the assumptions that 1) it was based on moderator exclusion; and 2) that the fuel cladding gap was not floodable.

b) Justify the ability of the fuel cladding to retain its integrity after the HAC tests so as to achieve moderator exclusion.

Section 6.2.1 .I, page 6-5, of the SAR states that the containment system of the MAP packages consists of the fuel rod cladding. Section 6.4.2.1.1, page 6-16, of the SAR states: "The fuel-clad gap is modeled as void to represent a dry gap. The fuel-clad gap within the fuel rods in the fuel assembly is not considered as floodable based upon the HAC testing results, discussed in Section 6.4.5.4." This is not consistent with the requirements set forth in 10 CFR 71.55, which requires the package to be sub-critical even if water were to leak into the containment system.

AREVA Response to Question 6-4:

Visual inspection of the fuel rod cladding after (see Response to RAI 4-2) the drop and fire tests performed for the MAP demonstrate that the containment boundary (fuel rod cladding) remains intact and leak-free during all normal and hypothetical accident conditions. The immersion tests further specified in 10 CFR 71 (c)(5) for fissile and (6) all packages, require immersion equivalent to an external water pressure of 21.7 lbf/in2, however intact and leak-free rods can tolerate much higher pressures and remain moderator free. Thus, moderators are not expected to flood the fuel-cladding gap.

10CFR 71.55 (c) allows exemptions provided that no single packaging error would permit leakage and appropriate measures are taken before each shipment to ensure that the containment system does not leak. Leak tests are performed as part of the manufacturing process prior to shipment to ensure the containment boundary does not leak. Furthermore, assemblies are handled and packed with great care with no event postulated as being more severe than the HAC.

However, in order to add additional conservatism to the criticality safety assessment, the calculations are revised to include water flooding in the fuel-cladding gap.

NRC Question 6-5:

Explain how the fuel-cladding gap can remain dry after the puncture and immersion test.

Section 6.4.5.4, page 6-29, of the SAR states that fuel rod cladding did not crack and rupture after testing under the HAC described in Section 2.12. The staff reviewed the HAC testing in Section 2.12 and found that the puncture was conducted on the packaging instead of the containment boundary, which is the cladding.

AREVA Response to Question 6-5:

The MAP package, like most others, utilizes an external shell to protect the containment boundary from external impacts. As required by regulation, the package was tested in its usual assembled condition. Thus, the containment boundary is not directly challenged by the puncture ram or penetration rod drop. This is typical for any radioactive materials shipping package.

The external shell is required to ship the materials; thus, the shipping package performance tests are representative of actual shipping conditions and demonstrate that cladding breach does not occur.

However, in order to add additional conservatism to the criticality safety assessment, the calculations are revised to include water flooding in the fuel-cladding gap.

NRC Question 6-6:

Provide an explanation on the behavior of the k_{eff} curves as a function of the package array size, in Figure 6-29.

Figure 6-29 shows the change of k_{eff} as a function of package array size with the FLIP1 configuration. From this figure, it can be observed that the k_{eff} value increases first, and then goes down as the number of packages increases. Finally, the k_{eff} value jumps from 0.9356 to almost 0.9420. This curve does not seem to be consistent with common understanding of the physics of a fissile system.

AREVA Response to Question 6-6:

The majority of the behavior noted is attributed to the statistical uncertainty associated with the k_{eff} values shown in Figure 6-29. The corresponding KENO VI cases were run with 280,000 histories (280 generations with 1000 neutrons per generation), and resulted in 1σ Monte Carlo uncertainties on the order of 0.0015-0.0020. The cases were rerun with 1,000,000 histories (1000 generations with 1000 neutrons per generation), and the 1σ Monte Carlo uncertainty was reduced to ~0.0010.

The calculated k_{eff} + 2 sigma values versus container array size for these rerun cases conforms more closely to the expected behavior. k_{eff} + 2 sigma increases monotonically from 24 to 30 packages, drops slightly by a statistically insignificant amount from 30 to 32 packages, and then continues to rise monotonically from 32 to 40 packages.

Note that the seemingly odd behavior in k_{eff} versus package array size noted for the original 280K-history cases was also statistically insignificant due to the relatively large 2 sigma values associated with those cases.

Additionally, note that a monotonically-increasing behavior in k_{eff} versus package array size is not necessarily the expected result over the full range of package array sizes. This is due to the fact that a larger package array size, in terms of number of containers, may have less cubic array geometry than a smaller package array size. This would result in a higher probability per package that a neutron will escape from the array system, which may provide enough negative reactivity to offset the positive reactivity associated with increasing the number of containers in the array.

The figure and text have been clarified in the SAR.

Attachment C

CD Electronic Copy
MAP-12/MAP-13 Package
Safety Analysis Report (SAR)

AREVA NP INC.
An AREVA and Siemens company

3315 Old Forest Road, P.O. Box 10935, Lynchburg, VA 24506-0935
Tel.: (434) 832-3000 - Fax: (434) 832-3840